Final Report

Design of an Urban Air Mobility vehicle for low-emissions take-off and landing

AE3200: Design Synthesis Exercise

KoriAir

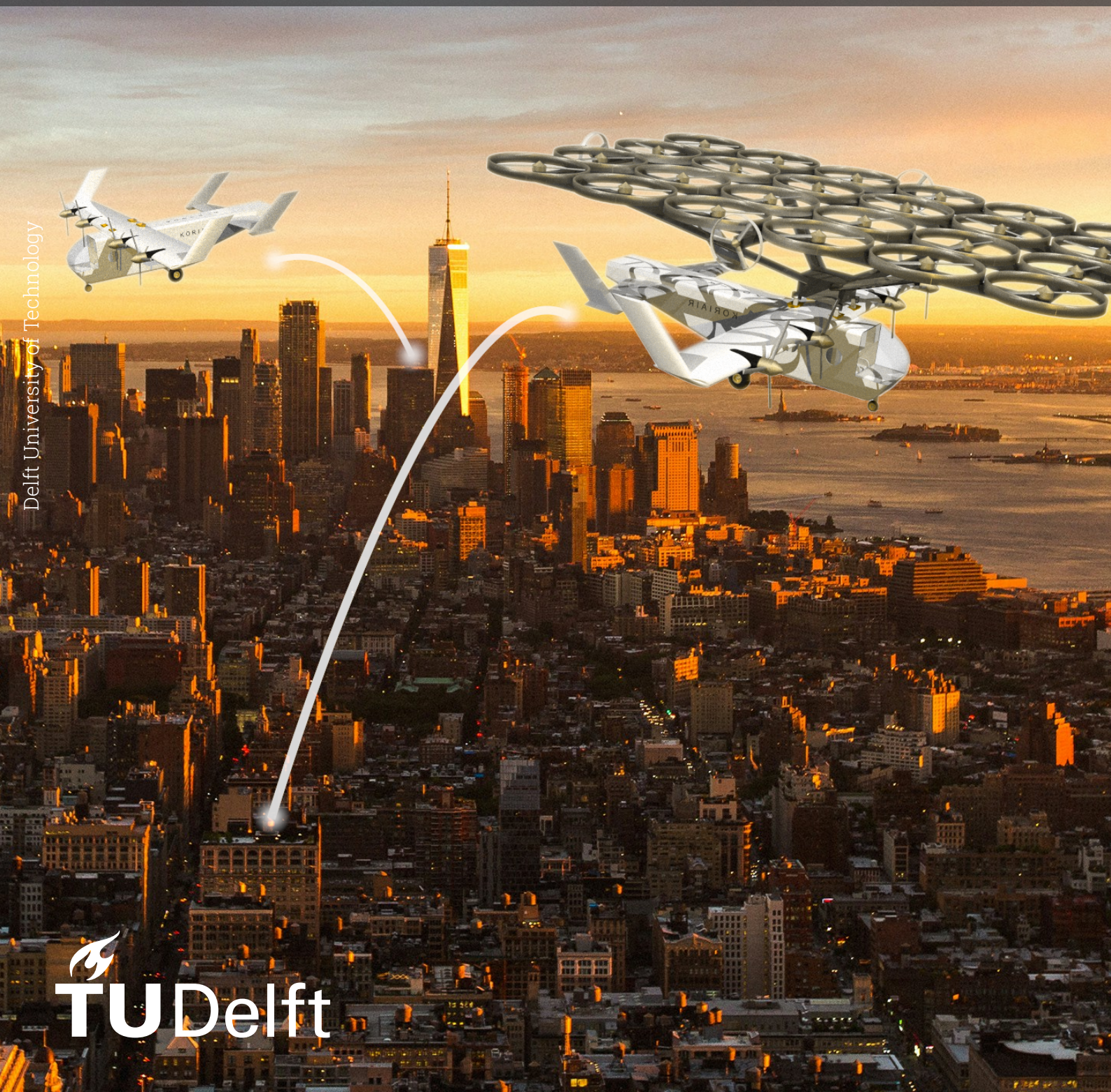

Delft University of Technology

TU Delft

Final Report

Design of an Urban Air Mobility vehicle for low-emissions take-off and landing

by

Bovino, L.
Ciunel, W.
Claps, S.
de Waart, B.J.W.
Fernandez Gutierrez, M.
Kim, J.
Leermakers, H.
Libes, T.
Ochman-Bates, M.
Slobbe, C.

for the completion of the Design Synthesis Exercise
at Delft University of Technology

Project duration:	April 22, 2024 – June 28, 2024
Supervisor:	Dr. L. T. Lima Pereira
Coaches:	R. Tian, Z. Xu

Cover Image: https://unsplash.com/photos/aerial-photography-of-cityscape-z-fpG7D7buk
[Accessed 18 June 2024]

TU Delft

This page is intentionally left blank.

Executive Overview

Low-Emissions Take-off and Landing Procedure for UAM vehicle

Students: L. Bovino, W.B. Ciunel, S. Claps, B.J.W. de Waart, M. Fernandez Gutierrez, J. Kim, H. Leermakers, T. Libes, M. Ochman-Bates, C. Slobbe

Supervisor: Dr. L. T. Lima Pereira

Coaches: R. Tian, Z. Xu

Introduction

As cities grow and populations become denser, the need for efficient transportation increases. The project KoriAir sets out to address this demand by designing an Urban Air Mobility (UAM) vehicle capable of vertical take-off and landing (VTOL). Along with the vehicle, the supporting infrastructure is designed specifically to allow for efficient and quiet operation. The design aims to compete with conventional ground transportation and current UAM vehicles, offering a faster, more convenient, quiet, and sustainable experience.

Market Analysis

The current industry landscape is investigated through a market analysis to assess the financial feasibility and market opportunity of UAM vehicles. The UAM market is fairly young. As of 2022, the market is valued at USD 2.31 billion[1], in stark contrast to conventional urban transport market that is valued at USD 300 billion.

To verify the potential of the designed product, key stakeholders are identified. These are passengers, transport companies, municipalities, aircraft regulators, and urban communities. Then, the required performance was analyzed in comparison with industry leaders such as Joby Aerospace, EHang, Volocopter and Vertical Aerospace. Since the UAM market does not currently exist on a large scale, the competitive capabilities were analyzed against other existing means of transport, such as trains or cars. The comparison was made for 3 missions: intracity (8 km in London), regional (30 km in London), and intercity (50 km in the Netherlands). As a result, it was proved that KoriAir provides significant travel time reduction while still maintaining an acceptable price. In the current state of the market, KoriAir is expected to gain market power in connecting suburbs with the city centers. A strengths, weaknesses, opportunities, and threats analysis of the UAM market was constructed to distinguish the design's position in the market and help establish its requirements. There market is young and there is a lot of room for innovation, so the need for development of energy efficient and quiet vehicles, capable of vertical take-off and landing, is clear.

Project Objective

The need for a more efficient and quiet UAM vehicle can be characterized by the following mission need and project objective statements. These statements will set the stage for the design and development work which will follow throughout this project.

Mission Need Statement:
"The UAM vehicle shall perform a more efficient and quiet take-off and landing within an urban environment than current air taxi vehicles."

Project Objective Statement:
"The objective of this project is to design a UAM vehicle and its supporting infrastructure that allows for more efficient and quiet operation than current air taxi vehicles."

[1] https://www.linkedin.com/pulse/urban-air-mobility-market-divya-jadhav-xmqjf [Accessed on 1 May 2024]

Requirements

With the scope of the project established, the key stakeholders of the project were identified. They include aircraft regulators, urban communities, municipal authorities, passengers, and transport service providers. From these, the key stakeholders of the design were identified to be the passengers and the transport service providers. As direct users of the UAM vehicle, their needs drove the generation of the key requirements of the design, which are presented below.

1. The UAM vehicle shall not produce noise more than 120 dBA in sound power level during take-off and landing [50].
2. The UAM vehicle shall have operating costs equal to or less than 1.00 euro/pax/km [50].
3. The UAM vehicle shall be fully chargeable in 30 minutes [50].
4. The acquisition cost of the vehicle and its supporting infrastructure shall not exceed 5 million euros.

On the other hand, the main requirements which are expected to specifically drive the design of the product are presented as in the following list.

1. The MTOW of the vehicle and its supporting infrastructure system shall not exceed 3175 kg [16].
2. The UAM vehicle shall be able to provide transport up to 50 km range [50].
3. The UAM vehicle shall have a cruise speed of 200 km/h [50].
4. The take-off and landing area shall not exceed a square of 12 x 12 m^2[2].
5. The weight of the payload shall not be less than 420 kg[3].
6. The take-off time shall be less than 100 s [5].
7. The landing time shall be less than 100 s [5].
8. The total installed power of the motors of the UAM vehicle shall be lower than 1,000 kW [50].
9. The UAM vehicle shall be able to achieve vertical acceleration of at most 2 m/s^2 or 0.2 g [5].
10. The UAM vehicle shall be able to achieve vertical acceleration of at most -2 m/s^2 or -0.2 g [5].

Design Option Trade-off

Following the market and requirements analysis, different potential design options were identified and analyzed to assess their competency in meeting the project objective for UAM vehicles. They varied from conventional VTOL designs to reinventing the current systems by developing solutions which have not been explored and matured by other companies. As a result of the analysis, the following five designs were chosen to be further developed for the trade-off stage of the project.

- Tilt-rotor VTOL vehicle
- Lift and cruise VTOL vehicle
- Multicopter
- Single lifting vehicle assisting the VTOL of a conventional aircraft
- Multiple lifting vehicles assisting the VTOL of a conventional aircraft

The first three designs already exist in the current UAM market. On the other hand, the latter two designs are new in the field. While two-vehicle concepts exist in the conceptual phase, the idea of using assisting vehicles only for take-off and landing is quite innovative.

An initial sizing was conducted for each of the design configurations in order to perform a complete and comprehensive trade-off. The main parameters which were analyzed were the general size and dimensions of the vehicle, its MTOW, the power requirements during cruise and take-off, the energy consumption during cruise flight and the noise produced during take-off. The design options were ranked based on their optimization of the parameters, with the conclusion of the single lifting vehicle design combined with a conventional aircraft for cruise flight.

[2]https://moaams.org/pdf/HelipadRecommedations.pdf [Accessed on 1 May 2024]
[3]https://lhconsulting.com/ [Accessed on 1 May 2024]

Final Design

Based on the trade-off, the final design selected was a two-vehicle configuration, consisting of a vehicle that would provide power and thrust for vertical take-off and landing (lifting vehicle), and a vehicle that provides horizontal thrust for the cruise part of the flight regime (cruise vehicle). The lifting vehicle is a multicopter, using 24 rotors to provide vertical thrust and four other rotors for gust mitigation. The cruise vehicle is a light electrical conventional commuter aircraft. A typical flight path is visualized in Figure 1. This is a simplified overview.

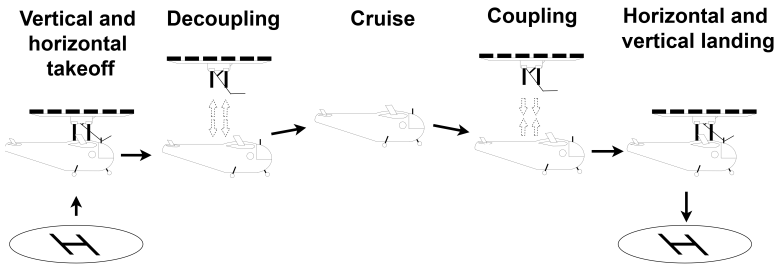

Figure 1: *A simplified visualisation of a typical flight mission*

The benefits of the design option chosen lie in the ability to optimize the design's performance for different parts of the flight regime. The vehicles will be physically connected together by a coupling mechanism before take-off. The lifting vehicle will execute the vertical take-off with the cruise vehicle attached, and once the transition altitude of 450 m has been reached, the cruise vehicle will begin producing lift from its own propulsion system. Before climbing, the coupling mechanism will decouple the vehicles and the cruise vehicle will execute the cruise phase of flight alone. At the end of the cruise phase, a different lifting vehicle will take-off from the destination vertiport and align itself with the cruise vehicle such that they can couple again. The coupled configuration will slow down horizontally, reduce its altitude, and land vertically at the vertiport.

The final lifting and cruise vehicle assembly is shown in Figure 2.

Figure 2: *Rendering of the final assembly*

Following the render, the most important dimensions and parameters of both the cruise and lifting vehicle are presented in Table 1.

Table 1: *Most important system parameters*

Parameters	Values	Units
Cruise Vehicle		
Wingspan	11.9	m
Length fuselage	7.45	m
Number of propellers	4	-

Continued on next page

Table 1: *Most important system parameters (Continued)*

Propeller radius	1.0	m
Engine type	Geiger Engineering HPD40D	-
Engine power	40	kW
Lifting Vehicle		
Number of rotors	24	-
Rotor radius	0.69	m
Engine type	Geiger Engineering HPD20SD	-
Engine power	20	kW
Design Mission		
Total energy consumption	30	kWh
Cost per trip	50	€/pax
CO_2 emissions	0.23	kg/kWh
Emitted noise during cruise	63	dBA

Cruise Vehicle Design

The design of the cruise vehicle closely resembled the procedures for a general aviation aircraft under certification specification CS-23. To begin with, the subsystems main parameters were designed, including the wing, fuselage, empennage, propulsion system, and landing gear. Their values were iterated upon until an acceptable converging design was met.

The wing design was based on the wing loading diagram and optimized for cruise performance while restricting the wingspan to fit within the vertiport area restrictions. The high lift devices were designed to achieve a low stall speed, which ensures the lifting vehicle does not have to travel too far.

For the fuselage, the design was based on the consideration that it should provide enough space to house the payload, batteries, avionics system, and other components while minimizing its drag. It must be noted that the fuselage is not pressurized, as the vehicle will not reach high altitudes. The design process was based on equations from Raymer [53].

The propulsion system design involved sizing the propellers, motors, and battery. Blade element theory was used to size the propellers, and a motor was selected based on its required characteristics.

After the main subsystems had been sized, a class II weight estimation was performed following Raymer's approach [53]. This estimation took parameters from the class I weight estimation and from the subsystem designs. The requirements are also taken into account during the class II weight estimation, which is shown below.

Table 2: *Results of the cruise vehicle class II weight estimation*

Component	Mass [kg]
Wing	139
Fuselage	222
Coupling mechanism	150
Horizontal tail	34
Vertical tail	26
Main landing gear	70
Nose landing gear	15
Engines (including propellers)	96
Flight controls	16
Electrical	42
Avionics	23
Operative empty weight (OEW)	**940**

Continued on next page

Table 2: *Results of the cruise vehicle class II weight estimation (Continued)*

Battery mass	**237**
Payload mass	**420**
Maximum take-off weight (MTOW)	**1597**

Lifting Vehicle Design

In the case of the lifting vehicle, most subsystems were sized using Raymer [53]. Based on the component, equations for general aviation aircraft or helicopter/multicopter were used. The fuselage of the lifting vehicle was sized to house the battery and avionics of the vehicle, as well as provide structural integrity. The propulsion system was designed in a similar way to that of the cruise vehicle. For noise considerations, the number of rotors was maximized. Finally, for the landing gear a skid structure was chosen as it is less complex, lightweight, and provides good ground stability. A retraction mechanism was included to allow for the coupling mechanism to operate under the vehicle. Once the main subsystems were sized, the weight estimation for VTOL vehicles was performed applying the approach from Raymer [53].

Table 3: *Results of the lifting vehicle class II weight estimation*

Component	Mass [kg]
Fuselage	35
Coupling	128
Landing gear	105
Engines	135
Electrical	70
Avionics	62
Rotors with ducts	211
OEW	**746**
Battery mass	**229**
Take-off mass without cruise vehicle	**975**

Coupling Mechanism

The concept of a coupling mechanism to allow two vehicles to physically connect in air is a fairly innovative concept. The coupling mechanism design included load-bearing elements and guiding mechanisms to ensure alignment and secure attachment without requiring precise initial positioning.

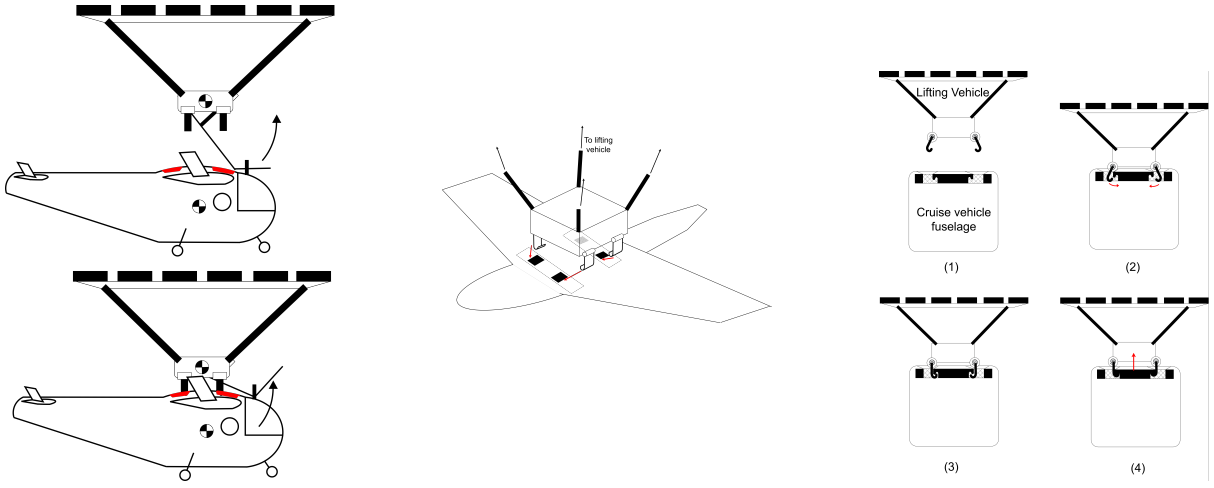

(a) *Mechanical guiding* **(b)** *Rigid connection points* **(c)** *Rigid connection creation*

Figure 3: *Overview of coupling procedure*

The mechanical guiding mechanism was idealized as a boom structure with a hydraulic system for

final alignment of the aircraft. This mechanism pulls the cruise vehicle towards the lifting vehicle.

The rigid coupling design involved four hooks on the lifting vehicle connecting with the front and rear spars of the cruise vehicle's center wing box (CWB). The hooks are designed to survive event with three hooks failing. Stress concentration factors were applied to the hook and spar designs, ensuring robustness against critical stresses. It was possible to achieve a precision of 11 cm in the positioning of the lifting vehicle. Moreover, the control system enables coupling in under 5 seconds, even in gusty conditions of 9.1 m/s wind speed.

Infrastructure and Operations

To ensure the VTOL infrastructure is well integrated in the urban community, it was necessary to design the infrastructure. Essential components of heliports were included, such as the final approach and takeoff area (FATO), touchdown and liftoff area (TLOF), and necessary lighting. Specific requirements, such as the dimensions of the TLOF and FATO, were highlighted, along with additional equipment like battery charging stations, emergency kits, and noise measurement instruments. Vertiport placement was also analysed in the context of Amsterdam and the Randstad area, taking into account existing and future heliports/vertiports, public transport links and access for emergency services.

Route optimization software implementation into the system's flight management systems was also discussed. The usage of a Provider of Services for UAM (PSU) to support route planning and ensure compliance with regulatory and operational requirements is recommended for further detailed design. This system would facilitate efficient airspace usage and coordination with air traffic control (ATC), ensuring safe and optimized flight paths.

Noise

Reduced noise emission were a key requirement for the design. Design choices to reduce noise level included selecting the number and size of rotors and blades to minimize noise, specifically the blade passing frequency (BPF). A higher number of rotors allowed for shrouds or ducts, reducing noise and radius size. A BPF of 80 Hz was achieved for the lifting vehicle, keeping harmonics below 1000 Hz. Ducts were designed based on experiments by Hubbart [25], with a hollow section filled with noise-reducing foam. Noise estimation methods for rotors and propellers considered near-field and far-field effects, applying correction factors for various parameters. Doppler effects and A-weighting were also considered ensuring noise was not perceived in sensitive frequency ranges. The values of the final overall A-weighted sound pressure levels (OASPL) values of the estimation are shown in Table 4. Additionally, the noise estimation was also performed for the Volocity vehicle, designed by Volocopter, to compare the acoustic emissions of both designs.

Table 4: *Results of the noise estimation*

Flight phase	KoriAir OASPL [dBA]	Volocity OASPL [dBA]
Vertical take-off	77	80
Horizontal take-off	67	-
Cruise	63	66

Cost

An initial estimation of the expected cost for the development of the vehicle was made. This estimate used class II cost estimations for subsystems, materials, testing, manufacturing, and other general costs. The development costs for the preliminary design were estimated by multiplying the expected days of work by the average salary of a worker in the Netherlands, with around 40 hours of work per week. This brought the costs to the following per design phase.

Table 5: *Cost estimation*

Design phase	Cost [M€]
Research and Development	5.7
Production	0.9
Operational	1.4
Regulatory and Certification	25
Project planning	0.033
Total	33

Technical Risk Assessment

Throughout the design process, identifying, analyzing and mitigating risks is a crucial element of succeeding in designing a functioning and safe vehicle. The technical risks identified for the design were updated and adapted throughout the further (sub)system detailing. Those classified as having the highest risk score were identified as listed below.

- The lift vehicle does not couple with the cruise vehicle during take-off and/or landing.
- A strong wind gust occurs when the vehicles are in close proximity of each other but not coupled.
- The lift vehicle collides with the cruise vehicle.
- The lift vehicle does not decouple with the cruise vehicle during take-off and/or landing.
- The control systems of the cruise and/or lift vehicle fail.
- All rigid coupling connection points fail.

Different mitigation and contingency strategies were set up to reduce the overall likelihood and consequence of these risks. Those strategies related to reducing the likelihood included designing systems with fail-safe or safe-life principles, which was done by implementing redundant (sub)systems or additional design safety factors. On the other hand, contingency strategies exist to reduce the consequence of risks, and these were more similar for different types of events. For example, many consequences could be reduced by performing an emergency landing procedure in a nearby location or diverting to the nearest vertiport for immediate landing if a critical (sub)system were to fail.

Sustainable Development Strategy

The sustainable development strategy of KoriAir addresses both the way sustainability is taken into account in the design of the vehicle and the way the product contributes to the sustainability of the overall urban environment. This strategy addresses the environmental, social, and economic aspects of KoriAir. To monitor the sustainability of the project, the following key performance indicators (KPIs) were considered.

- CO_2 emitted per km (kg)
- Noise level during all phases of vehicle operation (dBA)
- Ground area for VTOL infrastructure (m^2)
- Energy consumption for production, operation and recycling of the vehicle (kWh)
- Battery lifetime (km)
- Battery waste production per km of chemical compound disposed (moles)

In order to compare the sustainable operation of KoriAir to other modes of transport, the following table was made to illustrate the time, cost, noise emission and energy consumption of KoriAir compared to alternative inter/intra-urban transport. Note that noise level is measured at a distance of 100 m. The energy consumption of the eVTOL vehicle from Archer Aviation was based on its commercially available range and battery capacity characteristics, whilst KoriAir's was based on the battery specifics of the Joby S4 battery used for both vehicles and its mission range.

Table 6: *Performance of KoriAir compared to other means of transport*

	Intra-city (8 km)				Regional (30 km)				Inter-city (50 km)			
Transport	Time [min]	Price [€/pax]	Noise [dBA]	Energy consumption [kWh]	Time [min]	Price [€/pax]	Noise [dBA]	Energy consumption [kWh]	Time [min]	Price [€/pax]	Noise [dBA]	Energy consumption [kWh]
Train	19	3.3[1]	62 [47]	24	40	6.5[1]	62 [47]	90	28	14.5[2]	62 [47]	150
Car	45	1.4[3]	53 [43]	4.8	80	5[3]	53 [43]	18	45	5.4[3]	53 [43]	30
Taxi	45	35[4]	53 [43]	5.6	80	80[4]	53 [43]	21	45	110[5]	53 [43]	35
Helicopter [15]	5	390[6]	89	140	10.5	390[6]	89	520	15.5	390[6]	89	860
Archer Aviation	5	28[8]	61[7]	10	10	105[8]	61[7]	25	16	165[8]	61[7]	45
KoriAir	5.5	8	77	10	12	30	77	20	18	50	77	30

[1] https://tfl.gov.uk/fares/find-fares/tube-and-rail-fares [Accessed on 17 May 2024]
[2] 2nd/1st class prices based on: https://www.ns.nl/ [Accessed on 17 May 2024]
[3] Consumption of 9l/100km, 1.75€/l
[4] https://tfl.gov.uk/modes/taxis-and-minicabs/taxi-fares [Accessed on 17 May 2024]
[5] https://www.taxicentrale-schiphol.nl/en/ [Accessed on 17 May 2024]
[6] https://www.batterseahelicopter.com/helicopter-hire-prices/ Assumed price independent of distance in the specified range. [Accessed on 17 May 2024]
[7] https://news.archer.com/how-loud-is-an-evtol [Accessed on 21 June 2024]
[8] https://www.autofutures.tv/topics/-the-sky-is-no-longer-the-limit—-archer-aviation-to-offer-6-minute-evtol-flights-to-the-airport—/s/57e93aea-44fc-44b8-9f88-84afca6c1412 [Accessed on 21 June 2024]

As shown in the table, KoriAir can compete with all other means of transport. Travel time compared to all ground vehicles is largely reduced, especially for regional distance. Compared to helicopters, KoriAir offers similar performance in terms of time for a small fraction of helicopter rental price. Additionally, KoriAir is assumed to operate as an on demand service for much lower prices than a traditional taxi. Therefore, with lower prices and travel times, it is estimated to capture the majority of taxi demand. Finally, when compared to trains KoriAir's price is higher, however, the travel is significantly reduced. KoriAir is not expected to target the entire demand of train commuters, it can still be an attractive option for people living far away from the station.

Further Recommendations

The presented design remained at preliminary level, thus several recommendations for further research were drawn. Apart from further detailing the design of all subsystems, two areas requiring special attention were identified. First of all, the process of coupling shall be further developed. Emphasis must be put on modelling the aerodynamic interaction between the vehicles, analyzing the structural dynamic loading, and designing a more advanced control system. The second aspect requiring special attention is the operation of the vehicles. In cooperation with airworthiness authorities, certification standards should be issued. Additionally, further use case analysis must be performed to establish the optimum range for coupling procedures. Further development in the aforementioned fields will support KoriAir's entering into market. Additionally, it will create new design opportunities for the entire aviation industry.

Nomenclature

Symbol	Definition	Unit
A	Area	[m^2]
AR	Aspect ratio	-
C_D	Drag coefficient	-
C_L	Lift coefficient	-
e	Oswald efficiency factor	-
E	Energy consumption	[J]
$ED_{battery}$	Battery energy density	[J/kg]
h	Altitude	[m]
h_f	Fuselage height	[m]
$\frac{L}{D}$	Lift-to-drag ratio	-
l	Length	[m]
M	Mach number	-
m	Mass	[kg]
$MTOW$	Maximum Take-Off Weight	[kg]
n	Load factor	-
P	Power	[W]
r	Radius	[m]
R	Range	[km]
S	Surface area	[m^2]
T	Thrust	[N]
t	Time	[s]
t	Thickness	[s]
V	Velocity	[m/s]
w	Width	[m]
α	Angle of attack	[°]
η	Efficiency	-
ρ	Air density	[kg/m^3]
ρ_{mat}	Material density	[kg/m^3]
ω	Rotational speed	[rad/s]

Contents

1

Introduction

Imagine a city, where not only trains, trams, metros, and buses transport the citizens through their area. Small air taxi vehicles fly through the air, fast, efficient and quietly, whilst transporting the passengers to their desired locations. This dream is the main drive behind the market of Urban Air Mobility (UAM), a growing sector filled with exciting and promising ideas. Nonetheless, many concept vehicles run into problems. The impact of air vehicles flying around a crowded urban area should not be neglected. Emissions, noise pollution, and integrating the vehicle into the city's infrastructure are all factors of UAM vehicles which impact their urban environment. The objective of the KoriAir project is to design a UAM vehicle and its supporting infrastructure that allows for a more efficient and quiet operation than current air taxi vehicles. The aim of this report is to showcase the design of the KoriAir vehicle, which is the end product of the project.

In the first weeks of the project, the mission that the KoriAir vehicle needed to perform was analyzed. The functional requirements of the design were identified and several feasible design options were generated. After a thorough analysis and trade-off of these design options, a two-vehicle configuration was selected as the design to proceed with. KoriAir's revolutionary two-vehicle configuration, consisting of a lifting vehicle and a cruise vehicle, allows for a more efficient cruise, take-off, and landing, as the vehicle that provides vertical flight capabilities decouples from the cruise vehicle once it generates sufficient lift. Hence, the cruise vehicle does not carry the weight of the lifting vehicle during the cruise phase of flight. In this report, the process of designing the (sub)systems of the vehicles will be described, as well as different analyses on characteristics of the design, such as its aerodynamics, stability and control, and structural capabilities.

In this report, the following structure has been used. In Chapter 2, the objective of the project and the design process will be discussed in more detail. Next, in Chapter 3, the market of UAM will be analyzed, and in Chapter 4 the functions and requirements of the design will be discussed. After defining the gap in the market and the requirements the system should fulfill, the (sub)systems of the cruise vehicle and lifting vehicle will be designed in Chapter 5 and Chapter 6 respectively. The design of the mechanism that ensures both vehicles can be coupled and decoupled safely and efficiently will be laid out in Chapter 7. Following these design chapters, the performance of the system will be analyzed in Chapter 8, along with the architecture of the internal systems present, such as hard- and software systems, will be explained in Chapter 13. Next, a further analysis regarding the aerodynamics, structural, and stability and control characteristics will be discussed in Chapter 9, Chapter 10 and Chapter 11, respectively. A more detailed discussion into the noise mitigation techniques employed in the design of the system will be addressed in Chapter 12. To conclude the main design of the system, Chapter 14 will illustrate the verification and validation methods used to ensure the design models and tools are indeed correct. The operation and infrastructure integration of the design in an urban environment will be explained in Chapter 15, whilst the production, manufacturing and assembly plan in Chapter 16. Then, the sustainable development strategy of the design will be included in Chapter 17. The main technical risks of the design, as well as the reliability, availability, maintainability, and safety (RAMS) will be assessed in Chapter 18 and Chapter 19. Resources will be allocated in Chapter 20 and the costs of the design will be discussed in Chapter 21. Finally, the compliance of the design with its initial requirements and the future development of the project will be presented in Chapter 22 and Chapter 23. The report will end with the main conclusions of the design, as well as the most important recommendations for further design in Chapter 24.

2

Design Objective

In this chapter, the objective and process of the project of the design will be described. Designing does not happen successfully without a clear definition of the need and the project objective statement. The need statement describes the gap that is to be filled by the design. For the KoriAir project, this gap is related to the disadvantages of the market of Urban Air Mobility. Therefore, the need statement has been formulated as follows.

Need Statement:
Urban Air Mobility must not disturb the environment with noise and pollution emissions.

This statement leads to the mission that the design needs to perform.

Mission Need Statement:
The Urban Air Mobility vehicle shall perform more efficient and quieter operations in an urban environment than current air taxi vehicles.

The objective of the KoriAir project logically flows from the mission need statement above.

Project Objective Statement:
The objective of the KoriAir project is to design an Urban Air Mobility vehicle and its supporting infrastructure that allows for more efficient and quieter operation than current air taxi vehicles.

2.1. Stakeholder Requirements

One of the crucial first steps in a design project is identifying its stakeholders and their wishes. Stakeholders are the parties that have an interest or concern in the project. The definition of the stakeholders of the KoriAir project will be explained in Chapter 3. The identified key stakeholders of the KoriAir project are the aircraft regulators, the municipality, the urban community, the passengers and transport service providers. The requirements imposed through the desires and wishes of these key stakeholders have been listed in Table 2.1.

Table 2.1: *List of stakeholder requirements*

ID	Stakeholder Requirement
Aircraft Regulators	
REQ-STK-1	The UAM vehicle and infrastructure system shall adhere to applicable aircraft regulations.
REQ-STK-2	The UAM vehicle shall not interfere with the airspace assigned to commercial aircraft.
REQ-STK-3	The UAM vehicle shall communicate with the air traffic control.
REQ-STK-4	The UAM vehicle and infrastructure shall undergo regular maintenance checks.
Municipality	
REQ-STK-5	The UAM vehicle and infrastructure system shall be as environmentally friendly as possible.
REQ-STK-6	The UAM vehicle and infrastructure system shall not disrupt daily urban activity.
REQ-STK-7	The UAM infrastructure shall include designated landing and takeoff areas.
REQ-STK-8	The UAM infrastructure shall integrate with existing urban transportation networks.
REQ-STK-9	The UAM vehicle and infrastructure system shall have emergency response protocols.
Urban Community	
REQ-STK-10	The UAM vehicle shall be as quiet as possible.

Continued on next page

Table 2.1: *List of stakeholder requirements (Continued)*

REQ-STK-11	The UAM vehicle shall be as safe as possible.
Passengers/Transport Service Providers	
REQ-STK-12	The UAM vehicle shall transport passengers.
REQ-STK-13	The UAM vehicle shall be as low-cost as possible.
REQ-STK-14	The UAM vehicle shall transport passengers as fast as possible.
REQ-STK-15	The UAM vehicle shall provide comfortable transport.
REQ-STK-16	The UAM vehicle shall provide transportation as frequently as possible.
REQ-STK-17	The UAM infrastructure shall provide convenient access.
REQ-STK-18	The UAM vehicle shall be able to cover common urban transportation distances.

As can be seen in the table above, the requirements imposed by aircraft regulators are mainly related to regulations. The municipality has an interest in the implementation of the KoriAir project in its urban area, regarding the environment, convenient transportation and policies. The urban community is mostly concerned with the quietness and safety of the project. Finally, the passengers and transport service providers impose requirements related to comfort, cost, and performance. Many mission and (sub)system requirements flow down from these stakeholder requirements. These requirements are verifiable and more specific than the ones from the stakeholders, and they will be used when designing the different subsystems of the KoriAir vehicle. The compliance with these requirements will be checked in Chapter 22. To ensure a design that meets the requirements, they will be checked at the end of this design phase. This covers both the specific ones for the subsystems, and, therefore automatically, the ones imposed by the stakeholders.

2.2. Design Process

In the process of designing the KoriAir vehicle, the mission to be performed needed to be analyzed. The functions and requirements that the vehicle has to perform were identified in order to approach the design project with a clear idea of what the design is required to do. Some of these requirements have been discussed in Section 2.1. Several design options had to be considered in order to cover the range of concepts that could fit within the constraints set by the requirements. Some concepts were considered in more depth and preliminary sizing of these concepts was performed. Finally, the design option that was deemed to be most feasible and would provide the largest benefits in terms of efficiency and noise emissions was selected. This design option was a two-vehicle configuration, consisting of a vehicle that would provide power and thrust for vertical take-off and landing, and a vehicle that provides horizontal thrust for the cruise part of the flight regime. Throughout this report, these vehicles will be referred to as the lifting vehicle and the cruise vehicle, respectively. The lifting vehicle is a multicopter, using multiple rotors to provide vertical thrust. The cruise vehicle is a small electrical conventional commuter aircraft.

The benefits of the design option chosen lie in the ability to optimize the design's performance for different parts of the flight regime. In the process of analyzing current concepts in the field of Urban Air Mobility, it was concluded that their struggle with efficiency and noise was mostly related to the need to combine vertical take-off and landing performance with cruise performance in one vehicle. Air taxi vehicles like helicopters often have problems with larger ranges, as their rotors have to provide great amounts of power to fly horizontally at higher cruise speeds. Other vehicles with propellers that provide horizontal thrust, like lift-plus-cruise vehicles, also have disadvantages. Lift-plus-cruise vehicles have two separate sets of rotors; one that provides vertical and one that provides horizontal thrust. This adds dead weight to the aircraft which leads to the snowball effect of needing more thrust, thus heavier batteries and propulsion systems, once again leading to more dead weight. For these reasons, a design was selected that has a separate lifting vehicle providing vertical thrust, that decouples once the cruise vehicle has enough horizontal velocity to generate enough lift. At the end of the cruise phase, the lifting vehicle couples again with the lifting vehicle. The coupled configuration would slow down horizontally, reduce altitude, and land.

The two-vehicle configuration described above requires a mechanism that allows for the coupling between the lifting and cruise vehicle. This coupling mechanism is a crucial and innovative part of the design, as there are currently no comparable examples of such a mechanism in aviation. The design of this coupling mechanism will be highlighted in Chapter 7. Other subsystems of both vehicles also need to be sized and designed to allow for the coupling, as well as to optimize their performance. The design of these subsystems of the cruise vehicle and lifting vehicle can be found in Chapter 5 and in Chapter 6 respectively.

2.3. Analysis Procedures

Along with designing a cruise and lifting vehicle come many analyses and assessments of different aspects of the KoriAir project. Firstly, the current and potential market of Urban Air Mobility needs to be analyzed. This entails identifying stakeholders, competition, and customers. This market analysis can be found in Chapter 3. It is also important to define the functions that the design must perform. This can be done through a functional flow diagram, which depicts the logical flow of all functions that need to be performed for the mission of the design to be successful. The functional analysis can be found in Chapter 4. After designing the different subsystems of the design, the performance of the vehicles, such as the flight profile and loading diagrams, has to be analyzed. The flight profile, as well as the loading diagrams, are crucial parts of the design to show its feasibility. The performance analysis of the system can be found in Chapter 8.

After the general system design, there are several subsystems that need further investigation and definition of characteristics. For instance, the aerodynamic aspects of the vehicles, including a drag estimation and lift distribution, are inspected in Chapter 9. Furthermore, the structural integrity of the design and defining structural characteristics is crucial. These structural considerations will be highlighted in Chapter 10. Another critical aspect, especially with regard to the coupling phase of the flight regime, is the controllability of the aircraft. The lifting vehicle needs to be able to fly as close to the cruise vehicle as necessary for the coupling to happen. For this, a well-performing controller is needed. The stable nature of the aircraft needs to be confirmed as well. The stability and control characteristics of the design are discussed in Chapter 11.

Additionally, an important aspect of the mission is its quiet operation. Therefore, the noise that is produced by the vehicles needs to be analyzed. The noise analysis and potential mitigation strategies will be covered in Chapter 12. Also, a sensitivity analysis of the system consisting of the designs of the subsystems and their weights will be performed in order to confirm the robustness of the final design. The sensitivity analysis, as well as the verification and validation procedures, can be found in Chapter 14.

Finally, the mission need statement does not only considers a vehicle to be designed. Its supporting infrastructure is also part of the design project. The vertiport layout, the route planning and overall logistics with regard to the infrastructure of the KoriAir project are highlighted in Chapter 15. All of these different inspections lead to a well-covered and robust design as an end product of the KoriAir project.

3

Market Analysis

The objective of the market analysis is to establish the competitive cost and volume of the market for the product and the services it can provide, as well as a prediction and the establishment of new markets. This allows for determining where the vehicles being designed will fit in the market, and thus ensures a profitable launch. First, the stakeholders will be outlined in Section 3.1. Then the competition in the UAM market is covered in Section 3.2. This is important in order to determine where the design can fill a gap in the market, and thus lead to a successful integration in society. This is followed by a SWOT analysis and a discovery of potential customers, respectively in Section 3.3 and Section 3.4.

3.1. Stakeholders

The stakeholders include all entities that are affected by and can affect the mission. The following list presents all the stakeholders to the best of the team's knowledge. The stakeholders will be classified based on their impact on the system. Figure 3.1 is an interest-influence plot, visualizing how important each stakeholder is to the overall system. From the plot, the key stakeholders are *passengers, transport service providers, aircraft manufacturers and local urban communities*. This will be taken into account when performing the rest of the market analysis.

- Aircraft regulatory bodies
- Transport service providers
- Aircraft manufacturers
- Infrastructure providers
- Software contractors
- Passengers
- Investment groups
- Insurance companies
- Research institutions
- Emergency services
- Local urban community
- Local and national government
- Tourism boards
- Real estate developers
- Energy service providers

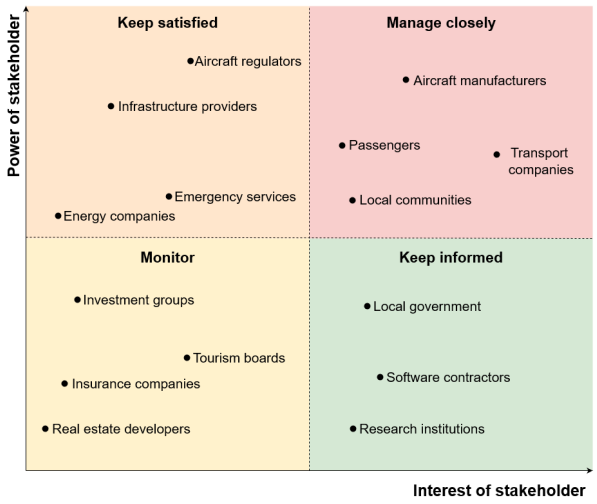

Figure 3.1: *Graph detailing the importance of each stakeholder to the system*

3.2. Competition

The current state of the UAM market finds only a few companies leading this industry. Table 3.1 shows the key players in the UAM market and specifications of their designs, including existing helicopters. It must be noted that at this stage of development, most of the revenue is from pre-orders as no UAM vehicles have been certified yet.

Table 3.1: *Key market players and designs in the UAM industry*

Company	Aircraft type	Passengers	Range [km]	Cruise speed [km/h]	MTOW [kg]	Noise emissions during cruise at 500 meters elevation [dBA]
Joby S4	Multi-Tiltrotor	4	160[1]	320[1]	2404[1]	45[1]
EHang EH216-S	Multicopter	2	35[2]	100[2]	620[2]	-
Lilium Jet	Tiltduct	6	250[3]	250[3]	3175[3]	-
Volocopter VoloCity	Multicopter	4	65[4]	90[4]	900[4]	48[4]
Urban Aeronautics	Fancraft	4	150[5]	235[5]	1930[5]	55[5]
Tetra Mk-5	Multicopter	1	260[6]	260[6]	567[6]	-
Archer Midnight	Multi-Tiltrotor	4	80[7]	240[7]	3175[7]	46[7]
Vertical Aerospace VX4	Multi-Tiltrotor	4	161[8]	240[8]	-	-
Bell 407	Helicopter	6	612[9]	224[9]	2268[9]	-
Bell 427	Helicopter	5	520[10]	250[10]	2880[10]	-
MD 900	Helicopter	6	350[11]	282[11]	3080[11]	-

[1] https://evtol.news/joby-aviation-s4-production-prototype [Accessed on 19 June 2024]
[2] https://evtol.news/ehang-216/ [Accessed on 19 June 2024]
[3] https://evtol.news/lilium-gmbh-lilium-jet-7-seater [Accessed on 19 June 2024]
[4] https://evtol.news/volocopter-volocity/ [Accessed on 19 June 2024]
[5] https://evtol.news/urban-aeronautics-cityhawk/ [Accessed on 19 June 2024]
[6] https://evtol.news/tetra-aviation-mk-5 [Accessed on 19 June 2024]
[7] https://evtol.news/archer/ [Accessed on 19 June 2024]
[8] https://evtol.news/vertical-aerospace-VA-1X [Accessed on 19 June 2024]
[9] https://www.maunaloahelicopters.edu/library/Rotorcraft_Flight_Manuals/Bell_Helicopter/407.pdf [Accessed on 19 June 2024]
[10] https://www.helimax.pl/en/helicopters/207-bell-427 [Accessed on 19 June 2024]
[11] https://www.paramountbusinessjets.com/private-jet-charter/aircraft/mcdonnell-douglas-md-900-explorer [Accessed on 19 June 2024]

Since none of these UAM vehicles have entered service so far, to analyze the possibilities of KoriAir, the current market of urban transport is analyzed. For reference, usage of public transportation in London was investigated. Based on data from January 2018[1], between Inner and Outer London - which covers about 30km - there are about a million journeys per weekday. Additionally, around 3 million journeys per weekday are made within Inner and Outer London. This number shows that in a big city like London, public transportation is a major method of transportation used by inhabitants and that the KoriAir vehicle must be more attractive than public transportation. In order to be competitive against public transportation, it must be cost-competitive, easily accessible, and most importantly, must be able to transport the users quickly and comfortably.

In addition to commuting within the agglomeration, the range of 50 km allows for a competition with the regional trains. For instance, this range can cover the majority of the Randstad area including connection between Schiphol Airport and The Hague or Rotterdam. According to 2022 NS statistics[2], daily, 106 000 passengers use the route connecting Schiphol Airport with Rotterdam and The Hague. Furthermore, the trains operate only from a specified station, and following NS statistics it was observed that around 50% of passengers arrive to the station using municipal public transport. Compared to

[1] https://data.london.gov.uk/dataset/origin-and-destination-of-public-transport-journeys [Accessed on 16 May 2024]
[2] https://dashboards.nsjaarverslag.nl/reizigersgedrag/ [Accessed on 16 May 2024]

trains, KoriAir is closer to door-to-door service, which largely reduces transfer time.

To gain market power, KoriAir aims to provide better service than other possible means of transport. Compared to public transport and cars, the main goal is to reduce the travel time, while still maintaining an acceptable price. Additionally, helicopter rentals exist which provide fast transport within the city, however, due to the reduced availability following noise restrictions and high prices they are not widely accessible. By reducing the price and noise, KoriAir may increase the demand in this market segment.

To improve travel time, the requirement of cruise speed being 200 km/h was introduced. Furthermore, to remain competitive in terms of price, the requirement of operating cost being no higher than 1€/km/pax was defined. Using these values, the performance of KoriAir was compared for three types of missions: intracity, regional, and intercity. As a reference for intracity mission, a trip between two underground stations in Zone 1 in London (Notting Hill Gate - Liverpool Street) was used. Reference mission for regional travel is also defined within London, connecting two Elizabeth Line stations - West Drayton and Liverpool Street. The intercity mission was analyzed on the example of the journey between Schiphol Airport and Rotterdam Centraal station. Travel times were estimated using Google Maps as a reference for ground vehicles, specifications of Eurocopter EC130 [15].

Table 3.2: *Performance of KoriAir compared to other means of transport*

	Intra-city (8 km)			**Regional (30 km)**			**Inter-city (50 km)**		
Means of Transport	Time [min]	Price [€/pax]	Noise at 100 m distance [dBA]	Time [min]	Price [€/pax]	Noise at 100 m distance [dBA]	Time [min]	Price [€/pax]	Noise at 100 m distance [dBA]
Train/Subway	19	3.3[1]	62 [47]	40	6.5[1]	62 [47]	28	14.5/25[2]	62 [47]
Car	45	1.4[3]	53 [43]	80	5[3]	53 [43]	45	5.4[4]	53 [43]
Taxi	45	35[5]	53 [43]	80	80[5]	53 [43]	45	110[6]	53 [43]
Helicopter [15]	5	390[7]	89	10.5	390[7]	89	15.5	390[7]	89
Archer Aviation	5	28[9]	61[8]	10	105[9]	61[8]	16	165[9]	61[8]
KoriAir	5.5[10]	8[10]	77[10]	12[10]	30[10]	77[10]	18[10]	50[10]	77[10]

[1] https://tfl.gov.uk/fares/find-fares/tube-and-rail-fares [Accessed on 17 May 2024]
[2] 2nd/1st class prices based on: https://www.ns.nl/ [Accessed on 17 May 2024]
[3] Consumption of 9l/100km, 1.75€/l
[4] Consumption of 6l/100km, 1.75€/l
[5] https://tfl.gov.uk/modes/taxis-and-minicabs/taxi-fares [Accessed on 17 May 2024]
[6] https://www.taxicentrale-schiphol.nl/en/ [Accessed on 17 May 2024]
[7] https://www.batterseahelicopter.com/helicopter-hire-prices/ Assumed price independent of distance in the specified range. [Accessed on 17 May 2024]
[8] https://news.archer.com/how-loud-is-an-evtol [Accessed on 21 June 2024]
[9] https://www.autofutures.tv/topics/-the-sky-is-no-longer-the-limit—-archer-aviation-to-offer-6-minute-evtol-flights-to-the-airport—/s/57e93aea-44fc-44b8-9f88-84afca6c1412 [Accessed on 21 June 2024]
[10] Values are taken from analysis performed later in the report

As shown in Table 3.2, KoriAir can compete with all other means of transport. Travel time compared to all ground vehicles is largely reduced, especially for regional distance. Compared to helicopters, KoriAir offers similar performance in terms of time for a small fraction of the helicopter rental price. Additionally, KoriAir is assumed to operate as an on demand service for much lower price than a traditional taxi. Therefore, with lower price and travel time, it is estimated to capture the majority of taxi demand. Finally, when compared to the train the price is higher, however it comes with time savings and denser number of stations. Note that public transport in the cities is often partially funded by local authorities. If UAM service would also partially funded, then the final price for a customer would also decrease. KoriAir is not expected to target the entire demand of train commuters, it can still be an attractive option for people living far away from the station.

For large urban areas it is expected that the regional mission will dominate the utilization of KoriAir.

According to Demographia World Urban Areas annual report[3], the 100 largest urban areas in the world with a population larger than 500,000 cover between 1250 and 11350 km^2. Additionally, the availability of the public transport is lower outside city centers. KoriAir, with a cruise speed of 200 km/h and on-demand service will provide a fast and convenient substitution to the public transport outside of city centers. With a range of 50 km it can cover the majority of existing metropolitan areas for a one-way trip from the suburbs to the agglomeration center. Thus, commuters travelling from their home outside the city center to their workplace in the city center are the most important demographic KoriAir aims to provide service to.

3.3. Customer Analysis

Although at the moment there are no UAM vehicles in operation, there is an expected demand for them based on current uses of helicopters and private transportation vehicles. Possible use cases and sectors for UAM vehicles are listed below.

- Air taxi: Although this sector still requires much development because of the infrastructure needed, the market of air taxi services will create demand for the KoriAir vehicle, especially in cities with high traffic numbers. As mentioned in Section 3.2, there exists a large market potential in suburbs-center commuters.
- Air metro: For bigger UAM vehicles and only certain stations where UAM vehicles can park, it could be an option for crowded cities to add one more public transport option. However, this is currently unlikely as most prototypes of UAM vehicles only transport four passengers.
- Package delivery: UAM vehicles could be used to transport a package from the distribution centres just outside the city or to intra-urban locations.
- Military/Medical: UAM vehicles could be used to deliver time-sensitive medical goods or to transport patients.
- Tourism: UAM vehicles could be used for sightseeing around sites of interest.

3.4. SWOT Market Analysis

After defining the key market players, components and stakeholders, an overall analysis of the market for VTOLs can be done. This includes discussing the Strengths (S), Weaknesses (W), Opportunities (O) and Threats (T) of the vehicle and its integration in the global market. In Table 3.3 the results of the SWOT analysis are shown.

Table 3.3: *SWOT analysis table*

Strengths	**Weaknesses**
Currently, less traffic on skies than on roads Straight paths to destinations are faster than roads Small take-off distance Environmental benefits Diverse applications Low operational and maintenance costs	Current UAM are quite big and hard to park in cities UAM vehicles are not a proven product Infrastructure challenges with landing pads, air traffic management disturbing aerial wild life Safety concerns regarding possible catastrophic failures Operational barriers concerning integrating UAM in congested airspace
Opportunities	**Threats**
High demand in cities as traffic increases & possibility for innovation Market expansion No active UAM in use yet Open market Segment with high financial ceiling	Source of energy Aircraft regulation developments Noise levels depending on propulsion method Possible high price of operation If eVTOL low life expectancy of batteries High competition by older/more experienced competitors Social resistance

One simple takeaway from Table 3.3 are the relative points for strengths and opportunities versus weaknesses and threats. At the moment, UAM VTOL vehicles seem to have many hurdles and challenges, which is typical for emerging technology. The largest hurdles to overcome in design and

[3]http://www.demographia.com/db-worldua.pdf [Accessed on 22 May 2024]

market share are the large competition from more conventional competitors such as taxis and buses. Also, it is complicated for the final design to inspire the same confidence in terms of reliability and safety to the end users. This will be considered during the generation of the design option tree by considering both established aircraft designs and new ones. By studying both the current state of the market and conducting a SWOT analysis, a gap in the market for inexpensive and quiet flight was identified. The design should fill this gap, while achieving high speeds and vertical take-off and landing capability.

Strategic Product Issues

When launching a product, it is crucial to analyze market saturation. Although there are currently no active UAM (Urban Air Mobility) vehicles available in urban cities, there are a few promising prototypes in development. Figure 3.2 shows the segmentation of the VTOL vehicle market. It is preferable for the design to avoid the red area because it has relatively high cost without additional complexity. Instead, the design should focus on reducing the cost. Thus, the design should fall in or under the "4-seater UAM VTOL vehicle" of Figure 3.2. In this green area the costs are minimized, without adding unnecessary complexity which could introduce risks.

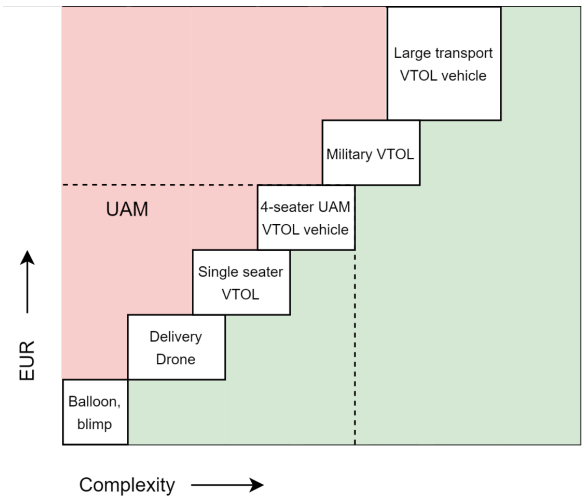

Figure 3.2: *Segmentation of the supply side of the VTOL vehicle market*

3.5. Conclusion

The current market situation indicates the need for UAM within cities, as increasing traffic congestion and the desire to travel faster power this emerging market. The analysis of the stakeholder needs, and current competition show a clear market gap. The vehicle, which can fly up to 50 km with a cruise speed of 200 km/h while maintaining the cost of 1€/km/pax, can fill this market gap. Its range covers the majority of the existing large urban areas. The possibility to travel 6 to 8 times faster than a traditional taxi for a third of the price will make the KoriAir project a successful one.

Analyzing the current UAM market also indicates the possible improvements to be made. These are reducing noise, ground footprint, and improving the infrastructure, will lead the design process of the final product. Moreover, the SWOT analysis will also be used to emphasize some parts of the design to maximize its utilization. SWOT indicates that the operating cost, noise, airspace use, and infrastructure optimization will be the area of special interest in the design. The design incorporating noise reduction and low cost will fill the existing market gap in UAM.

4

Functional Analysis

Functional analysis is important because it ensures that all operational requirements and constraints are systematically addressed. The functions that the design should perform dictate what the system is required to do. In this chapter, the functions of the vehicle system are visualized with a Functional Flow Diagram (FFD) in Section 4.1 and a Functional Breakdown Structure (FBS) in Section 4.2.

4.1. Functional Flow Diagram

To understand what is desired from the final design, an FFD was created, which displays all functions that should be performed in the mission in their logical flow. This flow was divided into three main functions: perform pre-operations, perform operation, and perform end-of-life operations. In the first function, the organization of the certification, infrastructure, and vehicle shipment logistics that must be performed by the system in order to operate the vehicle are displayed. Note that this function starts when the vehicle has already been designed and manufactured. The second function is the most detailed one, as it is most relevant in designing the UAM vehicle system and its subsystems. By analyzing the functions the vehicle needs to perform, it was ensured that no functional requirements are overlooked and every step in the operational mission can be performed. Note that there are also several checks introduced with "OR" and "AND" boxes. Finally, the third function highlights the operations at the end of the vehicle's life. Here, several steps related to part/material recycling and disposal can be taken. Note that at the bottom of every lower-level function the relevant (sub)system has been indicated.

4.2. Functional Breakdown Structure

In the FBS, the functions that have been generated in the FFD were arranged in a hierarchy. They are based on the same main functions of the FFD, and are then separated into the activities and operations which should be executed by the system. Note that this diagram does not include "OR" and "AND" boxes. This structured approach facilitated requirement generation, as well as the verification and validation of those requirements. The FFD is shown first in Section 4.2 and the FBS in Section 4.2.

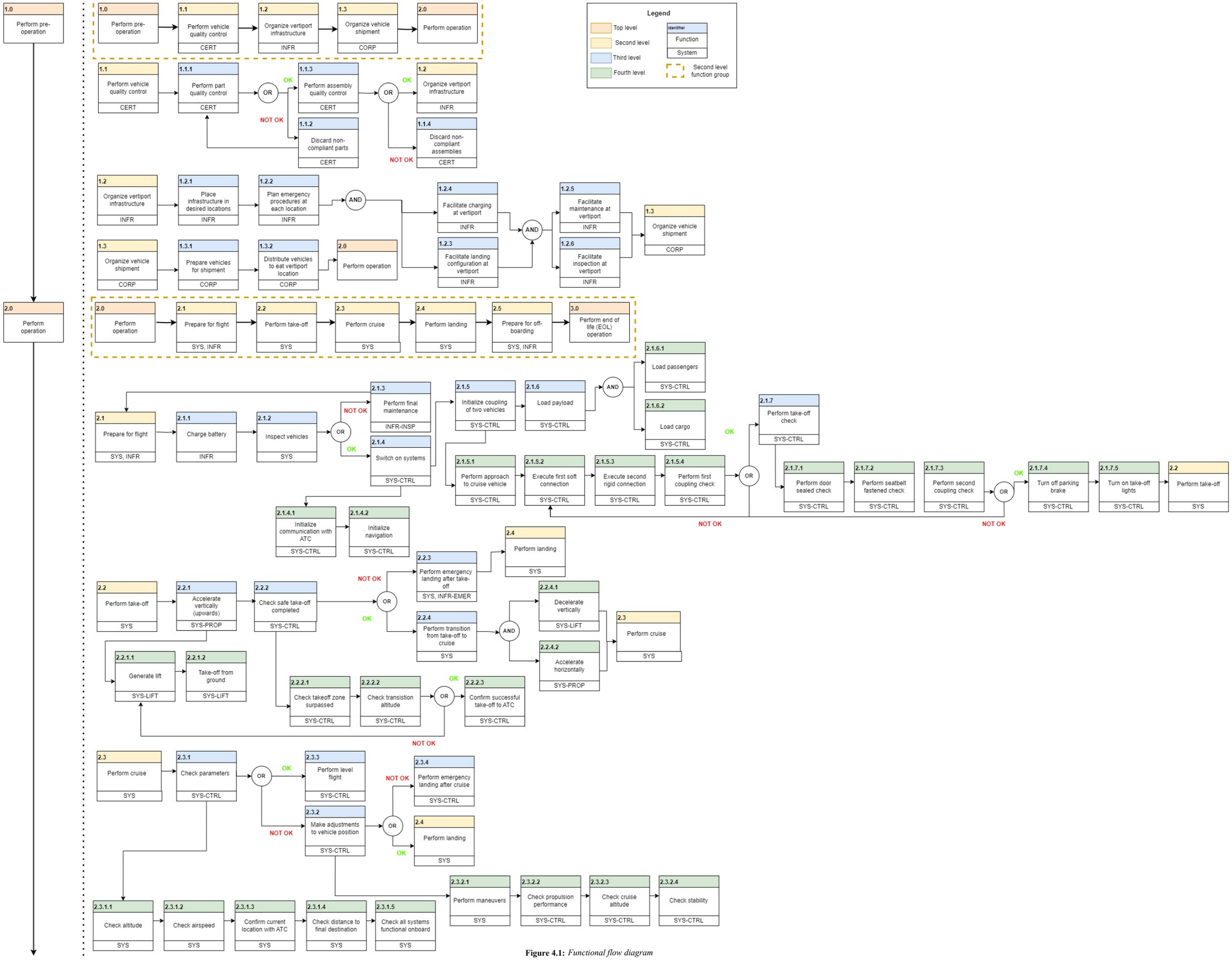

Figure 4.1: *Functional flow diagram*

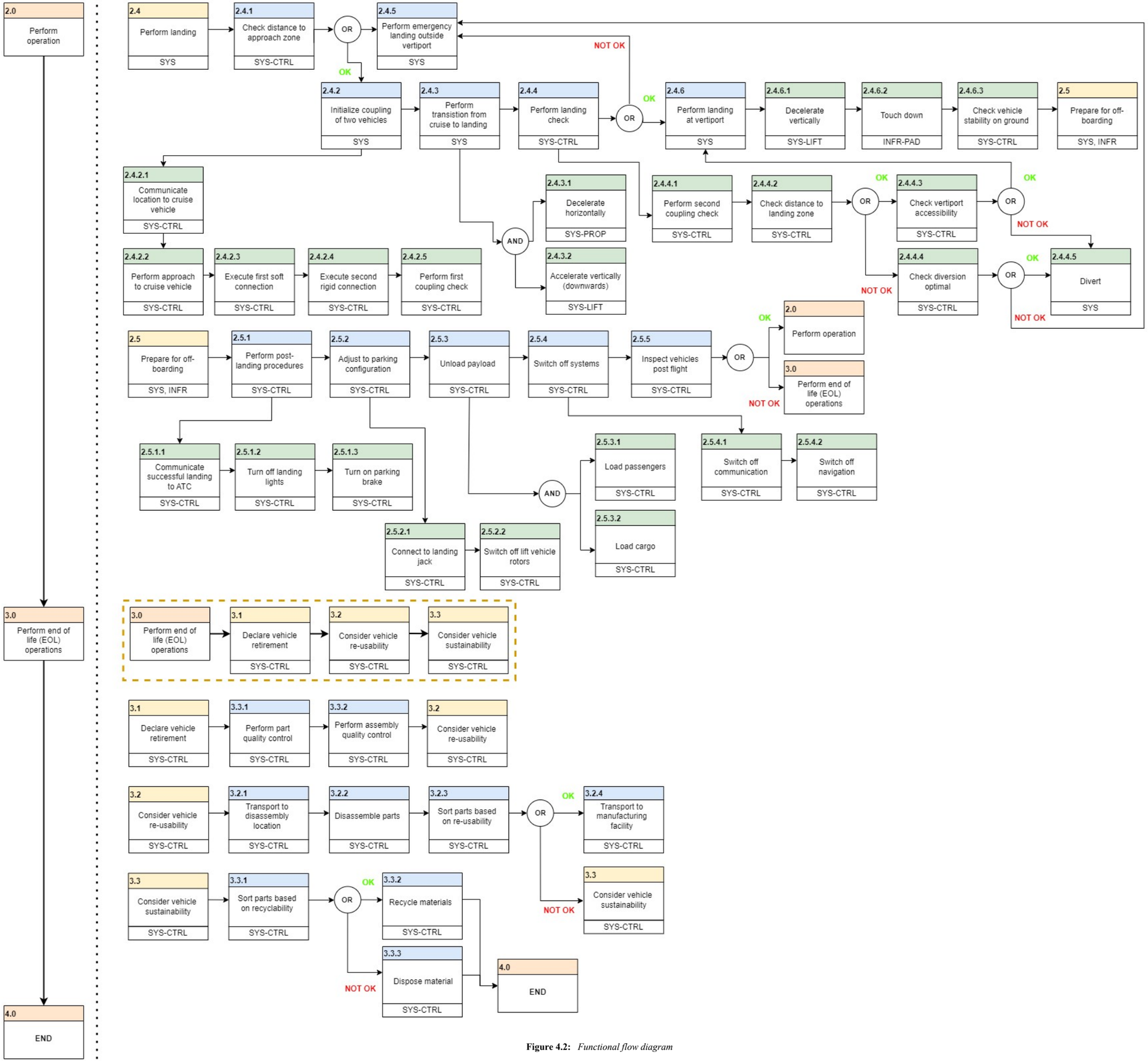

Figure 4.2: *Functional flow diagram*

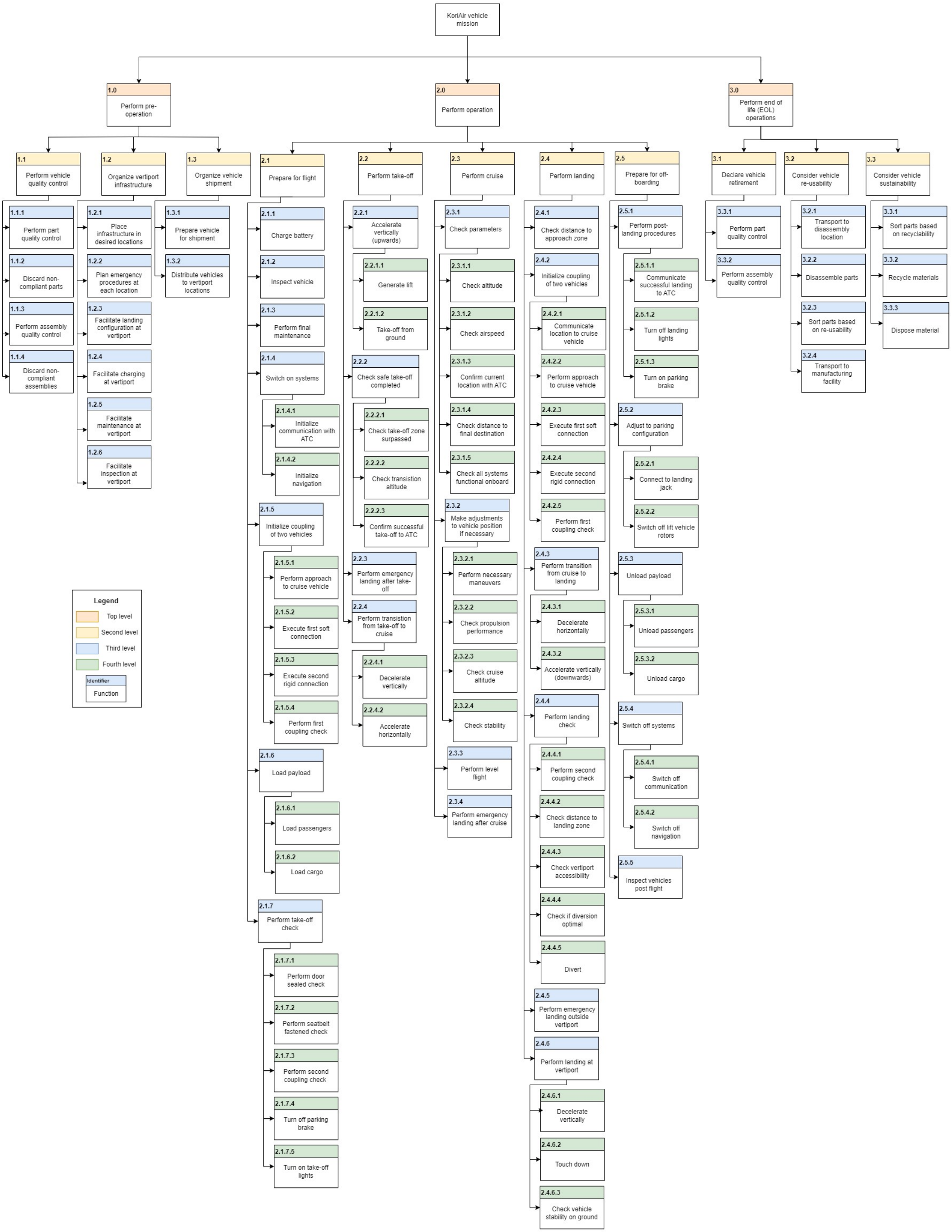

Figure 4.3: *Functional breakdown structure*

5

Cruise Vehicle Design

The cruise vehicle performs the largest segment of the flight. It is therefore designed optimal cruise efficiency. Firstly, the design of the subsystems that are most relevant and that need to be known in order to carry out a weight estimation will be described in Section 5.1. In this section, the objectives of the design process of a subsystem, as well as the assumptions made and the process of designing the subsystem, will be described. Then in Section 5.2, a Class II weight estimation, which depends on parameters that have been assumed or calculated in Section 5.1, will be carried out. Furthermore, the position of the center of gravity will be calculated. Designing an aircraft is an iterative process. In the iterations, the updated weight of the aircraft, as well as the center of gravity position, will be used to update the design of the subsystems, and subsequently estimate the weight and center of gravity position of the aircraft again. These iterations will continue until the updated weight of the aircraft is within a 1% margin of the last iteration.

5.1. Subsystem Design

An initial step in designing the cruise vehicle is setting up functions for the subsystems. The parameters of the subsystems that need to be defined to be able to carry out the weight estimation are found through these functions, which can be used to iterate over. The subsystems that will be discussed in this section are the wing, the fuselage, the empennage, the propulsion subsystem, and the landing gear.

5.1.1. Wing Design

The first subsystem to design is the wing. This crucial part of the cruise vehicle generates the lift which is required to keep the vehicle in the air. In this section, the sizing of the parameters that describe the wing planform will be described. More detailed information about the aerodynamic design and analysis of the wing is provided in Chapter 9.

Objectives and Requirements

In the process of designing the wing subsystem, the main requirement is that the wing is designed to be able to provide enough lift to carry the weight of the cruise vehicle. Furthermore, the span of the wing should be smaller than 12 meters due to the dimensions of the vertiport. There are more aerodynamic requirements, such as stall characteristics, however, most of them will be discussed in Chapter 9.

Assumptions

The assumptions made in the process of designing the wing are listed below.

- *The aspect ratio of the wing is 7.5.* This value is assumed to maximize glide performance, whilst fitting the wingspan into the vertiport.

Design Process

The design of the wing starts from the power and wing loading diagram in Section 8.1. From this diagram, a limiting wing loading $\frac{W}{S}$ of 829 N/m^2 due to landing constraints was selected as the starting point. This wing loading can be used to find the surface area of the wing S. Furthermore, the wing span can be calculated through the aspect ratio AR, which was assumed to be 7.5. The taper ratio was set to be 0.79 for the optimal lift distribution in cruise for the NACA 2418 airfoil that was

selected. More information on these aerodynamic considerations can be found in Chapter 9. From the taper ratio λ, the length of the root chord c_r, tip chord c_t, wingspan b, and mean aerodynamic chord $\bar{c}$ can be calculated. All of these calculations can be seen in Equation 5.1. High lift devices will be explained in Section 9.2.2.

$$S = \frac{W}{(W/S)} \qquad b = \sqrt{S\,AR} \qquad c_r = \frac{2S}{(1+\lambda)b} \qquad c_t = \lambda c_r \qquad \bar{c} = \frac{2}{3} c_r \frac{1+\lambda+\lambda^2}{1+\lambda} \tag{5.1}$$

The sweep of the quarter chord of the wing $\Lambda_{c/4}$ is zero degrees. This is due to the low Mach number during cruise [1]. Furthermore, the thickness-to-chord ratio is a result of the airfoil that has been selected. More information about high lift devices and control surfaces on the wing will be given in Chapter 9.

5.1.2. Fuselage Design

The fuselage of the cruise vehicle houses the main subsystems, like avionics. There should also be enough space to travel comfortably, while minimizing the drag to obtain optimal efficiency. This section will cover the requirements of the fuselage design.

Objectives and Requirements

The shape of the fuselage should be aerodynamic and strong enough to integrate the wings, empennage, propellers, landing gear, and the coupling mechanism.

Assumptions

Before the sizing of the fuselage can start, certain assumptions have to be made. These are mentioned below.

- *No aisle is present in the fuselage.* The amount of passengers is low enough to allow boarding via a door. Additionally, flights will take less than 30 minutes, so the passengers do not need to leave their seats during the flight.
- *Values for the seat width, armrest width, shoulder height, floor height, longitudinal length of a seated passenger, and clearance for head height are obtained from literature* [59]. These values are standard to use to design the interior cabin.
- *The dimensions and the weight of the luggage per passenger is 0.55 x 0.4 x 0.2 m^3 and 12 kg.* The size corresponds to a standard-seized carry-on bag. There will be no specific designed compartment inside the cabin for the passengers to store their luggage. Their luggage will be placed underneath the seats or on the passenger's lap during flight.
- *The fuselage is not pressurized.* Given the low cruise altitude, of approximately 1200 m, it was established that pressurizing the cabin is not necessary. This means that a non-circular cross-section can be used, as stress distributions due to pressurization do not play a significant role. This eases manufacturing of the fuselage and provides flexibility in designing the fuselage.

Design Process

The design of the cabin of the fuselage starts from the number of passengers. It was decided to have two rows of two seats abreast. With Equation 5.2 [53], the length of the cabin section can be computed.

$$l_{cabin} = \frac{n_{pax}}{n_{sa}} k_{cabin} \tag{5.2}$$

In this equation, n_{pax} and n_{sa} are the number of passengers and number of seats abreast, and k_{cabin} is a constant which determines the length of a row, which equals 1.08 for single aisle aircraft. The width of the cabin consists of two seats with a width of 45 centimeters, three armrests of 5 centimeters, and 2 centimeters clearance between the outer armrests and the wall to ensure enough space for structural elements, cables, and other elements such as interior lining [1]. This led to an inner cabin width of 1.09 meters.

The cabin height consists of the height of the headroom of the cabin, which is 1.30 meters, and the floor thickness, which is 15 centimeters. This leads to a cabin height of 1.45 meters. For the outer

dimensions of the cabin, 4 centimeters of wall are added to the width and height of the cabin, leading to dimensions of 1.13 by 1.49 meters. The largest dimension of the cabin, which is the cabin length, is needed to calculate the total length of the fuselage, as shown in Equation 5.3 [53].

$$l_{fus} = h_{cabin} \cdot \phi_f \tag{5.3}$$

Here, ϕ_f is the fineness ratio and indicates the ratio between the fuselage length and its maximum diameter. For a fixed cross-sectional area, a fineness ratio of 3 is optimal [24]. Most subsonic aircraft, however, have a fineness ratio between 6 and 8. To increase the tail arm and make the tail cone longer to allow for a more aerodynamic shape, a fineness ratio of 5 was selected. The length of the tail cone can also be determined with a similar formula as for the length of the fuselage. This is given in Equation 5.4 [54].

$$l_{tail\ cone} = D_{max} \cdot \lambda_s \tag{5.4}$$

Here, λ_s is the slenderness ratio, which indicates the taper of the tail cone. A slenderness ratio that is too high will lead to steep taper of the tail cone and earlier flow separation. A slenderness ratio of 2.5 was selected. Finally, the only length missing to fully determine the distribution of section of the fuselage is the length of the nose cone. Since the aircraft will have no pilots, no extra cockpit will be taken into account. The systems of the aircraft will be mainly hidden in the internal structure of the aircraft, and will not be accessible for passengers. This will still take up some space, also needed for the aerodynamic shape of the fuselage, but it will not be as significant as the room needed for one or two pilots and their required instrumentation. Thus, the length of the nose cone can be calculated with Equation 5.5.

$$l_{nose\ cone} = l_{fus} - l_{tail\ cone} - l_{cabin} \tag{5.5}$$

5.1.3. Empennage

Based on the planform of the wing, as well as the center of gravity excursion, the empennage of the cruise vehicle can be designed.

Objectives and Requirements

The function of the empennage is to provide stability and control for the aircraft. The horizontal tail needs to provide a moment around the center of gravity of the aircraft to counteract the moment caused by the lift of the wing and provide longitudinal stability. This entails generating lift at a certain distance from the center of gravity. Increasing this tail arm leads to less lift needed for the same moment, leading to a smaller tail surface, and thus lower weight. The vertical tail, on the other hand, needs to provide lateral stability for the aircraft. The objective in the design of the empennage is to provide enough stability whilst minimizing the weight of the tail.

Assumptions

The assumptions made in the process of designing the empennage are listed below.

- *An H-tail configuration is used.* To create space for the coupling to take place, two vertical tailplanes are attached to the tip chord of the horizontal tail. These vertical tailplanes were sized similarly to a conventional configuration, as the H-tail configuration would not have a significant influence on the performance of the empennage in regard to stability.

Design Process

For the design of the tailplanes, a tail volume coefficient needs to be selected. With the tail volume coefficients, the area of the tailplanes can be found through parameters that describe the wing's tailplane. The formula for the horizontal and vertical tail volume coefficients can be seen in Equation 5.6 [1].

$$C_H = \frac{S_H l_H}{S_w \bar{c}} \qquad C_V = \frac{S_V l_V}{S_w b} \tag{5.6}$$

Here, l_H and l_V are the distances between the quarter chord of the mean aerodynamic chord of the wing and the quarter chord of the horizontal and vertical tail, respectively. S_w, $\bar{c}$ and b are the surface

area of the wing, the mean aerodynamic chord, and the wingspan. These tail volume coefficients were taken from reference data of similar aircraft. This led to values of 0.5 and 0.03 for the horizontal and vertical tail volume coefficient, respectively [45, 53]. Winglets have been neglected when selecting values for the tail volume coefficients. When the wing parameters, as well as the tail lengths, are filled in Equation 5.6, the area of the horizontal and vertical tail can be calculated. Next, the sweep angle, taper ratio and aspect ratio for the tailplanes were determined to be 0° at quarter chord, 0.45 and 4 for the horizontal tail, and 40° at the leading edge, 0.75 and 1.5 for the vertical tailplanes. These values come from reference aircraft [1]. The surface area of the vertical tailplane found with Equation 5.6 needs to be halved to account for the two vertical tailplanes of the H-tail configuration. From these parameters, all other parameters that describe the planform of the horizontal and vertical tail can be calculated similarly to the approach in Section 5.1.1.

5.1.4. Propulsion

The propulsion subsystem encompasses both the engine and the propellers. The subsystem takes, as an input, both the thrust required by the aircraft and the desired velocity during take-off or landing and in cruise. The model used to size the propeller was used for both the lifting vehicle and the cruise vehicle, with only the inputs changing. In this section, assumptions in the process of setting up the model, as well as the model itself, will be described.

Objectives and Requirements

The propulsion system of the cruise vehicle should be able to provide the thrust for horizontal speed. The power and thrust delivered by the engines and propeller should be sufficient to perform all phases of the flight regime. The goal in the process of designing this subsystem is maximizing efficiency, whilst minimizing weight and noise.

Assumptions

The assumptions used during the design on the propulsion subsystem are listed below.

- *The hub of the propeller ends at 15% of the blade radius.* In the blade region until 20% very low thrust is generated. A hub radius of 15% will thus have a negligible effect on the thrust generated, whilst increasing the strength of the propeller [12].
- *The cruise vehicle has four wing-mounted engines.* Due to the nature of the coupling, in which a hook will attach to the cruise vehicle, it was determined that the cruise vehicle should have four wing-mounted rotors. By allocating the cruise vehicle with four rotors, they can be sized smaller due to the decreased thrust required by each rotor. Additionally, four smaller propellers will allow for more clearance during coupling and add redundancy in the case one of them becomes inoperative.
- *The material used for the propeller is carbon fiber.* Most propellers nowadays are made of carbon fiber, due to its relatively low density and strong load-bearing qualities.
- *The airfoil NACA 2440 was selected for the blades of the propeller.* This airfoil was deemed suitable for the propeller due to its thickness [14].
- *The Mach number at the tip of the blade for optimal conditions is set at 0.4.* At this Mach number at the tip, the total battery to motor efficiency is 93%, whilst additional gearbox losses bring the total system efficiency to about 90% [53].
- *The blade chord length is constant and 0.10 meters.* This value allows for enough thrust whilst minimizing the weight of the propellers.
- *The coefficients of lift and drag are taken as a constant 1.4 and 0.036 respectively across the blade.* It was calculated that the Reynolds number for the airflow was consistently over 1 million across the blade. Therefore, the lift and drag coefficients of the chosen airfoil could be obtained from Javafoil, and they could be assumed to be constant along the blade.

Design Process

The design of the propulsion subsystem aims to size the main parameters of the propellers, namely: the number of blades, the number of rotors and the rotor radius. Once the propeller has been sized, an appropriate engine can be chosen to power the propellers. It was decided that four engines

would be better than two for reduced noise emissions. The choice of four engines leaded to smaller engines, which produce less noise. However, these engines also had to have relatively low rotational speeds. This is why the choice was made to use the Geiger Engineering HPD40D. It provides the necessary power at an RPM of 2600, which was the lowest RPM compared to the other options. The inputs needed to design these parameters are the power required and the desired velocity of the aircraft. By developing the code to take these as inputs, one model can be used for both the lifting and cruise vehicle. To design the propeller, the performance indicators used are propeller efficiency (in cruise), noise generated by the propeller, propeller mass and the thrust and torque coefficients. The combination of number of blades, number of rotors, and propeller radius which yield the best combination of efficiency, noise, and mass will be chosen for the design.

To calculate the efficiency and thrust generated from the propellers, blade element theory was implemented[1]. This is a simplified method in which the propeller is divided into a number of sections across the radius of the blade, and for each section a set of equations can be solved by iteration. The results of each section are summed across the blade to predict the performance of the complete propeller. The blade is split into a specified number of sections starting from the hub radius, which is not lifting and omitted from the analysis. The hub radius is assumed to be 15% of the total propeller radius.

The forces produced by the propeller, as well as the angles and flow velocities, are shown in Figure 5.1. θ is the pitch angle of the propeller blades and α is the angle of attack of the blade with respect to the airflow. Furthermore, the lift and drag produced by the blade can be represented as a component along the axis of rotation of the propeller, the thrust T, and a component perpendicular to this axis, the torque Q.

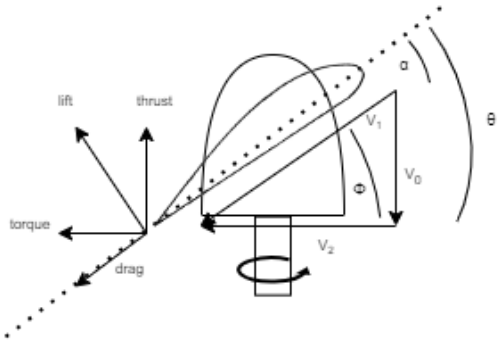

Figure 5.1: *Simplified representation of a propeller and the relevant angles, forces, and velocities*

In blade element theory a system of equations has to be solved in order to find the thrust and torque of a particular blade section. The system of equations to be solved can be seen in Equation 5.7 and 5.8.

$$\Delta T = \frac{1}{2}\rho V_1^2 c(C_L \cos\phi - C_D \sin\phi)B \cdot dr \qquad \Delta Q = \frac{1}{2}\rho V_1^2 c(C_D \cos\phi + C_L \sin\phi)Br \cdot dr \tag{5.7}$$

$$\Delta T = 4\pi\rho V_\infty^2 (1+a)a \cdot dr \qquad \Delta Q = 4\pi r^3 V_\infty (1+a)b\Omega \cdot dr \tag{5.8}$$

In these equations, c is the chord of the blade, which is assumed to be constant and 10 cm, ϕ is the difference between the angle of attack α and the pitch angle of the blade θ, B is the number of blades, and r is the radius of the propeller. Additionally, a and b are the axial and angular inflow factors. C_L and C_D are the lift and drag coefficients of the blade, which are dependent on the airfoil chosen. For these propellers, a NACA 2440 airfoil was selected, which came with a lift coefficient of 1.40 and a drag coefficient of 0.036 [14]. The velocities in this system have been drawn in Figure 5.1. Here, V_1 is the section local flow velocity vector, and V_0 and V_2 are its axial and angular local flow velocity

[1]https://www.aerodynamics4students.com/propulsion/blade-element-propeller-theory.php [Accessed on 5 June 2024]

components. These velocities can be found through Equation 5.9. Here, V_∞ is the free stream velocity and Ω is the rotation speed of the propeller in radians per second.

$$V_1 = \sqrt{V_0^2 + V_2^2} \qquad \alpha = \theta - \arctan\frac{V_0}{V_2} \qquad V_0 = V_\infty(1+a) \qquad V_2 = \Omega r(1-b) \tag{5.9}$$

With these equations, the system of equations can be solved for ΔT, ΔQ, a and b, at every section of the blade. An initial guess is made for the axial and angular inflow factors a and b. Then, the equations are iterated until the inflow factor falls within 0.1% of the previous iteration. When the factors have converged, the total thrust and torque can be found by summing ΔT and ΔQ for every section. The total thrust and torque can be converted to their dimensionless coefficients by Equation 5.10. When the thrust and torque coefficients are known, the efficiency of the propeller can be calculated with Equation 5.10.

$$C_T = \frac{T}{\rho n^2 D^4} \qquad C_Q = \frac{Q}{\rho n^2 D^5} \qquad \eta_{prop} = \frac{JC_T}{2\pi C_Q} \qquad J = \frac{V_\infty}{nD} \tag{5.10}$$

In these equations, n is the rotational speed of the propeller in revolutions per seconds, D is the diameter of the blade, and J is the advance ratio. Now, the efficiency and the total thrust provided by a propeller is known. With the propeller efficiency, thrust produced, the mass of the propeller, as well as a noise estimate obtained from Chapter 12, an optimal combination of the number of blades and the radius of the propeller can be found for all of these parameters.

As mentioned above, an important requirement for the propulsion subsystem is that it needs to provide enough thrust in the critical part of the flight regime, which is during the horizontal in-air take-off phase, as the drag from both the cruise and lifting vehicle need to be counteracted. The thrust can be calculated from the equations of motion during horizontal take-off, as shown in Equation 5.11

$$T = D + (m_{LV} + m_{CV})(g \sin\alpha_{h,TO} + a) \tag{5.11}$$

In this equation, m_{LV} and m_{CV} are the mass of the lifting and cruise vehicle, and $\alpha_{h,TO}$ and a are the angle of attack at take-off and horizontal acceleration. The drag D depends on the maximum velocity in this flight regime, which is 1.15 times the stall speed, is calculated with estimated drag coefficients and areas. This drag estimation can be found in Chapter 9. The thrust required per rotor is a quarter of the outcome of Equation 5.11.

5.1.5. Landing Gear

The landing gear is needed to support the cruise vehicle's weight during ground procedures and take-off and landing operations. Under normal conditions the aircraft will make a vertical landing supported by the lifting vehicle, however, the cruise vehicle should be able to perform a stand-alone conventional horizontal landing, in case of an emergency or malfunction of the coupling system.

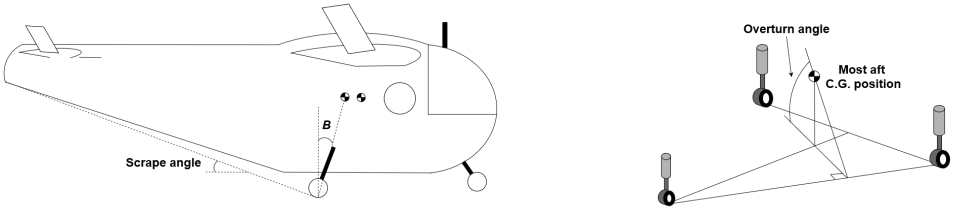

Figure 5.2: *Angles of interest during landing of the cruise vehicle*

Objective and Requirements
The function of the landing gear is to support the weight of the aircraft when parked, allow the aircraft to move during ground operations, and make the aircraft capable of performing emergency horizontal landings. The landing gear should absorb landing shocks and taxiing shocks, provide braking capability and not damage the surface it lands on.

Assumptions
- *The landing surface can be of Type 1, Type 2 and Type 3 [1].* If the aircraft suffers malfunction in an urban environment, it should be able to land on either paved roads, grass fields and traditional runaways.
- *The landing is not retractable.* To avoid complexity and an increase in weight of the aircraft, the landing gear will be fixed.

Design Process
The landing gear can be designed based on a number of constraints. To land, the aircraft will minimize its velocity by flying near its maximum lift coefficient, at 1.15 times the stall speed, which was calculated to occur at an angle of attack of 11 degrees in Chapter 9. Following from this requirement, minimum requirements for the scrape angle and B angle, illustrated in Figure 5.2, of 11 degrees were imposed. Combining these two restrictions yields a feasible region for the height of the main landing gear and its position along the length of the fuselage. From this feasible set, the most forward main landing gear position is chosen. Next, using the calculated most forward and most aft cg, a feasible set for the location of the nose landing gear is chosen such that the nose landing gear supports between 8% and 15% of the weight of the aircraft. The lower bound was imposed so that the landing gear is able to both steer the aircraft, while the upper constraint was imposed so that the aircraft can break effectively, without the wheels locking. To allow the aircraft to perform sharp turns and maintain stability during ground operations, the overturn angle was constrained to be lower than 55°. Using this requirement, a feasible region for the track width of the main landing gear was created, and the smallest track width was chosen [1].

5.2. Class II Weight Estimation
In order to obtain a more detailed estimation for the mass of the cruise vehicle, a class II weight estimation has to be performed. This consists of estimating the individual component weights of the aircraft based on parameters that have been calculated in the Section 5.1 or assumed based on literature or reference aircraft. This weight estimation was performed using the method outlined in Raymer's book [53]. Note that the inputs for all the formulas below are in imperial units, such as feet, inches, and pounds. Refer to Raymer's book for details about the units of every formula. Finally, the position of the center of gravity of the also needs to be calculated. The outcome of the weight estimation and center of gravity excursion will be used to update the design of the subsystems.

5.2.1. Wing Weight
To estimate the weight of the wing of the cruise vehicle, Equation 5.12 can be used.

$$W_{wing} = 0.036 S^{0.758} W_{fw}^{0.0035} \left(\frac{AR}{\cos^2 \Lambda}\right)^{0.6} q^{0.006} \lambda^{0.04} \left(\frac{100 t/c}{\cos \Lambda}\right)^{-0.3} (N_z W_{dg})^{0.49} \tag{5.12}$$

As the aircraft will be electric, the wing fuel weight W_{fw} will be zero. According to Raymer [53], this parameter can therefore be left out. Furthermore, the wing area S, aspect ratio AR, sweep angle of the quarter chord Λ, dynamic pressure in cruise q, taper ratio λ, and the thickness-to-chord ratio t/c are results of the wing design performed in Section 5.1.1. Furthermore, the design gross weight, which is the MTOM, W_{dg} needs to be input as well. This parameter will have an initial value of 1092 kilograms and will be updated later through the Class II weight estimation. Finally, the ultimate load factor N_z needs to be defined. Therefore, two new requirements were created. The chosen value for the load factor requirement stems from the CS-23 regulations for commuter aircraft [17].

Table 5.1: *Additional requirements for wing design*

Identifier	Requirement
REQ-STK-11-MIS-38	The UAM vehicle shall be able to sustain a maximum load factor of 2.5 during all normal flight maneuvers.
REQ-STK-11-MIS-39	The UAM vehicle shall be able to withstand an ultimate load factor N_z of 3.75.

5.2.2. Fuselage Weight

To estimate the weight of the fuselage, Equation 5.13 can be used.

$$W_{fuselage} = 0.052 S_f^{1.086} (N_z W_{dg})^{0.177} l_V^{-0.051} (L/D)^{-0.072} q^{0.241} + W_{press} \tag{5.13}$$

$$S_f = 0.65(2 l_{fus} w_{fus} + 2 l_{fus} h_{fus}) \tag{5.14}$$

The exposed area of the fuselage S_f is estimated through sizing the fuselage as a rectangular box with the height (h_{fus}), width (w_{fus}), and length (l_{fus}). This is multiplied by 0.65, to account for the reduction in fuselage area due to the tail and nose cone. Furthermore, l_V is the length between the quarter chord point of the mean aerodynamic chord of the wing and the quarter chord point of the vertical tail, as has been described in Section 5.1.3. Furthermore, L/D is the lift-to-drag ratio that is assumed to be 15 based on reference aircraft [38]. W_{press} is the weight penalty due to pressurization. As the cruise vehicle flies at an altitude of approximately 1200 meters, the cabin does not need to be pressurized, so this weight penalty goes to zero. Finally, the dynamic pressure at cruise q, the ultimate load factor N_z, and the design gross weight W_{dg} have already been described in Section 5.2.1.

5.2.3. Empennage Weight

The weight of the horizontal and vertical tail can be estimated using Equation 5.15 and Equation 5.16 respectively.

$$W_{ht} = 0.016 (N_z W_{dg})^{0.414} q^{0.168} S_{ht}^{0.896} \left(\frac{100 t/c}{\cos \Lambda} \right)^{-0.12} \left(\frac{AR}{\cos^2 \Lambda_{ht}} \right)^{0.043} \lambda_{ht}^{-0.02} \tag{5.15}$$

$$W_{vt} = 2 \cdot 0.073 \left(1 + 0.2 \frac{H_t}{H_v} \right) (N_z W_{dg})^{0.376} q^{0.122} \left(\frac{S_{vt}}{2} \right)^{0.873} \left(\frac{100 t/c}{\cos \Lambda_{vt}} \right)^{-0.49} \left(\frac{AR}{\cos^2 \Lambda_{vt}} \right)^{0.357} \lambda_{vt}^{0.039} \tag{5.16}$$

Firstly, the ultimate load factor N_z, the design gross weight W_{dg}, the dynamic pressure q, the thickness-to-chord ratio of the wing t/c, the sweep angle at quarter chord of the wing Λ, and the aspect ratio of the wing AR have all been described in Section 5.1.1 and Section 5.2.1. Furthermore, the area of the horizontal and vertical tail S_{ht} and S_{vt}, the sweep of the horizontal and vertical tail Λ_{ht} and Λ_{vt}, and the taper ratio of the horizontal and vertical tail λ_{ht} and λ_{vt} have been described in Section 5.1.3. Additionally, the ratio of the height of the horizontal tail above the fuselage to the height of the vertical tail above the fuselage $\frac{H_t}{H_v}$ could be reduced to zero, as the H-tail configuration is used [53]. Finally, the vertical tail weight formula was adjusted to take into account the two separate vertical tailplanes.

5.2.4. Landing Gear Weight

The following equations were used to estimate the weight of the main and nose landing gear.

$$W_{mg} = 0.095 (N_z W_l)^{0.768} (L_m/12)^{0.409} \tag{5.17}$$

$$W_{ng} = 0.125 (N_z W_l)^{0.566} (L_n/12)^{0.845} \tag{5.18}$$

In these equations, W_l is the design gross weight at landing, which is equal to the MTOW of the cruise vehicle and the lifting vehicle combined. Furthermore, L_m and L_n are the lengths of the landing gear struts, which have been defined in Section 5.1.5, in inches. Finally, N_z is the ultimate landing load factor, which will be specified through creating two additional requirements. The same load factor as for the weight of the wing was chosen.

Table 5.2: *Additional requirements for landing gear design*

Identifier	Requirement
REQ-STK-11-MIS-38-SYS-TEC-8.5.1	The UAM vehicle shall be able to sustain a maximum load factor of 2.5 during all landing maneuvers.
REQ-STK-11-MIS-39-SYS-TEC-8.5.2	The UAM vehicle shall be able to withstand an ultimate load factor of 3.75 during landing.

5.2.5. Battery Weight

A crucial component of the total weight of the aircraft is the weight of the battery. The battery needs to provide the energy used to perform the flight. The mass of the battery can be calculated through Equation 5.19.

$$m_b = 1.5\frac{E_{used}}{E_{sb}\eta_b} \tag{5.19}$$

In this equation, E_{sb} is the specific battery energy, which is assumed to be 235 Wh/kg [42], the same specific energy as the Joby S4 prototype battery, and η_b is the efficiency of the battery, which is assumed to be 0.9 [53]. A safety margin of 1.5 is added to allow for battery failure. Furthermore, the energy used by the cruise vehicle E_{used} can be calculated through Equation 5.20.

$$E_{used} = P_{used}t = P_{TO}t_{TO} + P_{climb}t_{climb} + P_{cruise}t_{cruise} + P_{loiter}t_{loiter} \tag{5.20}$$

$$P_{TO} = (m_{CV} + m_{LV})a_{h,TO}V_{h,max} \quad P_{climb} = \frac{m_{CV}\cdot g}{\eta_p}\left(ROC + \frac{V_{climb}}{L/D}\right) \quad P_{cruise} = P_{loiter} = D_{cruise}V_{cruise} \tag{5.21}$$

The energy used is divided into the phases of the flight for which the cruise vehicle needs to provide power: horizontal take-off, climb to cruise altitude, cruise, and eventual loitering. In these equations, m_{CV} and m_{LV} are the mass of the cruise vehicle and lifting vehicle respectively. Additionally, η_p is the efficiency of the propeller. There are also a number of parameters which depend on the flight profile, which will be described in more detail in Section 8.2.10. The times in Equation 5.20 are also defined in this section. These parameters are $a_{h,TO}$, $V_{h,max}$, ROC, V_{climb}, and V_{cruise}. The lift-to-drag ratio L/D and the drag in cruise D_{cruise} have been described in Chapter 9. Finally, the power used in cruise is equal to the power used for loitering.

5.2.6. Miscellaneous Weights

The masses of subsystems were estimated through formulas, without the need for detailed sizing, as described in this section. Firstly, Equation 5.22 can be used to estimate the weight of the entire propulsion system. This requires a number of engines, as well as a weight of the uninstalled engine. The aircraft has four wing-mounted engines. As a starting point for the weight of the uninstalled engine, it was assumed that HPD40D motors were installed, which are from the company Geiger engineering[2], and have a weight of 12 kg.

$$W_{en,installed} = 2.575W_{en}^{0.922}N_{en} \tag{5.22}$$

In this equation, W_{en} and N_{en} are the weight and number of engines, respectively. Next, the weight of the flight controls can be estimated using Equation 5.23, which only depends on previously obtained parameters.

$$W_{fc} = 0.053l_{fus}^{1.536}b^{0.371}(N_zW_{dg}\cdot 10^{-4})^{0.8} \tag{5.23}$$

[2]https://www.geigerengineering.de/en/avionics/products [Accessed on 28-5-2024]

The weight of the hydraulics in the aircraft will be estimated using Equation 5.24. This requires the design Mach number in cruise, as well as a value for K_h, which is a parameter based on the design Mach number. This can be taken to be 0.05 for low subsonic general aviation aircraft, according to Raymer [53].

$$W_{hydraulics} = K_h W_{dg}^{0.8} M^{0.5} \tag{5.24}$$

For the weight estimation of the avionics, a value for the weight of the uninstalled avionics W_{uav} needs to be estimated. This was taken to be approximately 2% of the operative empty mass of the aircraft. The weight can then be calculated using Equation 5.25 [53].

$$W_{avionics} = 2.117 W_{uav}^{0.933} \tag{5.25}$$

Equation 5.26 can be used to find an estimation for the weight of the electrical components of the vehicle. As the aircraft does not contain a fuel system, the weight of the electronics only depends on the weight of the avionics, described above.

$$W_{electrical} = 12.57(W_{fuel\ system} + W_{avionics})^{0.51} \tag{5.26}$$

The weight of the air conditioning, anti-ice and furnishings can then be estimated using Equation 5.27, with some of the previously obtained parameters. Finally, N_p is the amount of people on-board, which is just the four passengers.

$$W_{air\ conditioning\ and\ anti-ice} = 0.265 W_{dg}^{0.52} N_p^{0.68} W_{avionics}^{0.17} M^{0.08} \tag{5.27}$$

$$W_{furnishings} = 0.0582 W_{dg} - 65 \tag{5.28}$$

Finally, the weight of the coupling mechanism has been estimated as 150 kilograms. This takes into account the different components of the coupling mechanism that are attached to the cruise vehicle, as well as the weight due to structural reinforcements to include the coupling mechanism. More details on how this weight was estimated can be found in Chapter 7.

5.2.7. Center of Gravity Excursion

For more analysis of the control and stability of the aircraft, the center of gravity of the aircraft needs to be obtained. Additionally, the empennage and landing gear design depends on the position of the center of gravity. Therefore, the excursion of the position of the center of gravity is included in the iterations.

The MTOW of the aircraft consists of three components: the operating empty weight (OEW), the battery, and the payload. The first step in finding the center of gravity is exploring the center of gravity of the OEW. This component of the weight of the aircraft can be divided into two smaller components: the wing group (WCG), of which the center of gravity position is related to the distance from the leading edge of the mean aerodynamic chord of the wing, and the fuselage group (FCG), of which the center of gravity position is related to the fuselage itself. The wing group consists of the wing and the engines, as they are wing-mounted. The fuselage group consists of the fuselage, the empennage, and fixed equipment. The fixed equipment consists of flight controls, hydraulics, avionics, electrical, air conditioning and anti-ice, and furnishings. The landing gear has been neglected in the calculation of the center of gravity, as its influence is insignificant [1]. Note that in the weight of the engines, the propellers, fairings, and nacelles are also included.

Here $\left(\frac{x}{c}\right)$ and $\left(\frac{x}{l_{fus}}\right)$ represent the distance from the wing position or nose of the aircraft as fractions of the wing's chord length and the fuselage length, respectively. To find the center of gravity of the OEW, the center of gravity of the wing group with respect to the fuselage needs to be found. This position can be found through the leading edge of the mean aerodynamic chord, which is calculated through Equation 5.29.

$$X_{LEMAC} = X_{FCG} + \bar{c}\left[\left(\frac{x}{c}\right)_{WCG}\frac{M_W}{M_F} - \left(\frac{x}{c}\right)_{OEW}\left(1 + \frac{M_W}{M_F}\right)\right] \tag{5.29}$$

Here, M_W and M_F are the mass fractions of the wing group and fuselage group with respect to the MTOW. Furthermore, the center of gravity position of the OEW with respect to the chord of the wing $\left(\frac{x}{c}\right)_{OEW}$ is assumed to be 0.25, based on reference aircraft [1]. Subsequently, the center of gravity of the OEW can be found with Equation 5.30.

$$X_{CG,OEW} = \frac{\left(X_{LEMAC} + \left(\frac{x}{c}\right)_{WCG}\right) W_{WCG} + X_{FCG} W_{FCG}}{W_{WCG} + W_{FCG}} \tag{5.30}$$

With the center of gravity position of the OEW calculated, now the center of gravity position of the MTOW can be calculated by adding the battery and payload to the OEW (Equation 5.31). The center of gravity of the payload $X_{payload}$ is assumed to be in the middle of the cabin, and the center of gravity of the battery $X_{battery}$ is assumed to be 1 meter behind the cabin (for batteries in the tail cone). The mass and center of gravity position of the OEW and the payload, as well as the OEW and the battery can be calculated by leaving the battery or payload respectively out of Equation 5.31.

$$W_{MTOW} = W_{OEW} + W_{batt} + W_{payload} \quad X_{CG,MTOW} = \frac{X_{CG,OEW} W_{OEW} + X_{batt} W_{batt} + X_{payload} W_{payload}}{W_{MTOW}} \tag{5.31}$$

The four center of gravity positions as well as their weights, namely of solely the OEW, the OEW and the battery, the OEW and the payload, and the OEW, battery and payload combined (MTOW), can be graphically shown in a loading diagram. This loading diagram will be shown later in this chapter with the final results. From the four center of gravity positions, the most aft and forward center of gravity positions can be selected and used in calculations for the empennage and landing gear.

5.3. Final Design Specifications

After several iterations, the MTOW of the cruise vehicle and the parameters describing the different subsystems, that influence the weight of the vehicle, converged. In the following subsections, these parameters will be summarized.

5.3.1. Wing Design

The wing subsection was designed as described in Section 5.1.1. The parameters in Table 5.3 describe the design of the wing of the cruise vehicle.

Table 5.3: *Parameters describing the design of the wing*

Symbols	Parameters	Values	Units
AR	Aspect ratio	7.5	-
S	Wing surface area	18.9	m^2
b	Wingspan	11.9	m
$\Lambda_{c/4}$	Quarter chord sweep angle	0	°
λ	Taper ratio	0.79	-
c_r	Root chord length	1.77	m
c_t	Tip chord length	1.40	m
$\bar{c}$	Mean aerodynamic chord	1.63	m
t/c	Thickness-to-chord ratio	0.18	-
-	Airfoil	NACA 2418	-

More detailed information about the lift distribution of the wing, lift and drag coefficients, twist, and dihedral can be found in Chapter 9.

5.3.2. Fuselage Design

The fuselage of the cruise vehicle was designed according to the procedure in Section 5.1.2. These have been summarized in Table 5.4. Note that the dimensions that are included in the table are the outer dimensions of the fuselage.

Table 5.4: *Parameters describing the design of the fuselage*

Symbols	Parameters	Values	Units
l_{cabin}	Length of the cabin	2.16	m
w_{cabin}	Width of the cabin	1.13	m
h_{cabin}	Height of the cabin	1.49	m
l_{fus}	Length of the fuselage	7.45	m
$l_{nose\ cone}$	Length of the nose cone	0.82	m
$l_{tail\ cone}$	Length of the tail cone	4.47	m
-	Scrape angle	26	°

5.3.3. Empennage Design

The H-tail was designed in Section 5.1.3. The parameters describing its design are summarized in Table 5.5. Note that the parameters for the planform of one vertical tailplane are presented.

Table 5.5: *Parameters describing the design of the empennage*

Symbols	Parameters	Values	Units
Horizontal Tail			
S_{ht}	Surface area	5.1	m^2
Λ_{ht}	Sweep angle at quarter chord	0	°
λ_{ht}	Taper ratio	0.45	-
A_{ht}	Aspect ratio	4	-
$c_{r_{ht}}$	Root chord length	1.6	m
$c_{t_{ht}}$	Tip chord length	0.70	m
b_{ht}	Wingspan	4.5	m
MAC_{ht}	Mean aerodynamic chord	1.2	m
Vertical Tail (one tailplane)			
S_{vt}	Surface area	1.1	m^2
Λ_{vt}	Sweep angle at quarter chord	42.8	°
λ_{vt}	Taper ratio	0.75	-
A_{vt}	Aspect ratio	1.5	-
$c_{r_{vt}}$	Root chord length	0.99	m
$c_{t_{vt}}$	Tip chord length	0.74	m
b_{vt}	Wingspan	1.3	m
MAC_{vt}	Mean aerodynamic chord	0.87	m

5.3.4. Propulsion Design

The propulsion subsystem, which mainly consists of the four rotors and engines, has been designed to provide enough thrust. The parameters that describe the propellers as well as the compatible engine are shown in Table 5.6.

Table 5.6: *Parameters describing the design of the propulsion subsystem*

Symbols	Parameters	Values	Units
R_{prop}	Propeller radius	1.0	m

Continued on next page

Table 5.6: *Parameters describing the design of the propulsion subsystem (Continued)*

B	Number of blades	3	-
n_{prop}	Number of propellers	4	-
-	Blade airfoil	NACA 2440	-
-	Blade material	Carbon fibre	-
c_{blade}	Blade chord	0.1	m
R_{hub}	Hub radius	0.15	m
Ω	Rotational speed	2600[6]	RPM
-	Engine type	Geiger Engineering HPD40D	-

5.3.5. Landing Gear Design

The procedure in Section 5.1.5 calculated the ideal landing gear position for the main and nose landing gear. The landing gear parameters have been summarized in Table 5.7.

Table 5.7: *Parameters describing the design of the landing gear*

Symbols	Parameters	Values	Units
h_{LG}	Landing gear height	0.40	m
x_{MLG}	Distance of main landing gear from nose	3.5	m
y_{MLG}	Distance of main landing gear from fuselage centerline	1.0	m
x_{NLG}	Distance of nose landing gear from nose	0.50	m

5.3.6. Weights

The resulting weights of the components have been shown in Table 5.8. Additionally, the OEW and the MTOW have been calculated. Note that the value for operational empty mass does not contain the battery mass.

Table 5.8: *Results of the class II weight estimation*

Component	Mass [kg]
Wing	139
Fuselage	222
Coupling mechanism	150
Horizontal tail	34
Vertical tail	26
Main landing gear	70
Nose landing gear	15
Engines	96
Flight controls	16
Hydraulics	6
Electrical	42
Avionics	23
Air conditioning & anti-ice	36
Furnishing	63
OEW	**940**
Battery mass	**237**
Payload mass	**420**
MTOW	**1597**

5.3.7. Center of Gravity Excursion Results

The center of gravity position of the cruise vehicle was calculated using the center of gravity of its components (Section 5.2.7). These numbers and the results of the excursion are in Table 5.9. Note that the battery is located in the tailcone, while the propulsion subsystem is placed on the wing. These values put the vehicle in the static margin.

Table 5.9: *CG excursion results*

Position	Value	Unit
X_{LEMAC}	2.7	m
$(\frac{x}{c})_{propulsion}$	0.3	-
$(\frac{x}{c})_{wing}$	0.25	-
Fuselage	3.0	m
Empennage	6.7	m
Fixed equipment	2.2	m
Battery	4.0	m
Payload	2.50	m
Most forward	2.7	m
Most aft	3.3	m
MTOW	2.9	m

With these parameters specified, the cruise vehicle is visualised in Figure 5.3.

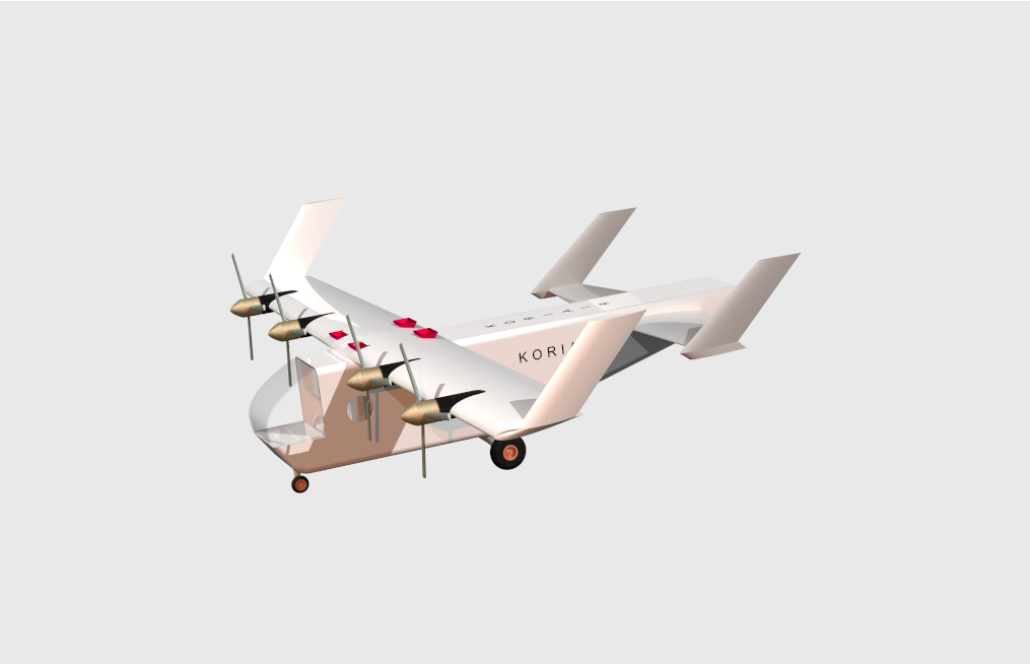

Figure 5.3: *Rendering of the cruise vehicle*

6

Lifting Vehicle Design

The lifting vehicle is used to provide thrust to lift the vehicle into the air, to let the cruise vehicle take off at an altitude of 500 meters. The most relevant subsystems will be designed in the sections below, after which the total weight of the lifting vehicle will be calculated. As was explained in Chapter 5, designing is a reiterative process, and therefore, a loop over both the lifting vehicle and the cruise vehicle needs to be performed to find converging values for their weights and parameters describing their subsystems. In Section 6.1, the fuselage, landing gear, and propulsion subsystem are designed. Then in Section 6.2, the method for estimating the weight of the different subsystems and the total weight of the lifting vehicle are described. Finally, in Section 6.3 the parameters describing the subsystems and their weights are summarized.

6.1. Subsystem Design

The first phase of designing the lifting vehicle starts by setting up the main subsystems. These are the coupling mechanism, fuselage, landing gear, propulsion subsystem, and the battery. The coupling mechanism will not be discussed in detail in this section; due to its complexity it will be explained in Chapter 7. In the sections below, the design of the subsystems will be described, with the relevant requirements and assumptions made.

6.1.1. Fuselage Design

The fuselage of the lifting vehicle does not need to transport the passengers, unlike the fuselage of the cruise vehicle. It needs to carry the battery and several other avionics systems. In the sections below, the design process of the fuselage will be described.

Objectives and Requirements

The fuselage shall house the battery and avionics systems of the lifting vehicle. Therefore, it shall have enough volume to house these subsystems, as well as provide structural integrity. The aim in designing the fuselage is minimizing its shape and weight, whilst providing the necessary volume and structural integrity.

Assumptions

- *The fuselage will house at least twice the battery volume.* Through this requirement, the fuselage will provide enough volume for the battery as well as other subsystems.

Design Process

The fuselage is sized as a hollow box. The dimensions of the box need to allow for enough volume in the fuselage. To analyze its structural integrity, the bending stresses induced by the forces acting on the fuselage were analyzed and stringers were designed to support the fuselage. The bending stresses σ_z acting on the fuselage could be calculated with Equation 6.1.

$$\sigma_z = \frac{(M_x I_{yy} - M_y I_{xy})y + (M_y I_{xx} - M_x I_{xy})x}{I_{xx} I_{yy} - I_{xy}^2} \qquad I_{xx} = \frac{l_x l_y^3}{12} \qquad I_{yy} = \frac{l_y l_x^3}{12} \qquad I_{xy} = 0 \tag{6.1}$$

Here I_{yy}, I_{xx} are the moments of inertia about the x and y axis, respectively, and I_{xy} is the product moment of inertia. l_x and l_y are the length of the box in the x and y directions. The moments M_x and M_y are found with the lift and weight and the position at which they act. The maximum stresses for a set of dimensions can be compared with the yield stress of carbon fibre, the material that was selected

for the fuselage. This returns a length, width, height and thickness of the wall of the fuselage, as well as additional stiffener dimensions to support the structure.

6.1.2. Landing Gear Design

The multicopter requires landing gear for when it is not connected to the cruise vehicle. The landing gear has a skid-like structure, as is more often seen in helicopter-like vehicles. Skids are less complex, more lightweight, and provide good ground stability. However, due to the way the coupling between the cruise and the lifting vehicle is designed, there is no room for a fixed landing structure under the landing vehicle. Thus a retraction mechanism is required.

Skid

As described above, adopting a skid-like landing structure allows for a relatively simple landing gear. The structure consists of two longitudinal hollow cylinders, with on each bar two diagonal skids. A simple visual representation is given in Figure 6.1 to show the structure.

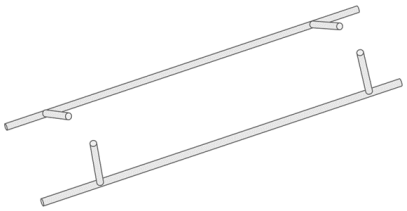

Figure 6.1: *A sketch of the skid landing gear*

Objectives and Requirements

The skid structure shall be able to sustain the weight of the multicopter when it lands and takes off. This will also include additional forces due to downward acceleration. It should absorb shocks such that the delicate electrical components inside the fuselage of the lifting vehicle will not be damaged. The skid structure shall be as light as possible while keeping into account the other requirements. Additionally, while the lifting vehicle is on the ground, the skid shall provide good stability. This means the vehicle is not easy to tip over. The ease of manufacturability of the skid structure should also be taken into account.

A requirement set by regulations for multicopters, similar to CS-23 for aircraft, is about the ground stability the skid landing gear provides. In this case, the minimal angle between the center of gravity location of the vehicle and the point of contact between the skid and the ground is 27 degrees [28].

Assumptions

The assumptions for the design of the skid structure are listed below.

- *The skid structure - both the longitudinal and diagonal parts - are completely circular.* This assumption follows from the landing gear designs of light helicopters and multicopters.
- *The skid structure is completely hollow, except for the parts where the diagonal parts connect to longitudinal part.* While the structure is designed to withstand all the loads when it is completely hollow, it was decided to fill these higher points of stress to ease the loads transfer in these points. This will distribute the stress more evenly through the structure, which will be beneficial in reducing fatigue failure.
- *The length of the longitudinal part is 3 m.* As the multicopter's center of gravity is relatively high due to the elevated placement of the rotors and ducts, the landing gear must be sufficiently long to maintain stability and prevent tipping.
- *The skid structure has a minimal thickness of 0.01 m.* Arising from manufacturing considerations, the lower bound for the thickness of the skid structure was set to 0.01 m.

- *The design of the skid structure will be based on a landing case where the lifting vehicle touches down with one point of the skid structure first; so that one diagonal part will carry the full weight of the vehicle momentarily.* In the event of an uneven landing, the landing gear structure should be able to support the full weight of the vehicle.
- *A safety factor of 1.5 is adopted when calculating the maximum stresses and shear forces in the skid structure.* On top of the above requirement, a safety factor of 1.5 was selected.
- *Landing gear material* The landing gear material was constrained to aluminium alloys only. This was done to their isotropic properties, light weight to strength characteristics and good fatigue endurance.

Design Process

Since there is one geometrical restriction of the skid structure coming from the minimal angle between the center of gravity of the multicopter and the point of contact of the skid with the ground, this was the start of the design. It gave the initial dimension of the longitudinal part of the skid.

Then, the compressive force on the skid is determined. This is simply done by dividing the total mass of the lifting vehicle by the cross-sectional area. This included the safety factor mentioned earlier. Also, the full weight of the lifting vehicle is compressing one diagonal skid part in the most extreme landing case. This is considered in the calculations.

Subsequently, the shear stress in the structure is calculated. This can be done with Equation 6.2[1].

$$\tau = \frac{VQ}{It} = \frac{4}{3}\frac{F}{A}\left(1 + \frac{D_{out} \cdot D_{in}}{D_{out}^2 + D_{in}^2}\right) \tag{6.2}$$

In this equation, F is the magnitude of the force causing shear, A is the cross-sectional area of the skid, and D_{out} and D_{in} are the outer and inner diameter of the skid, respectively. With the known stresses in the structure, the type of material and the dimensions of the skid structure are changed. The strongest, most lightweight option for the material of the skid is AL-7075 T6, an aluminium alloy with high strength.

Retraction Mechanism

The retraction mechanism will move the skid structure to flight configuration before the lifting vehicle connects to the cruise vehicle. Similarly, the skid structure will be moved downwards when the landing vehicle is landing on its own. This will be the case when it returns to the vertiport when it has brought the cruise vehicle in the air, or when an emergency situation is present. The design of the retraction mechanism entails various factors, which are covered in the coming sections.

Objectives and Requirements

The purpose of the retraction mechanism is to retract the skid during flight and during the coupling. Retraction during flight will improve the performance of the lifting vehicle. Retraction of the landing skid during coupling is of utmost importance; otherwise, the cruise vehicle will not be able to connect with the lifting vehicle. It is required that the retraction of the skid can be completed in five seconds.

Assumptions

The assumptions made in order to calculate the necessary parameters for the retraction mechanism are listed below.

- *The center of mass is in the longitudinal part of the skid structure.* This is not be the actual situation, as the diagonal part of the skid will move the center of mass slightly closer to the pivot point. However, assuming the center of mass is in the longitudinal part is a conservative assumptions, as the theoretical displaced mass is larger than occurs in reality.

[1]https://www.ae.msstate.edu/tupas/SA2/chA14.6_text.html [Accessed on 10 June 2024]

- *The center of mass moves a quarter of a circle, i.e. 90 degrees.* As of now, the exact shape of the fuselage is not known in detail, and thus it is difficult to analyse how the far the skid landing gear can be moved upwards. Thus, it is assumed that the landing gear can move maximal 90 degrees.
- *A safety factor of 1.2 is applied to the required force to move the landing gear.* This safety factor is included to encounter for small factors that are not explicitly considered in the following calculations, e.g. friction of the mechanism. Also, it will make sure that the restoration mechanism functions under all circumstances.
- *The weight of the linkages, fasteners, reinforcements, and other miscellaneous components is 5 % of the weight of the skid structure.* Since there are hardly any comparable retractable skid landing gears, it is not possible to make use of statistical relations for the weight of these components. Therefore, a percentage of the total weight of the landing gear will be used for the weight of the miscellaneous parts.

Design Process

There are three options to retract the landing gear: a hydraulic, electric, or mechanical system. Since the lifting vehicle is unmanned, a mechanical system is not a possible option. The choice between a hydraulic or electric system is more nuanced. Hydraulic systems are commonly used in retraction mechanisms for landing gear. They, however, are generally heavier than electrical systems because of the pumps, fluid reservoirs, valves, actuators, and plumbing components. Also, hydraulic systems require more maintenance. An electrical system is more easily integrated with a digital system, and maintenance is simpler. However, the motor must have enough remaining power that is not used for the flight surfaces and propulsion system to power the retraction mechanism. Given the advantages of the electrical system in terms of weight, complexity, and integration into the existing structure, this option will be further designed.

The novel aspect of the design of this subsystem is that skid landing gear structures, the structure is nearly always fixed to the fuselage of the craft. There are only two examples in history when a retractable skid landing gear is developed; the Bell Cobra 209/AH-1F[2], and the Lockheed XH-51[3]. Both these helicopters have been fully functional flying helicopters, but the design was changed before mass production was started (in the case of the Bell 209 model), or other prototypes were built (in the case of the Lockheed XH-51).

The design of the retraction mechanism starts with determining the required force to move the skid. For this, Newton's second law of motion can be used. The acceleration will be composed of two parts; the gravitational acceleration and the acceleration due to the retraction or extension. This is shown in Equation 6.3.

$$a_{tot} = g + \frac{2\pi r \ \frac{1}{4}}{t^2} \tag{6.3}$$

An additional safety factor of 1.2 is taken in the calculation of the total required force, to account for unknown factors such as friction, weather conditions, etc. Subsequently, the required torque can be calculated. This is done with the equation given in Equation 6.4.

$$\tau = F \cdot r \tag{6.4}$$

In this equation, r is the radius of turn. In the case of the skid structure, it is the vertical part of the structure. The torque is needed to select an appropriate gear reduction system. The force is needed to select an actuator that is strong enough. With the mass and the dimensions of the skid structure calculated in the section above, these can be calculated. This leads to a required force of approximately 930 N and a torque of 465 Nm. An example of an actuator than can be used is a linear actuator able to provide a force up to 1000 N[4]. An example of a gearbox that is able to provide 528 Nm of torque and thus will be able to pull the skid structure up is a worm gearbox[5].

[2]https://www.nhahistoricalsociety.org/ah-1g-bell-209-huey-cobra-snake-helicopter/ [Accessed on 10 June 2024]
[3]https://en.wikipedia.org/wiki/Lockheed_XH-51 [Accessed on 10 June 2024]
[4]https://www.transmotec.com/product/DLA-12-40-A-150-HS2-IP65/ [Accessed on 10 June 2024]
[5]https://nl.rs-online.com/web/p/gearboxes/2166642?gb=s [Accessed on 10 June 2024]

6.1.3. Propulsion Design

The propulsion subsystem of the lifting vehicle shall provide the upward thrust to lift itself, as well as the cruise vehicle, up. This subsystem consists of the rotors, engines, nacelles, and fairings. The procedure for designing the rotors is the same as for the propellers of the cruise vehicle in Section 5.1.4. Therefore, this method will not be repeated. However, the assumptions made, and specific information used in the process of designing the rotors for the lifting vehicle will be discussed in this section.

Objectives and Requirements

The purpose of the propulsion subsystem is to lift the vehicles into the air. The lifting vehicle achieves this with propellers that provide upward thrust. For the sake of stability, multiple rotors are used, such that thrust differentials can be used to control the aircraft and to perform maneuvers.

Assumptions

The assumptions specific to the lifting multicopter are listed below. Assumptions from Section 5.1.4 are not repeated.

- *The lifting multicopter will have 24 rotors.* It is crucial to design the lifting multicopter for control, such that the coupling process can be performed smoothly. Therefore, the number of rotors is constrained more by maneuverability than efficiency. However, the propulsion design will still take into account the number of blades and propeller radius to try to maximize efficiency and minimize noise and weight.

Design Process

The design process for noise and weight remains the same as explained in Section 5.1.4.

The method described in Section 5.1.4 finds the optimal combination of number of blades and radius based on the propeller efficiency, thrust produced and noise emitted by the propeller, and the mass of the propeller. An important requirement for the propulsion system is that the rotors shall provide enough thrust to lift both vehicles to the horizontal in-air take-off altitude of 500 meters. The thrust can be calculated from the equations of motion at the most critical point in this phase of the flight, which is shown in Equation 6.5.

$$T = C_D \frac{1}{2} \rho V_{v,max}^2 S + (m_{LV} + m_{CV})(a_{v,TO} + g) \tag{6.5}$$

In this equation, $V_{v,max}$ is the maximum vertical velocity, m_{LV} and m_{CV} are the mass of the lifting and cruise vehicle, and $a_{v,TO}$ is the vertical acceleration of the vehicles. The drag coefficient and surface area for vertical flight are estimated in Chapter 9.

The main difference in the lifting multicopter design is efficiency. As seen in Equation 5.10, the efficiency decreases as V_∞ decreases. It then becomes zero when the lifting vehicle hovers ($V_\infty = 0$). Thus, in this case, efficiency is not a useful metric for propeller design.

For vehicles which hover, such as helicopters and multicopters, the figure of merit is used instead to determine efficiency. It is the non-dimensional ratio between the ideal power required to hover and the actual power required to hover and can shown as a relationship with the thrust coefficient computed with Equation 6.6.

$$\text{FM} = \frac{\frac{C_T^{3/2}}{\sqrt{2}}}{\frac{\kappa C_T^{3/2}}{\sqrt{2}} + \frac{\sigma C_{d0}}{8}} \tag{6.6}$$

Here, κ is the non-ideal loss factor, C_{d0} is the zero-lift drag coefficient, C_T is the thrust coefficient and σ is the rotor solidity with typical values ranging between 0.05 and 0.12 for helicopters. From the above equation, it follows that the figure of merit increases as the thrust coefficient increases. In the case of the lifting vehicle with $\kappa = 1.15$ and, $\sigma = 0.1$ the figure of merit is computed to be 0.85. This value represents excellent hovering performance for a helicopter rotor and therefore is suitable for the

multicopter lifting vehicle[6]. These values, together with Equation 6.10, the power required for take-off is 941 kW, and for landing it is 770 kW.

Four small outwards facing rotors with a radius of 0.5 meters are added on the sides of the lifting vehicle. Finally, ducts have been added to the 24 rotors on top to reduce the noise that they produce. These ducts also increase the thrust produced by the rotors and therefore, the radius of the rotors could be adjusted. More about these ducts and their sizing can be found in Chapter 9.

6.2. Class II Weight Estimation

This section will detail the class II weight estimation method for each important vehicle system.

6.2.1. Airframe Weight

The airframe is assumed to be composed of three separate components: fuselage, arms, and coupling mechanism. The weight of the fuselage can be determined by calculating the volume of the box with stiffeners designed in Section 10.2. Then, the weight is simply determined by multiplying it by the chosen material density, in this case Aluminum 2024. The same principle is applied for the arms, which are modelled as an I beam. Since the calculation does not account for the weight of rivets, fasteners, and any other detailed structural elements, the obtained value for the mass of the fuselage and arms is multiplied by 2. For the coupling component, the mass is calculated in Section 7.3.

6.2.2. Landing Gear Weight

The weight of the landing gear of the lifting vehicle can be split into two components: the weight of the landing gear itself, and the weight of the retraction mechanism. The weight of the landing gear itself is a result of calculating the volume of the skid structure and multiplying it with the specific density. The weight of the retraction mechanism can be divided up in three parts. The weight of the gearbox and the actuator are treated separately, and extra miscellaneous weight due to linkages, fasteners, and reinforcements is considered as well. The fraction this last component takes up was already mentioned in Section 6.1.2. Thus, the weight of the landing gear can be calculated with Equation 6.7.

$$W_{landinggear} = 1.02 \cdot W_{skid} + W_{gearbox} + W_{actuator} + 0.05 \cdot W_{skid} \tag{6.7}$$

The gearbox and actuator specified in Section 6.1.2, have a weight of respectively 14.8 kg and 0.990 kg. The weight of the skid structure can be calculated by determining the volume and multiplying it with the specific density of AL-7075 T6. An extra factor of 2% of the weight of the skid structure was added to account for welding the longitudinal and diagonal parts together.

6.2.3. Propulsion Weight

The weight of the propulsion subsystem consists of the weight of the engines as well as the rotors. Firstly, the weight of the engines is found through multiplying the weight of the engine by the number of engines, which is 24, and multiplying the entire weight by 1.2 to take into account nacelles and fairings.

$$W_{engines} = 1.2 W_{engine,uninstalled} N_{engines} \tag{6.8}$$

Furthermore, the calculation of the mass of the rotors is shown in Equation 6.9.

$$m_{rotor} = \rho_{material} B \left(\frac{t}{c}\right)_{blade} c_{blade}^2 \tag{6.9}$$

The resulting value can be multiplied with 24 to find the weight of all rotors together. The weight of the ducts was also added to this value.

6.2.4. Battery Weight

The weight of the battery can be calculated through the energy that is used by the lifting vehicle during its flight regime. This energy used can be found by multiplying the power required in every phase of

[6]https://eaglepubs.erau.edu/introductiontoaerospaceflightvehicles/chapter/helicopters-vtol/

the flight regime, by the time corresponding to that phase. The power required is determined using Equation 6.10.

$$P = \frac{1}{\eta_{mech} FM} \sqrt{\frac{(f_w T)^3}{2\rho A_{disk}}} \tag{6.10}$$

Power required at a given time depends on the required thrust T, and air density ρ at this time instance. This value is corrected with the mechanical efficiency η_{mech}, assumed to be 0.97, fuselage down wash factor f_w, assumed to be 1.10, and the figure of merit FM, assumed to be 0.7.

The lifting vehicle is used for take-off and landing mission phases specified in Section 8.2. To determine the battery weight, the additional time of 10 minutes of loitering is added. Loitering after take-off is performed with the cruise vehicle attached, however it is assumed that the cruise vehicle is also capable of providing power, therefore it produces lift for itself. Furthermore, the additional time was added for maneuvering: 20 seconds for maneuvering without the cruise vehicle, 20 seconds for maneuvering with cruise vehicle, and 10 seconds for coupling. For each of the aforementioned phases, thrust required can be determined based on the required acceleration. The energy required for the take-off mission is determined also taking into account the possibility for a landing with the cruise vehicle attached after loitering. The power required is then multiplied by time for the associated phase of the mission, and the energy is determined.

Due to the requirement for landing with the cruise vehicle attached, the take-off mission is used for the battery weight estimation. Having the energy E for the mission, the battery weight can be determined using Equation 6.11.

$$m_{battery} = \frac{E}{E_{sb} \eta_{battery}} \tag{6.11}$$

The specific energy density E_{sb} was assumed to be 235 Wh/kg and the battery system efficiency was assumed to be 0.9 [53].

6.2.5. Miscellaneous Weights

For the coupling mass estimation, the team designing was asked to provide an upper limit on the hook of the lifting vehicle. The expected maximum mass of the coupling mechanism is of around 200 kg

The avionics are key in the lift vehicle, as it has to coordinate with the cruise vehicle for take-off and landing procedures. Additionally, it is completely unmanned, thus additional avionics are expected. Initially, a similar amount of avionics as the cruise vehicle was taken at 40 kg. To find the mass of the avionics as a whole, Equation 6.12 from Raymer [53] for general aviation planes was used.

$$W_{av} = 2.117(W_{uav}^{0.933}) \tag{6.12}$$

6.3. Final Design Specifications

The weight of the lifting vehicle and the parameters describing its different subsystems were found after a number of iterations. In the following subsections, these parameters will be summarized. More details about some of the subsystems will be specified in other chapters of this report.

6.3.1. Airframe Design

A crucial part of the lifting vehicle is the fuselage that houses the battery and avionics systems, as well as the arms that connect the fuselage to the rotors. The design of the airframe is described in Section 10.1. After determining the required space for the battery, the dimensions of the fuselage can be calculated. These have been summarized in Table 6.1.

Table 6.1: *Parameters describing the design of the fuselage*

Symbols	Parameters	Values	Units

Continued on next page

Table 6.1: *Parameters describing the design of the fuselage (Continued)*

$V_{battery}$	Battery volume	0.11	m^3
$l_{fuselage}$	Fuselage length	1.00	m
$w_{fuselage}$	Fuselage width	1.00	m
$h_{fuselage}$	Fuselage height	0.50	m
$t_{fuselage}$	Fuselage wall thickness	0.001	m
$n_{stiffener}$	Number of stiffeners	1	-
$h_{stiffener}$	T stiffener height	0.12	m
$t_{stiffener}$	T stiffener thickness	0.02	m

Apart from the fuselage, the airframe of the lifting vehicle consists also of the arms supporting the rotors. The description of the design of those is provided in Section 10.1. The final parameters are given in Table 6.2.

Table 6.2: *Parameters describing the design of the arms*

Symbols	Parameters	Values	Units
l_{arm}	Arm length	5.2	m
h_{arm}	Beam height	0.28	m
w_{arm}	Beam width	0.04	m
t_{web}	Web thickness	0.001	m
t_{flange}	Flange thickness	0.001	m
Φ	Angle between the arm and the fuselage	27	°

6.3.2. Landing Gear Design

The landing gear of the lifting vehicle consists of the skid and a retraction mechanism. Some parameters describing this design and necessary to estimate its weight are presented in Table 6.3.

Table 6.3: *Parameters describing the design of the landing gear*

Symbols	Parameters	Values	Units
l_{skid}	Skid length	3	m
h_{skid}	Skid height	0.5	m
θ	Skid angle	30	°

6.3.3. Propulsion Design

The propulsion system of the vehicle consists of 24 rotors, with noise reducing ducts, providing vertical thrust, 4 smaller rotors on the sides to provide control, and engines for all of these rotors. The rotors described below are the 24 on top. The 4 smaller ones are different in a sense that they have a radius of 0.5 meters and do not have ducts.

A relatively small engine was picked in order to reduce the noise. This caused an increase to the number of propellers to 24 and reduced the possible engines. Afterwards, to further reduce noise, an engine with enough thrust and power but the lowest possible RPM was picked. The choice was made for the Geiger engineering HPD20SD engine which had an RPM of only 2600, while providing enough power to support the vehicle.

Table 6.4: *Parameters describing the design of the propulsion subsystem*

Symbols	Parameters	Values	Units
R_{rot}	Rotor radius	0.69	m

Continued on next page

Table 6.4: *Parameters describing the design of the propulsion subsystem (Continued)*

B	Number of blades	2	-
n_{rot}	Number of rotors	24	-
-	Blade airfoil	NACA 2440	-
-	Blade material	Carbon fibre	-
c_{blade}	Blade chord	0.05	m
R_{hub}	Hub radius	0.15	m
Ω	Rotational speed	2600[10]	rpm
-	Engine type	Geiger Engineering HPD20SD	-

6.3.4. Weights

The resulting weights of the components have been shown in Table 6.5. Additionally, the operating empty weight and the maximum take-off mass have been calculated. Note that the value for operational empty mass does not contain the battery mass.

Table 6.5: *Results of the class II weight estimation*

Component	Mass [kg]
Airframe	35
Coupling	128
Landing gear	105
Engines	135
Electrical	70
Avionics	62
Rotors with ducts	211
OEW	**746**
Battery mass	**229**
MTOW without cruise vehicle	**975**

With these parameters specified the lifting vehicle can be visualized with Figure 6.2.

Figure 6.2: *Rendering of the lifting vehicle*

7

Coupling Mechanism and Processes

Coupling is a crucial part of the performance of the two vehicles, and therefore requires detailed analysis. In this chapter, the most critical aspects impacting the feasibility of the novel coupling mechanism are discussed. This mainly includes a structural analysis of the rigid coupling elements. A brief description behind the logic of the design process is also given, as well as qualitative descriptions behind some operations of the coupling.

7.1. Background and Assumptions

A rigid connection must exist between the cruise and lifting vehicle. This 'coupling' is critical to the operation of the system. The design of the coupling system includes the physical load-bearing elements that hold the vehicles together, as well as any guiding mechanisms that bring the connecting elements together. The attachment process of the load bearing elements must not require precise alignment of the two aircraft to begin the coupling, but must eventually lead to a robust connection. This is why both physical connections and control systems are to be used. When a full connection is established, a form of locking mechanism is engaged to provide a secure connection between the vehicles. Furthermore, it is clear that the control subsystems of the cruise and lifting vehicles must provide some minimum level alignment before any physical alignment takes place. This means that the design of the control subsystem is significantly important for the coupling procedure.

Because of the expected volatility of the situation, two distinct elements of the physical coupling procedure are proposed: mechanical guiding, followed by a rigid coupling that finalizes the transition of the system from two aircraft to one. The mechanical guiding is intended to aid the control systems of the aircraft in bringing them closer together to align them. The mechanical guiding must have some level of compliance to allow for motion between the aircraft to occur without the connection disengaging. Within the mechanical guiding mechanism a load limiter should be integrated in order to protect the aircraft at some critical condition.

Before more detailed design steps are taken, a decision about the location of the coupling mechanism must to be made. It was decided that the coupling mechanism should be implemented in such a way that the lifting vehicle picks up the cruise vehicle from the top. This decision was made for a few reasons, which were mainly operational and structural:

- Passengers and cargo need to be unloaded and loaded quickly and safely. If the lifting vehicle is under the cruise vehicle, this is problematic. This is also important for evacuating passengers.
- There is limited ground space allowed for both vehicles on ground at take-off and landing. With the lifting vehicle on the bottom, more clearance would be required.
- The cruise vehicle has a high-wing configuration. Because of this, the load on the wings is introduced into the fuselage in the top of the aircraft. Locating the cruise vehicle's connection points near this structure would be more efficient, because a structure for the load path between lifting and cruise vehicle would be present. However, it is still necessary to create a structure to accommodate the connection points and the relatively high force concentrations associated with them.

When the two aircraft are close together, the rigid coupling is ready to engage. The rigid coupling elements are ideally above their respective connection points, however their pivots are modified with springs so that they can find their way to a good connection position and lock into place. During the

release procedure, these rigid connections will be actuated as the cruise vehicle increases its lift, and the two vehicles will detach.

7.2. Design of Mechanisms

In this section, more details about the design of the coupling mechanisms are documented. This includes mechanical guiding to finalise the alignment of the aircraft and the rigid coupling mechanism.

7.2.1. Design of the Rigid Coupling

The rigid coupling element of the coupling system consists of four hooks on the lifting vehicle, which form a strong connection with the airframe of the cruise vehicle through the front and rear spars of its center wing box (CWB). The decision to have the rigid coupling occur through the front and rear spars of the CWB of the cruise vehicle was made to simplify construction. Generally, the wing box of the cruise vehicle can be split into the outer wing boxes (OWBs), which are situated in the wings, and the CWB, which is connected to the two OWBs and is integrated into the airframe of the cruise vehicle. Sizing the CWB this way will simplify the introduction of cruise vehicle loads in the coupling mechanism, as they are occurring in a structure that is already optimized for efficient force introduction of critical loads. The CWB and OWBs, the joint between the two and the integration of the CWB into the airframe of an aircraft, are critical parts of aircraft structural design and are well-developed in literature. Therefore, the structural sizing of the coupling mechanism for the lifting vehicle will focus on the hooks, and for the cruise vehicle on the front and rear spar of the CWB. A notional drawing of the top of the cruise vehicle and the bottom of the lifting vehicle is shown in Figure 7.1a. The arrangement of hooks and the general points of contact with the spars can be seen.

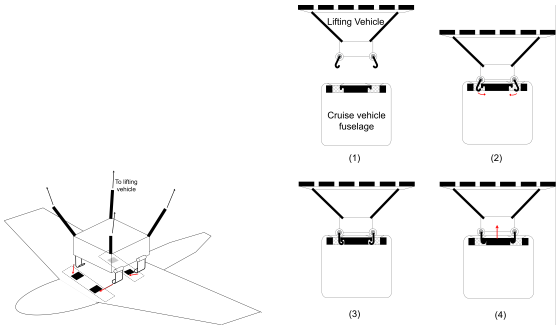

(a) *Vehicles ready for coupling* **(b)** *Vehicle coupling procedure*

During coupling, the hooks of the lifting vehicle connect with these spars through four holes in the top of the fuselage in the region on top of the CWB. A high level process of the rigid coupling is shown in Figure 7.1b which shows the shaded cross section from Figure 7.1a. The hooks are held in a retracted position while the vehicles come closer together. Once the vehicles are aligned, the hooks are released and the torsional springs swing them into place. If there is misalignment, the angled walls of the entry points of the hooks aid in the re-centering of the hooks. As the cruise vehicle reduces the lift it produces, it comes to rest on the hooks, transferring more load to the lifting vehicle.

The front two holes in the fuselage are located in the front spar of the CWB, and the two rear holes are located in the rear spar of the CWB. The connection points are separated by 1 m (x_{sep}) both in the X and Y direction. At this stage of design this assumption is used because it is less than the fuselage width (1.13 m) and it is not possible to size the exact length of the wing spar at this point. Furthermore, the exact location of the front and rear spars of the OWBs is not known and so the separation of the connection points in the X direction was also made 1 m. This is reasonable for a root chord of c_r =1.77 m and so the separation of the spars along the X-axis can conceivably be higher. The arrangement of these holes can be seen in Figure 7.2a. In Figure 7.2b, the meshing elements of the coupling mechanism are detailed. This hook is an idealized hook with a square cross-section and width w_{hook}, as seen in the figure.

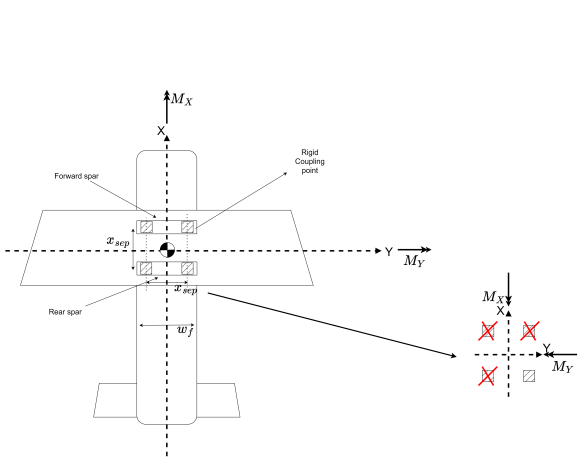

(a) *Arrangement of rigid coupling points on top of vehicle*

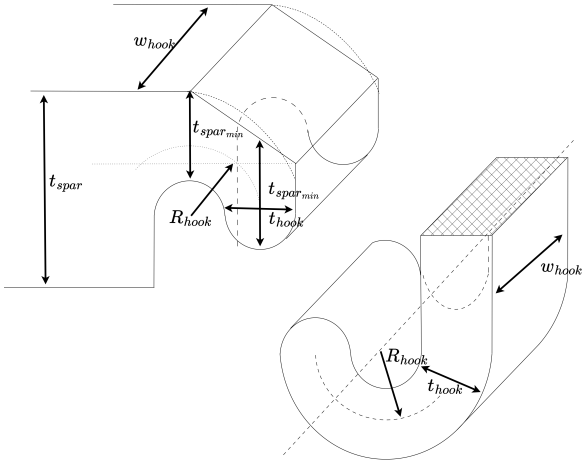

(b) *Detailed geometry of hook meshing*

The hook illustrated in the figure is sized based on the most critical condition, specifically the situation when three connections have failed and the lifting vehicle is supporting the entire weight of the cruise vehicle through one connection. Most importantly, it must also sustain moments generated by the cruise vehicle around the X and Y axes. The connection points are arranged around the center of gravity of the cruise vehicle, as shown in the Figure 7.2a. A free body diagram for the hook and part of the spar is shown in Figure 7.3a.

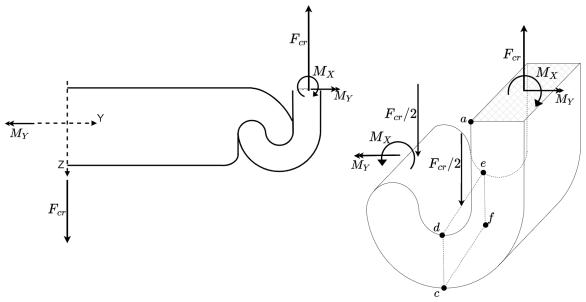

(a) *Free body diagrams of hook with idealized load transfer*

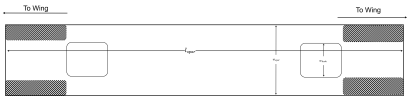

(b) *Top view of the idealized spar*

The critical loading $F_{cr} = n_{safety} MTOW\ g$ includes a safety factor of 2 applied to the loading of the cruise vehicle to account for the critical nature of the structure. This does not take into account stress concentration effects, which will be introduced later. The distance between the two points of force application on the hook in Figure 7.3a is assumed to be much smaller than the distance of the hook from the center of gravity of the cruise vehicle, such that the forces applied there are equal. For now, assuming that the hook can sustain the applied moments, critical stress locations can be located. These are Point 'a' for maximum axial stress and Point 'c' for maximum shear stress.

The stress at Point A is calculated based on the direct axial stress due to the weight of the cruise vehicle, and the moments around the X- and Y- axes in Figure 7.2a.

$$\sigma_a = \sigma_{direct} + \sigma_{M_X} + \sigma_{M_Y} \tag{7.1}$$

The shear stress at Point C is calculated based on the direct shear force due to the weight of the vehicle, the torsion around the Y-axis acting on face *cdef*, as well as the moment around the X-axis.

$$\tau_c = \tau_{direct} + \tau_{T_Y} + \tau_{M_X} \tag{7.2}$$

The region within the spar where the hook will make contact was also sized for a certain height (h) and width (w). At this stage, the rectangular face outlined by h and w is assumed to carry all the direct

shear loads introduced by the hook, as well as the shear introduced by torsion around the Y-axis and moments around the X-axis. This is a structural idealization, which also over-designs this region of the spar. The maximum shear is calculated with Equation 7.3

$$\tau_{spar} = \tau_{direct} + \tau_{T_y} + \tau_{M_X} \tag{7.3}$$

As mentioned, the connection points will be subject to stress concentrations. The geometries being considered are complex, so a much more detailed analysis of the stresses should be done in the future. However, as with such a critical structure, some stress concentrations will already be applied now, as far as is possible given the understanding of the geometry at this point. For crane hooks, a stress concentration factor of 1.56 can be found [52, p. 462]. This is applied to the hook in the coupling mechanism. Within the spar, as one moves from right to left, the spar thickness increases dramatically from h to t_{spar}, and is characterized by the curve, or shoulder filet, with radius R. Hardy and Pipelzadeh [23] found stress concentration factors for such geometries but with different proportions. Nevertheless, the paper finds that for very high values of ratios of a shoulder fillet in shear, similarly large as the spar being characterized, the stress concentration factors tend to a constant value. Using the dimensions indicated in Table 7.1 a stress concentration factor of 1.8 is selected.

The dimensions for the hook and spar are detailed in Table 7.1. These values were determined after some iterations to find a selection of parameters for which the critical stresses were not surpassed. The hooks will be the end points to the arms, which hang down from the lifting vehicle and transmit the load from the hooks to the lifting vehicle, as shown in Figure 7.3a. For an initial estimate of the mass, it is assumed that the arms have the same cross-section as the hook base. The total mass of the arms and spars is also given. They are made out of Titanium 6AI-4V because of its good strength and fatigue properties, which is appropriate for such a critical aspect of the design. The spar must be modified to accommodate a connection to the OWBs using some form of splice joint. The details of this splice joint are left for further designs, however it is necessary to check that the spar will resist the wing loading. The moment produced at the root of the wing can be calculated with Equation 7.4 where two assumptions are made; the cruise vehicle experiences a maximum lift loading of F_{max} due to a loading factor N_z of 3.75, and that the lift acts as two components through the midpoint of each wing at distance $b/4$. Here the force is equivalent to the half the load factor multiplied by the weight of the aircraft.

$$M = Fd = 0.5 N_z m_{cv} g \frac{b}{4} \tag{7.4}$$

Assuming that each spar in the CWB resists half of these loads, and that only the shaded region in Figure 7.3b transmits the loads to the rest of the spar, which is an underestimation, the maximum axial stresses due to wing bending can be calculated. Having these shaded regions with a titanium thickness of 2 cm was found to be more than sufficient to resist the loading. Shear loads were found to be two orders of magnitude smaller for these dimensions, and so are not critical.

The final dimensions of the hook and spar are shown in table Table 7.1. The length of the spar is assumed for now to be equal to the width of the fuselage, w_{fus}. There is no robust structural feature which can make the hook and spar resist moments on its own. It was assumed that it would do so inherently, and the hook and arm dimensions were sized for stresses accordingly. In Figure 7.4, a mechanism is suggested that is a starting point for a more detailed design of the hook. In the diagram, a bar swings into a notch within the hook. A release mechanism is implemented such that this bar is released when the main part of the hook makes contact with the spar. The two contact points can now support loads in opposite directions and generate a moment couple that can resist moments. The mechanism also introduces a clamping action to the design that secures the hooks more effectively.

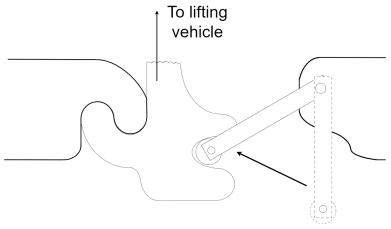

Figure 7.4: *Mechanism conceptualization for hook clamping*

Finally, consideration should be given to the quality of the contact between hook and spar. It would be beneficial to line the surfaces of the spar where the hook makes contact with some form of durable elastic material such as rubber. This would avoid any high force concentrations, and distribute the loads more effectively on spar and hook.

7.2.2. Design of Mechanical Guiding

The mechanical guiding mechanism will consist of a long boom-like structure that is actuated using a hydraulic system. It will finalize the alignment of the two aircraft by entering a loop on the cruise vehicle and pulling it towards the belly of the lifting vehicle. This loop will either close around the boom or a gripping mechanism on the boom with activate around loop. The boom will be actuated using a hydraulic system.

As seen in Figure 7.5, the the boom for mechanical guiding enters the cable loop on the cruise vehicle, and it is pulled upwards by the actuation of the hydraulic piston. Due to the shape of the boom, the cable will be pushed into corner of the boom, which will align the centers of gravity of both cruise and lifting vehicle, and therefore the rigid coupling. Only when the loop is in the corner of the boom will the mechanism be activated. The details of this mechanism are left for future studies, but its necessity stems from the need to be able to force the cruise vehicle, using the hydraulic system, in both positive and negative z-direction. The base of the boom and piston must allow for some movement around the three axes as relative motion between the aircraft needs to be allowed. This needs to be combined with some form of torque limiting device that will cause the mechanism to fully disengage at some threshold.

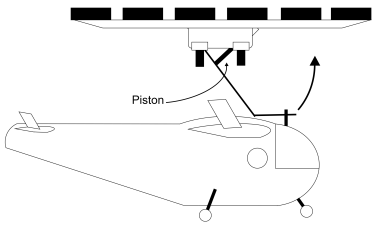

Figure 7.5: *Mechanical Guiding Concept*

It was decided to size the piston based on forces expected due to gusts, with a safety factor of 2 applied. For CS-27 regulations, this implies gusts with speeds up to 9.1 m/s [16]. Locating the piston close to the pivot/base of the boom allows the aircraft for plenty of safe space to manoeuvre in the event of a gust. Assuming that the lifting vehicle will start mechanical guiding to the cruise vehicle with a separation of 2 m, a boom of length just over 4 metres was chosen, which includes the bend and allows for some margin. For this situation, the piston would have to generate just under 10000 N of force to counter gust effects. The length of the boom was chosen because of the ability of the control systems of the two aircraft to be within a certain range of each other. The base of the boom would allow for some rotation around two axes, but no torsion of the boom would be allowed. The base of the piston shall also have freedom to rotate and follow the boom.

7.3. Final Values

Table 7.1 gives the final dimensions for the spar and hook. The mass of the hook includes an over estimate of the amount of material needed to create the pivot onto which the hook-arm are attached.

Table 7.1: *Hook and spar dimensions*

Parameter	Value
t_{hook} [m]	0.05
w_{hook} [m]	0.105
R_{hook} [m]	0.05
$t_{spar_{min}}$ [m]	0.065
t_{spar} [m]	0.115
x_{sep} [m]	1.0
w_{spar} [m]	0.145
l_{spar} [m]	1.13
Hook weight (4 hooks including arms) [kg]	128
Spar weight (2 spars) [kg]	150

The boom for mechanical guiding is made of Aluminium-7075 which is sufficient for the predicted stresses. The boom weighs 35.1 kg. The mass of the piston attached to the boom is based on an existing piston with sufficient stroke (actuation distance) and force (1000 N). Such pistons exist and can be sourced commercially[1]. An example piston with ball joints has a mass of 35 kg.

The coupling mechanism has been sized from a structural point of view using limited literature due to the lack of current resources available. Therefore, the safety factors and stress concentration factors applied yield a design with large margins. This is supported by the rather heavy spars for the CWB. The next steps in the design will include computational methods to judge the effectiveness of the coupling mechanism structure and further define the details regarding its actuation and clamping mechanisms.

[1]https://www.hydrauliek24.nl/dubbelwerkende-cilinder-70x40x1000mm-met-kogelgewricht [Accessed on 14 June 2024]

8

System Performance Analysis

Analyzing the performance of the vehicles helps to investigate and show that the design adheres to the requirements. With more details known about the design of the vehicles, their performance can be analysed. Firstly, power and wing loading diagrams are constructed and shown in Section 8.1. Then, the flight profile of the vehicles is discussed in detail in Section 8.2. Finally, the load factor diagram, showcasing the magnitude of the loads that the cruise vehicle has to sustain during flight, is included in Section 8.3.

8.1. Wing and Power Loading Diagram

An initial step in analyzing the performance of the design is setting up a wing and power loading diagram. In this diagram, the inverse of power loading W/P is plotted against wing loading W/S in several parts of the flight regime, to visualize the limiting conditions for the design. This diagram allows for an evaluation of the design space, where feasible combinations of power loading and wing loading exist, and what the required power and wing area are in relation to the weight for those design points. From these values, subsystems like the wing could be designed in Section 5.1.1. In the following paragraphs, the limits due to stall speed, take-off, landing, cruise, and climb will be discussed.

8.1.1. Stall Speed

The first limit set is the stall speed. The cruise vehicle shall not fly at speeds lower than this stall speed. CS-23 regulations [17], which are specified for general aviation aircraft, under which category the cruise vehicle falls, prescribe a stall speed of maximally 61 kts or 31 m/s[1]. The maximum allowed wing loading for stall speed is described in Equation 8.1. At this point, the maximum lift coefficient $C_{L_{max}}$ is assumed to be 1.8, which is taken from similar aircraft [1].

$$\frac{W}{S} = \frac{1}{2}\rho V_S^2 C_{L_{max}} \tag{8.1}$$

8.1.2. Take-off

For take-off, a statistical parameter is used to find the relation between power loading and wing loading. This so called Take-off Parameter (TOP) is defined as in Equation 8.2. According to Raymer [53], the TOP for the assumed take-off distance of 500 meters is 160. Finally, σ is the ratio of air density at take-off altitude to air density at sea level and $C_{L_{TO}}$ is the takeoff lift coefficient.

$$TOP = \frac{W}{S}\frac{W}{P}\frac{1}{C_{L_{TO}}}\frac{1}{\sigma} \qquad C_{L_{TO}} = \frac{C_{L_{max}}}{1.1^2} \tag{8.2}$$

8.1.3. Landing

The limiting wing loading for landing can be determined through Equation 8.1 using the approach speed $V_{s_{land}}$ instead of stall speed. According to CS-23 regulations[1] the approach speed can be related to the landing distance s_{land}, which was assumed to be 500 meters, as in Equation 8.3. That yields the following formula for the limiting wing loading for landing.

[1]https://www.easa.europa.eu/en/document-library/certification-specifications/group/cs-23-normal-utility-aerobatic-and-commuter-aeroplanes#cs-23-normal-utility-aerobatic-and-commuter-aeroplanes [Accessed on 24 May 2024]

$$\frac{W}{S} = \frac{1}{2}\rho \frac{s_{land}}{0.5915} C_{L_{max}} \qquad V_{s_{land}} = \sqrt{\frac{s_{land}}{0.5915}} \tag{8.3}$$

8.1.4. Cruise

In cruise conditions, the available power is equal to the power required, which is equal to the drag multiplied by the velocity. Knowing that the available power is equal to the brake shaft power multiplied by the propeller efficiency ($P_a = \eta_p P_{br}$) and using the drag polar, a formula for the power loading related to the wing loading in cruise can be set up. The derivation of the formula, and the formula itself, is given in Equation 8.4 respectively [1]. Note that a correction for altitude is added in the form of $\left(\frac{\rho}{\rho_0}\right)^{3/4}$. A cruise altitude of 1200 meters was assumed. Furthermore, a zero-lift drag coefficient C_{D_0} of 0.03 and an Oswald efficiency factor e of 0.8 was assumed, according to reference aircraft[2].

$$\frac{\eta_p P_{br}}{W} = \frac{C_D \frac{1}{2}\rho V^3}{(W/S)} = \frac{C_{D_0}\frac{1}{2}\rho V^3}{(W/S)} + \frac{W}{S}\frac{1}{\pi A R e \frac{1}{2}\rho V} \rightarrow \frac{W}{P} = \eta_p \left(\frac{\rho}{\rho_0}\right)^{3/4} \left[\frac{C_{D_0}\frac{1}{2}\rho V^3}{(W/S)} + \frac{W}{S}\frac{1}{\pi A R e \frac{1}{2}\rho V}\right]^{-1} \tag{8.4}$$

8.1.5. Climb

The limiting relations between rate of climb and climb gradient are defined in 8.5 [1].

$$\frac{W}{P} = \frac{\eta_p}{ROC + \frac{\sqrt{\frac{W}{S}}\sqrt{\frac{2}{\rho}}}{1.345\frac{(AR\ e)^{3/4}}{C_D^{1/4}}}} \qquad \frac{W}{P} = \frac{\eta_p}{\sqrt{\frac{W}{S}}\left(\frac{c}{V} + \frac{C_D}{C_L}\right)\sqrt{\frac{2}{\rho C_L}}} \tag{8.5}$$

A rate of climb ROC of 5 m/s is assumed, according to the minimum of 4.5 m/s set by CS-23 regulations[3]. A climb gradient $\frac{c}{V}$ of 0.083 is assumed from CS-23 regulations as well.

8.1.6. Final Diagram

All limits have been set up and the diagram is plotted in Figure 8.1.

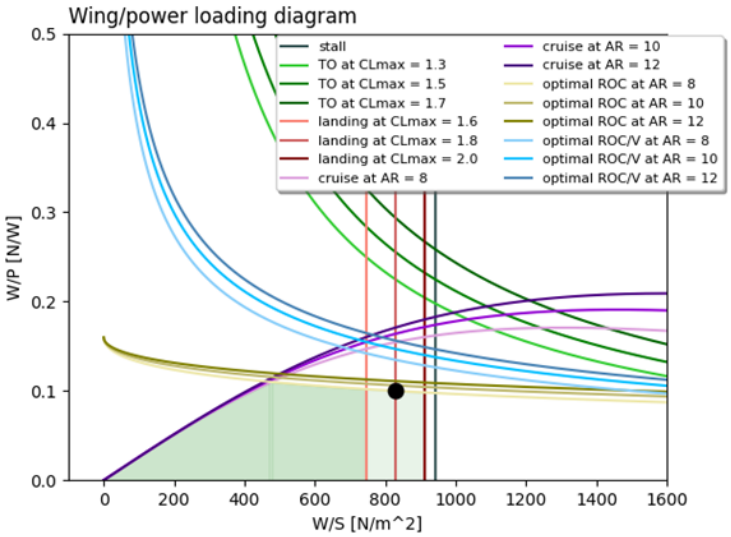

Figure 8.1: *$W/S - W/P$ diagram for the cruise vehicle*

[2]http://wpage.unina.it/fabrnico/DIDATTICA/PGV_2012/MAT_ESERCIT_GEN/CDo_Estimation.pdf [Accessed 15 May 2024]

[3]https://www.easa.europa.eu/en/document-library/certification-specifications/group/cs-23-normal-utility-aerobatic-and-commuter-aeroplanes#cs-23-normal-utility-aerobatic-and-commuter-aeroplanes [Accessed on 16 May 2024]

Note that the maximum lift coefficients and aspect ratios have been varied. The feasible design space is indicated with green. Light green is used to indicate the design space for landing with a maximum lift coefficient between 1.6 and 2.0. The upper right corner of the design space corresponds to the maximum feasible wing loading for a minimum power loading; note that $\frac{W}{P}$ is the inverse of the power loading. When a maximum lift coefficient of 1.8 is assumed, the values found at the point indicated in the diagram are a wing loading of 829 N/m^2 and a power loading of 10.0 W/N.

8.2. Flight Profile

Defining what the different parts of the flight regime of the cruise vehicle look like is a crucial part of analyzing the performance of the design. Furthermore, the velocities and duration of the different flight phases are inputs of the energy calculations which have been carried out in Section 5.2.5. In this section, the design mission of a range of 50 kilometers will be analyzed. The flight regime of the design mission can be split into seven parts. The first phase is the vertical take-off. Here, the lifting vehicle provides the power to lift the cruise vehicle into the air vertically. In the second phase, the cruise vehicle starts to provide forward thrust, such that its wings can generate enough lift to sustain its own weight. At the end of this phase, the lifting vehicle decouples and flies back. In the third phase, the cruise vehicle climbs to the cruise altitude, and in the fourth phase, the cruise vehicle performs its cruise. After this phase, the cruise vehicle descends to an altitude where the lifting vehicle cruises, and at the end of this phase, the lifting vehicle recouples. In the last two phases, the vehicles slow down horizontally, and descend vertically until they land at the vertiport. All of these phases will be described in more detail below.

8.2.1. Vertical Take-off

From the requirements, the vertical acceleration of the vehicles at take-off $a_{v,TO}$ is 2 m/s^2. The vertical speed $V_{v,TO}$ at which the vehicles climb is set at a value of 6 m/s. The altitude which needs to be reached by the vehicles before the next phase starts is 450 meters. The vertical distance that needs to be travelled differs depending on the altitude of the top of the buildings off of which the vehicles take off. To obtain a maximum duration for this first phase of the flight regime, the vertiport can be assumed to be at sea level. It takes three seconds and almost fourteen meters to achieve the vertical speed of 6 m/s with the vertical acceleration of 2 m/s^2. This time and distance is doubled as the vehicles decelerate in the same time and distance. The remaining distance of 423 meters is traveled in less than 71 seconds at the vertical speed of 6 m/s. This means the vertical take-off phase takes a total time $t_{v,TO}$ of approximately 77 seconds.

8.2.2. Horizontal In-air Take-off and Decoupling

When the altitude of 450 meters is reached, the lifting vehicle generates enough lift to keep both vehicles at constant altitude. Then, the engine of the cruise vehicle starts providing thrust, such that a horizontal acceleration $a_{h,TO}$ of 1.6 m/s^2 is reached. As a result of the horizontal direction of flight, the wings of the cruise vehicle start generating lift through the incoming airflow. The rotors of the lifting vehicle will produce less lift by lowering their rotational speed. This is required because the cruise vehicle will start sustaining its own lift by the generated lift. The combination of vehicles are still connected and should keep a constant altitude. Once the vehicles reach the stall speed of the cruise vehicle, enough lift is generated by its wings to keep itself in the air. For safety, however, the lifting vehicle will only decouple once a horizontal speed of 1.15 times the stall speed is reached. This safety margin of 1.15 is chosen because under normal circumstances, take-off from a runway occurs at between 1.1 and 1.2 of the stall speed. With a minimal vertical acceleration of 2 m/s^2 and the stall speed calculated according to the general lift formula with the maximum lift coefficient of the cruise vehicle, the speed at which the cruise vehicle and lifting vehicle can decouple is just under 30 m/s. This means it would take the combination of vehicles approximately 19 seconds and 282 meters. This means that the entire take-off phase takes up 100 seconds.

When the lifting vehicle and the cruise vehicle have decoupled at 1.15 the stall speed, they continue to fly independently. From this point, the lifting vehicle has to fly back to the vertiport or couple with

another cruise vehicle. The cruise vehicle continues its flight to the destination vertiport. These phases of the flight will be analyzed separately in more detail below.

8.2.3. Climb to Cruise of the Cruise Vehicle

Once the lifting vehicle has been decoupled, the cruise vehicle can start climbing to the cruise altitude of 1200 meters. It will already have been accelerating at this point. The climb happens with a rate of climb of 4.5 m/s. The optimal horizontal speed to climb can be calculated with Equation 8.6 [53].

$$ROC = \frac{P_{installed}}{m} \cdot \frac{\eta_p}{g} \cdot \frac{V_{horizontal}}{\frac{L}{D}} \tag{8.6}$$

In this equation $\frac{P_{installed}}{m}$ is the installed power in kW per kg of the cruise vehicle. As a result, the cruise vehicle will climb with a speed of approximately 45 m/s or 162 km/h. This means that it will accelerate during climb as well, since this speed is higher than the speed the vehicle has directly after decoupling. Assuming full acceleration after decoupling, the climb starts with an initial speed of about 30.5 m/s, at 300 m distance of the vertiport location. Given a vertical acceleration of 2 m/s^2 and a horizontal acceleration of 1.6 m/s^2, gives approximately a climb acceleration of 2.5 m/s^2. This means the optimal speed for climb is obtained after a little less than 6 seconds. The minimum rate of climb of 4.5 m/s will be obtained earlier. This not a problem however. Taking a conservative approach however, means that the entire climb phase will take approximately 167 seconds, and a horizontal distance of 7500 m is covered during the climb phase of the cruise vehicle.

8.2.4. Cruise of the Cruise Vehicle

Once the cruise vehicle reaches the cruise altitude, it will level out and accelerate to the nominal cruise speed of 200 m/s. It will do so again with an acceleration of 1.6 m/s^2. Assuming the aircraft does not lose speed during the level-off, this takes approximately 7 seconds. Then the cruise vehicle performs level flight at the specified cruise vehicle, and might change flight altitude according to instructions from the Air Traffic Control.

8.2.5. Descent to Coupling Altitude of the Cruise Vehicle

Once the cruise vehicle is at a specified distance from the vertiport where it will land, it will initiate its descent. The rate of descent is 9 m/s. Lowering the altitude to the required 450 m for coupling will take approximately 167 seconds. Descent is usually performed at cruise velocity [53], unless this creates unrealistic high descent angles. In this case, the descent angle at cruise velocity and with specified rate of descent will be 9.3°. This is a relatively high angle, but not uncommon; it is justified by the specific type and duration of the mission. Thus, the first part of the descent will be performed at cruise speed. However, the cruise vehicle is required to fly near 1.15 times the stall speed when it levels out at 450 m altitude. It is therefore expected that it slowly reduces its velocity during the initial descent, so that it flies at approximately 35 m/s when it reaches coupling altitude. This is done gradually. Thus, the horizontal distance covered is roughly 7150 m.

8.2.6. Horizontal In-air Landing

This phase starts where the cruise vehicle further reduces it velocity until it attains the required 1.15 times the stall speed. The multicopter aligns with the cruise vehicle and couples. The combination of the two vehicles decelerates until zero horizontal speed is obtained. This is done similarly as for the horizontal landing. It will thus also take approximately 19 seconds and a distance of 300 meters. At that point, the vehicles will be directly above the vertiport.

8.2.7. Vertical Landing

The vertical landing of the two vehicles will be comparable to the vertical take-off in terms of acceleration, velocity, travelled distance, and time it takes. Thus, the total landing procedure will take just under 100 seconds.

8.2.8. Climb to Cruise of the Lifting Vehicle

After the cruise vehicle and lifting vehicle decouple at an altitude of 450 m, and the cruise vehicle accelerates away from the lifting vehicle, the lifting vehicle can perform multiple different types of flight. This depends on the demands of the Air Traffic Control tower. The case analyzed in the following subsection will be the most critical one; the lifting vehicle is required to gain a higher altitude and loiter at that altitude until it has permission to either couple with a cruise vehicle or land independently.

Thus, after decoupling, the lifting vehicle will have a velocity of approximately 30 m/s. It will decelerate horizontally and accelerate vertically to obtain an altitude of 700 m. This horizontal deceleration will be performed because straight, vertical acceleration is the most efficient way for the lifting vehicle to climb, due to its design. It is assumed the vehicle again has a maximum horizontal acceleration of (-)1.6 m/s^2, and a maximum vertical acceleration of (-)2 m/s^2. This is a conservative approach since these are the same accelerations the vehicle can obtain while coupled with the cruise vehicle. It is much lighter in this case since it does not carry the lifting vehicle. Therefore, once the cruise vehicle is decoupled and a safe distance away, the lifting vehicle will put its power to vertical acceleration. Climbing for 700 m, with the specified acceleration, and a maximum vertical velocity of 6 m/s, and then again decelerating to obtain zero vertical velocity - this is again a conservative approach - this part will take about 57 seconds. The horizontal speed during this maneuver will reduce due to the drag. Assuming the drag is proportional to the speed, since only a small altitude increase does not alter the air density much, and Newton's second law, the following differential equation can be constructed, Equation 8.7.

$$\frac{dV}{V^2} = \frac{C_D}{m} dt \tag{8.7}$$

The drag coefficient is the drag coefficient of the lifting vehicle in horizontal flight, which is 0.4. The variable m signifies the mass of the lifting vehicle. Integrating both sides of the equations, solving for the integration constant with the initial condition of V(0) = 30 m/s, allows solving for horizontal speed when the lifting vehicle reaches the loiter altitude. This is about 17 m/s. The lifting has then covered a horizontal distance of approximately 1350 m. Then, again depending on the commands of the ATC, the lifting vehicle can either hover in the air until further instructions or fly to another vertiport.

8.2.9. Cruise of the Lifting Vehicle

Assuming the most critical case in which the lifting vehicle has to fly to the closest vertiport, not the one it has taken off from, the lifting vehicle will accelerate to obtain a cruise speed of 30 m/s. It is assumed the average distance between intra-city vertiports is 10 km, which will be further explained in Section 15.2. The lifting vehicle will start its descent to the coupling altitude in a similar way as the ascent to the cruise altitude, but in an opposite manner. Therefore, it is expected this will take approximately the same time and distance. Once the lifting vehicle has obtained a speed of 30 m/s it is ready to couple with a cruise vehicle and safely guide both of them to the vertiport location.

Another possibility is that no cruise vehicle close by requires assistance with landing. In that case, the lifting vehicle will continue its flight at an altitude of 700 m until it nears the vertiport location. The required horizontal distance to reduce its horizontal velocity to 0 m/s is approximately 300 m. At the same instant the lifting vehicle is reducing its horizontal velocity, it will start descending. The earlier-mentioned acceleration and maximum vertical velocity cause this maneuver to take about 120 seconds.

8.2.10. Flight Profile Diagram

A visual representation of the flight phases, described above, is a flight profile diagram. Two of those diagrams have been constructed, one for the lifting vehicle and one for the cruise vehicle. They are the result of the explanations and calculations described in the sections above. The flight profile for the lifting vehicle is shown in Figure 8.2, the one for the cruise vehicle in Figure 8.3.

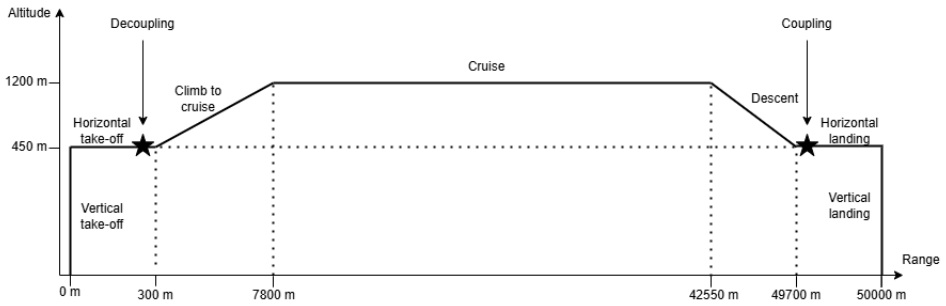

Figure 8.2: *A flight profile for the cruise vehicle*

Note that the diagram has not been drawn to scale. Also, there is a margin for both the vehicles after decoupling to remain in horizontal flight. This is in order to obtain an appropriate horizontal distance before the cruise vehicle, and possibly the lifting vehicle as well, start ascending.

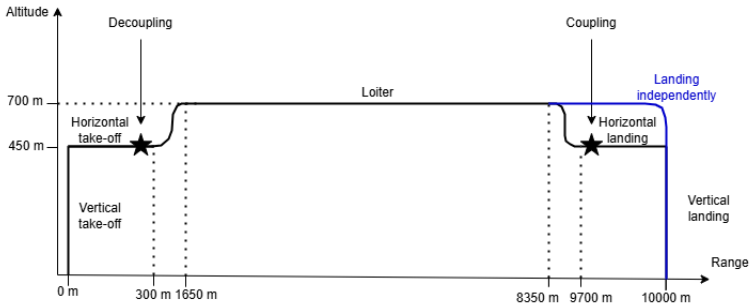

Figure 8.3: *A flight profile for the lifting vehicle*

In Figure 8.3, the blue line indicates the flight path of the lifting vehicle if it will not couple and land with a cruise vehicle. This will not a non-standard flight path, since optimal use of the lifting vehicle will ensure that is always takes off and lands with a cruise vehicle attached. In short, a flight mission looks as visualised in Figure 8.4.

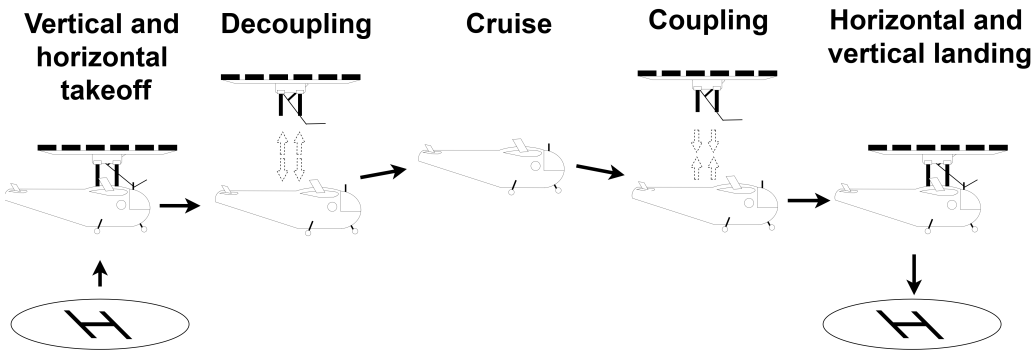

Figure 8.4: *A simplified visualisation of a typical flight mission*

8.3. Load Factor Diagram

During operations, the cruise vehicle will experience maneuver and gust loads. To size the aircraft, both the maximum and minimum loads need to be found, which is done using the load factor diagram. This diagram relates the speed of the aircraft to the load factor it experiences, defined as the lift produced by the aircraft over its weight.

The maneuver load envelope shows the load factor an aircraft experiences during maneuvers at different airspeeds. To construct this diagram, Equation 8.8 is used. The load factor increases quadratically

with velocity, occurring at the maximum lift coefficient configuration, as depicted by the blue line in Figure 8.5. Similarly, a negative load factor can be achieved by performing a downward maneuver. The load factor is bounded by regulatory requirements at a maximum of 3.8 and a minimum of -1.5 [17]. Beyond these points, increasing the velocity does not increase the load factor, as shown in Figure 8.5. The maximum speed the aircraft can achieve is its dive speed, which corresponds to a load factor of zero. Connecting velocities and their corresponding load factors yields the maneuver envelope.

$$n = \frac{\rho V^2 C_L}{2\,W/S} \tag{8.8}$$

When a gust acts on the aircraft, it will have a velocity v in the direction of the airfoil and a velocity u perpendicular to the direction of the airfoil. The angle of attack will temporarily be increased, as shown in Equation 8.9. Using a small angle approximation, and assuming that $v << V$, the difference in load factor can be calculated with the second part of Equation 8.9 using the lift slope C_{L_α} of the aircraft. According to CS-23 regulations, the aircraft must withstand different gust speeds for its different velocities at cruise, dive, and speed at its greatest possible angle of attack [17]. The gust speeds can be both positive and negative. Assuming that the aircraft is in level flight, a value of one is added to the calculated change in load factor to get the experienced load factor. Connecting the required load factors for each velocity and respective gust speed yields the gust load envelope, illustrated by the red line in Figure 8.5. Finally, the maximum and minimum load factors to design for are given by the highest and lowest load factors of the combined maneuver and gust loading diagrams, illustrated in Figure 8.5.

$$\Delta\alpha = \arctan\frac{u}{V+v} \qquad \delta n = \frac{pVC_{L_\alpha}u}{2W/S} \tag{8.9}$$

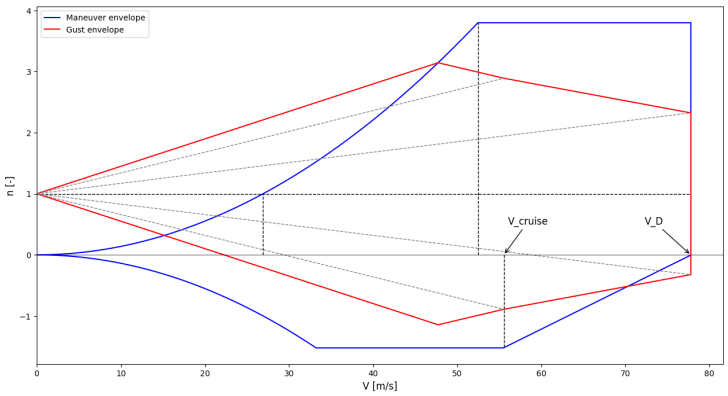

Figure 8.5: *V-n diagram for the cruise vehicle*

From Figure 8.5, the maximum load factor was found to be 3.75. This value is critical for the design process, ensuring that the aircraft's structure is robust enough to handle the most severe conditions it may face during operation. It will dictate the structural requirements of the aircraft, guiding the selection of materials, component design, and safety margins.

9

Aerodynamic Characteristics

In order to more accurately calculate the performance of the vehicles, the design and aerodynamic characteristics of the wing of the cruise vehicle are analysed in detail. Thus, after the initial wing sizing was performed based on the wing loading diagram, a more detailed aerodynamic analysis was conducted. First, the lift distribution and stall location over the wing were analyzed in order to minimize the drag and optimize the stall location. Then, Javafoil was used to select an airfoil and perform the initial analysis of its 2D characteristics. Subsequently, XFLR5 was used to translate these 2D characteristics into a 3D analysis of the aerodynamics of the cruise vehicle.

9.1. Airfoil Selection

Given the vehicle's mission, the airfoil was chosen to optimize cruise efficiency. This entails selecting an airfoil that produces its largest lift over drag ratio at the cruise lift coefficient, which was computed using Equation 9.1. Using the previously determined wing loading, which is given in Section 8.1, along with the cruise speed V_{cruise} and the density from the requirements, a cruise lift coefficient of 0.49 was obtained.

$$C_{l,cruise} = \frac{W}{S} \frac{2}{\rho V_{cruise}^2} \tag{9.1}$$

The airfoil with 2% camber provides an efficient lift generation capability. During cruise, the wing must produce sufficient lift to counteract the vehicle's weight, while simultaneously minimizing its drag. This camber level helps achieve a favorable lift-to-drag ratio, crucial for efficient cruising. Additionally, an 18% thickness-to-chord ratio enhances the structural integrity of the wing compared to a thinner airfoil. While this characteristic is usually more relevant for larger aircraft, in this case the higher ratio is beneficial for the vehicle's wing structure, which will be required to support the loads of the coupling mechanism as well as the predicted aerodynamic loads without excessive deformation. This thickness also allows for a relatively smooth airflow, reducing form drag and maintaining efficient lift production. The maximum camber position at 40% of the chord length results in a pressure distribution that minimizes adverse pressure gradients, contributing to smoother airflow over the wing and enhancing aerodynamic efficiency during cruise. The NACA 2418 airfoil design ensures a predictable and smooth stall behaviour, which is beneficial for maintaining control at various speeds and during different flight phases. During cruise, having an airfoil that behaves predictably near stall conditions increases its safety and reliability, whilst also improving handling characteristics and simplifying its operations and maintenance.

From the C_l - C_d plot in Figure 9.1, it was found that the maximum lift over drag ratio of the airfoil occurs between a lift coefficient of 0.49 and 0.55. As this corresponds to the cruise lift coefficient, this airfoil was deemed suitable to perform cruise in the most efficient way.

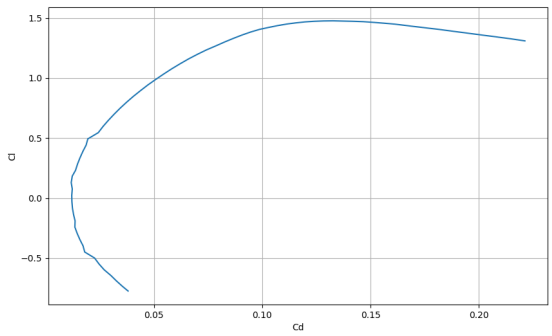

Figure 9.1: *C_l - C_d plot for the airfoil*

9.2. Wing Planform Configuration

To facilitate coupling and provide clearance for the propellers, a high-wing configuration was chosen. This configuration not only enhances operational flexibility but also improves ground clearance for the propellers, reducing the risk of damage during takeoff and landing. Additionally, the high-wing design contributes to better visibility for the pilots, enhancing overall safety.

The ideal lift distribution for a wing in order to minimize drag resembles an elliptical loading [27]. This lift distribution can be altered by modifying wing parameters. It was found that a low taper ratio would yield the lift distribution closest to an elliptical loading. However, due to the taper, the tip chord is smaller than the root chord, resulting in a lower Reynolds number at the tip. This causes the wing to stall near the tip first, which is unacceptable as it introduces a rolling moment and can result in the loss of aileron control. Therefore, wing twist was introduced in order to lower the angle of attack near the tip, significantly affecting the lift distribution.

As twist tends to introduce structural challenges into the structure, it was decided that the twist would be kept to the minimum necessary to avoid tip stalling. Using Javafoil, the required twist for every taper ratio analyzed was determined. These taper and twist combinations were then input into XFLR5 in order to obtain the lift distribution. The lift distributions produced at an angle of attack of 2.5 degrees, corresponding to the cruise condition, were exported to a Python script to calculate the root mean squared deviation (RMSD) between this lift distribution and an elliptical lift distribution. The combination with the lowest RMSD was considered the optimal configuration for the cruise vehicle. This resulted in a taper ratio of 0.79 and a washout of 2.1 degrees, meaning the tip of the airfoil has an angle of attack 2.1 degrees lower than the root at all times. The final lift distribution of the wing at the cruise angle of attack, obtained from XFLR5, is illustrated in Figure 9.2 with the red line. The gray line shows the ideal elliptical distribution.

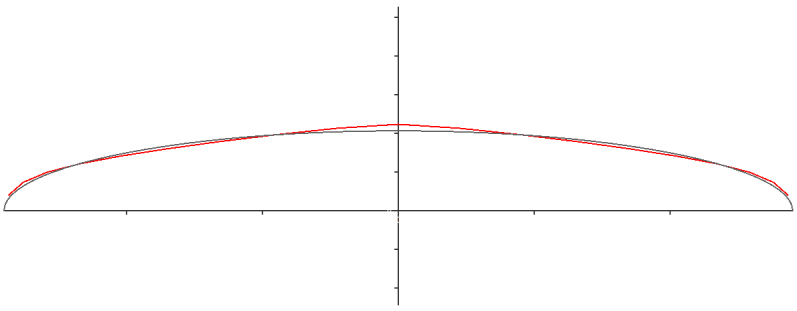

Figure 9.2: *Lift distribution during cruise*

9.2.1. Aileron Sizing

In order to size the ailerons, the requirements for roll were taken into account. The cruise vehicle was deemed to be a class I aircraft according to MIL-F-8785 [41], requiring a roll performance of 60 degrees

in 1.3 seconds. The time required to achieve a certain bank angle change $\Delta\phi$ and the roll rate P are defined by Equation 9.2.

$$\Delta t = \frac{\Delta\phi}{P} \qquad P = -\frac{C_{l_{\delta a}}}{C_{l_p}}\delta a\frac{2V}{b} \tag{9.2}$$

The aileron control derivative $C_{l_{\delta a}}$ and the roll damping coefficient C_{l_p} are calculated using Equation 9.3, where S_{ref} is the reference surface area of the wing. The aileron effectiveness τ used in Equation 9.3 was found using Figure 9.3.

$$C_{l_{\delta a}} = \frac{2c_{l\alpha}\tau}{S_{ref}b}\int_{b_1}^{b_2} c(y)ydy \qquad C_{l_p} = -\frac{4(c_{l\alpha}+c_{d_0})}{S_{ref}b^2}\int_0^{b/2} y^2c(y)dy \tag{9.3}$$

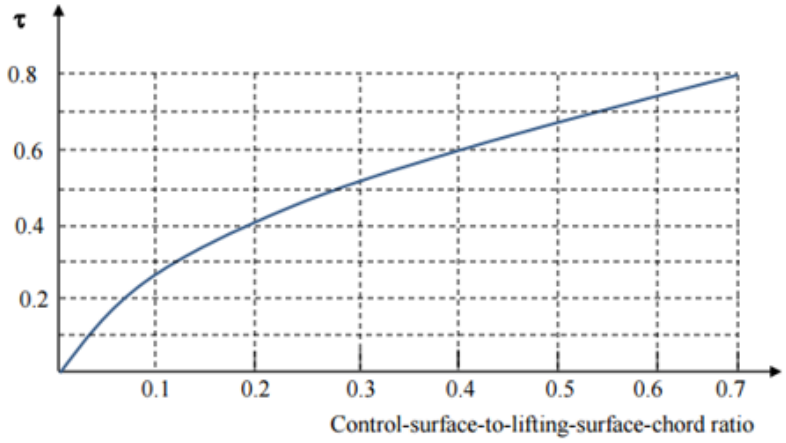

Figure 9.3: *Aileron effectiveness*

Having the ailerons start at 71% of the halfspan and end at 97%, with a 30% chordwise width, was deemed to be the best configuration for the vehicle in order to satisfy the roll requirement.

9.2.2. High Lift Devices

The airfoil selection led to a final decision on the NACA2418 airfoil, with a maximum clean lift coefficient of 1.4. This allows for an optimization of the vehicle's performance during cruise, as previously discussed in Section 9.1. However, during coupling and decoupling, the vehicle will need to fly at the lowest possible speeds to maximize coupling efficiency and safety. The coupling speed can be as low as 30 m/s, and for this case the wing should provide a higher lift than can be provided by the cruise configuration.

High Lift Devices (HLDs) are used to increase the maximum lift coefficient generated by the wing, with various types available depending on the required increase in $C_{L,max}$. Based on the clean $C_{L,max}$ of the wing of 1.5, and the maximum $C_{L,max}$ of 2.1 required to achieve a stall speed of 25 m/s, as this is the preferred stall speed, the HLD chosen should generate an additional $\Delta C_{L,max}$ of 0.7.

$$\Delta C_{L,max} = 0.9\Delta C_{l,max}\frac{S_{flapped}}{S_{ref}}\cos\Lambda_{HD} \qquad \Delta\alpha_{OL} = (\Delta\alpha_{OL})_{airfoil}\frac{S_{flapped}}{S_{ref}}\cos\Lambda_{HD} \tag{9.4}$$

Equation 9.4 was used to estimate the increase in maximum lift coefficient and the decrease in zero lift angle of attack. $\Delta C_{l,max}$ depends on the type of HLD used and is taken from Raymer [53]. With the sizing of the flaperons completed, the changes in $C_{L,max}$ and α_{OL} were estimated. It was found that the flaperons would increase the maximum lift coefficient by 0.15 and reduce the zero lift angle of attack by about 2 degrees.

Since a significant increase in $C_{L,max}$ was still required, double slotted flaps were selected. Their weight was estimated using Equation 9.5 [35], and found to be about 85 kg. According to Raymer

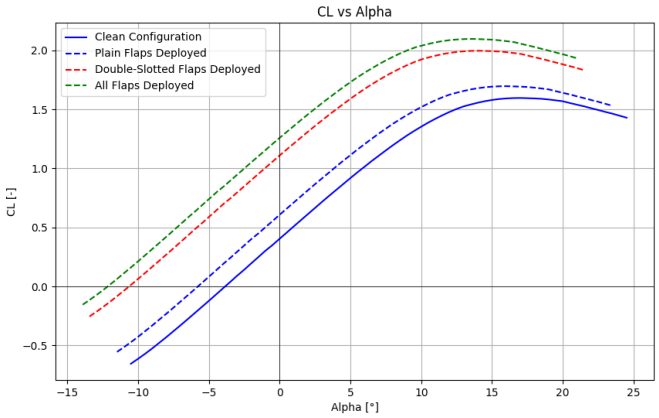

Figure 9.5: *Lift curve for the aircraft with and without HLD*

[53], $\Delta C_{l,max}$ for double slotted flaps is defined as 1.6 c'/c. The ratio c'/c is dependent on the flap type and deflection. Figure 9.4, along with Equation 9.6, can be used to determine $\Delta c/c_f$. Using the same chordwise flap length as the flaperons results in an increase in the maximum lift coefficient of 0.55 and a reduction in the zero lift angle of attack by nearly 5 degrees.

$$W_{TE_f} = 100 k_{TE_f} \left(1 + \sqrt{\frac{W_{TO}}{10^6}}\right) S_{TE_f} \tag{9.5}$$

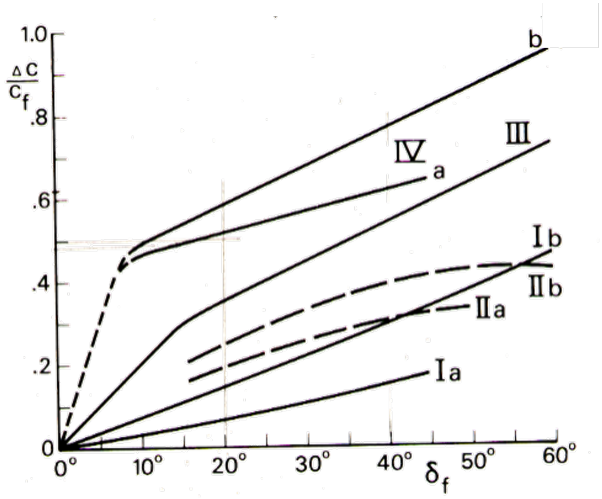

Figure 9.4: $\Delta c/c_f$ *as a function of flap deflection [59]*

$$c' = c + \Delta c \tag{9.6}$$

Given the low takeoff and landing speed requirements due to the coupling process, it was decided to introduce flaperons. This entails that the ailerons will also be used as plain flaps during the take-off and landing phases in order to maximize the lift coefficient. This results in an additional increase in $C_{L_{max}}$ of 0.15 and 2.4 degrees of decrease in zero lift angle of attack. Combining both flap systems results in a total increase in the maximum lift coefficient of 0.7, bringing the lift coefficient to the required value of 2.1. Additionally, the zero lift angle of attack decreases by 6.6 degrees, resulting in a new zero lift angle of attack of -8.8 degrees. The stall speed is then reduced to 25.4 m/s, occurring at an angle of attack of 11.2 degrees. The final lift polar with and without the high lift devices for the plane can be seen in Figure 9.5.

9.2.3. Winglets

Winglets are wingtip devices used to reduce the induced drag of a fixed wing vehicle. This is done by reducing the formation of wingtip vortices, which are created by the difference in air pressure on the upper and lower surfaces of the wing [61]. For the sizing and positioning of the winglets, the design guidelines outlined by Raymer [53] were followed.

The winglet design was optimized to reduce drag. It was decided not to include the bottom winglet panel, as it contributes significantly less to drag reduction. An analysis conducted by Whitcomb [61] indicated that the addition of a lower winglet in all flight conditions resulted in only marginal performance improvements. The NACA 8608 airfoil was selected for the winglets as winglets should typically have a higher camber than the wing's airfoil [53]. With the addition of winglets, the effective AR of the wings increases, which was computed using Equation 9.7, where h is the winglet height. According to Raymer [53], this winglet height can be taken as the tip chord of the wing.

$$AR_{eff} = AR(1 + \frac{h}{b})^2 \tag{9.7}$$

9.3. Oswald Efficiency Estimation

A method outlined by Nita [45] was used to estimate the Oswald efficiency factor of the aircraft. The method consists of computing a theoretical Oswald factor, which is subsequently corrected for the influence of the fuselage, zero lift drag and mach number. Firstly, a theoretical Oswald factor was obtained by using Equation 9.8, where Figure 9.6 was used to find $f(\lambda)$. Due to the effect of the twist on the wing, the function shifts to the right, with the chosen taper ratio of 0.79 corresponding to the point with the minimum value of $f(\lambda)$.

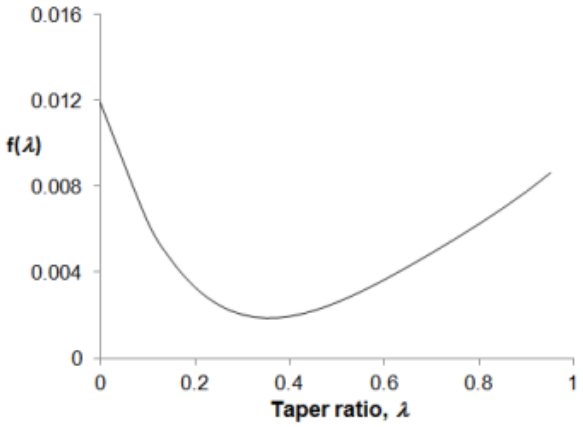

Figure 9.6: *Function of f(λ) [45]*

$$e_{theo} = \frac{1}{1 + f(\lambda)AR} \qquad e = e_{theo} k_{e,F} k_{e,D0} k_{e,M} \tag{9.8}$$

The Oswald efficiency factor was estimated using Equation (9.8). The equation takes into account the influence of the fuselage, zero lift drag and Mach number on the Oswald factor. The contribution from the fuselage can be calculated using Equation (9.9), where $\frac{d_F}{b}$ corresponds to the fuselage diameter over span ratio. The values for $k_{e,D0}$ and $k_{e,M}$ were obtained from Nita Equation (9.8). Using this method, the Oswald factor was estimated to be 0.78 with the inclusion of winglets.

$$k_{e,F} = 1 - 2\left(\frac{d_F}{b}\right)^2 \tag{9.9}$$

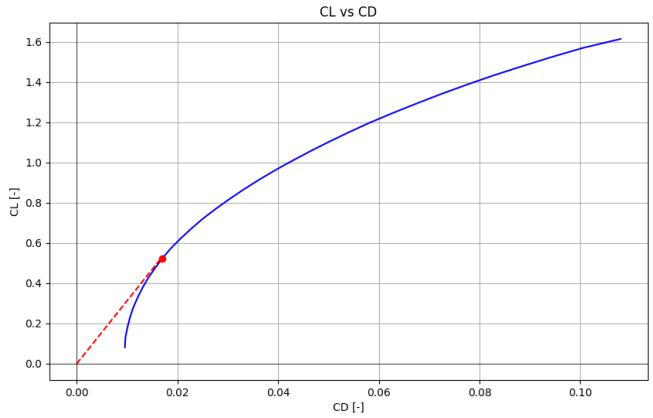

Figure 9.7: *Lift-drag polar for the aircraft*

9.4. Drag Estimation

In order to find values for the thrust required from the propulsion system, the drag needs to be estimated. To calculate the parasite drag of the cruise vehicle, a component buildup method was used, which estimates the drag of each component. This method uses the assumption that during cruise, the parasite drag of a well designed aircraft is composed of mostly flat-plat skin-friction and and pressure drag [53]. Equation 9.10 is used to calculate parasite drag.

$$C_{D_0} = \frac{\sum (C_{f_c}) FF_c \, Q_c \, S_{wet_c}}{S_{ref}} + C_{D_{misc}} \tag{9.10}$$

The terms C_f, FF, and Q represent the skin friction, the form factor, and the interference effects of each component on the component drag. The total component drag is computed as the product of these three values. Then, the total parasite drag of the aircraft is given by the sum of the components' drag and $C_{D_{misc}}$, which is an estimate of the drag of the flaps and the landing gear. Equation 9.11 estimates the form factor of the wing, tail, strut and pylon, and Equation 9.12 gives the form factor of the fuselage.

$$FF = \left[1 + \frac{0.6}{(x/c)_m}\frac{t}{c} + 100\left(\frac{t}{c}\right)^4\right]\left[1.34M^{0.18}\left(\cos\Lambda_m\right)^{0.28}\right] \tag{9.11}$$

$$FF_{fuselage} = \left(0.9 + \frac{5}{f^{1.5}} + \frac{f}{400}\right) \quad f = \frac{l}{d} = \frac{l}{\sqrt{(4/\pi)A_{max}}} \tag{9.12}$$

Similarly, to find the thrust required by the lifting vehicle both when coupled with the cruise vehicle and when in the decoupled configuration, its drag needs to be found. At this preliminary stage of the design, the shape of the lifting vehicle is not yet finalized, so to have conservative estimates, it was modelled as a rectangular box with an angled nose. The drag coefficients for simple shapes at given Reynolds number are known [24]. To find the drag coefficient of the lifting vehicle during horizontal flight, the body was modelled as an angled cube and the rotor hubs were modelled as a collection of cylinders. For vertical flight, when the lifting vehicle raises the cruise vehicle, the lifting vehicle was modeled as a cube. The wings and fuselage of the cruise vehicle were modeled as a flat plate and a long cylinder, respectively. This conservative modeling approach provides higher drag estimates, ensuring that there is a buffer for design uncertainties and performance variations. The final lift drag for the aircraft is shown in Figure 9.7.

10

Structural Analysis

Structural design is crucial for the final product as it integrates the design choices of the subcomponents and ensures the design operates safely. In order to finalize the structural design, suitable structural analysis must be performed to create a reliable design. This chapter presents the preliminary structural design choices made for KoriAir and the analysis behind its choices for both the lifting vehicle and the cruise vehicle. It starts with the description of the lifting vehicle airframe in Section 10.1, followed by the wing box design of the cruise vehicle, given in Section 10.2.

10.1. Lifting Vehicle Airframe

To ensure that the vehicle can operate as demanded, the structure must be able to withstand the load. The airframe of the lifting vehicle is assumed to be a box with four arms supporting the rotors. This section elaborates on the structural choices made for the lifting vehicle. The primary structural loads to which the lifting vehicle is subjected include bending, vibrations, and fatigue loading. The bending moment is caused by the thrust generated by the rotors, the weight of the vehicle, and the reaction forces due to the coupling mechanism. Fatigue loading is caused by cyclic loading. Vibrations are another important load case that shall be considered when designing the airframe of the lifting vehicle. The lifting vehicle has spinning rotors generating thrust. The magnitude of the thrust generated by the rotors is not uniform but fluctuates which causes the structure to vibrate.

For the lifting vehicle, both the fuselage itself and the arms supporting the rotors will be covered. This is done in Section 10.1.1 and Section 10.1.2 respectively. Before the analysis, the coordinate system that is adopted is defined in Figure 10.1.

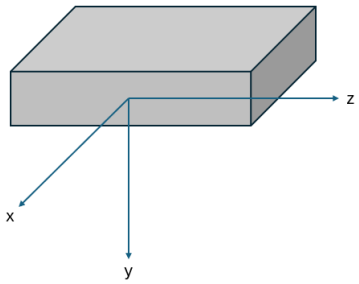

Figure 10.1: *Coordinate system for lifting vehicle analysis*

10.1.1. Fuselage Design

Firstly, the bending stress on the lifting vehicle caused by the loads applied to the vehicle was analyzed. The bending stress that the structure is subjected to is caused by the bending moments M_x and M_y. The relationship between the two is as given in Equation 10.1 [40].

$$\sigma = \frac{(M_x I_{yy} - M_y I_{xy})y + (M_y I_{xx} - M_x I_{xy})x}{I_{xx} I_{yy} - I_{xy}^2} \tag{10.1}$$

Here, I_{xx}, I_{yy} and I_{xy} correspond to the moment of inertia of the lifting vehicle. To utilize this equation, the moment and the area moment of inertia must be identified. For this analysis, the bending moment

in the x-direction was considered. The bending moment is transferred through the arms to the fuselage. Due to the symmetry of the box and the design choice of using the symmetric stiffeners, Equation 10.1 can be simplified to Equation 10.2.

$$\sigma = \frac{M_x y}{I_{xx}} \tag{10.2}$$

The main goal of this analysis was to ensure that the bending stress experienced by the structure is lower than the yield strength of the material, as exceeding this value can cause catastrophic failure. Therefore, the maximum value of y, which is half of the height of the box, was used. Another main objective is to reduce the weight of the lifting vehicle. Therefore, the iteration was done to minimize the weight whilst keeping the bending stress experienced by the structure lower than the yield strength of the material.

In addition, the stiffener type was chosen to ensure that the box is stiff enough to resist the bending moments. A higher area moment of inertia represents higher resistance to bending. Oftentimes, the L-shaped stiffener is used, as it provides an adequate amount of moment of inertia and has a lower weight than the I-beam. However, with the L-shaped stiffener, the polar moment of inertia must be calculated as the cross-sectional area is not symmetric about the x-axis and y-axis. This increases the complexity greatly. Therefore, a reverse T-shaped stiffener was used with its horizontal part attached to the skin, as its moment of inertia about the x-axis would be the same as the L-shaped and the weight would be very similar. The final parameters of the box have been summarized in Table 6.1.

10.1.2. Arm Design

Another part of the airframe which must be designed is the set of four arms supporting the rotors. They are modelled as I-beams. Similar to the fuselage, the main load is the bending caused by the rotors. Normal stress along the section can be calculated using Equation (10.1). However, the thrust T is not perpendicular to the arm. Therefore, the additional normal component must be added depending on the angle Φ between the fuselage and the arm. The stress which needs to be added is described by Equation 10.3 [40].

$$\sigma = \frac{T \sin \Phi}{A} \tag{10.3}$$

The same principle as for the design of the fuselage is applied. Multiple configurations of I-beam dimensions were considered and the lightest out of all meeting the requirement for the allowable stress was chosen.

Moreover, analysis on vibrations was conducted. Due to the spinning rotor, the aircraft is subjected to vibrations. The critical parts, subjected to vibrations, are the arms that connect the fuselage and the rotors. The arms are assumed to be beams, such that modal analysis can be conducted in order to ensure its integrity against vibrations.

The beam is in a diagonal orientation and no vibration in the x-axis is assumed. Thus, the beam is assumed to be a vertical spring with displacement in the y-axis. The spring's stiffness is equal to the beam's stiffness in the y-direction of the beams, as it is assumed that there is no displacement in the x-axis. The stiffness coefficient of the beam can be calculated with Equation 10.4.

$$k_g = \frac{3EI}{L^3 \sin \theta} \tag{10.4}$$

The engine produces undamped harmonically forced vibrations. Thus, the standard solution seen in Equation 10.5 [40] is used to perform a modal analysis. c_1 and c_2 are constants obtained from the initial conditions.

$$x(t) = c_1 \cos(\omega_n t) + c_2 \cos(\omega_n t) + \frac{f_0}{\omega_n^2 - \omega_f^2} \cos\left(\omega_f t + \phi\right) \tag{10.5}$$

The forcing frequency ω_f of the engine is assumed to be equal to the RPM velocity of the engine (2600 RPM = 43.334 Hz) in Hz and the force amplitude is assumed to be equal to the mass of the engines (6 engines) being supported (4.7 kg per engine). The natural frequency ω_n (108.51649104038394) is far from the forcing frequency, thus the structure should not undergo resonance.

The lifting vehicle is assumed to be a rectangular prism. While this assumption simplifies the calculation to make structural decisions for the lifting vehicle, it must be noted that this assumption also has consequences. One of the main consequences originates from neglecting the fact that the lifting vehicle may include circular parts to be more aerodynamic, which increases the weight. To take this into consideration, the weight of the structure was increased by a factor of 1.2. The final dimensions of the I-beams which form the the arms from the fuselage of the lifting vehicle to the rotors can be found in Table 6.2.

10.2. Wing Box Design

Another crucial structural element is the wing box of the cruise vehicle. In order to simplify the design process, the wing box has been modelled as a hollow rectangular box which is located in the wing. There are three main aspects to consider: torsion, bending, and shear. Before the analysis, the coordinate system must be defined. The common coordinate system which has its z-axis through its wing span and y-axis down toward the ground is used. More detail on the coordinate system can be found in Figure 10.2. The entire wing box structure consists of two different wing boxes, one on each side, and was assumed to be cantilevered on one end. Figure 10.2 is the free body diagram of one of the wing boxes.

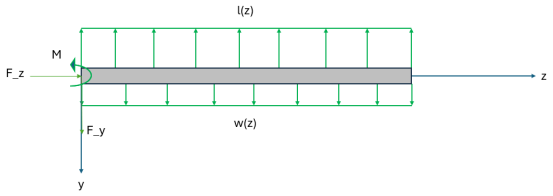

Figure 10.2: *Free body diagram of the wing box*

Firstly, the bending stress was analyzed. The distributed lift and the weight throughout the wing box introduce an internal bending moment, which causes bending stress. The internal bending moment can be found as a function of an axis along the wingspan with adopting a statics approach. Then, using Equation 10.1 the bending stress can be identified. As the wing box is symmetric about the x-axis and y-axis, I_{xy} is zero, and this leads to the equation that was used previously, e.g. Equation 10.2. It must also be noted that the thin-walled assumption was used when determining the moment of inertia. Figure 10.3 shows the free body diagram of the wing box cross-section.

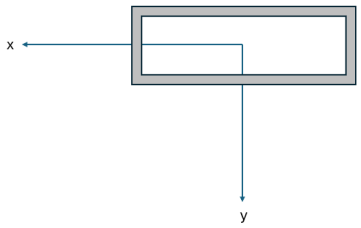

Figure 10.3: *Free body diagram of the wing box cross-section*

After the bending stress analysis, the shear stress also had to be analyzed. The shear stress is caused

by two different forces, namely the shear stress due to the shear force and due to torsion. This analysis can be done separately for the different load cases and it can be summed up to find the total shear stress experienced by the structure.

The distributed lift and the distributed weight introduce shear flow and shear stress into the structure. This leads to shear flow throughout the cross-section which is a quantity often used interchangeably with shear stress for thin-walled structures. The shear flow in a closed section due to the shear force can be found with Equation 10.6 [40].

$$q_s = -\frac{V_y I_{yy} - V_x I_{xy}}{I_{xx} I_{yy} - I_{xy}^2} \int_0^s t y ds - \frac{V_x I_{xx} - V_y I_{xy}}{I_{xx} I_{yy} - I_{xy}^2} \int_0^s t x ds + q_{s0} \tag{10.6}$$

In this equation, q_s is the shear flow in the specified section of the cross-section, and V_x and V_y are the shear force experienced by the cross-section in the x and y direction respectively. The t variable is the thickness of the section which the shear flow is being calculated for, and lastly x and y are the positions of the section expressed in local coordinate s. As mentioned previously, due to the cross-section's symmetry about the x-axis and y-axis the polar moment of inertia, I_{xy} is zero. Therefore the above equation can be simplified to the following, i.e. Equation 10.7.

$$q_s = -\frac{V_y}{I_{xx}} \int_0^s t y ds + q_{s0} \tag{10.7}$$

To utilize Equation 10.7, a cut should be made to establish a point where the shear flow is zero. This must be done prior to the calculation of the shear flow. Equation 10.7 identifies the changes in shear flow from one point to another. The integral should be taken from the point where the cut was made, which is the point where the shear flow is zero. Using this equation, the shear flow throughout the cross-section can be identified. The point where the maximum shear flow occurs can also be identified. The maximum shear is used to identify the maximum total shear flow experienced by the structure.

Secondly, the shear flow caused by torsion was identified using Equation 10.8 [40].

$$\frac{q}{t} = \frac{T}{2tA_m} \tag{10.8}$$

Due to the aerodynamic loads, the wing box is subjected to torsion T. The variable t is the thickness of the wing box and A_m is the area which the wing box covers. Using this equation, the shear flow was calculated. After calculating the shear flow caused by shear force and shear flow caused by torsion, they were added together and divided by the thickness to calculate the shear stress.

In order to minimize the weight of the structure while ensuring that it is structurally reliable, multiple iterations were performed. The main parameters that were optimized were the width and height of the cross-sectional area, and the thickness of the wing box skin. The ranges for which these parameters were set were based on the wing, to ensure that the wing box was not bigger than the wing itself. Additionally, some safety factors were applied. The lift was multiplied by the maximum load factor and a safety factor of 1.5. Additionally, the limits for the bending stress and shear stress were adjusted to ensure a sufficient gap between the stress that the structure experiences and the limit. After consulting with an expert [63], it was decided that 70% of the yield stress and the shear stress may be used as the limit.

After the iterations, it was identified that a titanium wing box would be the optimal design choice for the wing box. However, titanium is often not easily accessible and expensive. Its hard accessibility makes it difficult for maintenance or replacements. For a vehicle like KoriAir, which requires quick repairs, it would be more beneficial to build the wing box out of materials that are more accessible despite the increase in weight. Therefore, it was decided to build the wing box with Aluminum 2024. To elaborate a little further on the selection of material, the Aluminum 2024 was chosen over other

aluminum such as the 6061 and 7075, was due to the fact that it meets the requirements of yield stress and is already used for the aircraft. The latter reason played a significant role as it would make the maintenance or replacement of parts easily as this type of aluminum is also used in other parts of the aircraft.

Additionally, to ensure that the iterations were performed accurately, the calculations of the variables mentioned previously were also done manually to verify the iteration process.

The final values of the wing box are shown in Table 10.1.

Table 10.1: *Final dimensions of the wingbox*

Variable	Dimension
Width	0.54 m
Height	0.15 m
Thickness	4 mm
Mass	88.4 kg

10.3. Further Analysis

The performed structural analysis aimed to provide preliminary structural choices to be made for the aircraft. However, there are further analyses that could be made in the next stage of the design process. Firstly, buckling of the skin of the fuselage should be considered in detail. Buckling in fuselage skin is commonly found in modern aircraft. However, it must be verified that this would not lead to catastrophic failure of the structure. Concepts such as the Johnson parabola or Euler's critical loading can be used to analyze buckling of the structure. Secondly, the fatigue loading of the aircraft can be considered in more detail. Fatigue loading cases were not considered in detail in this report, as it was not feasible to conduct such an analysis with the currently available parameters. As KoriAir aims to become a new method of transportation for daily use, the aircraft will be subjected to cyclic loading. Therefore, fatigue analysis must be done in order to validate that the designs presented can withstand the load cycles that the wing box is subjected to.

Thirdly, the stress concentration due to the cutouts such as the doors and the windows must be analyzed. Due to these cutouts, the stress concentration is subjected to changes, and necessary reinforcement may be applied for the given conditions. This analysis helps to make the aircraft structurally safer. Lastly, further analysis regarding the failure mechanisms can be done in order to prevent catastrophic failures. The aircraft is subjected to many types of loadings. A reliable failure mechanism can ensure the product's safety and longer lifetime. Especially, mechanisms such as the fail-safe mechanism should be considered in order to ensure that the aircraft can still serve its purpose despite a minor failure.

11

Stability and Control Characteristics

As a result of the two-vehicle configuration, the stability and control characteristics are a crucial aspect of the system. A stable vehicle will return to its equilibrium position after a disturbance. For an aircraft, this means that when a gust moves the aircraft, it automatically returns to its original attitude. A controllable vehicle can be moved while in flight. Finding a balance between a controllable vehicle and a stable vehicle is important for safe and comfortable flight. Additionally, during coupling, stability and controllability is crucial to ensure gentle alignment of the two vehicles. In Section 11.1, the stability and control characteristics of the cruise vehicle will be described. Then in Section 11.2, the model for the simulation of the lifting vehicle motion is derived and the controller design is presentd.

11.1. Cruise Vehicle

To analyze the stability and controllability of the cruise vehicle, a scissor plot can be generated. This plot shows the limiting control and stability conditions and returns a feasible center of gravity range. The maximum center of gravity positions during flight must fall within this range.

11.1.1. Stability Limit

The constraints for stability and control are plotted in regard to the ratio of horizontal tail area to wing area $\frac{S_h}{S}$ on the y-axis and center of gravity position $\bar{x}_{cg}$ on the x-axis. Equation 11.1 shows the relation between these two parameters for the stability limit.

$$\frac{S_h}{S} = \frac{1}{\frac{C_{L_{\alpha_h}}}{C_{L_{\alpha_{A-h}}}}\left(1-\frac{d\epsilon}{d\alpha}\right)\frac{l_h}{\bar{c}}\left(\frac{V_h}{V}\right)^2}\bar{x}_{cg} - \frac{\bar{x}_{cg} - SM}{\frac{C_{L_{\alpha_h}}}{C_{L_{\alpha_{A-h}}}}\left(1-\frac{d\epsilon}{d\alpha}\right)\frac{l_h}{\bar{c}}\left(\frac{V_h}{V}\right)^2} \tag{11.1}$$

In this equation, l_h and $\bar{c}$ are the distance between the quarter chord of the tail and the wing, and the mean aerodynamic chord. Furthermore, SM is the static stability margin, which is 5% of the mean aerodynamic chord of the wing. Then, the lift curve slope of the tail $C_{L_{\alpha_h}}$ and of the tailless aircraft $C_{L_{\alpha_{A_h}}}$ are found with the aspect ratio AR and Oswald efficiency factor e of the tail and wing respectively. The Oswald efficiency factor can be found with the aspect ratio. The ratio of flow velocity along the tail over flow velocity along the wing $\frac{V_h}{V}$ is assumed to be one due to the position of the H-tail [46]. Finally, the downwash derivative $\frac{d\epsilon}{d\alpha}$ can be found with the quarter chord sweep of the wing, as well as correction factors for the aspect ratio, taper ratio, and the geometry of the aircraft. These calculations can be seen in Equation 11.2 and Equation 11.3.

$$C_{L_\alpha} = \frac{2\pi}{1+\frac{2\pi}{\pi AR e}} \qquad e = 1.78\left(1-0.045AR^{0.68}\right)-0.64 \qquad \frac{d\epsilon}{d\alpha} = 4.44\left(K_{AR}K_\lambda K_H\sqrt{\Lambda_{c/4}}\right)^{1.19} \tag{11.2}$$

$$K_{AR} = \frac{1}{AR} - \frac{1}{1+AR^{1.7}} \qquad K_\lambda = \frac{10-3\lambda}{7} \qquad K_H = \frac{1}{(2l_h/b)^{1/3}} \tag{11.3}$$

11.1.2. Control Limit

To analyze the controllability of the aircraft, Equation 11.4 can be used.

$$\frac{S_h}{S} = \frac{1}{\frac{C_{L_h}}{C_{L_{A-h}}} \frac{l_h}{\bar{c}} \left(\frac{V_h}{V}\right)^2} \bar{x}_{cg} + \frac{\frac{C_{m_{ac}}}{C_{L_{A-h}}} - \bar{x}_{ac}}{\frac{C_{L_h}}{C_{L_{A-h}}} \frac{l_h}{\bar{c}} \left(\frac{V_h}{V}\right)^2} \tag{11.4}$$

In this equation, the lift coefficient of the horizontal tail C_{L_h} is assumed to be -1, in line with a fully moving tail [46]. Furthermore, the lift coefficient of the tailless aircraft $C_{L_{A-h}}$ in landing configuration is 1.9. Then, the pitching moment coefficient around the aerodynamic center $C_{m_{ac}}$ when taking the high lift devices into account is -0.247 and the aerodynamic center itself is assumed to be at quarter chord of the mean aerodynamic chord of the wing [18, 60].

11.1.3. Scissor Plot

Combining the stability and control limits in a scissor plot leads to Figure 11.1.

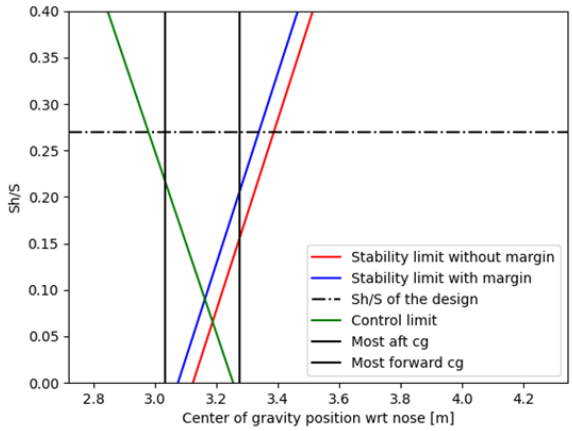

Figure 11.1: *The stability and control limits with regards to the CG position of the cruise vehicle*

In this plot, the stability limit with and without margin, as well as the control limit have been plotted. A horizontal line is plotted at the $\frac{S_h}{S}$ ratio that corresponds with the one of the design. Additionally, two vertical lines, representing the most forward and most aft center of gravity positions have been plotted. The most forward center of gravity corresponds with the center of gravity of the maximum take-off weight. The most aft center of gravity corresponds with the center of gravity of the vehicle without any payload. The center of gravity position of the vehicle with payload but without the battery was not considered, as this configuration would not be possible in flight. From the scissor plot, it can be concluded that the center of gravity positions fall between the stability and control limits. Therefore, it can be confirmed that the cruise vehicle is stable and controllable. Stall wake and recovery will be analyzed in further stages of the design.

11.2. Lifting Vehicle

The lifting vehicle is a multicopter, which is inherently unstable. Therefore, to ensure safe flight it requires an active control system which responds to any disturbances which can be encountered. Additionally, to allow coupling, the control system of the multicopter must provide highly accurate attitude and position control.

11.2.1. Control System Layout

An in-air landing procedure does not only require high control precision but also quick adjustments. The adjustment time is limited by the fact that the classical multicopter does not have a full control over its 6 degrees of freedom. Due to the thrust being directed always in the z direction in the body reference frame, it is impossible to control the motion in the horizontal plane, i.e. parallel to the Earth surface, without changing pitch and/or roll angle. This dependence is not an issue during most flight

phases. However, to achieve the required precision and speed for coupling, larger control over the multicopter is required.

The necessity of the independent control in every degree of freedom made a classical multicopter unfeasible for coupling. As a result, four additional smaller propellers were added on the sides of the multicopter to provide the possibility of adjustments during coupling. In order to maintain the low mass of the lifting vehicle, these propellers are used only for small position adjustments since they do not provide enough power to fully control the horizontal motion of the vehicle. Thus, the lifting vehicle can still be considered and modeled as a multicopter.

The lifting vehicle is controlled by adjusting the rotational speed of 24 main rotors and 4 adjustment propellers. The rotational speed is adjusted by a PD (proportional derivative) controller based on the difference between the desired and the actual position of the multicopter. Additionally, to provide a better response to gusts, the true airspeed is measured and also taken into account while calculating the control input. The airspeed can be measured by placing pitot tubes on the sides of the rotors panel. Note that to integrate pitot tubes, a supporting structure on the shrouds might be required. This structure must be taken into account while the shrouds are designed in detail. A detailed description of the controller is provided in Section 11.2.3.

11.2.2. Motion Model

To simulate the motion of the lifting vehicle, the model for quadcopter simulation and control proposed by Luukkonen [36] is used. This model was modified in order to adjust it to the design of the lifting vehicle.

Modifications

Firstly, to simplify the controller design, instead of 28 different rotational speeds, only 8 are taken. The upper surface of the lifting vehicle was divided into 4 sections, each of them containing 6 rotors. A section is represented by an equivalent rotor having a controllable rotational speed. To provide yaw control in 2 out of 4 section, the rotors rotate in the clockwise direction, while in the other 2 they rotate in the counterclockwise direction. The additional propellers, adjusting horizontal plane motion are modelled without the simplification. Therefore, the vehicle can still be represented as a quadcopter with the additional thrust vector components.

Adding four adjusting propellers acting in the horizontal body plane results in adding x^B and y^B components to the thrust vector. Furthermore, these propellers also create pitching and rolling moments following their placement in the rotors plane above the center of gravity. However, they are placed in such a way that they do not create yawing moments. This contribution modifies the thrust and torque vectors.

In Luukkonen's model [36], the aerodynamic drag is added by applying an additional force acting at the center of gravity. Additionally, the force is assumed to be linearly dependent on the velocity components in the inertial frame. To make the model more realistic, the lifting vehicle is modelled as two bodies: one box representing the fuselage and one grid of cylinders representing the rotors. The incoming airspeed vector is decomposed into 3 vectors, representing the airspeed perpendicular to the respective surfaces in the body frame ($V_{n_{x^B}}$, $V_{n_{y^B}}$, $V_{n_{z^B}}$). Then, the drag generated by each of the surfaces can be expressed by Equation 11.5. Drag coefficient values are chosen in the same way as in Section 9.4.

$$D = C_D \frac{1}{2} \rho V_n^2 S \tag{11.5}$$

Due to the unequal drag generated by rotors panel and fuselage, additional pitching and rolling moments are added. It is assumed that the drag acts at the center of gravity of each of the components. Therefore, following the symmetry of the vehicle with respect to $x^B z^B$ and $y^B z^B$ planes, no yawing moment is generated since the x^B and y^B coordinates of the centers of gravity align with the respective coordinates of the entire lifting vehicle. The aforementioned assumptions largely simplify the geometry and aerodynamic interactions of the lifting vehicle. Due to the novelty of the design and lack of

available stability or aerodynamic data for the ducted rotors, it is deemed sufficient to simulate the aerodynamics of the lifting vehicle this way at this design stage.

Translation Equations of Motion

Translation of the lifting vehicle is described using the position vector ξ.

$$\xi = \begin{bmatrix} x \\ y \\ z \end{bmatrix} \tag{11.6}$$

ξ describes the position of the lifting vehicle with respect to the fixed (i.e. non-moving and non-rotating) origin of the inertial reference frame. After applying the modifications to the model, the resulting equations of motion for the translational motion can be expressed as follows:

$$\ddot{\xi} = \mathbf{g} + \mathbf{T}^I + \mathbf{D}^I_{fus} + \mathbf{D}^I_{rotor} \tag{11.7}$$

The equation of translational motion consists of the gravity vector $\mathbf{g}$, thrust $\mathbf{T}^I$, drag components of the fuselage $\mathbf{D}^I_{fus}$, and rotors $\mathbf{D}^I_{rotor}$.

The gravity vector $\mathbf{g}$ can be expressed as a constant force acting in z-direction in the inertial reference frame.

$$\mathbf{g} = \begin{bmatrix} 0 \\ 0 \\ -g \end{bmatrix} \tag{11.8}$$

To express thrust vector in the inertial reference frame, the expression of this force in the body frame must be transformed using the transformation matrix from the body to the inertial reference frame $\mathbf{R}$.

$$\mathbf{R} = \begin{bmatrix} \cos\psi\cos\theta & \cos\psi\sin\theta\sin\phi - \sin\psi\cos\phi & \cos\psi\sin\theta\cos\phi + \sin\psi\sin\phi \\ \sin\psi\cos\theta & \sin\psi\sin\theta\sin\phi + \cos\psi\cos\phi & \sin\psi\sin\theta\cos\phi - \cos\psi\sin\phi \\ -\sin\theta & \cos\theta\sin\phi & \cos\theta\cos\phi \end{bmatrix} \tag{11.9}$$

Thrust in the body frame is modelled as the function of the rotor angular velocities of the rotors ω_i, the thrust constant for rotors k_{rotor}, and the thrust constant for propellers k_{prop}.

$$\mathbf{T}^B = \frac{1}{m}\begin{bmatrix} k_{prop}\left(\omega_5^2 - \omega_7^2\right) \\ k_{prop}\left(\omega_6^2 - \omega_8^2\right) \\ k\sum_{i=1}^{4}\omega_i^2 \end{bmatrix} \qquad \mathbf{T}^I = \mathbf{R}\mathbf{T}^B \tag{11.10}$$

The angular velocities ω_1, ω_2, ω_3 and ω_4 correspond to the equivalent rotors. Meanwhile, ω_5 and ω_7 correspond to the correcting propellers in the x^B direction, and ω_6, ω_8 to the correcting propellers in the y^B direction.

The drag components can be expressed using Equation 11.5 as the following:

$$\mathbf{D}^B = -\frac{1}{2m}\rho\mathbf{C_D}\boldsymbol{S}\left(\mathbf{V}^B_{air}\right)^2 \qquad \mathbf{D}^I = \mathbf{R}\mathbf{D}^B \tag{11.11}$$

$\mathbf{C_D}$ is the drag coefficient matrix composed of drag coefficients for the reference surface areas for the respective directions. Then, it is multiplied by the reference areas matrix $\boldsymbol{S}$.

$$\mathbf{C_D} = \begin{bmatrix} C^B_{D_x} & 0 & 0 \\ 0 & C^B_{D_y}S^B_{ref_y} & 0 \\ 0 & 0 & C^B_{D_z}S^B_{ref_z} \end{bmatrix} \qquad \boldsymbol{S} = \begin{bmatrix} S^B_{ref_x} & 0 & 0 \\ 0 & S^B_{ref_y} & 0 \\ 0 & 0 & S^B_{ref_z} \end{bmatrix} \tag{11.12}$$

The airspeed vector $\mathbf{V}^B_{air}$ is defined as the sum of the lifting vehicle velocity and wind speed expressed in the body frame. Solving Equation 11.7 gives the velocity of the lifting vehicle expressed in the

reference frame. Additionally, wind speed is also expressed in the inertial frame. Therefore, to obtain the airspeed in the body frame, the inertial airspeed $\mathbf{V}^I_{air}$ must be transformed using Equation 11.9.

$$\mathbf{V}^B_{air} = \boldsymbol{R}^{-1}\mathbf{V}^I_{air} \qquad \mathbf{V}^I_{air} = \begin{bmatrix} \dot{x} + V^I_{wind,x} \\ \dot{y} + V^I_{wind,y} \\ \dot{z} + V^I_{wind,z} \end{bmatrix} \tag{11.13}$$

Rotational Equations of Motion

The attitude of the lifting vehicle with respect to the inertial reference frame is described using roll ϕ, pitch θ, and yaw ψ angles. Following that, the attitude vector $\boldsymbol{\eta}$ in the inertial frame can be defined. The derivatives of the angles can be related to roll p, pitch q, and yaw r rate expressed in the body frame as the following [36]:

$$\dot{\boldsymbol{\eta}} = \begin{bmatrix} \phi \\ \theta \\ \psi \end{bmatrix} \qquad \dot{\boldsymbol{\nu}} = \boldsymbol{W}_\eta \dot{\boldsymbol{\eta}} \qquad \dot{\boldsymbol{\nu}} = \begin{bmatrix} p \\ q \\ r \end{bmatrix} = \begin{bmatrix} 1 & 0 & -\sin\theta \\ 0 & \cos\phi & \cos\theta\sin\phi \\ 0 & -\sin\phi & \cos\theta\cos\phi \end{bmatrix} \begin{bmatrix} \dot{\phi} \\ \dot{\theta} \\ \dot{\psi} \end{bmatrix} \tag{11.14}$$

First, the attitude equation can be expressed in the body frame [36].

$$\boldsymbol{I}\dot{\boldsymbol{\nu}} + \boldsymbol{\nu} \times (\boldsymbol{I}\boldsymbol{\nu}) + \boldsymbol{\Gamma} = \boldsymbol{\tau} \tag{11.15}$$

The attitude equation consists of the moment of inertia matrix $\boldsymbol{I}$ multiplied with the angular acceleration $\dot{\boldsymbol{\nu}}$, centripetal term $\nu \times (\boldsymbol{I}\boldsymbol{\nu})$, gyroscopic term $\boldsymbol{\Gamma}$, and external moment $\boldsymbol{\tau}$.

Since the lifting vehicle is symmetric about $x^B z^B$ and $y^B z^B$ planes, there are no products of inertia contributing to the moment of inertia matrix $\boldsymbol{I}$. Therefore, it can be expressed as follows:

$$\boldsymbol{I} = \begin{bmatrix} I_{xx} & 0 & 0 \\ 0 & I_{yy} & 0 \\ 0 & 0 & I_{zz} \end{bmatrix} \tag{11.16}$$

To reduce the gyroscopic effects from the propellers, and rotors, they are counter-rotating. Following that, $\boldsymbol{\Gamma}$ can be described using Equation 11.17.

$$\boldsymbol{\Gamma} = -I_r \begin{bmatrix} p \\ q \\ r \end{bmatrix} \times \begin{bmatrix} \omega_5 - \omega_7 \\ \omega_6 - \omega_8 \\ \omega_1 - \omega_2 + \omega_3 - \omega_4 \end{bmatrix} \tag{11.17}$$

Due to the modifications to the Luukkonen's model, there are additional contributions from the drag and correcting propellers to the external moment vector. Therefore, the external moment can be decomposed into its thrust component $\boldsymbol{\tau}_{thrust}$ and drag component $\boldsymbol{\tau}_{drag}$.

$$\begin{aligned} \boldsymbol{\tau} &= \boldsymbol{\tau}_{thrust} + \boldsymbol{\tau}_{drag} \\ \boldsymbol{\tau}_{thrust} &= \begin{bmatrix} l_{rot,cg,y} k \left(-\omega_2^2 + \omega_4^2\right) + l_{prop,cg} \frac{k}{12} \left(\omega_5^2 - \omega_7^2\right) + b \left(-\omega_6^2 + \omega_8^2\right) \\ l_{rot,cg,x} k \left(-\omega_1^2 + \omega_3^2\right) + l_{prop,cg} \frac{k}{12} \left(\omega_6^2 - \omega_8^2\right) + b \left(-\omega_5^2 + \omega 7^2\right) \\ b \left(-\omega_1^2 + \omega_2^2 - \omega_3^2 + \omega_4^2\right) \end{bmatrix} \\ \boldsymbol{\tau}_{drag} &= \begin{bmatrix} l_{panel,cg} C^B_{D_{y,panel}} \frac{1}{2}\rho \left(V^B_{air_y}\right)^2 S^B_{ref,panel_y} - l_{fus,cg} C^B_{D_{y,fus}} \frac{1}{2}\rho \left(V^B_{air_y}\right)^2 S^B_{ref,fus_y} \\ l_{panel,cg} C^B_{D_{x,panel}} \frac{1}{2}\rho \left(V^B_{air_x}\right)^2 S^B_{ref,panel_x} - l_{fus,cg} C^B_{D_{x,fus}} \frac{1}{2}\rho \left(V^B_{air_x}\right)^2 S^B_{ref,fus_x} \\ 0 \end{bmatrix} \end{aligned} \tag{11.18}$$

In Equation 11.18, $l_{rot,cg,x}$ and $l_{rot,cg,y}$ are the distances between the equivalent rotor location and the center of gravity in the x^B and y^B direction, respectively. Furthermore, $l_{prop,cg}$ and $l_{panel,cg}$ are

the distances between the center of gravity in the z^B direction and the correcting propeller locations. Finally, $l_{fus,cg}$ is the distance between the fuselage center of gravity location and the center of gravity in the z^B, and b is the torque constant.

Having all the components in the body frame, the equation of motion for the inertial frame can be formulated.

$$\begin{aligned}\ddot{\boldsymbol{\eta}} &= \frac{\mathrm{d}}{\mathrm{d}t}\left(\boldsymbol{W}_\eta^{-1}\right)\boldsymbol{\nu} + \boldsymbol{W}_\eta^{-1}\dot{\boldsymbol{\nu}} \\ \ddot{\boldsymbol{\eta}} &= \begin{bmatrix} 0 & \dot{\phi}\cos\phi\tan\theta + \dot{\theta}\frac{\sin\theta}{\cos^2\theta} & -\dot{\phi}\sin\phi\cos\theta + \dot{\theta}\frac{\cos\phi}{\cos\theta} \\ 0 & -\dot{\phi}\sin\phi & -\dot{\phi}\cos\phi \\ 0 & \dot{\phi}\frac{\cos\phi}{\cos\theta} + \dot{\phi}\frac{\sin\phi\tan\theta}{\cos\theta} & -\dot{\phi}\frac{\sin\phi}{\cos\theta} + \dot{\theta}\frac{\cos\phi\tan\theta}{\cos\theta} \end{bmatrix}\boldsymbol{\nu} + \boldsymbol{W}_\eta^{-1}\dot{\boldsymbol{\nu}}\end{aligned} \tag{11.19}$$

11.2.3. PD Controller

To control the motion of the lifting vehicle, a PD controller is used. As an input it takes the difference between the actual state and the desired state for all 6 degrees of freedom, which are used to determine the required forces and moments.

$$\begin{aligned} F_x^I &= m\left(K_{x,D}\left(\dot{x_d} - \dot{x}\right) + K_{x,P}\left(x_d - x\right)\right) \\ F_y^I &= m\left(K_{y,D}\left(\dot{y_d} - \dot{y}\right) + K_{y,P}\left(y_d - y\right)\right) \\ F_z^I &= m\left(K_{z,D}\left(\dot{z_d} - \dot{z}\right) + K_{z,P}\left(z_d - z\right)\right) \\ \tau_\phi^B &= I_x x\left(K_{\phi,D}\left(\dot{\phi_d} - \dot{\phi}\right) + K_{\phi,P}\left(\phi_d - \phi\right)\right) \\ \tau_\theta^B &= I_y y\left(K_{\theta,D}\left(\dot{\theta_d} - \dot{\theta}\right) + K_{\theta,P}\left(\theta_d - \theta\right)\right) \\ \tau_\psi^B &= I_z z\left(K_{\psi,D}\left(\dot{\psi} - \dot{\psi}\right) + K_{\psi,P}\left(\psi - \psi\right)\right) \end{aligned} \tag{11.20}$$

After transforming the force in the inertial frame to the body frame ($\boldsymbol{F}^B = \boldsymbol{R}\boldsymbol{F}^I$), the force components specified in the equation above can be substituted for $m\ddot{\boldsymbol{\xi}}$ in Equation 11.7. The moment components are assumed to be equal to the external moment defined in Equation 11.18. Note that for the drag calculation of forces and moments, the value for wind speed is taken with 0.1 s delay, which is comparable to the delay of the pitot tube measurement in an aircraft [7].

Following the substitution, the values for the rotational speeds of the rotors can be determined. However, they are calculated with a few limitations. First, for the correcting propellers it is assumed that only one of two propeller generates thrust for the same axis. In reality, during flight the propellers would not be fully switched off, however the difference in RPM remains the same. Thus, the behavior should be close to the simulated one. Additionally, the maximum rotational speed of the engine is 2600 RPM, therefore if any of the resulting rotation speeds exceeds this value, it is set to 2600 RPM. If it happens for the correcting propellers, the rotational speeds of the rotors are recalculated. Finally, it is assumed that the rotors cannot provide reverse thrust, so if one of them is expected to deliver negative thrust, the RPM is set to 0. Similarly to the correcting propellers, the main rotors would not stop rotating, however their rotational speed would be significantly low.

When the rotational speeds of the rotors are calculated, they are used as the inputs to the model. With this comes another constraint of the propellers - they do not react instantly. However, due to the usage of small propellers, their reaction time should be relatively low. Thus, at this stage of the design it is assumed that they react immediately to any changes. The effect of this assumption is that the reaction time of the entire system would be slower, which is taken into account while choosing the safety margins for the coupling time.

The controller was optimized for the assumed landing conditions (V_x = 35 m/s, h = 450 m). Final control gains are presented below.

Table 11.1: *Controller gains*

Parameter	Value
$K_{x,D}$	32.0
$K_{x,P}$	20.3
$K_{y,D}$	3.9
$K_{y,P}$	4.3
$K_{z,D}$	18.5
$K_{z,P}$	22.6
$K_{\phi,D}$	5.0
$K_{\phi,P}$	4.0
$K_{\theta,D}$	10.8
$K_{\theta,P}$	5.0
$K_{\psi,D}$	1.8
$K_{\psi,P}$	1.0

11.2.4. Results

The critical phase of the system is the two-vehicle coupling before vertical landing. To simulate the response of the lifting vehicle in difficult weather conditions, gusts were modelled as a disturbance input. The simulation yielded similar results, therefore the example of one of the performed simulations is shown here.

Gusts were modelled as cosine waves in wind speed. The amplitude of 9.1 m/s was chosen, as it corresponds to CS-27 regulations [16].

$$V_{air} = 9.1 \cos\left(k\pi t + \phi\right) \tag{11.21}$$

To make the conditions more random, different periods and phase shifts were chosen for different wind directions. For x: $k = 2$ and $\phi = 0$; for y: $k = 1$ and $\phi = \pi/6$; for z: $k = 3.1$ and $\phi = \pi/3$. The simulation was run for a sample landing procedure with an approach speed of 35 m/s. The results are shown in the graphs below.

As can be seen from Figure 11.2a, the required precision for coupling is achieved. Most importantly, the z position of the lifting vehicle remains within approximately 5 cm from the desired position at any moment in time. The y position remains almost constant during the approach. The only difference is for the x position, which settles at value between 0.40 and 0.45 m from the desired position. It is caused by the initial lower speed which cannot be overcompensated in later design phases. However, when the x position is settled, it is only required to slightly reduce in speed for the cruise vehicle to couple. Therefore, this difference can be accepted.

The speed of the vehicle in Figure 11.2b also perfectly meets the constraints of coupling. Firstly, the lifting vehicle is able to maintain the desired landing speed of 35 m/s, even in gusty weather conditions. Additionally, the velocity in every direction oscillates with a very small amplitude of less than 1 m/s. Following that, the speed response is also deemed sufficient for coupling.

Figure 11.2c shows the attitude of the lifting vehicle. To allow for smooth coupling without damaging the cruise vehicle, it is important to keep roll and yaw angles close to 0.0 rad. The pitch angle is larger, following the requirement to maintain proper horizontal speed. However, the guiding structure is designed in such a way that it allows for larger pitch angle for the lifting vehicle, which are necessary to fly with larger horizontal speed. Similarly, to the position and speed, the attitude of the lifting vehicle does not vary much when settled. Therefore, the last requirement is also met for the lifting vehicle to allow for coupling.

The aforementioned results prove excellent maneuverability of the lifting vehicle. Therefore, it was decided that during landing, the lifting vehicle would be responsible for any correcting maneuvers. The motion of the lifting vehicle in response to gust can be simulated using the stability derivatives of

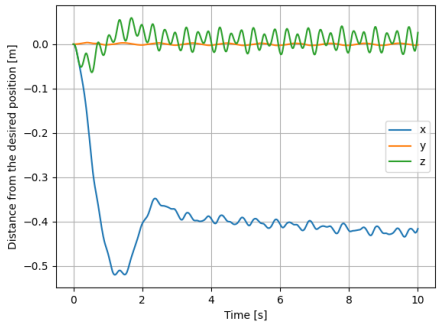

(a) *The distance from the desired position of the lifting vehicle in a 10 seconds span*

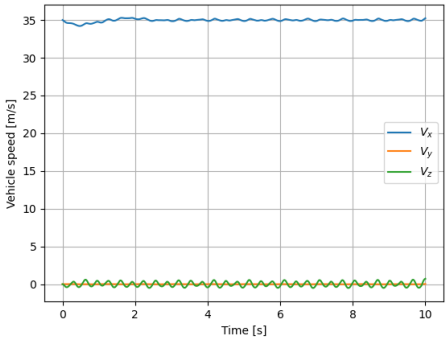

(b) *The speed of the lifting vehicle in a 10 seconds span*

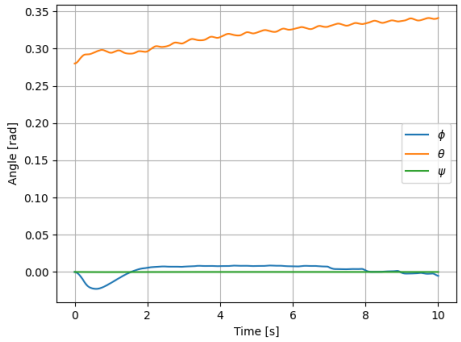

(c) *The attitude of the lifting vehicle in a 10 seconds span*

Figure 11.2: *The response of the lifting vehicle to a gust during landing*

the aircraft. However, these parameters are unknown at this stage of the design. Therefore, for the control subsystem design, the aim was to synchronize the motion of the lifting vehicle with the motion of a general light aircraft. The response of the aircraft to gust was modelled by a phugoid. The short period response of the aircraft was ignored due to the fact that before this motion becomes periodic, it is already damped. Following that, the motion of the aircraft in z direction was modelled as:

$$z(t) = A \sin(\omega t) \tag{11.22}$$

This position was used as an input to the controller of the lifting vehicle. The amplitude A was set to 7.5 m. This value is used due to the fact that the coupling procedure is assumed to start when the vehicles are 5 m from each other. Applying safety factor of 1.5 gives the amplitude. Then, the motion of the vehicle was simulated in 10 seconds time span, and root mean squared error of the position was calculated for different angular frequencies ω. The results are presented in Figure 11.3.

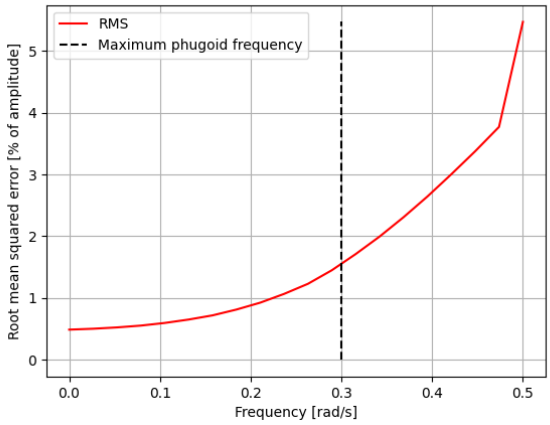

Figure 11.3: *Root mean squared error of the position for different frequencies of the phugoid*

As can be seen in the plot the lifting vehicle achieves an excellent performance in reaching the desired position. In the light aircraft phugoid frequency should not exceed 0.3 rad/s [58]. Thus, this value is taken as the limiting frequency at which the control subsystem must achieve high precision. As can be seen in Figure 11.3, root mean squared error for $\omega = 0.3$ rad/s is equal to 1.5%, which corresponds to the value of 0.1125 m for the assumed conditions. This result gives a clear indication that the control subsystem is sufficient for the purposes of coupling.

The dynamic, controlled response of the lifting vehicle shows that coupling can be achieved in a short period of time. Thanks to the installed correcting propellers, the lifting vehicle demonstrates excellent resistance to any disturbances affecting vehicles at low speed. It must be noted that the assumption of the instant response of the motors largely influences this result. Additionally, the simple drag model presented can be developed to provide a more detailed aerodynamic analysis, since the resulting drag of the surfaces was taken very preliminarily. On the other hand, only a simple PD controller was developed. Thus, it can be said that this model lays out a strong basis for further development of coupling mechanism. Taking the necessary margin for the inaccuracies in the model, coupling can take place within the acceptable time of 10 seconds when encountering maximum predicted gusts.

Furthermore, at this stage of the design, the control subsystem provides necessary margins. The mechanical guiding of the coupling mechanism is able to guide the vehicles up to 3 m difference. The precision provided by the control subsystem is 11.25 cm for 7.5 m vertical oscillation of the cruise vehicle. Following that, for the preliminary design, the coupling procedure can be confirmed as safe and quick.

12

Acoustic Emissions

Noise emissions is an important part to take into account when analysing the sustainability of the design, especially so when implementing the designs in an urban environment. This chapter describes the noise mitigation and analysis procedure. Firstly, the mechanics of rotor and propeller noise are explained in Section 12.1. Afterward, the design choices made with noise in mind are outlined in Section 12.2. Then, the design of the ducts and their effect are explained in Section 12.3. Subsequently, a noise estimation is performed for different phases of the flight in Section 12.4. The Doppler effect and A-weighting are then briefly discussed in Section 12.5 and Section 12.6, respectively. Finally, the results are shown in Section 12.7.

12.1. Rotor and Propeller Noise

The noise created by the vehicles can be classified into two main types: broadband noise and tonal noise. Broadband noise consists of sound that is produced over a wide range of frequencies, while tonal noise is concentrated at specific frequencies.

Tonal noise in rotors and propellers mostly consists of rotational noise, caused by the periodic passage of the blades through the air. This noise is most pronounced at the fundamental frequency of the rotor, which corresponds to the blade passage frequency, and its harmonics. The intensity of the noise tends to diminish with higher harmonics. Therefore, it is crucial to keep the fundamental frequency and the first few harmonics of the rotor out of the sensitive range for human hearing, which is between about 1000 and 4000 Hz[1]. Another source of tonal noise is blade vortex interaction, where a previously shed tip vortex interacts with a passing blade, creating an impulsive acoustic signal [6].

Broadband noise is predominantly comprised of airfoil self-noise. The two main contributors to airfoil self-noise are turbulent boundary layer trailing edge (TBLTE) noise and laminar separation bubble (LSB) noise. TBLTE noise occurs when the flow of a turbulent boundary layer passes by the sharp edge of an airfoil, converting kinetic energy to acoustic energy that propagates to the far field [33]. LSB noise arises due to flow separation over the airfoil, which then subsequently reattaches to create a laminar separation bubble [19]. This bubble influences aerodynamic performance and radiates noise.

12.2. Noise Design Choices

The noise produced, especially during take-off, was a significant factor influencing several design choices for the lifting vehicle. Specifically, the number and size of the rotors, as well as the number of blades per rotor, were selected with noise production in mind, particularly the frequency of the rotational noise. A high number of rotors was chosen to ensure a smaller radius, allowing for the addition of shrouds for noise attenuation. This not only reduced noise, but also decreased the required rotor radius from R_{old} to R_{new} due to the increase in thrust [49].

Since the design of the lifting vehicle incorporated a low number of blades, mostly for weight considerations, a low blade passage frequency (BPF) of 80 Hz was obtained. This is advantageous as it ensures that the first 12 harmonics remain below 1000 Hz. The blade passage frequency was obtained using Equation 12.1.

$$BPF = \frac{RPM}{60} B \tag{12.1}$$

[1]https://en.wikipedia.org/wiki/A-weighting[Accessed on 17/6/2024]

For the cruise vehicle, a BPF of 120 Hz was achieved, meaning that the first 8 harmonics are below 1000 Hz, which was deemed satisfactory for the design.

12.3. Shrouds

Installing shrouds around the rotors is crucial in order to provide the necessary noise mitigation for the vehicle. This section includes an estimation for the mass of the shrouds, the aerodynamic performance and the noise reduction the shrouds offer.

12.3.1. Aerodynamic Performance Estimation

Blade element momentum theory (BEMT) provides a relation between the expansion ratio of a shroud and the ratios of thrust, power, and area for open and shrouded rotors. Since the engines will remain unchanged, the power ratio was set to 1. The same applies to the thrust ratio, as the weight does not significantly change, and therefore the required thrust remains constant. The BEMT equation can then be simplified. The equation indicates that even for a shroud without an expansion ratio, the area of the rotors could still be halved. By maintaining the same area loading, the new radius of the rotors could be calculated. These equations can be seen in Equation 12.2.

$$\sigma_d = \frac{A_e}{A_0} \qquad \frac{P_{i,SR}}{P_{i,OR}} = \frac{1}{\sqrt{2\sigma_d}} \left(\frac{T_{SR}}{T_{OR}}\right)^{3/2} \left(\frac{A_{SR}}{A_{OR}}\right)^{1/2} \qquad A_{SR} = \frac{A_{OR}}{2\sigma_d} \qquad r_{SR} = \sqrt{\frac{r_{OR}^2}{2\sigma_d}} \tag{12.2}$$

The weight reduction W_{red} of the rotors was then computed using Equation 12.3. For simplicity, an expansion ratio of 1 was chosen for the design. A weight reduction of about 110 kg was obtained.

$$W_{red} = \rho B (R_{old} - R_{new}) \frac{t}{c} c^2 \tag{12.3}$$

12.3.2. Shroud Mass Estimation

In order to perform a mass estimation for the ducts, an initial design was required. Hubbard [25] conducted noise measurements on five different shrouds designs for a two- and five-bladed rotors. The rotor radius in the experiments was approximately 0.6 meters, with the rotor spinning at 3300 rpm. This setup was considered comparable to the design of the lifting vehicle, which has a rotor radius of 0.69 meters and an rpm of 2600. Consequently, one of the designs from the experiments was used to estimate the noise attenuation and the weight of the shrouds.

According to Hubbard [25], the length of the shrouds did not significantly impact noise attenuation. Therefore, it was decided that the smallest shroud would be suitable for this design, as it adds the least amount of weight. However, the smallest shroud in the experiment experienced thrust variation due to fluctuating flow conditions, leading to axial vibrations in the shroud. Therefore, shroud B was used as the reference shroud for the noise and mass estimation.

The airfoil coordinates provided by Hubbard [25] for shroud B were adjusted to make the chord length longer, maintaining the same chord length-to-rotor radius ratio as in the experiment. As the shrouds only have to carry their own weight and aerodynamic loads, a hollow section was decided upon, with walls made of carbon fiber and a thickness of 2 millimeters. The hollow section would then be filled with noise reducing foam. The approximation resulted in a mass of about 9 kg for one shroud, meaning about 216 kg for all the shrouds. This entails that the addition of shrouds for noise attenuation results in a weight penalty of approximately 116 kg, which was considered justified given the vehicle's mission.

12.3.3. Shroud Noise Reduction Estimation

To estimate the noise reduction provided by the shrouds on the lifting vehicle, the experimental results of Hubbard [25] were used. For shroud design B, a noise attenuation of about 6 dBA was achieved. This value will be used as an estimate to determine the noise produced by the lifting vehicle.

It is crucial to ensure that the flow remains unseparated on the shroud for effective noise attenuation. A shrouded rotor with separated flow can produce significantly more noise than an open rotor without a shroud. Although producing a detailed design of the shrouds is beyond the scope of this project, it is important to highlight that a detailed aerodynamic analysis should be conducted to ensure unseparated flow conditions are maintained throughout all phases of the mission.

12.4. Noise Estimation

As tonal noise generally tends to be more significant for rotors and propellers, it was deemed to be the most important source of noise for the design. A simple generalized method to estimate the tonal noise of rotors and propellers was outlined by Marte [37]. For the noise estimation of rotors, which corresponds to the lifting vehicle, the method takes into account rotor rotational noise and rotor vortex noise. For the noise estimation of propellers, corresponding to the cruise vehicle, two methods were described. The first one being able to estimate noise in the near-field, meaning within one propeller diameter of the propeller. This was used to obtain the noise estimation for the cabin. The second method provided an estimate for the far-field noise.

A MATLAB script was also obtained from one of the leading noise experts at the TU Delft to estimate tonal and broadband noise of a propeller. The script was used to verify the results of Marte's method for the tonal noise of the vehicles. Additionally, it was used to obtain an estimate of the broadband noise to confirm that no noise attenuation methods needed to be implemented to reduce broadband noise. The program calculates the tonal noise utilizing Hanson's model and the broadband noise using Amiet's theory [22][3].

12.4.1. Near-field Propeller Noise

The noise estimation for the near-field propeller noise can be summarized as follows. Firstly, a reference sound pressure level is obtained based on the power input of the propeller. Afterwards, a correction factor is applied to account for the number of blades and propeller diameter, calculated with Equation 12.4.

$$\Delta SPL = 20 \log \frac{4}{B} \qquad \Delta SPL = 40 \log \frac{15.5}{D} \tag{12.4}$$

Then, another set of correction factors were applied to account for the rotational speed of the propeller, the position of the fuselage with respect to the propeller, as well as the distance from the propeller to the point of interest. These were obtained from plots provided by Marte [37]. The final correction factor applied accounts for the effect of a reflecting surface, i.e. the fuselage. The original reference sound pressure level is then summed with the correction factors to estimate the overall sound pressure level at the point of interest. Then, an estimate of the harmonic distribution of the sound is obtained based on the fundamental frequency and its harmonics, as well as the tip Mach number. Finally, the harmonic levels are then combined to derive octave band levels.

This method has been used to estimate the noise in the cabin due to the propeller of the cruise vehicle during the horizontal take-off and cruise phases of the mission. An initial estimate for how much the noise is reduced due to the walls of the cabin was obtained from a study made by Grooteman [20]. The results of the study are depicted on Figure 12.1.

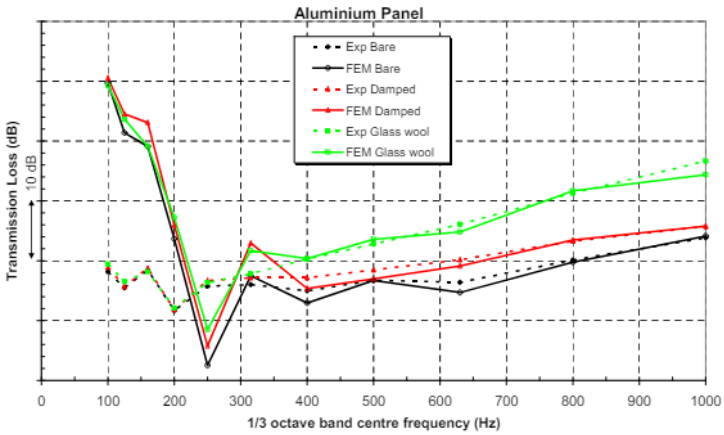

Figure 12.1: *Experimental (dotted) and numerical (solid) TL-curves for aluminum panel [20]*

The bare configuration of the panel was considered enough to obtain an initial estimate of the noise in the cabin, and was therefore used to obtain the SPL values. This was also used to obtain the noise in the cabin due to the lifting vehicle during the take-off phase.

12.4.2. Far-field Propeller Noise

For the far-field noise estimation of the propeller of the cruise vehicle, a similar method was used as for the near-field noise. The first few steps of the method are the same as for the near-field noise. However, instead of applying a correction factor for the position of the fuselage, the point of interest and the reflecting surface, correction factors were applied to account for the directionality of the sound, as well as the spherical spreading, where the latter is computed with Equation 12.5, where r is the distance from the observer to the center of the propeller. The rest of the correction factors are obtained from plots provided by Marte [37]. Afterward, the SPL values are obtained in the same way as for the near-field method. At the end, a final correction factor is added to the SPL values to account for the molecular absorption of sound in air, also obtained from a provided plot.

$$\Delta SPL = 20 \log (r - 1) \tag{12.5}$$

This method was used to estimate the noise on the ground during the horizontal take-off and cruise phases of the mission due to the propeller of the cruise vehicle.

12.4.3. Rotor Rotational Noise

To estimate the noise of the rotor rotational noise for the lifting vehicle, several parameters have to be calculated. These consist of the rotational Mach number, flight Mach number, the effective rotational Mach number and the angle between the rotor plane and the observer position. These were calculated using the equations in Equation 12.6, where n is the rotational speed, a the speed of sound, r the distance to the observer and i_d the incidence angle.

$$M_r = 0.8\frac{\omega R}{c} \qquad M_F = \frac{V}{c} \qquad M_E = \frac{M}{1 - M_F \cos\theta'} \qquad \theta' = \cos^{-1} x/r \tag{12.6}$$

$$\theta = \tan^{-1}\left[\frac{z}{(x^2 + y^2)^{1/2}}\right] - i_d\left[\frac{x}{(x^2 + y^2)^{1/2}}\right] \tag{12.7}$$

Afterward, using plots given by Marte [37], values for the harmonic sound pressure level were obtained based on values of the effective rotational Mach number, as well as the angle between the rotor plane and the position of the observer. The values were then corrected for thrust, disc loading and observer distance, yielding a value for the sound pressure levels at the relevant frequencies. Finally, Equation 12.8 was used to obtain the fundamental frequency of the noise.

$$f_f = \frac{\omega B}{2\pi(1 - M_F \cos\theta)} \tag{12.8}$$

12.4.4. Rotor Vortex Noise

To estimate the rotor vortex noise, Schlegel's equation for overall vortex noise at 300 ft, given by Equation 12.9, was used [37]. A_b describes the total blade area. The linear velocity of the 0.7 radius section of the rotor was calculated using Equation 12.10. The overall vortex noise SPL at any other distance was then estimated with the inverse square law, as seen in Equation 12.11.

$$SPL_{300} = 10 \log \frac{6.1 \cdot 10^{-27} A_b V_{0.7}^6}{10^{-16}} + 20 \log \frac{C_L}{0.4} \tag{12.9}$$

$$V_{0.7} = 0.7 \frac{\omega \pi D}{60} \tag{12.10}$$

$$SPL_x = SPL_{300} - 20 \log \frac{x}{300} \tag{12.11}$$

The peak frequency of the noise was then calculated using Equation 12.12. S_t corresponds to the Strouhal number, which was taken to be 0.28 [37]. The projected blade thickness h was calculated using Equation 12.13, where t_{blade} is the blade thickness, a is the chord length, and α the angle of attack.

$$f = \frac{V_{0.7} S_t}{h} \tag{12.12}$$

$$h = t_{blade} \cos \alpha + a \sin \alpha \tag{12.13}$$

This method, along with the rotor rotational noise estimation described in Section 12.4.3, was used to estimate the noise on the ground and in the cabin produced by the lifting vehicle during the vertical and horizontal take-off.

12.4.5. Accuracy of the Method

For the propeller noise, the accuracy of the near-field estimates was found to be within +5 to -9 dBA of the measured values, according to Marte [37]. However, for propellers with a diameter of less than 15 feet and a tip Mach number over horsepower ratio of less than 0.003, which is the case for the propellers of the cruise vehicle, this was found to reduce to ±3 dBA of the actual sound levels. A limited number of measurements were available to Marte [37] to compare the far-field estimation. For the measurements made, which went up to a distance of 500 ft, the accuracy of the far-field estimates were found to be within ±10 dBA. Marte [37] mentions that estimates for a distance larger than 500 ft are very dependent on variable atmospheric parameters, and the method should therefore only be used to obtain an initial estimation under ideal conditions.

The method was used to obtain a noise estimation for the vertical and horizontal take-off, and for the cruise conditions. The estimation was performed for the noise in the cabin and for an observer at various distances and angles.

12.5. Doppler Effect

The Doppler effect was considered during the cruise phase of the mission to ensure that the noise produced is not perceived at frequencies that are sensitive for the human ear. The frequency shift due to the Doppler effect can be calculated using Equation 12.14. When the observer is moving towards the source, the speed of the receiver v_r is added to the speed of sound. Conversely, when the source is moving away from the observer, the speed of the source v_s is added to the speed of sound.

$$f = \frac{c \pm v_r}{c \pm v_s} \tag{12.14}$$

Using the cruise speed and a stationary observer, it was found that the frequency would increase by a factor of 1.2. Consequently, the fundamental frequency increases to 156 Hz, meaning that the first six harmonics remain below 1000 Hz, instead of the previous eight. This adjustment was considered acceptable for the design.

12.6. A-weighting

A-weighting consists of applying a correction factor to the sound pressure level to account for the perceived loudness by the human ear, depending on the sound frequency. This is done by adding a correction factor to each SPL value at different frequencies. The A-weighting curve is shown in Figure 12.2. As illustrated, the human ear is most sensitive to frequencies between 1000 and 4000 Hz. Additionally, low frequencies, particularly those under 100 Hz, are not perceived as loudly by humans. This is significant as it means that the rotational noise of the lifting vehicle produced at its fundamental frequency will be perceived much less loudly than was initially estimated.

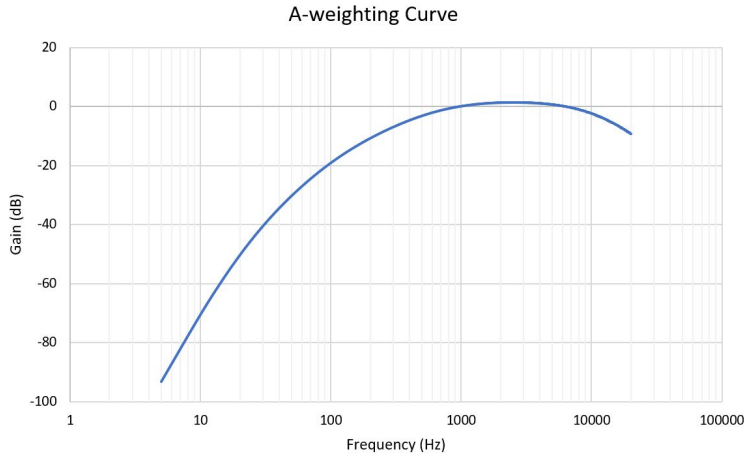

Figure 12.2: *A-weighting curve*

12.7. Results

The results of the noise estimation for different phases of the mission obtained by Marte's method [37] and the MATLAB program are outlined in Table 12.1 and Table 12.2, respectively. For the observer noise during the vertical take-off, a distance of 100 meters was taken. For the horizontal take-off, an observer position at 500 meters was taken. Additionally, the horizontal take-off accounts for the noise of both the lifting vehicle and the cruise vehicle, as there are instants where both vehicles are running at close to full power. The cruise sound pressure levels were calculated at the cruise altitude, i.e. 1200 meters.

Table 12.1: *Results of tonal noise estimation for different flight phases using Marte's method [37]*

Vertical take-off												
	Cabin						Observer					
Frequency range [Hz]	45-90	90-180	180-360	360-720	720-1440	OASPL	45-90	90-180	180-360	360-720	720-1440	OASPL
ASPL [dBA]	73.2	76.9	71.8	76.3	63.3	**81.13**	71.2	71.0	70.0	72.8	63.3	**77.6**
Cruise												
	Cabin						Observer					
Frequency range [Hz]	45-90	90-180	180-360	360-720	720-1440	OASPL	45-90	90-180	180-360	360-720	720-1440	OASPL
ASPL [dBA]	0	78.5	87.5	92.4	79.3	**93.9**	0	46.4	52.4	56.3	50.3	**58.8**
Horizontal take-off												
	Cabin						Observer					
Frequency range [Hz]	45-90	90-180	180-360	360-720	720-1440	OASPL	45-90	90-180	180-360	360-720	720-1440	OASPL

Continued on next page

Table 12.1: *Results of tonal noise estimation for different flight phases using Marte's method [37] (Continued)*

ASPL [dBA]	73.2	85.2	93.5	98.4	85.3	**99.9**	55.2	57.9	58.7	61.3	67.4	**69.3**

Table 12.2: *Results of tonal noise estimation for different flight phases using MATLAB program*

Vertical take-off						
	Observer					
Frequency range [Hz]	45-90	90-180	180-360	360-720	720-1440	OASPL
ASPL [dBA]	66.5	70.0	68.8	58.2	29.7	**73.6**
Cruise						
	Observer					
Frequency range [Hz]	45-90	90-180	180-360	360-720	720-1440	OASPL
Cruise ASPL [dBA]	0	45.9	49.2	53.2	53.7	**57.5**
Horizontal take-off						
	Observer					
Frequency range [Hz]	45-90	90-180	180-360	360-720	720-1440	OASPL
Horizontal take-off ASPL [dBA]	52.5	57.9	58.9	60.9	67.4	**69.2**

It can be seen from Figure 12.3 and Figure 12.4 that the OASPL values for the observer are very similar across both estimation methods, with the MATLAB program predicting slightly lower values. Therefore, the estimation was deemed accurate enough to consider REQ-STK-10-MIS-14 and REQ-STK-10-MIS-15 verified.

The Sound Power Level (SWL) of both tonal and broadband noise was plotted for the lifting and cruise vehicle in Figure 12.3 and Figure 12.4, respectively. The figures also include the A-weighted SWL. As can be seen on the figures, the tonal noise shows significantly higher sound power levels, with distinct peaks at various frequencies, especially in the low to mid-frequency range. In contrast, the broadband noise maintains a smooth and lower power level across the entire frequency spectrum. The difference in magnitude indicates that the contribution of broadband noise is minimal when compared to the tonal noise. Consequently, for the purposes of this project, the impact of the broadband noise was deemed insignificant relative to the much more pronounced tonal noise, and no broadband noise attenuation techniques will be implemented at this stage of the design.

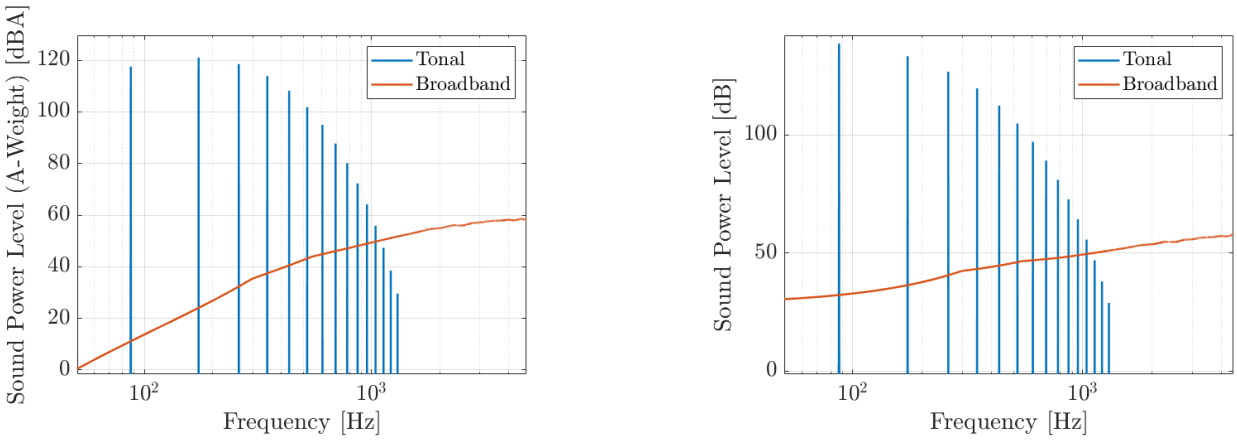

Figure 12.3: *Lifting vehicle (A)SWL vs frequency*

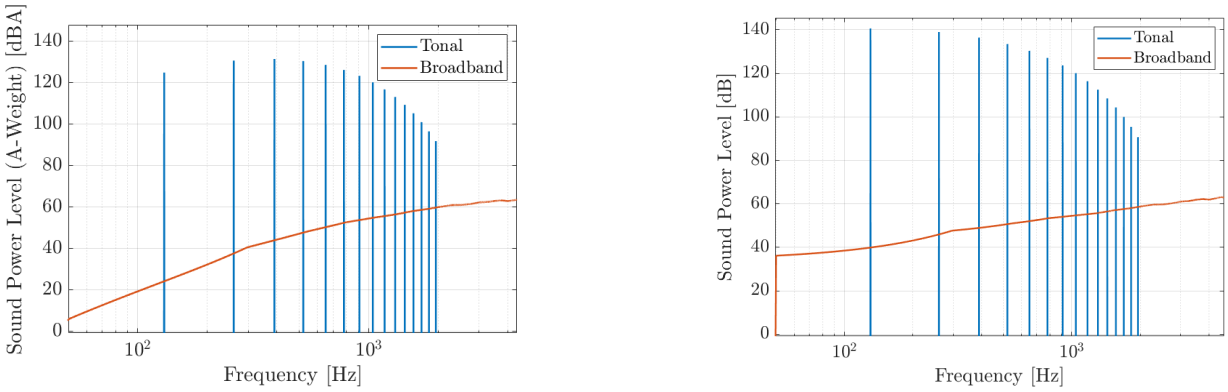

Figure 12.4: *Cruise vehicle (A)SWL vs frequency*

12.8. Cabin Noise Control

As can be seen in Table 12.1 and Table 12.2, the noise in the cabin was deemed unsuitable for a comfortable flying experience. This noise is primarily generated by the propellers of the cruise vehicle. Therefore, it was decided to implement active noise control (ANC) within the cabin to ensure the passengers can enjoy the flight without excessive noise.

According to a study performed by Kwon [31], the optimal configuration to perform ANC for maximum noise reduction consists of placing two speakers in a dipole configuration at the antinodes of related modes. Given that the engines are mounted on the wings, it was assumed that most of the cabin noise would originate from the walls adjacent to the wings. This results in an optimal setup where one speaker is positioned at the front of the cabin and the other at the rear. Figure 12.5 illustrates this positioning clearly. Using this configuration, a noise reduction of up to 70 dB can be achieved [31], ensuring passengers can enjoy the flight in the most comfortable way possible.

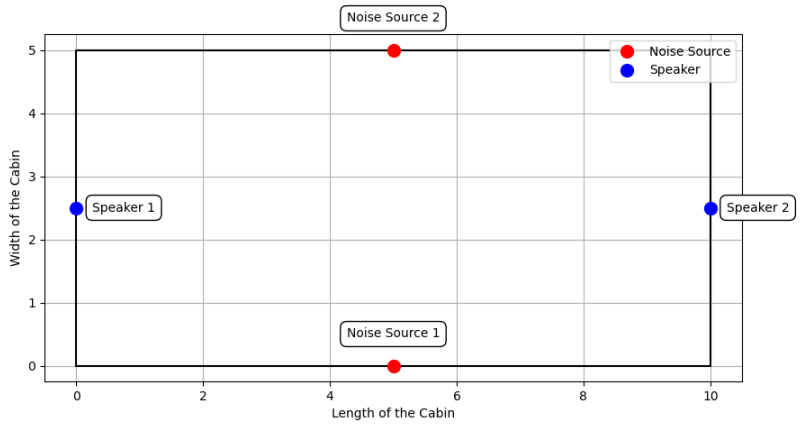

Figure 12.5: *Optimal speaker placement for active noise control in the cabin*

13

Internal System Architectures

Besides the design of the airframe of the vehicles, it is important to consider the avionics and subsystems as well. This chapter will provide an overview of the key components of these systems. It includes a hard- and software diagram in which the interactions between physical elements and the software is indicated. This diagram is discussed in Section 13.1. Then, in Section 13.2, the flow of power through the electrical equipment of the cruise vehicle is shown. Subsequently, a data handling diagram shows the flow of data between the lifting vehicle, the cruise vehicle, the ground system and the satellite system. It shows how data is processed. More details about this are given in Section 13.3. Finally, in Section 13.4, focuses on the flow of information between the lifting and the cruise vehicle specifically. This is an important part of the internal system architectures, since the coupling is a sensitive endeavor requiring high precision and thus good communication.

An simple overview of the main systems included in the communication infrastructure is given in Figure 13.1.

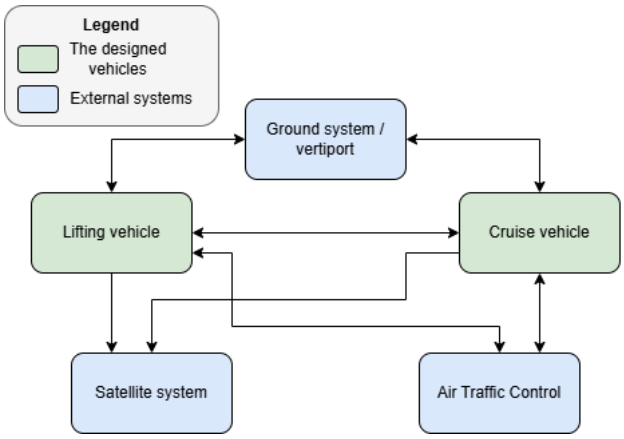

Figure 13.1: *General overview of the systems included in the communication infrastructure*

In this figure, the mentioned systems are not specified in detail. This will be done in the diagrams which are described in the following sections.

13.1. Hardware/Software Diagram

A hard- and software diagram aims to show the interaction of different physical components in the vehicle with each other through the use of software. In Figure 13.4, a distinction between the autopilot system of the vehicle and other internal systems is made. The autopilot system is shown with a light gray box. This hard- and software block diagram represents both the cruise vehicle and the lifting vehicle. Hardware components indicated with an asterisk are only present on the cruise vehicle. Essentially, this distinction results from the fact that passengers are present on the cruise vehicle, while the lifting vehicle will not carry people. Moreover, the propulsion system of the lifting vehicle is slightly different from the one of the cruise vehicle. The lifting vehicle does not have wings and will therefore not have trim and high-lift actuators. Additionally, the lifting vehicle has 24 rotors and 24 motors, which are not all included in the diagram to improve the readability of the diagram. Yet, the principle behind the relations between those components is similar.

13.2. Electrical Diagram

An Electrical Block Diagram (EBD) was created to illustrate the relationships and flow of electricity and power through the electrical equipment of the cruise vehicle. Components such as batteries, buses, switches, and relays are shown, to connect the main source of power of the vehicle to each (sub)system that requires electrical power. The batteries provide power to the vehicle, the buses serve as a central distribution point to provide power to the various vehicle systems and components, the relays facilitate automated switching of electrical power sources, which enhance system functionality and reliability [34]. On the other hand, the switches allow for manual control of the electricity flow, which are used to isolate circuits for maintenance in case of malfunction.

Note that Figure 13.4 is the same as for the lifting vehicle, with the only exception being the systems with an asterisk. Those systems are unique to the cruise vehicle and are not present in the EBD of the lifting vehicle.

13.3. Data Handling Diagram

A data handling block diagram was constructed to present the data flow through the system. The flow of data between the cruise vehicle, the ground system and a satellite system is shown. It is specified whether the signal is analog or digital, how and by what means the data is processed. The minimum outgoing bitrate of the mode S transponder is 60 kbps [9]. For the other components, it is complex to determine the exact amount of data that is sent and with what time interval. It can be assumed that the general data rate and computing power must be at least - but likely higher than - the same amount as that of a similar-sized electric aircraft. A higher amount is expected due to the high accuracy and precision required due to the coupling of the lifting and the cruise vehicle.

The general outline of the data flow from the vehicle to the satellite was taken from literature [57]. A low noise amplifier is often adopted after receiving the GPS signal from the satellite transmitting antenna[1]. This amplifies the weak signal and improves the signal-to-noise ratio. The use of a Kalman filter is common for the Attitude & Heading Reference System [13]. It provides an accurate estimate of the attitude and heading of the system, based on and by improving the data obtained from the inertial sensors. These sensors include accelerometers and gyroscopes. The system uses atmospheric sensors to further improve the accuracy of the estimations.

13.4. Communication Flow Diagram

The last diagram that shows the flow of information through the various systems involved is the communication flow diagram. This diagram focuses on the flow of information between the cruise and lifting vehicle specifically. The communication flow diagram is especially important since no human operator is involved and the coupling between the two aircraft is a crucial and precision-critical part of the mission. The required precision of the two systems is shown by the high amount of connection and visual sensors. Furthermore, both the cruise vehicle and the lifting vehicle have multiple ways of relaying their position to one another in terms of transponders, back-up transponders, broadcasting antennas, radio communication and an additional connection via a satellite. This ensures the vehicles will always be in contact with each other. Similar to the data handling diagram, quantities about the amount of data flow are uncertain at this stage of the design, and due to the novelty of the concept of coupling the two vehicles. It is therefore not included in the communication flow diagram.

[1]https://flightcrewguide.com/wiki/navigation/gps/gps-aircraft-installation-operation/ [Accessed on 4 June 2024]

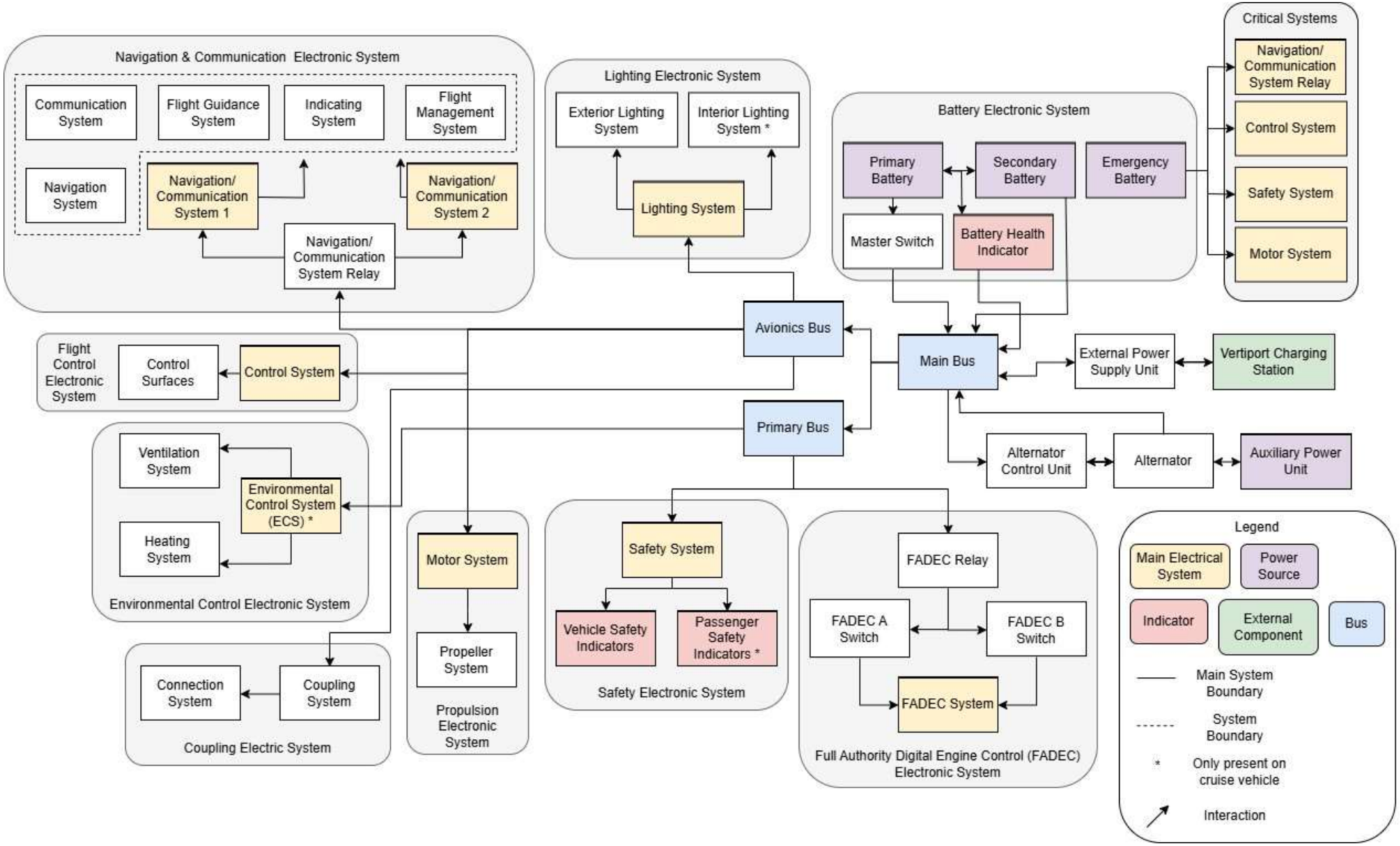

Figure 13.1: *Electrical block diagram*

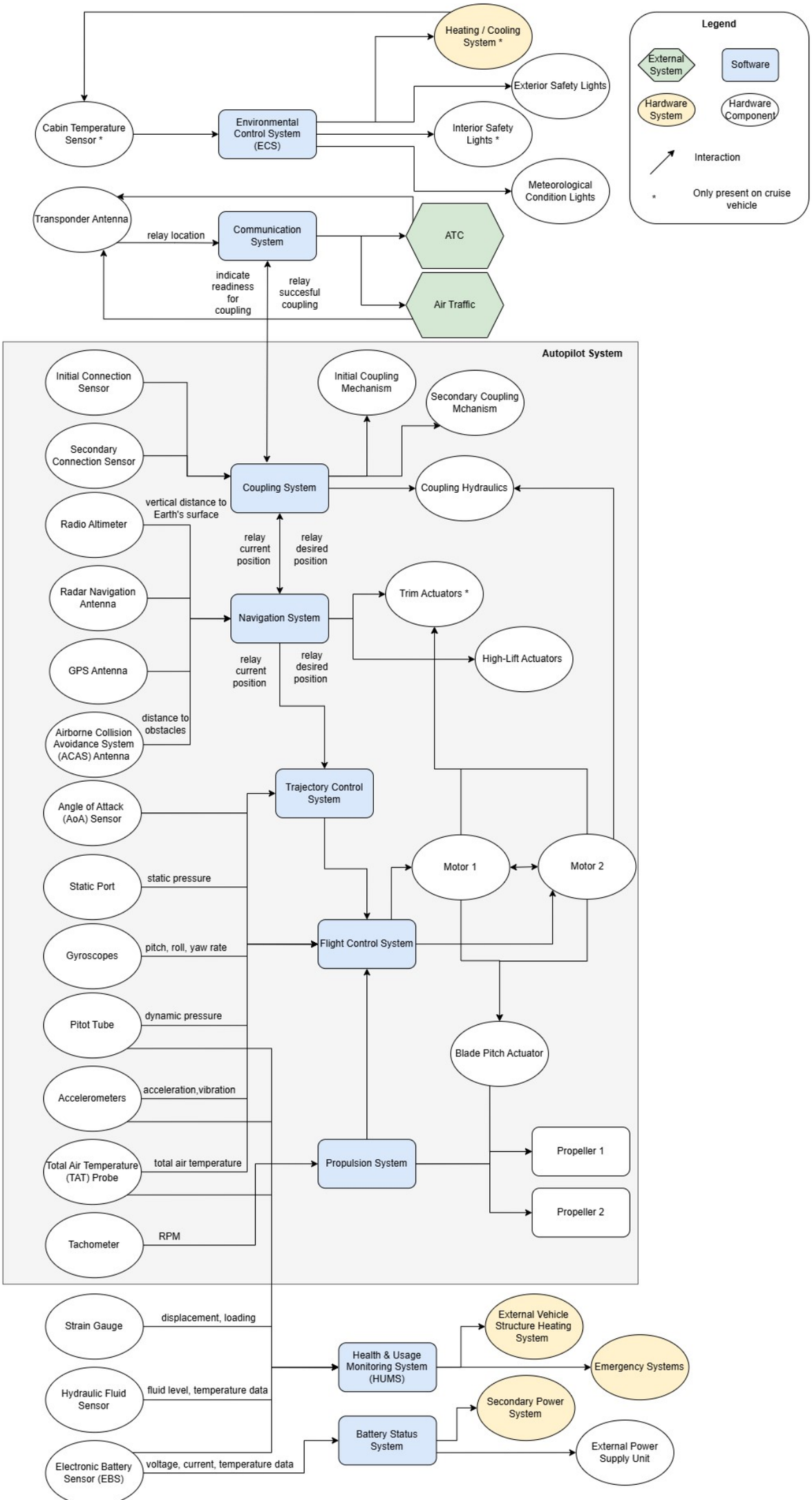

Figure 13.2: *Hardware and software diagram*

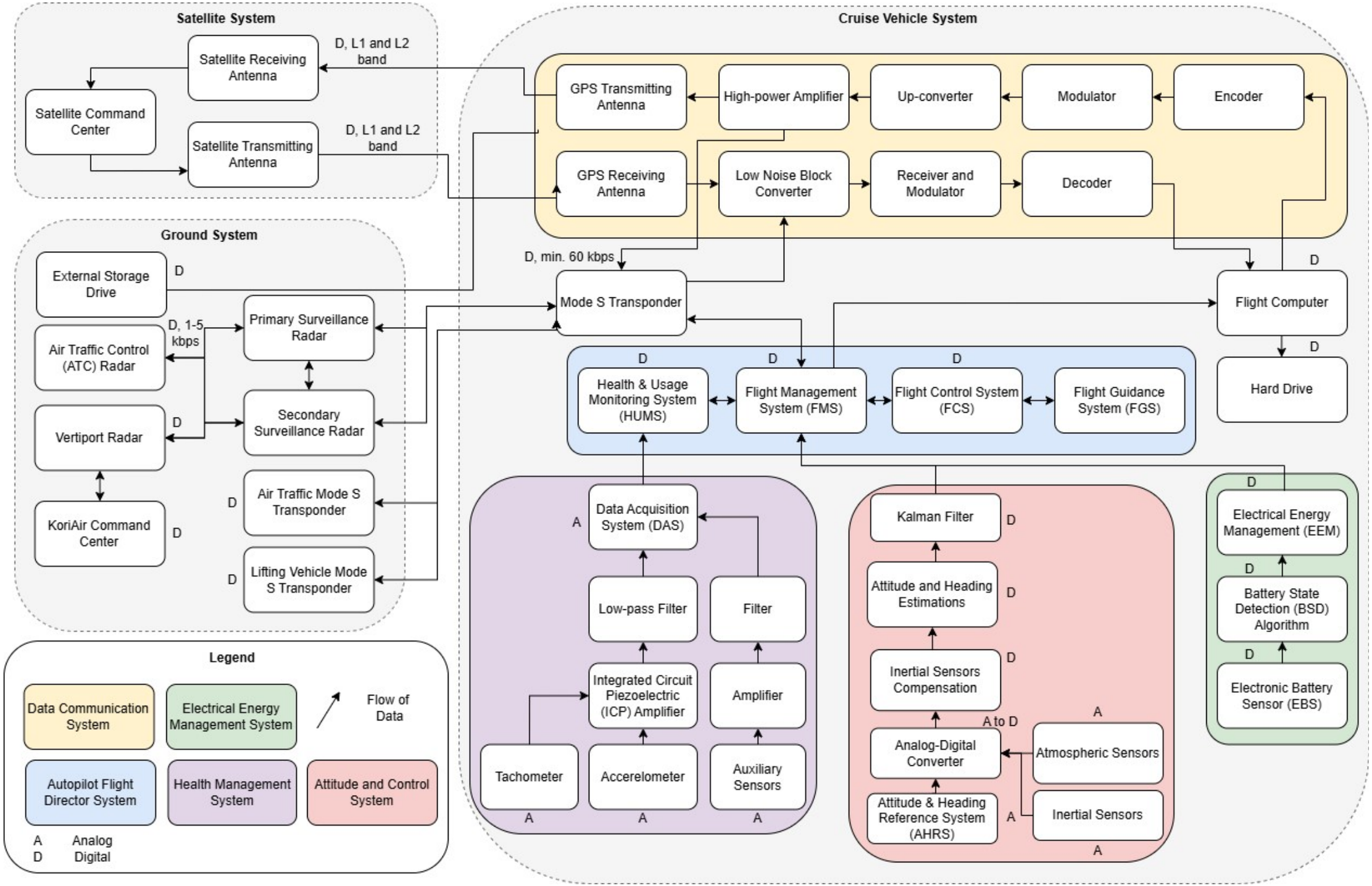

Figure 13.3: *Data handling diagram*

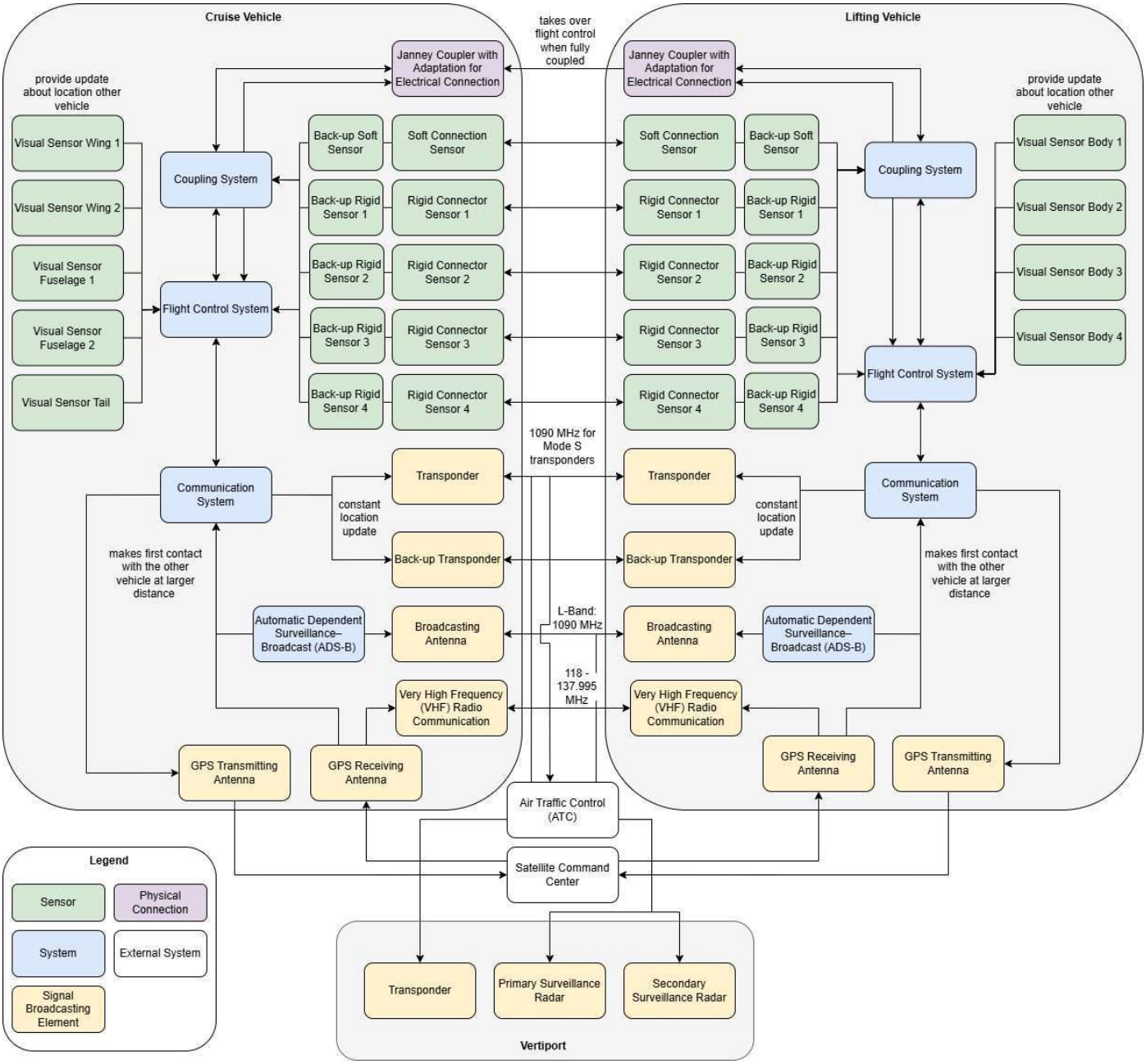

Figure 13.4: *Communication flow diagram*

14

Verification and Validation

To ensure that the performed simulation of and analysis on the design correctly represent reality, thorough verification and validation must be done. This process gives confidence in the results and points out the limitations which can be taken into account at later stages of the project. In this chapter, the performed verification and validation is presented in multiple parts. First, the overall scope of the process is described in Section 14.1. In Section 14.2 the procedures done for computational models are presented. This is followed by the description of the verification and validation for the final design in Section 14.3. Finally, the sensitivity analysis is provided in Section 14.4 as the last part of the validation process.

14.1. Verification and Validation Scope

Before the design process started, the scope of verification and validation procedures was defined. This report shows the preliminary design phase of the cruise and lifting vehicles with its coupling process. Therefore, verification and validation was done with respect to this stage of the design process, taking into account certain limitations and assumptions.

Many validation methods consist of experimental testing. Within the scope of this project, experiments were not possible. Therefore, validation of some parts of the design were left open. Especially for novel parts of the product, such as coupling, validation possibilities are limited at this point in the design process. For those parts, the analysis provided at this stage is verified to be free of any programming errors, however, it must be noted that no full certainty can be given without further testing and design detailing. Throughout the report, it is indicated whenever the analysis is limited due to a lack of details, time and resources. Moreover, plans for further analysis to improve the accuracy of the results are provided.

Another aspect limiting the verification and validation process is the simplification of many elements of the design to allow for preliminary analysis. Therefore, discrepancies might exist, especially in comparison to existing similar designs. On the subsystem level any simplifying assumptions were explicitly mentioned with the expected discrepancy compared to more detailed designs. Additionally, assumptions were made in a conservative manner to account for the lack of detail. Another method utilized to reduce uncertainty in the results which could not be sufficiently validated, was applying safety factors. With these measures taken, the design is expected to function properly when it is produced.

The verification and validation process was performed with respect to the limitations specified above. Note that while it was impossible to fully verify and validate the entire design, the results presented in the report form a basis for more detailed analysis. It is expected that these results will change, however, an initial analysis of the system has been performed.

14.2. Models Verification and Validation

Computational models form a large part of the design process, since they are used for the design of every subsystem to simulate its behaviour in different conditions. Verification of these models was done to assure that the design modelled by software accurately represents the chosen mathematical models. Verification of the created software was done in three different ways to reach full confidence in their veracity. It consisted of manual checking of the code, unit tests, and system tests.

Manual checking of a piece of code was done by a person who had not written that piece to have an independent insight on the implementation of the code. During this process, all of the inputs and lines of code were checked, and errors were corrected. Additionally, the integration in the final model was also initially verified manually.

For unit testing of the code, the following table illustrates the tests conducted on each vehicle (sub)system, as well as the expected output and the test result. For the cruise vehicle, inputs of example aircraft data provided in Raymer were given to the model to compare the model results to those provided in Raymer. These tests were done to ensure the class II weight estimation and sizing were correctly implemented from Raymer's design approach. Furthermore, to ensure proper functioning of the model, simple aircraft geometry were inputted and the model's results were compared to hand calculations of (sub)system weights and dimensions. For the lifting vehicle, since there are no relevant example aircraft from Raymer, this test type was not done. Instead, simple extreme values were given to the model to ensure its proper response to non-sensical inputs, as well as the hand calculation test performed for the cruise vehicle. The results are shown in the table below.

Table 14.1: *(Sub)system unit tests*

Subsystem	Input	Expected Output	Result
Wing	Raymer example aircraft data: MTOW, maximum load factor	Values similar to example aircraft	Passed
	Simple wing geometry: span, root and tip chord	Values similar to model output of taper, twist, etc	Passed
Fuselage	Raymer example aircraft data: fuselage dimensions, MTOW	Values similar to example aircraft	Passed
	Simple fuselage geometry: fuselage dimensions and L/D ratio	Values similar to model output of fuselage weight	Passed
Empennage	Raymer example aircraft data: AR, MTOW, tailplane volumes	Values similar to example aircraft	Passed
	Simple aircraft geometry: span, tailplane volumes	Values similar to model output of empennage weight	Passed
Propulsion	Raymer example aircraft data: MTOW, battery energy density	Values similar to example aircraft	Passed
	Simple aircraft parameters: MTOW, range, cruise speed	Values similar to model output of total power required	Passed
Landing Gear	Raymer example aircraft data: MTOW, maximum load factor	Values similar to example aircraft	Passed
	Simple aircraft parameters: MTOW, landing gear dimensions	Values similar to model output for landing gear weight	Passed
Airframe (lifting vehicle)	Simple aircraft geometry: MTOW, fuselage dimensions	Values similar to model output of airframe weight	Passed
	Extremely high MTOW	Extremely high values with model warning	Passed
Landing Gear (lifting vehicle)	Simple aircraft parameters: MTOW, strut dimensions	Values similar to model output of landing gear weight	Passed
	Extremely high MTOW, maximum load factor	Extremely high values	Passed
Propulsion (lifting vehicle)	Simple aircraft parameters: MTOW, range, cruise speed	Values similar to model output of total power required	Passed
	Extremely high MTOW, range, cruise speed	Extremely high values with model warning	Passed
Stability and control	The example values from Luukkonen [36]	Similar response from the model	Passed

In addition to unit testing, integration tests were performed. They were used to check whether

the values were correctly shared between subsystems, and each of the subsystems were updated accordingly in the design loop. Additionally, it was checked whether the final parameters of the subsystems allowed for the subsystem to perform its functions. The integration tests are summarized in the table below.

Table 14.2: *System integration tests and their results*

Subsystem	Input	Expected Output	Result
Wing	Final values for: wing surface area, maximum lift coefficient, stall speed	Lift at stall speed is larger or equal than the weight	Passed
	MTOW increases between iterations, stall speed and lift coefficient are constant	Wing surface area increases between iterations	Passed
Empennage	Wing area increases between iterations	Horizontal and vertical tail area increases between iterations	Passed
Propulsion	Drag estimation results, propeller parameters	Thrust is larger or equal to drag	Passed
	Drag increases between iterations	Thrust increases between iterations	Passed
Landing Gear	MTOW increases between iterations	Landing gear weight increases between iterations	Passed
	Center of gravity excursion, landing gear location, MTOW	Nose landing gear carries 8-15% of the weight of the vehicle	Passed
Airframe (lifting vehicle)	Thrust generated by rotors increases between the iterations	Mass of the airframe increases between iterations	Passed
Landing Gear (lifting vehicle)	MTOW increases between iterations	Landing gear weight increases between iterations	Passed
Propulsion (lifting vehicle)	MTOW of both vehicles, drag of both vehicles	Thrust is larger or equal to drag and weight	Passed
	MTOW increases between iterations	Required power increases between iterations	Passed

Validation was done mainly on the subsystem level. It was mainly done through comparison to available data and literature. For instance, many models were compared to the Cessna 172 and the Pipistrel Velis Electro due to the similarity of these aircraft to the cruise vehicle. For the lifting vehicle, due to the lack of experimental data on the multicopters, the validation was very limited. Existing vehicles that were used for comparison were helicopters and multicopter drones. The table with validation tests is shown below.

Table 14.3: *Validation testing per (sub)system model*

Subsystem	Input	Expected Output	Result
Wing	Reference aircraft data: MTOW, maximum load factor	Values similar to reference aircraft	Passed
Fuselage	Reference aircraft data: fuselage dimensions, MTOW	Values similar to reference aircraft	Passed
Empennage	Reference aircraft data: AR, MTOW, tailplane volumes	Values similar to reference aircraft	Passed
Propulsion	Reference aircraft data: MTOW, battery energy density	Values similar to reference aircraft	Passed
Landing Gear	Reference aircraft data: MTOW, maximum load factor	Values similar to reference aircraft	Passed
Airframe (lifting vehicle)	Reference aircraft data: MTOW, fuselage dimensions	Values similar to reference aircraft	Passed

Continued on next page

Table 14.3: *Validation testing per (sub)system model (Continued)*

Landing Gear (lifting vehicle)	Reference aircraft data: MTOW, strut dimensions	Values similar to reference aircraft	Passed
Propulsion (lifting vehicle)	Reference aircraft data: MTOW, range, cruise speed	Values similar to reference aircraft	Passed

14.3. Design Verification and Validation

When the design was produced, it also had to be verified and validated. Verification procedures for the design consisted of checking whether the design met the requirements. This was done by means of the compliance matrix in Chapter 22. Within the aforementioned scope, it was not possible to fully verify the model. However, whenever compliance with certain requirements could not be verified yet, a proposal was made on how to achieve compliance in further stages of the project. These are addressed in Chapter 22.

Due to time and resource limitations it was not possible to validate the entire design. Recommendations for this scope of validation include conducting full scale model testing in wind-tunnels, as well as vibration and structural load testing. Once the prototype model has met safety standards, initial flight tests should be conducted to ensure proper design functioning.

14.4. System Sensitivity Analysis

During a sensitivity analysis, one looks at how a variation of technical parameters influences the design and the requirements it meets. For the analysis, the altered parameters will be a variation of estimated component weights, battery specifications and operation logistics. The consequences of the changing parameters will be measured by analyzing how the final design varies and if the number of requirements met by the design varies. Performing a sensitivity analysis has several benefits: it helps identify the critical parameters that the design is sensitive to and assists in determining the robustness of the design.

To conduct the sensitivity analysis, each technical parameter (referred to as 'P'), will be subjected to a 10% increase or decrease in the direction that negatively impacts the design. Ten percent was chosen as contingency factor as it is the value that NASA uses when the design and subsystems layouts are determined [21]. The parameters selected for the analysis are those that have the most influence on the design. After implementing the change, the entire design procedure will be performed. The effect of the change will be measured by analyzing the difference in maximum take-off mass, power requirements and number of requirements met. Each parameter will be assigned a sensitivity score ranging from one to five, with the corresponding changes being: <1%, <3%, <5%, <10%, and >10%. These sensitivity levels will be valuable in future design stages, helping identify which parameters require more attention and should remain unchanged. As can be seen by Table 14.4, which summarizes the effects of a variation of technical parameters, the design is robust to these changes.

P1: Decrease in battery energy density The battery used in the design is not commercially available and is found in only one other aircraft. To investigate the effects of relying on such proprietary equipment, the energy density of the power source was reduced. The consequences of a 10% decrease in specific energy of the battery are a 3% and 4% increase in the total take-off mass of the cruise vehicle and lifting vehicle respectively. This parameter change does not affect the number of requirements met.

P2: Coupling mechanism mass and procedure Increasing the mass of the coupling systems found on both the lifting and cruise vehicle by 10% results in a 2% increase in the total mass of each vehicle and a 2% increase in the power required for both take-off and cruise. To the time required to couple both vehicles a greater variation was applied because this procedure is the first of its kind. Nonetheless, doubling the coupling time increased the mass and power requirements of both vehicles by negligible amounts (<0.1%). Increasing both mass and coupling time does not affect the requirements met.

P3: Heavier payload The consequence of increasing the payload mass by 10%, from 420 kg to 462 kg, results in an increase in the total mass of the cruise and lifting vehicles of 5% and 1% respectively. The take-off power of the lifting vehicle increases by 4% and the cruise power of the cruise vehicle increases by 3%. These changes do not significantly impact the final design, nor do they cause any requirements to be unmet.

P4: Increased cruise velocity Increasing the velocity of the cruise vehicle by 10% results in an increase of the power required during cruise of 5%. The mass of the cruise vehicle increases by 2% while the mass of the lifting vehicle is largely unchanged (<0.1%). The variation of this parameter does not have significant implications on the final design.

P5: Increased drag In the event that drag was underestimated due to the shape of the fuselage, landing gear drag or the lifting vehicle's ducts, the effect of increasing the drag of both vehicles during horizontal and vertical drag was investigated. A ten percent increase in the drag increases the lifting vehicle take-off mass by 2% and increases the cruise power required by 11%. The lifting vehicle's mass increases by a quarter of a percent while its take-off power increases by 4% due to the added weight from the cruise vehicle. The battery mass of the cruise vehicle increases by 8%, but there is enough space in the fuselage to accommodate the required extra volume. Overall, increasing the drag does not significantly alter the design of the aircraft.

Table 14.4: *System sensitivity analysis results displayed with sensitivity score*

	P1	P2	P3	P4	P5
Cruise vehicle mass	3	2	3	2	2
Lifting vehicle mass	3	2	1	1	1
Take-off power	2	2	3	2	3
Cruise power	2	2	3	3	5

As can be seen in Table 14.4, both aircraft are robust to variations in the technical parameters. A 10% change in input parameters results in a maximum of 5% change in the vehicle masses. Although the scenario with increased drag causes the most significant overall change — an 11% increase in the required cruise power — the masses of the lifting and cruise vehicles remain largely unchanged, and no additional requirements become unmet. From the system sensitivity analysis, the key technical parameters that have the largest influence on the design are the specific battery energy and payload mass. During the detailed design phase, special attention should be given to ensuring these parameters are optimized, as they have the greatest impact on overall performance and efficiency.

15

Infrastructure Integration

Besides, the design of the vehicles themselves, the design of the infrastructure is of great importance. Without a proper vertiport, the vehicles will not be able to perform a successful mission. In this chapter, the integration of the take-off and landing infrastructure in urban communities is discussed. To begin with, Section 15.1 details the components and layout of these components in the design of the vertiports, including safety areas, lighting and any additional equipment that is required for the vehicle configuration to safely and accurately land on the vertiport. Next, Section 15.2 covers the decisions made to select optimal locations for vertiports in urban cities. Two example cases are also analyzed, using Amsterdam for intra-city travel and the Randstad area for inter-city travel. Section 15.3 discusses the implementation of route optimization software and algorithms into the operation management systems of the vehicle. This chapter concludes with Section 15.4, which gives a description of the operations of the vehicle system throughout the entirety of its mission. This includes the flight operation modes, as well as the integration of the vehicle system in the existing infrastructure of urban environments.

15.1. Vertiport Design

The design of the vertiport infrastructure for the lift and cruise vehicle configuration is important for the integration of this system in urban environments. In order to size the vertiport, some of the heliport design standards from the International Civil Aviation Organization (ICAO) Annex 14, Volume II will be followed [26].

15.1.1. Vertiport Layout

The most basic elements included in the design of a heliport which will be present in the vertiport are the following:

- Final approach and takeoff area (FATO)
- Touchdown and liftoff area (TLOF)
- Clear approach and departure paths
- Safety zone
- Wind cone

The TLOF must be at least as long and wide as the rotor diameter of the largest vehicle to land on the vertiport [26]. In this case, the largest vehicle would be the cruise vehicle, however, the motor configuration size of the lifting vehicle is larger than that of the cruise vehicle, with a size of approximately 12 by 8 m. As a result, the TLOF will be designed as a 12 by 8 m area. The FATO will cover the TLOF, and as such will be a 12 by 12 m area. The safety zone will serve as the location for the battery charging station and storage for any basic operational and maintenance instruments (such as additional batteries, emergency kits, etc). Furthermore, a wind cone will be included on the vertiport to indicate the current wind direction, and based on the direction of the most predominant wind, an approach and departure path will be indicated with ground-based vertiport lighting.

An example of the standard heliport design and layout is illustrated in Figure 15.1. Note that the figure includes certain aspects of heliport design which will not be included in the vertiport, such as the paved taxiway.

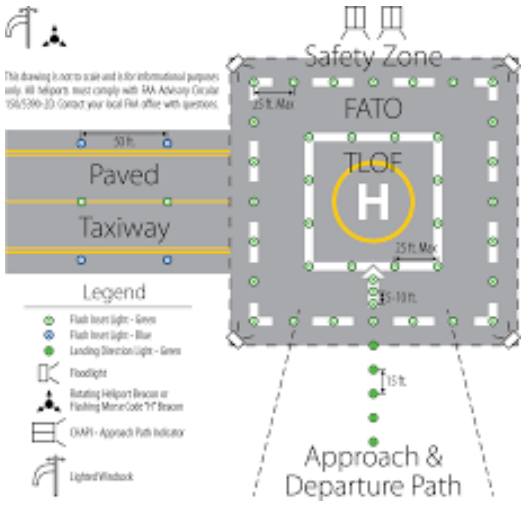

Figure 15.1: *Heliport design standards [26]*

15.1.2. Vertiport Lighting

The designated surfaces on the vertiport must also be surrounded by lighting to better delineate the areas during normal operation and during non-optimal meteorological conditions. Flush green lights (with a reading of about 100 candelas) will be used to define both the FATO and TLOF perimeter [26]. The standard is to use a minimum of four light fixtures per each side of the TLOF, of which one must be located on the corner of the each side. Lights can be spaced at a maximum of 7.6 m [26]. Additional useful visual aids include: floodlights, approach lights and obstruction lights. Obstruction lights are installed where required to mark objects in close proximity to the approach and departure path.

15.1.3. Landing Infrastructure

Once the lifting and cruise vehicle configuration has landed on the vertiport, a sliding jack will be used to support the lifting vehicle, as the landing gear of the cruise vehicle was not designed to support the total weight of both vehicles in the coupled configuration. This decision was made because otherwise the landing gear of the cruise vehicle would have been over-designed for the majority of its flight regime. As such, when the coupled vehicles land, the landing gear of the cruise vehicle will touchdown, and the rotors of the lifting vehicle will continue spinning to keep generating enough thrust to hover and counteract the weight of the vehicle. A sliding jack with a similar shape to a forklift, configured with wheels to support fast and easy movement, will be rolled under the lifting vehicle around the frame of the cruise vehicle. The jack will be extended to support rotors and counteract the total weight of the lifting vehicle, and once it is supported, the rotors will be shut down. The tool as a whole will have a c-shaped structure, with a lower horizontal beam to attach the wheels and have contact with the ground, a vertical beam (to be taller than the height of the cruise vehicle's wings), and a final horizontal beam (which will be located above the cruise vehicle's wings) to support the rotors of the lifting vehicle.

The jack will be included in every vertiport location to support the vertical landing of the vehicles. Additional equipment which will be present on the vertiport consists of:

- Charging port for battery recharging
- Spare batteries for battery replacement
- Emergency kit for first aid purposes
- Basic tools and instruments for operational maintenance and inspection
- Wheelchair accessibility items (e.g. a ramp)

15.2. Location Selection

In order to better determine the location for vertiports of KoriAir, the urban environment surrounding Amsterdam and the general Randstad area was analyzed. The main objectives which were considered

when determining vertiport locations were their distance to public transportation stations and residential areas. The former was minimized, and the latter was maximized, considering the general layout of the urban communities investigated. Furthermore, the location of vertiports (in this sense heliports), already constructed in the environment for private or commercial use was also considered. For this readily available infrastructure, the ground footprint of the heliport was estimated, and if it was equal to or greater than the 12 by 12 m area required for the KoriAir vehicle, then the infrastructure was considered accessible.

One final consideration which was made was the vertiport's proximity to the main central business district of urban cities, which was considered an important location for two main reasons. Firstly, the expected users for KoriAir vehicles are likely managerial and executive persons which will be attracted to the advantages that KoriAir has to offer (e.g. faster travel time than current intra-city travel). It is therefore beneficial to locate vertiports close to the central business district such that these persons can easily travel by foot to their respective working locations from the vertiport. Secondly, most high-rise buildings have an average roof area of about 1500 to 2500 m^2, which implies a width of about 30 to 50 m[1]. With this knowledge, it can be planned to implement vertiports on the rooftops of those high-rise buildings in case it meets the regulatory and operational restrictions for UAM vehicles within the city.

In the case of Amsterdam, the private and public heliports already present within the city were first located. The ground footprint of these heliports was then checked, and those which met the requirements for the KoriAir vehicles were concluded to be located at the Amsterdam UMC Hospital, Schiphol Airport and the commercial Amsterdam Heliport. At this point, two new vertiport locations were conceptualized in the two main central business districts of Amsterdam. Their exact locations are illustrated in Figure 15.2 below, with 'New Vertiport 1' being located only 10 minutes away by ferry to Amsterdam Centraal Station and 'New Vertiport 2' being located in the extremity of the green area surrounding the Johan Cruijff Arena, which is a 5 minute walk from the nearest train station.

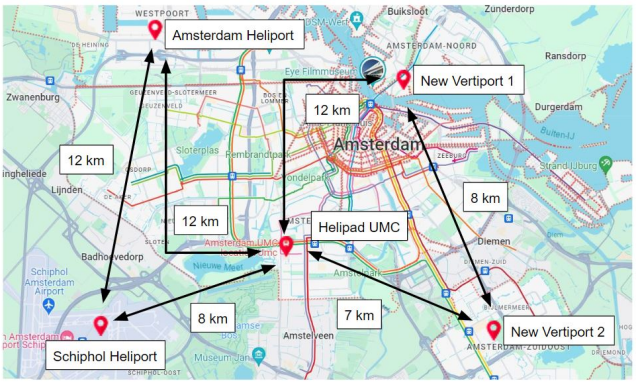

Figure 15.2: *Map of Amsterdam with existing and new vertiport locations*

As can be seen from the figure, the vertiport locations are indicated with a red symbol, and the route between vertiports is shown with a black arrow, including the approximate distance between respective vertiport locations. When constructing the routes, a direct path was initially attempted in order to reduce flight time, but in some cases the route had to be altered to avoid the main residential areas of Amsterdam. An example of this is the route from Helipad UMC to New Vertiport 1. The average distance seen for intra-city travel in Amsterdam was about 10 km, with a range from 7 to 12 km. Considering the cruise speed of 200 km/h and the take-off and landing time of 200 s, an estimate of about 10 minutes for Amsterdam intra-city travel was conceptualized.

For the case of inter-city travel, the Randstad area was also analyzed using only existing heliports. It was chosen to analyze only the transport with readily available heliports to demonstrate the universality of KoriAir vehicles and their easy implementation in urban environments. In this scope, only the

[1]https://en.wikipedia.org/wiki/List_of_skyscrapers_by_floor_area

main heliports of Amsterdam, The Hague, Rotterdam and Haarlem were considered and are shown in Figure 15.3 below.

Figure 15.3: *Map of the Randstad area with existing vertiports only*

The shortest distance illustrated is 15 km, the shortest distance from The Hague to Rotterdam. Estimated flight duration is about 15 minutes. For the medium distances of about 20 to 30 km, for travel between Amsterdam and Haarlem or a longer option from The Hague to Rotterdam, an average of about 20 minutes is estimated. The longest range of distances considered travelling from The Hague/Rotterdam to the Amsterdam, with a distance of around 50 to 60 km. This flight path is estimated to take about 25 to 30 minutes. These routes are more direct as it is expected that the vehicle will cruise at higher altitudes for longer flights, and thus the sound pressure level perceived at ground level in residential areas will be lower and less intrusive to the public.

An important requirement to consider is the amount of time it takes for emergency services to reach vertiport locations to assist in any possible emergency. The travel time for emergency services to the vertiports locations was decided to be less than 10 minutes. Each vertiport location was analyzed, and the results are shown in Table 15.1.

Table 15.1: *Response time of emergency services for all vertiport locations*

Vertiport Location	Travel Time [min]	Closest Hospital
Amsterdam		
New Vertiport 1	8	Bovenij Hospital
Amsterdam Heliport	10	ACIBADEM International Medical Center
Helipad UMC	-	UMC
New Vertiport 2	7	UMC Location AMC
Schiphol Heliport	3	According to regulations[1]
Helipad Red Cross Haarlem	-	Red Cross Hospital
Rotterdam		
Heliport Rotterdam Airport	3	According to regulations[1]
Heliport Maasstad	-	Maasstad Hospital
The Hague		
Heliport HMC Bronovo	-	HMC Bronovo
Heliport AHZ/Hagaziekenhuis	-	AHZ/Hagaziekenhuis

[1] https://ufuav.asn.au/wp/wp-content/uploads/2016/11/operations-manual.pdf [Accessed on 14 June 2024]

The travel time was calculated using the route a normal car would take. The expected reduction in

travel time due to the use of emergency vehicles equipped with visual and auditory signals has not been considered. Therefore, the actual time to the vertiports is expected to be less.

15.3. Route Optimization

Route optimization software and algorithms can be applied once the vertiport locations have been selected. In principle, the shortest path shall be the target in order to optimize battery usage and minimize energy consumption, and the flight path will be altered based on any obstacles or proximity to residential areas. Several papers have suggested route planning procedures to bring UAM vehicles to market in already complex and congested urban environments. For example, a paper investigating the routes and procedures for Supernal's UAM vehicle usage in the Los Angeles Metropolis [11], makes use of a Provider of Services for UAM (PSU). A PSU is an entity that supports UAM operators with meeting UAM operational requirements that enable safe, efficient, and secure use of the airspace. For the case of Supernal, the PSU acts as an interface between the UAM ecosystem and the Federal Aviation Administration (FAA), as it will be the primary service and data provider for its stakeholders [11]. The PSU aids in supporting UAM operators to meet regulatory and operational requirements for UAM operations within an urban environment. This includes the consideration of no-fly zones and operational restrictions within the airspace that must be avoided when planning the flight path of the vehicle.

It is proposed to implement the usage of PSU for KoriAir to optimize route planning in coordination with ATC. An example flow chart of communication between the PSU and ATC operations is shown in Figure 15.4 below. After the KoriAir user has made the flight request, the proposed flight path is submitted to the PSU. At this point, the PSU analyzes and confirms that the flight plan is complete, consistent with current advisories and restrictions, and strategically de-conflicted. It takes into consideration previously confirmed flight plans, Cooperative Operating Practices (COPs), UAM corridor capacity, airspace restrictions, vertiport resource availability, and adverse environmental conditions [11]. Once approved, it assigns a Globally Unique Flight Identifier (GUFI) to the flight plan, under which the vehicle chosen for operation is monitored and continuous telemetry data is communicated to the PSU network. This continuous monitoring allows for optimal airspace usage, predictive capabilities based on previous flight plans, system adaptations to changes in internal and external conditions, and a more streamlined operation that will avoid overburdening the existing collaboration with ATC.

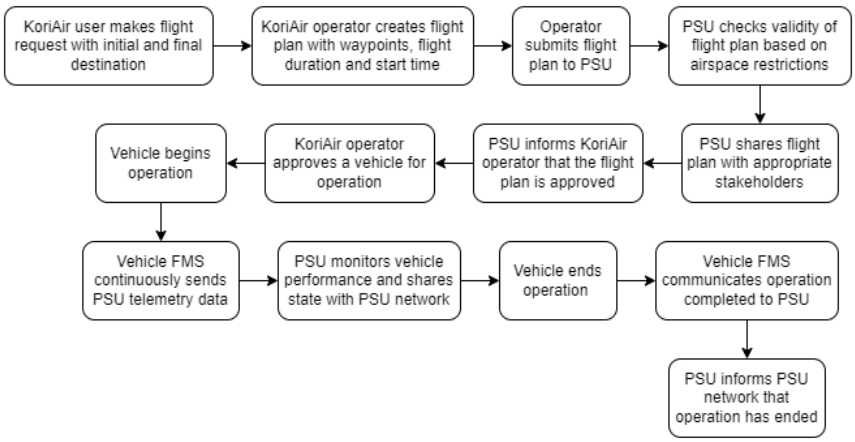

Figure 15.4: *PSU process workflow*

15.4. Operations and Logistics

This section describes the operation of the system for the complete mission. Using the functional flow diagram (FFD) in Section 4.2 as a starting point, the overall operations and logistics of the mission were presented. A diagram is also presented in Figure 15.5 to aid in the understanding of the operations

described.

Following from function 2.1 of the FFD, the preparation phase before flight consists of charging the batteries and inspecting the cruise vehicle. If the aircraft passes the inspection, the payload (cargo or passengers) is loaded and a final take-off check is performed. If the aircraft passes the final check, communication with city or regional air traffic control (ATC) is initialized and a request for take-off is presented. The navigation systems are enabled and the multicopter couples with the cruise vehicle from the air. Once the ATC request is granted, the take-off phase is initialized.

For take-off, the functions of block 2.2 are described here at a higher level. After the sliding jack is removed, the lifting vehicle accelerates the two vehicles vertically to take-off. In this way, the take-off procedure begins. If the take-off is deemed to be unsafe, an emergency landing is performed at the closest vertiport. Otherwise, a transition to cruise can be initialized. The forward propellers are activated and once a speed sufficient of maintaining level flight is achieved, the decoupling procedure can commence. A request for decoupling is sent to ATC and once accepted, the lifting vehicle separates from the aircraft and autonomously returns to the vertiport of departure, either to couple with another cruise vehicle or to land on the landing pad. The cruise vehicle will continue to cruise at the altitude specified by ATC.

During cruise, if a serious failure occurs, and an emergency landing is necessary, there are two landing options available. If the aircraft is sufficiently close to a vertiport and is able to maintain level flight, an emergency vertical landing procedure can be performed, which will be explained below. Otherwise, the aircraft will not be able to couple with a lifting vehicle and be forced to perform an emergency horizontal landing at a runway, empty road or field. A system of parachutes can be deployed to reduce the aircraft's vertical and horizontal momentum when nearing approach.

Once the aircraft is sufficiently close to its destination, a request will be sent to ATC and the vertiport's control system to begin the coupling phase. Once approved, a lifting vehicle will autonomously depart from the vertiport and fly towards the aircraft. Once the two vehicles are at a predetermined distance between each other, the cruise vehicle will reduce its speed to the maximum speed of the lifting vehicle. Then, using information transmitted from the cruise vehicle's navigational system, the lifting vehicle will align itself with the aircraft's flight path and speed, while maintaining a higher altitude than the latter. The lifting vehicle will slowly reduce the horizontal distance between the two vehicles, until it is directly above the aircraft. At this stage, the lifting vehicle will slowly descend towards the cruise vehicle and, once the two vehicles are sufficiently close, the coupling mechanism will activate. If the coupling is unsuccessful, the lifting vehicle will separate from the aircraft and perform another coupling attempt. If the second is unsuccessful, the lifting vehicle will return to the vertiport and a second will be sent to attempt coupling. If the second lifting vehicle is also unsuccessful, the aircraft will perform an emergency landing as explained in the section above.

If the coupling is successful, the lifting vehicle will keeps its propellers at idle and the aircraft will maintain its speed and continue at level flight. Once the aircraft reaches a distance of 300 meters from the vertiport, the cruise vehicle's engines' power will be reduced, slowing down the aircraft. The multicopter will increase the lift it provides to maintain a level flight. Once the aircraft is nearing the vertiport, the lifting vehicle will slow down the aircraft to a stop above the landing zone and begin a controlled vertical descent. Once vehicle touchdown is achieved, a sliding jack will support the vehicles while the lifting vehicle's propellers spin down. The payload is removed and the vehicles are charged.

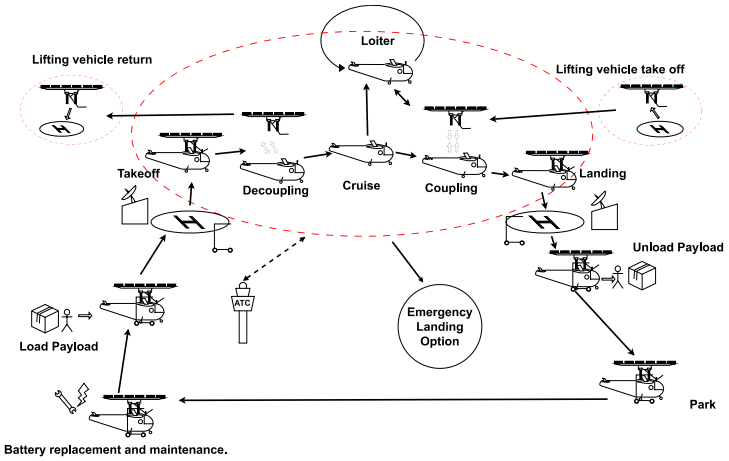

Figure 15.5: *Operations and logistics concept*

15.5. Comparative Characteristics

In order to place the operation of the KoriAir system in the market, it is important to compare its operation characteristics with other means of transport. The following table, originally in chapter 3, shows the time, cost, noise emission and energy consumption of KoriAir compared to alternative inter/intra-urban transport. Note that noise level is measured at a distance of 100 m. The energy consumption of the eVTOL vehicle from Archer Aviation was based on its commercially available range and battery capacity characteristics, whilst KoriAir's was based on the battery specifics of the Joby S4 battery used for both vehicles and its mission range.

Table 15.2: *Performance of KoriAir compared to other means of transport*

	Intra-city (8 km)				**Regional (30 km)**				**Inter-city (50 km)**			
Transport	Time [min]	Price [€/pax]	Noise [dBA]	Energy consumption [kWh]	Time [min]	Price [€/pax]	Noise [dBA]	Energy consumption [kWh]	Time [min]	Price [€/pax]	Noise [dBA]	Energy consumption [kWh]
Train	19	3.3[1]	62 [47]	24	40	6.5[1]	62 [47]	90	28	14.5[2]	62 [47]	150
Car	45	1.4[3]	53 [43]	4.8	80	5[3]	53 [43]	18	45	5.4[3]	53 [43]	30
Taxi	45	35[4]	53 [43]	5.6	80	80[4]	53 [43]	21	45	110[5]	53 [43]	35
Helicopter [15]	5	390[6]	89	140	10.5	390[6]	89	520	15.5	390[6]	89	860
Archer Aviation	5	28[8]	61[7]	10	10	105[8]	61[7]	25	16	165[8]	61[7]	45
KoriAir	5.5	8	77	10	12	30	77	20	18	50	77	30

[1] https://tfl.gov.uk/fares/find-fares/tube-and-rail-fares [Accessed on 17 May 2024]
[2] https://www.ns.nl/ [Accessed on 17 May 2024]
[3] Consumption of 9l/100km, 1.75€/l
[4] https://tfl.gov.uk/modes/taxis-and-minicabs/taxi-fares [Accessed on 17 May 2024]
[5] https://www.taxicentrale-schiphol.nl/en/ [Accessed on 17 May 2024]
[6] https://www.batterseahelicopter.com/helicopter-hire-prices/ Assumed price independent of distance in the specified range. [Accessed on 17 May 2024]
[7] https://news.archer.com/how-loud-is-an-evtol [Accessed on 21 June 2024]
[8] https://www.autofutures.tv/topics/-the-sky-is-no-longer-the-limit—-archer-aviation-to-offer-6-minute-evtol-flights-to-the-airport—/s/57e93aea-44fc-44b8-9f88-84afca6c1412 [Accessed on 21 June 2024]

16

Production Plan

It is important to thoroughly discuss the production of the vehicles to ensure efficient production planning and to address specific design-influenced processes and material considerations. In this chapter, the aspects of the manufacturing, assembly and integration of both the lifting and cruise vehicle will be discussed. The centerpiece of this chapter is the production plan, which is described in Figure 16.1. Some production processes are elaborated on, especially ones which are uniquely influenced by the chosen design. Manufacturing and material details are also briefly described when there are special considerations to be taken into account.

16.1. Production Processes

The production plan serves as a detailed step-by-step guide on how to manufacture the system. Due to the two-vehicle system, there are two branches in the production plan in Figure 16.1.

The production of both aircraft is split based on aircraft sub-assemblies. In general, the sub-assemblies correspond to subsystems of the vehicles. The production is based on sub-assemblies to increase efficiency during the manufacturing process, especially for large series products. For each sub-assembly, before manufacturing any parts, the materials and commercially available components must be ordered. Most components will be ordered if possible to reduce development costs, except for the more unique and specialized parts for the vehicle, such as the spars of the center wing box which must be able to accommodate coupling.

For all sub-assemblies, after parts and materials have been sourced, materials are processed into finished parts such that sourced and locally manufactured parts are ready for assembly. At this point, the assembly within each sub-assembly will proceed, which will sometimes be split into multiple sections. For example, the fuselage sub-assembly consists of a tail cone, nose and the center wing box. The interaction of each subsystem with other subsystems will also be taken into account during the processing and assembly phase. As a result, the sub-assemblies which have significant interactions need to be tested before their final assembly. For example, the propulsion system sub-assembly includes a step for testing with the power system. Some sub-assembly blocks also explicitly state the specific steps that need to be taken for structural integration of other subsystems - such as fittings for the wing to be integrated into the center wing box, or the engine mountings for aircraft propellers. Before heading to final assembly, the sub-assemblies undergo quality control to ensure that the sub-assemblies meet their specific requirements.

Once completed, the sub-assemblies must be assembled together to create the final system. The general order of events is described in the boxes titled 'Cruise Vehicle Assembly' and 'Lifting Vehicle Assembly'.

16.2. Important Consideration

At this stage, more details regarding the material and manufacturing aspects of the two vehicle configuration must be defined. This will include specifications on the coupling mechanism, the cruise vehicle wing box and the rotor ducts, which will be described in the following sections.

16.2.1. Coupling Elements

The hooks of the lifting vehicle and the spars of the center wing box (CWB) of the cruise vehicle serve as the coupling elements for the mechanism. These will be made of titanium due to its high strength

and fatigue properties. Because of the high tolerances required and the criticality of the coupling for operations, the hooks and spars will be machined. Machining is useful for complex parts, such as the spar and the necessary interior cavities for coupling and any clamping mechanisms that will be implemented. The primary disadvantage is cost but this is deemed acceptable based on the necessity of precision required for the parts being produced.

16.2.2. Cruise Vehicle Wing Box

As described in Chapter 7, the wing box will consist of a CWB which is in the fuselage, and two outer wing boxes (OWB) which are attached to the center wing box. The OWBs are manufactured using standard techniques already applied in the industry, and are composed of front and rear spars, ribs and flanges. The CWB is manufactured similarly, and thoroughly integrated into the airframe of the cruise vehicle. A key difference is that the front and rear spars are heavily modified to structurally accommodate for the loads introduced by the coupling mechanism.

Both CWB and OWB need to accommodate a joint to integrate the full wing box. This joint transfers the wing loading to the CWB from the OWBs and is a critical part of the aircraft structure. Testing of the full wing box will not only demonstrate that the wing loading can be sustained, but also that the CWB integration into the airframe of the cruise vehicle is sufficient for the coupling loads introduced.

16.2.3. Rotor Ducts

The shroud of the lifting vehicle rotors consist of an eliptical profile rotated around the axis of the rotors. The shape can be likened to a torus (or donut) where its circular profile has ben squashed to an ellipse. The shroud is made of carbon-fiber reinforced polymer (CFRP) and filled with a vibration-reducing foam. The shell will be made of two halves, manufactured using lay-up techniques. The hollow donut shape then covers the vibration-reducing foam if it is already solid. Otherwise, the two halves are put together and a liquid foam is filled into the hollow space through a small hole. The choice of which vibration-reducing foam to apply will be made in future development of the design, with a key choice driver being the foam density.

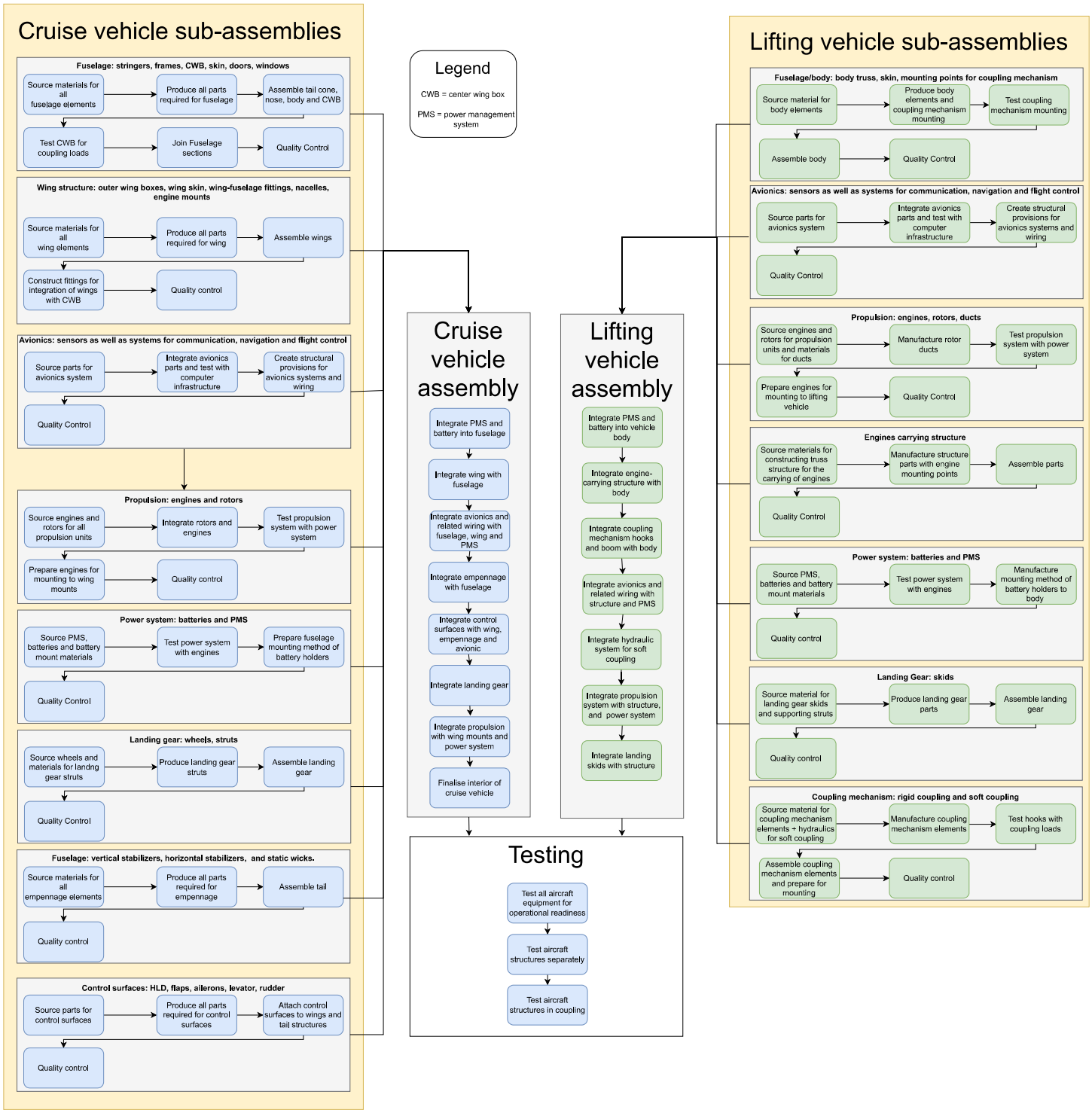

Figure 16.1: *Production plan diagram*

17

Sustainable Development Strategy

Sustainability is important because it minimizes environmental impact and enhances quality of life by reducing pollution and noise pollution. This chapter outlines the sustainable development strategy of KoriAir, which addresses the way sustainability is taken into account in the design and the way the product contributes to the sustainability of the overall urban environment. Key performance indicators (KPIs) are used to monitor the sustainability of the project. KPIs are quantitative measures that assign numerical values to the sustainability performance of an organization. They will be covered in Section 17.1. Then, various technological considerations related to the sustainability of the design will be discussed in Section 17.2.

17.1. Key Performance Indicators

KPIs are effective tools to break down the idea of sustainability into more tangible concepts, and to keep track of their values throughout the project. To measure the sustainability of the final design, the following KPIs were specified as being relevant to the project.

- **Carbon emission per km:** measure kilograms of CO_2 emitted per km
- **Noise level:** assess noise in dBA for each flight phase, with particular emphasis on take-off
- **Ground footprint:** measure the area required for take-off and landing infrastructure in m^2
- **Energy consumption for production, operation, maintenance, and recycling:** track energy usage in kWh for production, operation, maintenance, and recycling of the vehicle configuration
- **Battery lifetime:** track the number of km flown per battery cycle
- **Battery waste production per km:** analyze the battery waste in moles disposed per km (toxins released from battery waste include cadmium, lead, zinc, manganese, nickel, silver, mercury, and lithium [44])

17.2. Sustainability Aspects

Various factors need to be taken into account to meet the aforementioned KPIs. Comprehensive plans to meet the specific requirements will be discussed in the following sections. These will include the relevant (sub)systems most impacted by the requirements.

17.2.1. Air Pollution

The overall design of KoriAir should focus on both efficient energy use and environmentally free power sources. For this purpose, the design of KoriAir has an optimized aerodynamic design and prioritized the use of lightweight materials, such as aluminium and titanium alloys. Furthermore, the propulsion system of KoriAir has been designed to be electrically powered.

One of the relevant sustainability requirements for KoriAir is that it shall have a Global Warming Potential lower than that of a car running on diesel. Global Warming Potential is not an easily measurable parameter, and thus it was broken down into the most significant emissions from a diesel car. The following values for greenhouse gas emissions were found: 127 g of CO_2 per km[1], 800 mg of NO_2 per km[2], 15 mg of SO_2 per km [51] and 2.23 MJ of energy per km[3].

[1]https://www.transportenvironment.org/discover/diesel-true-dirty-story/ [Accessed on 1 May 2024]

[2]https://www.umweltbundesamt.de/en/press/pressinformation/real-nitrogen-oxide-emissions-of-diesel-passenger [Accessed on 13 May 2024]

[3]https://www.researchgate.net/figure/a-Well-to-wheel-energy-consumption-MJ-km-b-Well-to-wheel-vehicle-CO2-

The final sustainable development plan for air pollution reduction is summarized below.

- **Objective:** Minimize carbon emissions
- **Design actions:**
  1. Optimize aerodynamic design of the vehicle configuration
  2. Use lightweight materials:
  3. Implement an electric propulsion system:
- **Relevant (sub)systems:** Aerodynamics, Structures and Materials, Power and Propulsion

17.2.2. Battery Sustainability

After selecting KoriAir as an lithium-ion battery powered vehicle system, the significance of the batteries becomes an extremely important aspect of sustainability. The following section details the life-cycle sustainability assessment of a lithium-ion battery.

- **Resources required to make a lithium-ion battery:**
  The process of extracting and refining the resources necessary to create a lithium-ion battery is energy and environmentally expensive. The materials include bauxite, cobalt, lithium, and graphite which come from deposits across the world, which then must be transported and refined[4]. Global demand continues to rise year upon year. Estimations about greenhouse gas emissions related to batteries are generally done in kg CO_2 per kWh. Current projections range from 34 to 73 kg of CO_2 per kWh [32].
- **Recycling:**
  There are three methods for lithium-ion battery recycling: a heat-based smelting process called pyrometallurgical recycling, a liquid-based leeching process called hydrometallurgy recycling, and direct physical recycling. All methods aim to recover the base metals, however, they all release CO_2. For direct mechanical recycling, the most cost effective method, approximately 3.65 kg of CO_2 are emitted per kWh[5].
- **Battery end-of-life and disposal:**
  If the battery cannot be recycled, its end-of-life disposal still has an environmental impact. The batteries must be properly packaged to limit fire incidents and unwanted discharges [4]. To sum up the total impact of an non-recycled lithium-ion battery, each kg of battery produces about 6.7 kg of CO_2 [55].
- **Battery degradation:**
  Lithium-ion batteries begin to degrade immediately upon use. After 1000 to 2000 cycles, the battery will degrade to 80% of its original capacity[6]. However, most life cycle assessment studies ignore the greenhouse gas emissions due to degradation during the use phase [32]. Additionally, the batteries should not be completely discharged. Instead, they should be charged and discharged to about 80% of their total capacity to maintain lifetime[7].

To summarize the total battery life-cycle assessment in terms of CO_2 emissions, the following results are achieved. When an average value of 50 kg CO_2 per kWh is adopted for battery production, a mechanical recycling method with a 3.65 kg CO_2 per kWh emission is assumed, and CO_2 emission during use is neglected, the total CO_2 emission of the batteries during their lifetime can be estimated. When this is compared with the CO_2 emission of a diesel car, assuming its lifetime travel distance on average is 400000 km for about 15 years, the cruise and lifting vehicle produce over 20000 kg less CO_2 over a duration of 10 years. Furthermore, the CO_2 emissions for the production and recycling of the diesel car are not even taken into account.

The KoriAir system should be designed to use the minimum battery sizing possible to reduce the raw materials required. However, this minimum size must include margins to allow for charging and

emissions_fig1_257717286 [Accessed on 13 May 2024]

[4]https://www.innoenergy.com/uploads/2023/01/critical-raw-materials-in-li-ion-batteries.pdf [Accessed on 14 May 2024]

[5]https://floodlightinvest.com/recycling-of-lithium-batteries-and-ghg-emissions/ [Accessed on 13 June 2024]

[6]https://www.zitara.com/resources/lithium-ion-battery-degradation [Accessed on 15 May 2024]

[7]https://batteryuniversity.com/article/bu-808-how-to-prolong-lithium-based-batteries [Accessed on 15 May 2024]

discharging percentages for optimum battery health, along with margins for loiter time and reserve fuel. In addition, it would be beneficial to design the batteries to be easily accessible for maintenance and battery end-of-life. Ideally, all spent batteries will be recycled and their metals recovered. Another important aspect to note is as battery energy density improves, the system can make use of fewer batteries to achieve the same performance, reducing the overall weight of the vehicle as well as its environmental impact.

The final sustainable development plan for battery life-cycle sustainability is summarized below.

- **Objective:** Ensure efficient and sustainable battery use and recycling
- **Design actions:**
  1. Use lithium-ion batteries with optimal sizing
  2. Facilitate easy maintenance and recycling
  3. Ensure most up-to-date battery energy density technology is employed
- **Relevant (sub)systems:** Power and Propulsion

17.2.3. Energy Grid Source

It is crucial to assess the influence of the UAM infrastructure on the current electricity grid to support its transition to the renewable form. Currently, electricity grids cannot be considered a completely renewable source of energy due to their variability with weather conditions. In fact, the generation emissions factor for grid electricity has increased from 2022, from 0.19 to 0.23 kg CO_2 per kWh[8]. As such, the design of the UAM system shall be compatible with new Smart Energy Systems. Smart energy is the intelligent optimization of energy costs and efficiency using innovative technology to build and operate a sustainable energy management system [39]. To support Smart Energy Systems, models of UAM system utilization should be created in order to precisely estimate the demand of required energy at any given time. This could limit inefficient or over-excessive grid usage and support the resilience and reliability of electricity grids, as well as the reduction in costs for new grid infrastructure.

The final sustainable development plan for energy grid source optimization is summarized below.

- **Objective:** Integrate energy source with renewable and Smart Energy Systems
- **Design actions:**
  1. Design VTOL systems compatible with Smart Energy Systems
  2. Model energy demand for efficient grid usage
- **Relevant (sub)systems:** Performance, Power and Propulsion

17.2.4. Noise Levels

Noise pollution is another crucial aspect to consider, as it impacts the social acceptance and is an important part of the competition. The KoriAir system must not generate more than 80 dBA at a distance of 100 m during take-off and landing. In general, two types of aerodynamic noise are produced by vehicles, tonal noise and broadband noise. Tonal noise refers to noise emitted at a specific frequency. It was reduced by prioritizing multiple small rotors for the lifting vehicle vehicle, as opposed to less larger ones. Small rotors not only reduced noise but also aided in designing shrouds for the propellers, which further reduced noise emissions by about 5 to 10 dB [2].

Furthermore, active noise control (ANC) technologies were used to reduce the possible passenger disturbance due to noise levels during take-off and landing. An optimal configuration to perform ANC for maximum noise reduction was found to be two speakers in a dipole configuration at the antinodes of related modes [31]. Given that the engines are mounted on the wings, it was assumed that most of the cabin noise would originate from the walls adjacent to the wings. This resulted in an optimal setup where one speaker is positioned at the front of the cabin and the other at the rear. Using this configuration, a noise reduction to 70 dB can be achieved [31].

The final sustainable development plan for noise level reduction is summarized below.

[8]https://www.itpenergised.com/new-uk-grid-emissions-factors-2023/ [Accessed 24 June 2024]

- **Objective:** Ensure noise levels remain under 80 dBA from 100 m take-off, and limit those levels as much as possible during cruise
- **Design actions:**
  1. Reduce rotor diameter (and increase rotor number)
  2. Use propeller shrouds to reduce tonal noise
  3. Make use of active noise control technologies to further reduce noise within the vehicle
- **Relevant (sub)systems:** Power and Propulsion, Take-off and Landing Procedure

17.2.5. Infrastructure Integration

A full-scale integration of UAM vehicles includes the use of vertiports: small airports designed for vertical take-off and landing of vehicles. The integration of vertiports in an urban environment directly affects KoriAir's social, environmental and economic sustainability. First of all, the size of the VTOL area was determined to be limited by the average size of a helipad. Considering that helicopters are general socially accepted, even despite their significant noise emissions, it was determined that for an improved social sustainability of UAM vehicles, they should not require more space than a helipad, namely, no larger than 12 m by 12 m.

In terms of vertiport location, a constrast in objectives was found. To balance placing the vertiport sufficiently far from housing communities and sufficiently close to public transportation, it was decided to prioritize locations such as central business districts and non-residential areas which are still populated on a regular basis. Furthermore, each location was assessed to ensure a public transport station was situated not more than a 10 minute walk away. These characteristics were determined to be the most optimal in terms on integrating the vehicles into urban environments and optimizing their efficiency without causing additional noise disturbances.

Finally, to optimize KoriAir's routes between vertiports, the usage of the Provider of Services for UAM (PSU) was chosen. This entity provides real-time alerts and data regarding operational regulations and standards which UAM vehicles must adhere to. By processing vehicle flight paths, operations are directly confirmed, and if necessary flights are de-conflicted and rerouted to avoid restricted zones and sub-optimal weather conditions. In this way, vehicle operation is optimized and made more efficient, allowing for both operational costs and time saving benefits.

The final sustainable development plan for infrastructure integration is summarized below.

- **Objective:** Integrate vertiports effectively into urban environments
- **Design actions:**
  1. Design vertiports to be no larger than 12 m x 12 m
  2. Optimize vertiport locations to balance distance from housing and proximity to public transport stations
  3. Use the PSU entity to provide efficient and adaptive flight path planning and prioritize safe and fast operation
- **Relevant (sub)systems:** Infrastructure, Take-off and Landing Procedure, Performance

18

Technical Risk Assessment

Analyzing and mitigating risks is a crucial element of designing a functional and safe design. The technical risks of the design are shown in Section 18.1. An initial risk map will also be shown. In Section 18.2 and Section 18.3, different mitigation and contingency strategies will be put in place to reduce the overall risk score of each risk. A final risk map displaying the new risk scores after mitigation and contingency strategies are implemented will then be shown.

18.1. Identification of Technical Risks

Two parameters are proposed to assess the overall impact of a technical risk: the likelihood level and consequence level. The likelihood level is a measure of the chance or probability of a certain event occurring during the operating life of the vehicle. The following five categories of likelihood are specified:

- **Very likely (score 5):** There is a probability between 40 and 80% that it happens at least once.
- **Likely (score 4):** There is a probability between 20 and 40% that it will happen.
- **Moderate (score 3):** There is a probability between 5% and 20% that it will happen.
- **Unlikely (score 2):** There is a probability between 1% and 5% that it will happen.
- **Very unlikely (score 1):** There is a probability of less than 1% that it will happen.

The consequence level quantifies the negative impact of the result of a certain event or action which occurs during the project. As for likelihood, five categories of consequence are defined:

- **Catastrophic (score 5):** Mission failure or significant non-achievement of functions.
- **Critical (score 4):** Mission success is questionable, significant reduction in technical performance.
- **Major (score 3):** Significant obstruction of functions, requiring crucial corrections to deliver important parts of the mission.
- **Minor (score 2):** Some corrections are necessary to fulfill the mission.
- **Negligible (score 1):** Temporary delay in mission timeline, not endangering the outcome.

Using these categories, the overall risk score of a technical risk can be calculated by multiplying the likelihood score by the consequence score. This score will form the basis of the risk assessment process, in which risks can be rejected and must be reduced, accepted but must be monitored or simply accepted. Risk scores will be reduced with a mitigation or contingency strategy, which will be shown in the following sections.

A list of technical risks that have been identified can be seen in Table 18.1. The risks have been divided into the following categories: power (PWR), propulsion (PRP), control (CNTL), structure (STR), aerodynamics (ADYN), vertical take-off and landing (VTOL), safety (SFT), environment (ENV), certification (CRT) and coupling mechanism (CPL). A specific category was included for the coupling mechanism due to its novelty and relatively low TLR compared to the other vehicle subsystems.

Table 18.1: *Technical risks with corresponding likelihood, consequence and responsible person*

ID	Risk	L	C	Score
R-PWR-1	The cruise battery overheats during flight.	2	3	6
R-PWR-2	The cruise and/or lift battery does not charge between flights.	3	1	3

Continued on next page

Table 18.1: *Technical risks with corresponding likelihood, consequence and responsible person (Continued)*

R-PWR-3	The cruise battery does not supply enough power to another vehicle system.	2	5	10
R-PWR-4	The lift battery does not supply enough power to lift the cruise vehicle.	2	5	10
R-PWR-5	The cruise and/or lift battery degrades faster than expected.	3	3	9
R-PWR-6	The cruise and/or lift battery stops functioning completely during flight.	2	5	10
R-PWR-7	The electrical cabling system of the cruise and/or lift vehicle fails.	1	5	5
R-PWR-8	The cruise and/or lift battery stops functioning completely before flight.	1	5	5
R-PRP-1	The cruise and/or lift propulsion system does not provide enough thrust to take-off.	2	5	10
R-PRP-2	The propeller blades encounter icing conditions.	4	4	16
R-PRP-3	The cruise propulsion system does not provide enough energy to reach another vertiport.	2	5	10
R-PRP-4	One rotor stops functioning during flight.	2	4	8
R-PRP-5	All rotors stop functioning during flight.	1	5	5
R-CNTL-1	The cruise and/or lift communication system stops functioning during flight.	1	5	5
R-CNTL-2	The cruise and/or lift navigation system stops functioning during flight.	1	5	5
R-CNTL-3	The cruise and/or lift flight control system stops functioning during flight.	1	5	5
R-CNTL-4	The cruise vehicle loses communication with ATC.	2	4	8
R-CNTL-5	The cruise and/or flight guidance system stops functioning during flight.	1	5	5
R-CNTL-6	The stability of the UAM vehicle is disturbed by sub-optimal weather conditions.	4	3	12
R-CNTL-7	The stability of the cruise and/or lift vehicle is compromised during (de)coupling.	4	3	12
R-CNTL-8	The lift vehicle collides with the cruise vehicle.	2	5	10
R-STR-1	The cruise vehicle is imbalanced due to the weight distribution of the payload.	2	3	6
R-STR-2	The lift vehicle is imbalanced during flight.	2	2	4
R-STR-3	The door closing mechanism of the cruise vehicle fails.	1	2	2
R-STR-4	The coupling mechanism compromises the structural integrity of the cruise vehicle.	3	3	9
R-STR-5	The cruise and/or lift vehicle experiences fatigue above fatigue limit during coupling.	3	4	12
R-ADYN-1	The coupling mechanism introduces aerodynamic disturbances during flight.	4	2	8
R-ADYN-2	The lift-to-drag ratio is not sufficient for take-off and/or landing.	3	4	12
R-ADYN-3	The lift-to-drag ratio is not sufficient for cruise.	3	4	12
R-VTOL-1	The lift vehicle does not couple with the cruise vehicle during take-off and/or landing.	2	5	10
R-VTOL-2	No lift vehicles are available at a vertiport.	1	5	5
R-VTOL-3	The lift vehicle lands with the cruise vehicle outside the vertiport.	3	3	9
R-VTOL-4	The veriport is unavailable for landing.	1	4	4
R-VTOL-5	The lift vehicle does not decouple with the cruise vehicle during take-off and/or landing.	2	5	10
R-SFT-1	The cruise and/or lift vehicle collides with another air-vehicle during flight.	1	5	5
R-SFT-2	The parking brake fails.	2	4	8
R-SFT-3	A passenger emergency occurs during flight.	3	2	6
R-SFT-4	The cruise and/or lift vehicle lights fail.	2	3	6
R-SFT-5	An system failure occurs during flight.	2	5	10
R-ENV-1	The noise emissions do not meet the requirements for take-off and/or cruise.	3	2	6
R-ENV-2	The cruise and/or lift vehicle collides with urban community infrastructure.	2	5	10
R-ENV-3	The cruise and/or lift vehicle collides with avian wildlife.	3	3	9

Continued on next page

Table 18.1: *Technical risks with corresponding likelihood, consequence and responsible person (Continued)*

R-ENV-4	A lightning strike hits the cruise and/or lift vehicle.	2	4	8
R-CRT-1	The lift and cruise vehicle system does not meet certification requirements.	3	5	15
R-CRT-2	No certification exists for the lift and cruise vehicle system.	2	5	10
REQ-CPL-1	The control systems of the cruise and/or lift vehicle fail.	2	5	10
REQ-CPL-2	Strong wind gust occurs when the vehicles are in close proximity of each other but not coupled yet.	4	3	12
REQ-CPL-3	The limit loads of the soft coupling mechanism are exceeded.	3	3	9
REQ-CPL-4	The vehicles become slightly misaligned when the rigid coupling is being made.	4	2	8
REQ-CPL-5	All rigid coupling connection points fail.	2	5	10

As a result of Table 18.1, the risk map before mitigation and contingency strategies is shown in Table 18.2. Risks are identified by their identifiers and placed on the map based on their risk score. Risks with scores between 12 and 25 are categorized as 'red', indicating they must be reduced. 'Yellow' risks, with scores between 4 and 11, should also be reduced but can be accepted without action. 'Green' risks, with scores between 1 and 3, are considered low enough to be accepted.

Table 18.2: *Risk map before mitigation and contingency strategies*

Catastrophic	R-PWR-7,8 ; R-PRP-5 ; R-CNTL-1,2,3,5 ; R-VTOL-2, R-SFT-1	R-PWR-3,4,6 ; R-PRP-1,3 ; R-CNTL-8 ; R-VTOL-1,5 ; R-SFT-5 ; R-ENV-2 ; R-CRT-2 ; R-CPL-1,5	R-CRT-1		
Critical	R-STR-3 ; R-VTOL-4	R-PRP-4 ; R-CNTL-4 ; R-SFT-2 ; R-ENV-4	R-STR-5 ; R-ADYN-2,3	R-PRP-2	
Major		R-PWR-1 ; R-STR-1 ; R-SFT-4	R-PWR-5 ; R-STR-4 ; R-VTOL-3 ; R-ENV-3, R-CPL-3	R-CNTL-6,7 ; R-CPL-2	
Marginal		R-STR-2	R-SFT-3 ; R-ENV-1	R-ADYN-1 ; R-CPL-4	
Negligible			R-PWR-2		
	Very low	**Low**	**Moderate**	**High**	**Very high**

It can be seen that there are some risks in the red zone, which means their score must be reduced. The majority of the risks are currently located in the yellow zone, and there are only a few risks in the green zone.

18.2. Mitigation Strategies

One method to reduce the risk score of technical risks is by employing mitigation strategies. These are strategies which are used to reduce the likelihood of a risk occurring. In Table 18.3, the mitigation strategies for reducing the likelihood of the technical risks can be observed. Note that in some cases the mitigation is not expected to reduce the likelihood to the next lower level, therefore the same likelihood score is retained.

Table 18.3: *Technical risks with corresponding mitigation strategy*

ID	Mitigation strategy	Previous likelihood	Updated likelihood
R-PWR-1	Implement a thermal management system to automatically detect and cool battery system.	2	1
R-PWR-2	Employ a responsible person to monitor if battery is charging.	3	2
R-PWR-3	Size battery for a high power than actually required to have a safety factor.	2	1

Continued on next page

Table 18.3: *Technical risks with corresponding mitigation strategy (Continued)*

R-PWR-4	Size battery for a high power than actually required to have a safety factor.	2	1
R-PWR-5	Continuously monitor battery health and update predicted battery operational lifetime.	3	2
R-PWR-6	Employ a redundant battery and motor system to ensure continuous proper functioning if one battery fails.	2	1
R-PWR-7	Employ a redundant electrical cabling system to ensure continuous proper functioning.	1	1
R-PRP-1	Size the propulsion system for a high thrust than actually required to have a safety factor.	2	1
R-PRP-2	Equip propellers with anti-icing or de-icing systems.	4	2
R-PRP-3	Size the propulsion system for additional range than actually required to have a safety factor.	2	1
R-PRP-4	Design the propulsion system for redundancy to ensure proper functioning if one rotor fails.	2	1
R-CNTL-1	Implement a redundant communication system as a backup in case main system fails.	1	1
R-CNTL-2	Implement a redundant navigation system as a backup in case main system fails.	1	1
R-CNTL-3	Implement a redundant flight control system as a backup in case main system fails.	1	1
R-CNTL-4	Use a backup communication channel to contact ATC.	2	1
R-CNTL-5	Implement a redundant flight guidance system as a backup in case main system fails.	1	1
R-CNTL-8	Implement collision avoidance systems in the navigation system.	2	2
R-STR-1	Plan payload distribution before flight to optimize vehicle balance.	2	1
R-STR-2	Plan the placement of power system and all other vehicle systems to ensure optimal weight distribution.	2	1
R-STR-3	Design the door closing mechanism to have multiple locking points.	1	1
R-STR-4	Design the structure of the vehicle to sustain coupling mechanism loads with a safety factor.	3	2
R-STR-5	Design the structure of the vehicle to sustain coupling mechanism loads with a safety factor.	3	2
R-ADYN-2	Size the propulsion system for a higher thrust than required to have a safety factor.	3	2
R-ADYN-3	Size the propulsion system for a higher thrust than required to have a safety factor.	3	2
R-VTOL-1	Design a robust and reliable coupling mechanism with fail-safe systems.	2	2
R-VTOL-2	Communicate with vertiport crew to ensure lift vehicle is available for landing.	1	1
R-VTOL-3	Use precise GPS and accurate automated landing procedures.	3	2
R-VTOL-5	Implement manual override options for decoupling.	2	2
R-SFT-1	Implement collision avoidance systems in the navigation system.	1	1
R-SFT-2	Implement a redundant parking brake system.	2	1
R-SFT-4	Implement a redundant lighting system for the vehicle.	2	1
R-SFT-5	Ensure all critical vehicle systems have a redundancy to continue normal vehicle operation.	2	1
R-ENV-1	Implement operational techniques and noise reducing technologies to reduce noise emissions.	3	2
R-ENV-2	Implement collision avoidance systems in the navigation system.	2	1

Continued on next page

Table 18.3: *Technical risks with corresponding mitigation strategy (Continued)*

R-ENV-3	Implement collision avoidance systems in the navigation system.	3	2
R-ENV-4	Employ weather radar systems with real-time data predictions.	2	1
R-CRT-1	Conduct testing to ensure all systems in the lift and cruise vehicle meet certification standards.	3	2
R-CPL-1	Implement a redundant flight control system on both lift and cruise vehicles as a backup in case the main systems fail.	2	1
R-CPL-3	Design the soft coupling mechanism to sustain loads with an additional safety factor.	3	2
R-CPL-5	Design rigid coupling points to sustain loads with an additional safety factor.	2	1

18.3. Contingency Strategies

The second way of reducing risks is through reducing the consequence of the risk in case the event occurs. This type of risk management is called contingency. In Table 18.4 the contingency strategy for reducing the consequence of the technical risks can be observed. Once again, in some cases the contingency is not expected to reduce the consequence to the next lower level, therefore the same consequence score is retained.

Table 18.4: *Technical risks with corresponding contingency strategy*

ID	Contingency strategy	Previous consequence	Updated consequence
R-PWR-1	Divert to nearest vertiport for immediate landing.	3	1
R-PWR-2	Have spare charged batteries on location at each vertiport.	1	1
R-PWR-5	Have spare charged batteries on location at each vertiport.	3	2
R-PWR-8	Have spare charged batteries on location at each vertiport.	5	4
R-PRP-2	Divert to nearest vertiport for immediate landing.	4	3
R-PRP-4	Divert to nearest vertiport for immediate landing.	4	3
R-PRP-5	Divert to nearest vertiport/safe urban location for emergency landing.	5	4
R-CNTL-1	Perform an emergency landing without the communication system.	5	4
R-CNTL-2	Perform an emergency landing without the navigation system.	5	4
R-CNTL-3	Perform an emergency landing without the flight control system.	5	4
R-CNTL-4	Perform an emergency landing without ATC communication.	4	3
R-CNTL-5	Perform an emergency landing without the flight guidance system.	5	4
R-CNTL-6	Use active control surfaces to stabilize the vehicle.	3	1
R-CNTL-7	Use active control surfaces to stabilize the vehicle.	3	1
R-CNTL-8	Divert to nearest vertiport/safe urban location for immediate emergency landing.	5	4
R-STR-1	Use active control surfaces to stabilize the vehicle or perform emergency landing to correct weight distribution.	3	2
R-STR-2	Use active control surfaces to stabilize the vehicle or perform emergency landing to correct weight distribution.	2	1
R-STR-3	Implement manual override options for door operation.	2	3
R-STR-4	Divert to nearest vertiport for immediate landing.	3	3
R-STR-5	Divert to nearest vertiport for immediate landing.	4	3
R-ADYN-1	Use active control surfaces to stabilize the vehicle.	2	1
R-ADYN-2	Divert to nearest vertiport for immediate landing.	4	3

Continued on next page

Table 18.4: *Technical risks with corresponding contingency strategy (Continued)*

R-ADYN-3	Divert to nearest vertiport for immediate landing.	4	3
R-VTOL-1	Perform a separate emergency landing for each vehicle.	5	5
R-VTOL-2	Divert to nearest vertiport with an available lift vehicle.	5	3
R-VTOL-4	Divert to nearest vertiport for immediate emergency landing.	4	3
R-VTOL-5	Abort take-off and/or landing attempt and use manual decoupling procedures.	5	4
R-SFT-1	Divert to nearest vertiport for immediate landing.	5	4
R-SFT-2	Stop vehicle operation until parking brake is restored.	4	2
R-SFT-3	Equip vehicle with basic necessary emergency equipment.	2	1
R-SFT-4	Stop vehicle operation until lighting system is restored.	3	2
R-SFT-5	Divert to nearest vertiport for immediate emergency landing.	5	4
R-ENV-1	Conduct an immediate review to repair of the propulsion system.	2	2
R-ENV-2	Divert to nearest vertiport for immediate landing.	5	4
R-ENV-3	Divert to nearest vertiport for immediate emergency landing.	3	2
R-ENV-4	Divert to nearest vertiport for immediate emergency landing.	4	3
R-CRT-1	Conduct an immediate review and repair of affected systems.	5	4
R-CRT-2	Apply for other valid certification categories or develop interim operational guidelines.	5	4
R-CPL-1	Perform an emergency landing of both vehicles separately without their control systems.	5	4
R-CPL-2	Employ flight control system to realign vehicles for coupling to begin.	3	2
R-CPL-3	Divert to nearest vertiport/safe urban location for immediate emergency landing.	3	2
R-CPL-4	Employ flight control system to realign vehicles for rigid coupling.	2	1
R-CPL-5	Override soft coupling and divert to nearest vertiport or safe urban location for immediate emergency landing.	5	4

With the mitigation and contingency strategies applied to the identified risks, the risk scores can now be updated and a new risk map can be made. The map is shown in Table 18.5. Note that no risks are in the red area anymore, and most risks have moved to the green area. Therefore, the new risk map is deemed acceptable, with R-VTOL-1 being the most important risk to monitor.

Table 18.5: *Risk map after mitigation and contingency strategies*

Catastrophic	R-PWR-3,4,6,7 ; R-PRP-1,3	R-VTOL-1			
Critical	R-PWR-8 ; R-PRP-5 ; R-CNTL-1,2,3,5 ; R-SFT-1,5 ; R-ENV-2	R-CNTL-8 ; R-VTOL-5 ; R-CRT-1,2 ; R-CPL-1,5			
Major	R-PRP-4 ; R-CNTL-4 ; R-STR-3 ; R-VTOL-2,4 ; R-ENV-4	R-PRP-2 ; R-STR-4,5 ; R-ADYN-2,3 ; R-VTOL-3			
Marginal	R-STR-1 ; R-SFT-2,4	R-PWR-5 ; R-ENV-1,3 ; R-CPL-3		R-CPL-2	
Negligible	R-PWR-1 ; R-STR-2	R-PWR-2	R-SFT-3	R-CNTL-6,7 ; R-ADYN-1 ; R-CPL-4	
	Very low	**Low**	**Moderate**	**High**	**Very high**

19

RAMS Analysis

Reliability, Availability, Maintainability and Safety (RAMS) plays a vital role in ensuring the KoriAir design has an optimal and safe performance. In this chapter the RAMS analysis is conducted. The characteristics of RAMS are compared to existing similar designs, and then adapted based on the unique subsystems of the final design. The reliability characteristics are addressed in Section 19.1, the availability in Section 19.2, the maintainability in Section 19.3, and the safety in Section 19.4.

19.1. Reliability

As the KoriAir design is a significantly novel engineering concept, it was decided to compare the most important (sub)systems of the two vehicle configuration to existing concepts which already have estimates for RAMS characteristics. The reliability of a system is defined as its "ability to accomplish a required function, in given conditions, during a given time interval" [48]. The analysis of KoriAir's reliability is mainly based on the reliability of the system's batteries, motors, coupling mechanism and airframe structure, as those (sub)systems are the ones which are most imperative to the system's functionality.

19.1.1. Battery

The battery used for both vehicles is the proprietary lithium-ion battery from the Joby S4 eVTOL UAM vehicle. The battery has a specific energy of 235 Wh/kg or 500 kWh/m^3. This battery pack is formed from cells with a capacity of 288 Wh/kg. While there are no battery characteristics available commercially, Joby has demonstrated the battery is capable of more than 10000 representative flight cycles[1]. Lithium-ion batteries are widely used in electric vehicles due to their high energy density, efficiency, and relatively long lifespan. Typically, they can last for 150,000 to 300,000 km for a typical long-range electric vehicle[2]. The important aspect to consider when using lithium-ion batteries is overheating, however, with the continuous improvement of battery technology and battery management systems, it is expected that the safety and reliability of lithium-ion batteries in general will improve.

19.1.2. Motors

The motor of the cruise vehicle is HPD32D from Geiger engineering. These engines are electric permanent magnet synchronous motors (PMSMs). These are used frequently in automotive, aerospace and other transportation vehicle industries. The HPD32D motor is used in the Elektra Eagle aircraft, which is an observation and communication plane[3]. This vehicle has an endurance of 12 hours, and has been in operation since 2017 with no significant incidents. In fact, the manufacturer, Elektra Solar, states that their Elektra Eagle UAS (unmanned version), with triple redundant Elektra Solar autopilot (power supply, sensors, and flight control computer) and double redundant actuators, ensure absolute safety for fully autonomous flight missions[3].

The lifting vehicle uses the same type of motor but a smaller variation, namely the HPD20SD. An electronically limited version of this engine is used in the "Birdy" aircraft, a single-seater motor glider [56]. It also comes from the same manufacturer as the cruise vehicle motor and is frequently used

[1]https://aviationweek.com/business-aviation/aircraft-propulsion/opinion-will-evtols-disrupt-traditional-aircraft-values [Accessed 13 June 2024]

[2]https://www.iberdrola.com/innovation/lithium-ion-batteries [Accessed June 13 2024]

[3]https://www.elektra-solar.com/products/elektra-eagle-solar/ [Accessed 14 June 2024]

in high endurance aircraft. Additionally, as the lifting vehicles has 28 motors, 24 in a six by four configuration at the top of the vehicle and four additional motors at the sides for additional control, the vehicle ensures significant motor redundancy in case of failure.

19.1.3. Coupling Mechanism

The reliability of the coupling mechanism is the most concerning aspect of the design due to its novelty. With this in mind, the design of the mechanism was given most importance throughout the preliminary design phase of the system, and multiple safety factors and redundancies were added to ensure the mechanism is fail-safe. In fact, there will be four connection points from the lifting vehicle to the cruise vehicle, however, the structure has been designed to be fully functional with three of those connection points failing. This significantly increases the reliability and confidence in the coupling mechanism, as it is expected that during normal operation of the system, the structures are more than secure when coupled together.

19.1.4. Airframe Structure

The material used for the airframe structures is Aluminum 2024 T6, which has many benefits such as high strength-to-weight ratio and good fatigue and corrosion resistance[4]. This makes it a very strong material choice for the airframe, and in fact it is often used in the aviation industry for aircraft to maximize performance while minimizing weight and sustaining cyclic loads and stresses. The long-term usage of this aluminum alloy, along with its strong mechanical and fatigue resistance properties, strengthens the reliability characteristics of the airframes.

The cruise vehicle will have wing supported by a central wing box and spars. The reliability of these structures in the wing design for a general aviation aircraft is generally high, thanks to advanced materials, rigorous design and testing protocols, and robust inspection and maintenance practices. These components are designed to endure the loads and stresses experienced during all phases of flight, including those due to the coupling mechanism. Continuous improvements in materials science, and structural analysis techniques contribute to the confidence in the reliability of the structure. Following the aforementioned specifics of the airframe, it is expected that the reliability of the airframe structure is similar to the reliability of the airframe structure in the modern aircraft.

19.2. Availability

The availability of a system is defined as its "ability to be able to accomplish a required function, in given conditions, at a given moment, supposed that the external means are present" [48]. The main components which impact the availability of KoriAir are the materials used for the airframe, the energy density required for optimal battery performance, the control system of the coupling mechanism and the infrastructure in an urban environment on which to implement the KoriAir vertiports.

19.2.1. Airframe Materials

The airframe of both vehicles will be composed of Aluminum 2024 T6, whilst the coupling mechanism will be made of Titanium 6AI-4V. As already mentioned in Section 19.1, Aluminum 2024 T6 is widely used in the aviation industry. It is also quite easy to access, as the manufacturing and supply chains for the alloy are well-established and provide a robust supply network[4]. Its demand is only expected to increase in the coming years, as many industries are being driven by economic growth, and the shift to more sustainable practices will also push for a higher recycling rate of aluminum.

On the other hand, Titanium 6AI-AV, like many titanium alloys, is more expensive to manufacture and is less readily available in the market. The supply chain for titanium in general is more complex than for aluminum, involving more processing and post-processing activities which increase its acquisition cost[5]. Titanium 6AI-AV is the most commonly used titanium alloy, especially in the aviation industry, due to its unique combination of high strength, light weight and corrosion resistance properties. As advancements in titanium production techniques increase, such as powder metallurgy and additive

[4]https://asm.matweb.com/search/SpecificMaterial.asp?bassnum=ma2024t6 [Accessed 13 June 2024]
[5]https://www.xometry.com/resources/materials/all-about-titanium-alloy-6-4/ [Accessed 13 June 2024]

manufacturing, it is expected that the cost of titanium alloys will decrease over time and be more available in the technological market.

19.2.2. Battery

Lithium-ion batteries are significantly prevalent in many technological devices used in the current day. They are the main power source for phones, laptops, electric vehicles and many other electronics. However, there are some challenges in the lithium-ion battery production process. The batteries rely on scarce and finite resources such as lithium, cobalt, and nickel, which raises some concerns about long-term availability and geopolitical risks that arise during raw material extraction. The demand for these materials continues to increase, therefore it is imperative to acquire a stable and consistent supply chain. Furthermore, currently the battery used by Joby is not commercially available on the market. It is expected that with the current trend of continuous technological advancements in battery energy density, acquiring such a battery by the time the system is ready for operation will not be an impediment.

19.2.3. Coupling Mechanism

The TRL of the coupling mechanism is the main hindrance of this system. The ability of two flying vehicles to synchronize during flight and rely on a non-conventional control system to couple is not tested yet. While the preliminary design of the control system shows that it is possible, the additional flight tests shall be performed to confirm the availability of the system. The concept which this system is most similar too is the in-air refueling system, which has been researched and tested recently for military aircraft.

In fact, during a second flight test campaign by Airbus Defense and Space, conducted in November 2023, the Auto'Mate demonstrator showcased the potential of Autonomous Assets Air to Air Refueling (A4R) operations flying with five unmanned drones under the control of an A310 MRTT tanker, using advanced AI-based relative navigation and cooperative control technologies[6]. Similar to the design of the coupling mechanism, Airbus is focusing on three primary key technological foundations: navigation, communication and control. The Auto'Mate system can achieve unprecedented levels of position accuracy by combining cameras, high-precision satellite global positioning, and LiDAR (Light Detection And Ranging) sensors with AI and sensor fusion algorithms[6]. Furthermore, the autonomous control systems are capable of managing critical flight parameters and guaranteeing coordination between vehicles, ensuring a safe and efficient operation with collision avoidance functionality.

19.3. Maintainability

The maintainability of a system is defined as its "ability to be restored in an operating state, during a time interval [0,t], when the maintenance operations are accomplished with given means, as a determined program" [48]. In order to keep the system operational, it must be easily maintainable as well. The main components of the system which will require maintenance are the airframe structures, motors, and batteries.

19.3.1. Airframe Structure

As Aluminum 2024 T6 can be susceptible to corrosion. To improve its operational performance and reduce the occurrence of maintenance activities, protective coatings are commonly used[4]. While this will improve its corrosion resistance properties, it is advised to regularly inspect the structure to ensure it is up to standard. Due to its widespread usage, the tools and expertise required for aluminum maintenance are generally readily available, and standard techniques such as welding and cold working can be used to restore the mechanical properties of the material. Non-destructive testing (NDT) methods can also be used to detect cracks, corrosion, and other defects.

In the case of Titanium 6Al-4V for the coupling mechanism, the material requires minimal maintenance activities for corrosion protection, although inspection is still recommended to ensure regular integrity

[6]https://www.airbus.com/en/newsroom/stories/2023-11-aerial-refuelling-without-human-intervention [Accessed 13 June 2024]

of the structure. In general, titanium can be more challenging to repair due to strong mechanical properties, therefore more specialized techniques must be used to avoid damaging the unique structure of the material. NDT methods such as ultrasonic testing and X-ray scanning are commonly used, as these methods can detect internal defects that might not be visible on the surface[5].

19.3.2. Motors

Performing maintenance on electric motors is relatively straightforward and less labor-intensive compared to internal combustion engines. With fewer moving parts, no oil changes, and a simpler overall design, electric motors require less frequent and less intensive maintenance. Regular inspection of the motor system is generally sufficient to ensure a safe and reliable operation of an electric vehicle. The configuration of 24 motors at the top of the lifting vehicle can pose an additional challenge in terms of accessibility in case maintenance in required. If a certain motor is to experience a fault, it will be more difficult to conduct maintenance to repair it due to it being very closely located to many other motors. In this case, it may be easier to disassemble the entire unit of six motors from which it originates and then reassemble the unit once the motor is repaired. Additionally, if one of the motor components fails, it is generally cheaper and simpler to replace all the components of the motor instead of replacing only the singular part[7]. This applies for both the cruise and lifting vehicle, as they have the same type of motor with only a different size.

19.3.3. Battery

Batteries in electric vehicles are the most maintenance heavy element. A lithium-ion battery's charge and discharge cycle must be ideal for the battery health to remain in optimal state for as long as possible. A well-maintained battery could last between 3 and 5 years[7]. Additionally, lithium-ion batteries are expensive and relatively hard to recycle, with only 5% of their components being recyclable[8].

19.4. Safety

Due to the non-conventionally of the system, it is of key to assess the overall safety of the design. The safety of a system is defined as the "ability of a system to generate to itself and to its environment, in given conditions, catastrophic or hazardous events with an acceptable level of risk" [48]. During the design of a general aviation aircraft, safety is always considered as the ultimate priority. With this in mind, applying redundancies and safety factors to all critical systems, structures, and components is imperative. Engineering design mainly operates with two differing safety approaches: the safe-life approach and the fail-safe approach. The former is based on the principle of designing the components of the system to not fail during the operational life of the system. This is mainly done by applying safety factors during the analysis and design phases, such that the structures are designed to withstand loads and stresses which are stronger than those they are predicted to experience. The latter concept is based on the principle of designing the system as a whole to continue safe operation even in the event of a failure. This means that the failure of a non-critical part will not lead to a catastrophic system. To ensure this, redundancies and secondary components are usually included, both to critical and non-critical systems, to allow for the system to complete an operation cycle (a flight). The faulty system can thus be repaired and replaced to facilitate continued fail-safe operation.

These design safety philosophies can be applied to the systems and components in KoriAir, depending on the part. If a component can be inspected and repaired, the fail-safe principle is applied and considerations are made on the rate of inspection and maintenance of the part. If a component cannot be easily inspected, the safe-life principle is applied and the part undergoes extensive testing and quality control to ensure it will not fail during normal operation. The main technical risks which impact the safety of the system are discussed in Chapter 18, along with the mitigation and contingency strategies to reduce the likelihood & consequence of the event. The most important risks will be continuously monitored, to ensure a continued safe operation.

[7]https://www.imeche.org/news/news-article/electric-aircraft-pose-new-challenges-for-maintenance-and-repair [Accessed 13 June 2024]

[8]https://www.continentalbattery.com/blog/can-lithium-batteries-be-recycled [Accessed 13 June 2024]

20

Resource Allocation

To effectively manage costs and technical resources throughout development of the design, it is important to set up and maintain a detailed resource allocation. This chapter describes how the resources will be allocated in the design of the system. In Section 20.1, the development of a methodology for estimating cost and time is described. Resource allocation of the various (sub)systems of the design is covered in Section 20.2. This chapter ends with a contingency plan, which is discussed in Section 20.3.

20.1. Methodology Cost and Time

Since eVTOL UAM vehicles are in initial phase of development, most specifications are not publicly available. Therefore, as the eVTOL UAM's take-off regime is similar to a helicopter's and the cruise regime is similar to a conventional aircraft, both were used to identify the ranges. This simplification will be elaborated on in the following sections. It also must be noted that as the chosen configuration consists of a lifting vehicle (LV) and a cruise vehicle (CV), the masses, power, and costs of acquisition will be given separately for each vehicle.

First, the estimated development time for each task by taking into account the expected time to complete it. A margin of half the expected time was added as an upper limit for contingency. The contingencies are given in a range in order to take into account unexpected delays. In the case of development time, contingencies of two days were used for all tasks. For the cost, the working hours per day was multiplied by the number of working days, the number of people working and the average wage in the Netherlands for 40 hours of work per week, with €27.26 an hour[1]. This resulted in the expected development cost.

20.2. Cost of Subsystems

For the propulsion department, the main development component is the motor. The mass of the motors used for the lifting vehicle is 4.7 kg per motor [2]. The weight of each installed engine is displayed in the table [53]. A contingency of 21% is applied on both margins based on NASA's contingency strategy used for preliminary design phases. The same is done for the cruise vehicle, which uses four heavier motors of 12 kg each. The complete weight estimation for the propulsion system of the cruise vehicle was performed in Chapter 5, and for the lifting vehicle in Chapter 6.

For the cruise vehicle the mass of the fuselage was calculated in Chapter 5 using a class II weight estimation from Raymer [53]. This is examined in more detail in Chapter 5. For the lifting vehicle the mass was estimated using the equation seen in Chapter 6 [62]. Additional development time was considered due to the two vehicle configuration requiring additional structural integration.

The coupling mechanism is one of the most critical components of the system. Therefore, resource allocations on mass, power, cost, and time must be enforced. For the mass budget, a maximum estimated mass of 200 kg was determined in Chapter 7. The development cost and time estimations are based on the same methodologies described in Section 20.1.

As only the cruise vehicle will have wings, the majority of the workload of this department be centered

[1]https://www.statista.com/statistics/537968/average-hourly-wage-in-the-netherlands-by-working-hours/ [Accessed 6 June 2024]

[2]https://www.geigerengineering.de/en/avionics/products [Accessed on 6 June 2024]

around the aerodynamics system. Additionally, this department will focus on the aerodynamic interaction of the cruise vehicle and the lifting vehicle during the coupling process. The mass of the wings was calculated using the class II estimation [53]. This is explored in more detail in Chapter 5. The standard contingencies of 21% were applied according to the NASA contingency strategy [29].

The performance department determines the expected masses and costs initially using a class II estimation. Contingencies of 21% are applied to both [29]. The expected time was estimated to be around 30 days minimum and up to 34 days. For cost, the previously explained calculation was performed.

Stability and control includes all the control surfaces and computer systems required to maneuver the vehicle system. The mass of the avionics was estimated for both the lifting vehicle and the cruise vehicle using Raymer's sizing equations for general aviation aircraft [53]. Additionally, the hydraulics, electrical system, flight control and tail systems were sized using Raymer and its class II weight estimation [53]. This is shown in more detail in Chapter 5. During normal cruise, the horizontal propellers of the lifting vehicle are not used. these 4 propellers are for special maneuvers and to maintain stability occasionally. The Power of these 4 engines adds up to 80 kW of continuous and 100 kW of peak power[3]. The cost of the avionics system was estimated from [8] and the time expected to be spent designing this subsystem is 20 days. Additional development time considerations were included due to the increased complexity and precision is required for this subsystem.

Safety and certification consists of procedures and regulations which much be met in order to operate the system once the design is finalized. Around five days of total work are expected for this, and these will be stretched over time to review the quality of all subsystems. The same method as Section 20.1 is used for the cost and time margins. It must be noted that the certification development time does not account for the actual time needed to certify the system. It only consists of the time to plan and develop the testing and assurances for certification. It must also be noted that with the configuration used, the time needed for this department has increased compared to other design concepts. The coupling mechanism has never been used in this context or application, therefore more precautions are needed to ensure the system can safely operate.

An overview of the budget estimations for the different subsystems discussed above is shown in Table 20.1.

Table 20.1: *Budget estimation for the different subsystems*

Subsystem	Parameters	Lower	Target	Upper
Propulsion	Mass LV [kg]	203	257	311
	Mass CV [kg]	80	101	123
	Power LV [kW]	384	480	576
	Power CV [kW]	128	160	192
	Development cost [€]	3490	3926	4362
	Development time [days]	16	18	20
Structures	Mass LV [kg]	23	30	36
	Mass CV [kg]	120	152	185
	Development cost [€]	3926	4362	4798
	Development time [days]	18	20	22
Coupling Mechanism	Mass LV [kg]	142	180	217
	Mass CV [kg]	94	120	145
	Development cost [€]	7852	8724	9596
	Development time (2 people) [€]	18	20	22

Continued on next page

[3]https://www.geigerengineering.de/en/avionics/products[Accessed on 18 June 2024]

Table 20.1: *Budget estimation for the different subsystems (Continued)*

Aerodynamics	Mass wing CV [kg]	82	103	125
	Development cost [€]	2102	2522	2943
	Development time [days]	10	12	14
Performance	Battery mass LV [kg]	158	200	242
	Battery mass CV [kg]	180	228	275
	Payload mass CV [kg]	331	420	508
	Development cost [€]	5465	6305	7146
	Development time [days]	26	30	34
Stability and Control	Mass LV [kg]	49	63	76
	Mass CV [kg]	18	23	27
	Mass hydraulics CV [kg]	3	4	5
	Mass electrical CV [kg]	33	42	51
	Mass flight controls CV [kg]	8	11	13
	Tailplane (horizontal + vertical) [kg]	38	49	59
	Power LV [kW]	80	80	100
	Development cost [€]	3783	4204	4623.52
	Development time [days]	18	20	22
Safety and Certification	Development cost [€]	1472	1892	2312
	Development time [days]	7	9	11

20.3. Contingency Management

As explained in each section, a certain range including a reserve or contingency was implemented for each budget value. In order to progress with the design development, a contingency management plan was created to address unexpected events or risks that could impact the project's timeline, budget, or quality. A contingency plan is generally implemented when a certain risk occurs, and it will outline the actions to be taken to mitigate the consequence of the event. The contingency plan for this system will take into account a couple of key aspects:

1. **Critical areas:** Based on the requirements for the system, some key budgets can be identified. Namely, the mass and cost for each subsystem. As a result, these areas have been given a larger contingency range (around 20 to 30%) and will be heavily monitored as the design develops.
2. **Risk assessment:** During the risk assessment phase, the contingencies can be increased or decreased based on the level of risk associated with each specific budget calculation. This is then iterated upon as more accurate estimations of the risks are developed.
3. **Contingency trigger:** The contingency range aims to include unforeseen budget increases during the design process. However, if there are any large changes to the design, this should trigger a larger contingency change in the budgets. The budgets shall be iterated upon to include any significant differences in the project. The contingencies shall be larger than 21% for mass and power, as used by NASA [29].
4. **Potential new budgets:** As the design develops, additional balancing of different properties of the design could arise. If so, additional contingencies will be added to the budget.

21

Costs and Profit Estimation

For the continuation of the design of the KoriAir vehicles and infrastructure, it is important to estimate the expected material, man-hour, and other costs. In this chapter, the expected post-project costs are estimated in Section 21.1. This includes the flight tests, material, tooling, and quality control costs. The cost breakdown structure diagram in then illustrated in Section 21.2. Finally, the Return on Investment (RoI) is calculated in Section 21.2.

21.1. Origin of Costs

Due to the innovative concept design, empirical cost estimations were employed from Raymer when available, and some estimations were based on similar designs. Statistical estimations were made for the flight test costs, in which two flight tests were assumed. Equation 21.1 was used, where FTA is flight test number and W_e is empty weight [53].

$$C_F = 2498 W_e^{0.3} 25 V^{0.822} FTA^{1.21} \tag{21.1}$$

Furthermore, the material costs (C_M), tooling hours (H_y) and quality control hours (H_Q), Equation 21.2, Equation 21.3 and Equation 21.4 were used, respectively. In these equations, Q refers to the number of units to be produced in the next 5 years (1 unit was assumed).

$$C_M = 22.1 W_e^{0.5} V^{0.621} Q^{0.799} \tag{21.2}$$

$$H_y = 5.99 W_e^{0.777} V^{0.696} Q^{0.263} \tag{21.3}$$

$$H_Q = 0.076 C_M \tag{21.4}$$

Finally, the crew cost per vertiport (C_C), Equation 21.5, was assumed for a two people (on ground) crew, where W_0 is the take-off gross weight.

$$C_C = 70.4 V (V \frac{W_0}{10^5}) + 168.8 \tag{21.5}$$

The preliminary (sub)system development costs were estimated in Chapter 20, which were based on their development time. The costs for the final design were based on the method described in Chapter 20. An estimation of 100 working days to complete the design, in which 10 people work eight hours per day. The design optimization is assumed to take 25 days. The cost for the final CAD model was assumed to be in the order of magnitude of 10k.

All other costs that did not originate from Raymer are displayed here in Table 21.1.

Table 21.1: *Costs Breakdown*

Parameters	Value	Origin
Costs Material testing [€]	300k	Common aircraft design service[8]
Cost of the Landing pad [€]	3k	From a common heliport service[10]
Certification [€]	25 million	Taken from a general aviation aircraft[12]

Continued on next page

Table 21.1: *Costs Breakdown (Continued)*

Project Planning costs [€]	32720	Method of Chapter 20

The remaining costs upper expected limits were assumed. The cost breakdown structure, illustrating the total cost of the system broken down into research and development, production, operation, regulatory and certification, and project planning costs. Those costs are further broken down into various categories, seen in Figure 21.1.

21.2. Return on Investment

The Return on investment (RoI) is used to quantify the profitability of a product [13]. It is a ratio of the net return over the initial investment. This means that the final value of investment of KoriAir at a certain point in the future needs to be compared to the initial cost of developing and producing its vehicles. From research on the market of UAM, it was estimated that the revenue of the entire market would be USD 50 billion in 2032[14]. Assuming that KoriAir achieves a market share of 1% by this time, it means that the revenue of the KoriAir project in 2032 is estimated to be USD 500 million.

To determine the cost of the vehicle, development costs as well as production costs need to be taken into account. The development costs consist of all costs made in order to develop the design until a point where it can be produced and operated. This value does not return for every newly produced vehicle. The development costs were estimated in Section 21.1 as USD 33 million. Production costs are the costs made in the process of producing the KoriAir vehicle and therefore return for every vehicle that is being produced. These production costs have been estimated in Section 21.1 as well, as USD 900k per vehicle. In order to make a profit off of the vehicles, and adhering to the requirement of a maximum of USD 2.2 million as the price for the KoriAir vehicle, the price of the vehicle has been set to USD 2 million. With a revenue of USD 500 million and a price per vehicle of USD 2 million, it can be estimated that 250 vehicles will have been sold.

With Equation 21.6 the RoI can be calculated. The total revenue is the number of vehicles multiplied by their price. The total costs are subtracted from this. These costs involve the development costs as well as the production costs for each vehicle.

$$RoI = \frac{(n_{vehicles}P) - (C_{dev} + C_{prod}n_{vehicles})}{C_{dev} + C_{prod}n_{vehicles}} \tag{21.6}$$

Filling in the number of sold vehicles $n_{vehicles}$, which is 250, the price per vehicle P, which is USD 2 million, the development costs C_{dev}, which is USD 33 million, and the production costs C_{prod}, which is USD 900k, a RoI of 94% was found. This is a high return on investment, which could be explained by the low development costs and the high expected market value, as UAM is a fast-growing and promising market. However, this rough estimate should be reconsidered once more details are known about development and production costs, as well the development of the market.

[13]https://www.investopedia.com/articles/basics/10/guide-to-calculating-roi.asp [Accessed on 19 June 2024]

[14]https://www.globenewswire.com/news-release/2024/03/13/2845402/0/en/Urban-Air-Mobility-UAM-Market-Size-Share-Study-Projected-to-Reach-USD-49-09-Billion-By-2032-Report-by-Polaris-Market-Research.html [Accessed on 19 June 2024]

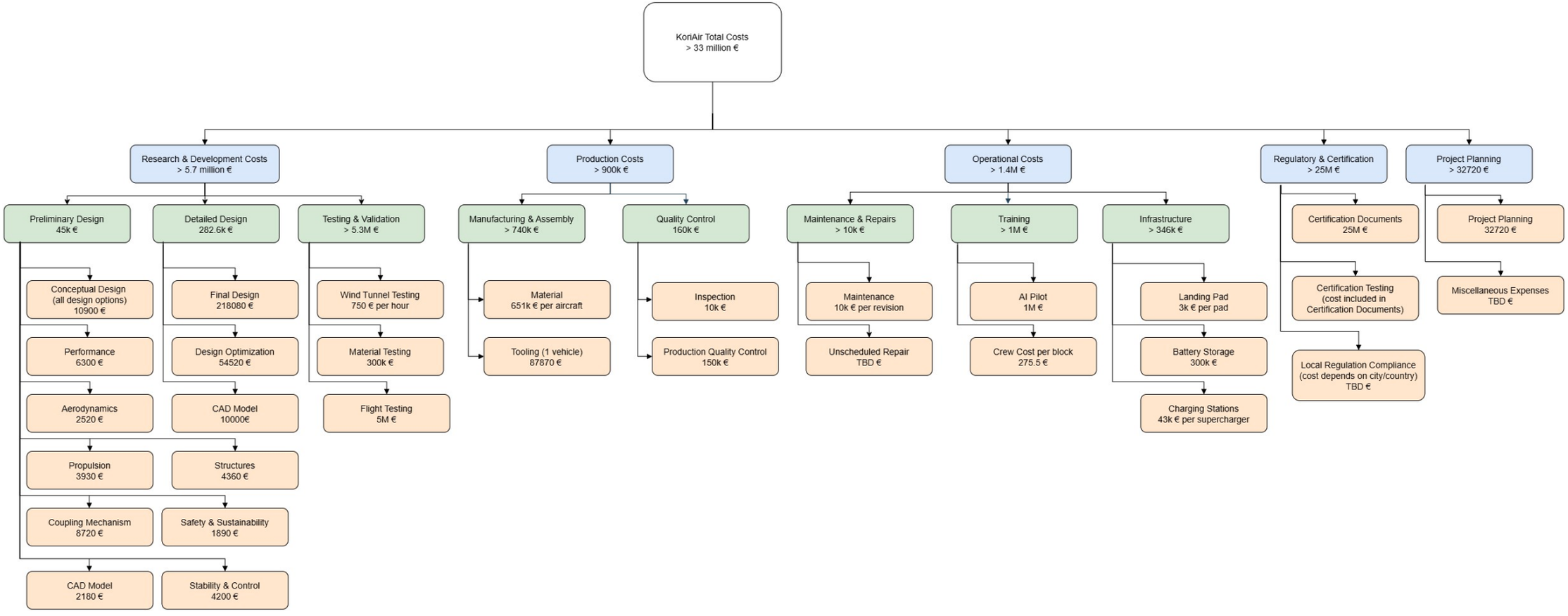

Figure 21.1: Cost breakdown diagram

22

Compliance and Feasibility

It is crucial to ensure that the design meets the requirements consistently throughout the entire process, not just at the final phase. This will prevent problems in later stages. At that moment, considerable modifications to the design would be costly, time-consuming, and complex. Thus, in the current preliminary design phase of the vehicles, a compliance matrix is set up. This matrix is shown in Section 22.1. Some requirements call for a more in-depth explanation than a simple check. Therefore, the compliance matrix is followed by a feasibility analysis in Section 22.2, where those requirements and the requirements that are not yet met are discussed in detail.

22.1. Compliance Matrix

Below, in Table 22.1, the compliance matrix for the requirements is given. The stakeholder requirements are not covered in this matrix, as the mission requirements flow down from these requirements. Also, due to stakeholder requirements being formulated in their language, they are not specific enough to determine whether the requirements are fulfilled by the design.

In the compliance matrix, requirements that are met by the current design are indicated with a checkmark. Requirements that are not fulfilled are indicated with a cross mark. For some requirements, the actual value of the design is given in this cell as well. The asterisks indicate that the requirements, whether the design meets them or not, require further explanation. The clarification is given in section 22.2.

22.2. Feasibility Analysis

The feasibility analysis provides a detailed overview explaining why some requirements are too comprehensive or specific to be fully addressed at this stage of the design process, or, in the case a requirement is not met, why that is the case. It indicates what adjustments might be needed in order to fulfil those requirements. First, the rationale of the more complex requirements is given in Section 22.2.1. Then in Section 22.2.2, the explanation and proposed modifications are covered.

Table 22.1: *Compliance matrix of the mission, system, and subsystem requirements*

Identifier: REQ-STK-	Requirement	Met	Location
Mission Requirements			
1-MIS-1	The UAM vehicle shall meet the certification standards of FAR Chapter 21.17 [51].	✓*	Chapter 8
2-MIS-2	The UAM vehicle shall adhere to the boundaries of the TBD airspace that it is assigned.	✓	Chapter 15
3-MIS-3	The UAM vehicle shall communicate with the air control tower during operation.	✓	Section 13.4
4-MIS-4	The UAM infrastructure shall allow for visual inspection to be conducted.	✓	Chapter 15
4-MIS-5	The UAM infrastructure shall allow for regular in-operation maintenance activities.	✓	Chapter 15
5-MIS-6	The UAM vehicle shall have a Global Warming Potential that is lower than a car running on diesel [51].	✓*	Section 17.2.2
5-MIS-7	The UAM vehicle and infrastructure parts shall have a recyclability of TBD %.	*	
5-MIS-8	The UAM vehicle shall have an operational lifetime of at least 12 years.	*	
6-MIS-9	The operation of the vehicle shall not structurally damage the surrounding infrastructure elements during its flight regime.	✓*	Chapter 11
7-MIS-10	The landing and takeoff area shall occupy the same area as a heliport or smaller.	✓	Section 15.1
8-MIS-11	The designated landing and takeoff zones shall not be further away than 10 minutes of walking from other public transportation station stops.	✓	Section 15.2
9-MIS-12	The designated landing and takeoff zones shall be accessible for emergency services within 10 minutes.	✓	Section 15.2
9-MIS-13	The UAM infrastructure shall include emergency kits.	✓	Section 15.1.3
10-MIS-14	The UAM vehicle shall not produce noise more than 80 dBA in sound pressure level during take-off and landing from 100 m [51].	* 77.6 dBA	Section 12.7
10-MIS-15	The UAM vehicle shall not produce noise more than 80 dBA in sound pressure level during cruise from 1200 m.	* 63.5 dBA	Section 12.7
11-MIS-16	The UAM vehicle shall include emergency kits, containing life jackets, parachutes, seat belts, and first aid kits.	✓	Section 5.1.2
12-MIS-17	The UAM vehicle shall transport four passengers [51].	✓	Section 5.1.2
13-MIS-18	The UAM vehicle shall have operating costs equal to or less than 1,00 EUR/PAX/km [51].	*	
13-MIS-19	The UAM vehicle acquisition cost shall be equal to or less than 5 million euros per unit [51].	✓	Chapter 21
14-MIS-20	The UAM vehicle shall have a cruise speed of 200 km/hr [51].	✓	Chapter 5
15-MIS-21	The UAM vehicle shall have seating capacity for each passenger.	✓	Section 5.1.2
16-MIS-22	The UAM vehicle shall be fully chargeable in 30 minutes [51].	*	
16-MIS-23	The turnaround time per flight shall be less than 30 minutes.	*	
17-MIS-24	The UAM vehicle shall be accessible for wheelchair users.	✓*	Section 5.1.2
17-MIS-25	The UAM infrastructure shall be accessible for wheelchair users.	✓*	Section 5.1.2
18-MIS-26	The UAM vehicle shall be able to provide transport up to 50 km range [51].	✓	Chapter 5 Chapter 6
9-MIS-27	The UAM vehicle shall be able to perform an emergency landing during its entire flight regime.	✓	Section 8.2
18-MIS-28	The UAM vehicle shall have a block time of less than 4 minutes for a 7 km interurban mission. [6]	*	
18-MIS-29	The UAM vehicle shall have a block time of less than 12 minutes for a 30 km extra-urban mission. [6]	*	
15-MIS-30	The UAM vehicle shall provide weather control during flight.	✓	Chapter 13
18-MIS-31	The UAM vehicle shall have enough range to divert in case the designated landing area is not available.	✓	
18-MIS-32	The UAM vehicle shall have enough range to loiter in case the designated landing area is not available.	✓	Chapter 5 Chapter 6

Continued on next page

Table 22.1: *Compliance matrix of the mission, system, and subsystem requirements (Continued)*

11-MIS-33	The UAM vehicle shall incorporate redundancy in its subsystems	✓	Chapter 5 Chapter 6
11-MIS-34	The UAM vehicle shall not fly under extreme weather conditions (8 Beaufort).	✓	Chapter 13
11-MIS-35	The UAM vehicle shall include thermal management systems in the propulsion and power subsystems.	*	
11-MIS-36	The UAM vehicle shall perform stable flight in its entire flight regime.	✓	Chapter 11
1-MIS-37	The UAM vehicle shall include a flight control system.	✓	Chapter 13 Chapter 11
11-MIS-38	The UAM vehicle shall be able to sustain a maximum load factor of 2.5 during all normal flight maneuvers	✓	Chapter 10
11-MIS-39	The UAM vehicle shall be able to withstand an ultimate load factor of 3.75	✓	Chapter 10
System Requirements			
Sustainability			
5-MIS-6-SYS-CON-1.1.1	The UAM vehicle shall emit no more than 127 g of CO_2 per km [54].	*	
5-MIS-6-SYS-CON-1.1.2	The UAM vehicle shall emit no more than 0.08 g of NO_x per km [44].	*	
5-MIS-6-SYS-CON-1.1.3	The UAM vehicle shall emit no more than 0.001 g of SO_2 per km [12].	*	
10-MIS-14-SYS-CON-1.2.1	The UAM vehicle shall produce less than 120 dBA in sound power level during take-off and landing.	× 137.4 dBA	Section 12.7
10-MIS-14-SYS-CON-1.2.2	The UAM vehicle shall generate noise during take-off and landing for no more than TBD minutes per day.	*	
5-MIS-7-SYS-CON-1.3.1	The UAM vehicle shall consist of at least 80% of parts that can be recycled.	*	
5-MIS-7-SYS-CON-1.3.2	The UAM infrastructure shall consist of TBD % of parts that can be recycled.	*	
Environment			
3-MIS-3-SYS-CON-2.1.1	The UAM vehicle shall coordinate its flight with the local air traffic control agencies.	✓	Chapter 13
5-SYS-CON-2.3.1	The UAM vehicle shall have less than 5 bird strikes per 10 000 flights.	*	
6-MIS-9-SYS-CON-2.2.1	The UAM vehicle shall not have a vertical velocity at touchdown of more than 2 m/s.	✓	Section 8.2
2-MIS-2-SYS-CON-2.4.1	The minimum separation distance between two UAM vehicles shall be at least 152 m [1]	✓	Chapter 11
Safety			
1-MIS-1-SYS-CON-3.2.1a	The UAM lifting vehicle shall meet the certification standards of CS-27.	✓	Chapter 6
1-MIS-1-SYS-CON-3.2.1b	The UAM cruise vehicle shall meet the certification standards of CS-23.	✓	Chapter 5
2-MIS-2-SYS-CON-3.1.1	The UAM vehicle shall adhere to municipal regulations in which it operates.	✓*	Chapter 15
11-MIS-16-SYS-CON-3.3.1	The UAM vehicle shall include safety gear for all passengers.	✓	Section 5.1.2
11-MIS-16-SYS-CON-3.3.2	Emergency evacuation procedures shall be performed within 90 seconds.	*	
2-MIS-2-SYS-CON-3.1.2	The UAM vehicle shall have a collision avoidance systems capable of detecting both airborne and ground-based obstacles.	✓	Chapter 13
5-MIS-8-SYS-CON-3.2.2	The UAM vehicle shall achieve a maximum allowable failure rate of critical systems of less than 10^{-9} per flight hours.	*	
9-MIS-27-SYS-CON-3.3.3	The UAM vehicle shall be able to perform an emergency landing during take-off.	✓	Chapter 5 Chapter 6
9-MIS-27-SYS-CON-3.3.4	The UAM vehicle shall be able to perform an emergency landing during cruise.	✓	Chapter 5 Chapter 6
9-MIS-27-SYS-CON-3.3.5	The UAM vehicle shall be able to perform an emergency landing during landing.	✓	Chapter 5 Chapter 6
4-MIS-4-SYS-CON-3.1.3	The UAM vehicle shall undergo regular in-operation inspection daily.	*	
4-MIS-5-SYS-CON-3.1.4	The UAM vehicle shall undergo regular in-operation maintenance every 300 flight hours.	*	
11-SYS-CON-3.4.1	The software of UAM vehicle shall be compliant with DO-178C.	*	
9-SYS-CON-3.3.6	The UAM vehicle shall act as a Faraday cage in case of a lightning strike.	✓*	Chapter 10

Continued on next page

Table 22.1: *Compliance matrix of the mission, system, and subsystem requirements (Continued)*

9-SYS-CON-3.3.7	The UAM vehicle shall carry one fire extinguisher.	✓	Section 5.1.2
11-MIS-35-SYS-CON-3.5.1	The UAM vehicle shall have a cooling system for batteries and engines.	*	
4-MIS-5-SYS-CON-3.1.5	The UAM vehicle shall have a guide for performing maintenance available for maintenance mechanics.	✓	**??**
Resources			
16-MIS-23-SYS-CON-4.1.1	The loading and unloading of the payload shall not take up more than 3 minutes.	*	
7-MIS-10-SYS-CON-4.2.1	The take-off and landing area shall fit in a 12 x 12 m square [43].	✓	Chapter 15
Payload			
12-MIS-17-SYS-CON-5.1.1	The UAM vehicle shall transport 320 kg of passengers [7].	✓	Chapter 5
12-MIS-17-SYS-CON-5.2.1	The UAM vehicle shall transport 100 kg of luggage. [7]	✓	Chapter 5
12-MIS-17-SYS-CON-5	The weight of the payload shall not exceed 420 kg [7].	✓	Chapter 5
15-MIS-21-SYS-CON-5.2.2	The UAM vehicle shall have at least 0.63 m^3 storage space for total passenger luggage [28].	×*	Chapter 5
17-MIS-24-SYS-CON-5.1.2	The UAM vehicle shall have at least 2.5 m^3 cabin volume.	✓ 3.6 m^3	Chapter 5
12-MIS-17-SYS-CON-5.1.3	Ingress and egress for passengers shall be possible.	✓	Section 5.1.2
Take-off and Landing			
6-MIS-9-SYS-CON-6.2.1	The transition altitude shall be at least 450 m.	✓	Section 8.2
6-MIS-9-SYS-CON-6.1.1	The horizontal distance between lift-off and reaching transition altitude shall not exceed 300 m.	✓	Section 8.2
Performance			
14-MIS-20-SYS-TEC-1.6.1	The UAM vehicle shall fly at a cruise altitude of at least 1200 m.	✓	Section 8.2
18-MIS-26-SYS-TEC-1.1.1	The UAM vehicle shall have a nominal range of 50 km.	✓	Section 8.2
18-MIS-26-SYS-TEC-1.3.1	The UAM vehicle shall be able to fly for 10 min after reaching the first point of intended landing place. [49]	✓	Chapter 5 Chapter 6
18-MIS-26-SYS-TEC-1.4.1	The take-off time shall be less than 100 s. [6]	✓	Section 8.2
2-MIS-2-SYS-TEC-1.4.2	The landing time shall be less than 100 s. [6]	✓	Section 8.2
2-MIS-2-SYS-TEC-1.5.1	The UAM vehicle shall have a minimal climb rate of 4.5 m/s. [49]	✓	Chapter 6
18-MIS-28-SYS-TEC-1.2.2	The UAM vehicle shall be able to achieve vertical acceleration of at least 2 m/s^2 at any given time during cruise.	✓	Chapter 5
18-MIS-28-SYS-TEC-1.2.3	The UAM vehicle shall be able to achieve horizontal deceleration of at least 1.6 m/s^2 at any given time during landing.	✓	Chapter 6
18-MIS-28-SYS-TEC-1.2.1	The UAM vehicle shall be able to achieve vertical acceleration of at least 2 m/s^2 at any given time during take-off. [6]	✓	Chapter 6
9-MIS-27-SYS-TEC-1.5.2	The UAM vehicle shall have a maximum descent rate of 10 m/s during normal operation.	✓	Chapter 5
Propulsion			
18-MIS-28-SYS-TEC-2.2.1	The UAM vehicle and infrastructure shall be able to provide thrust in the direction perpendicular to the flight.	✓	Section 6.3.3
18-MIS-28-SYS-TEC-2.1.1	The UAM vehicle shall be able to achieve horizontal acceleration of at least 1.6 m/s^2 at any given time during take-off.	✓	Section 6.3.3
18-MIS-28-SYS-TEC-2.1.2	The UAM vehicle shall be able to achieve horizontal acceleration of at least 1.6 m/s^2 at any given time during cruise.	✓	Section 5.1.4
18-MIS-28-SYS-TEC-2.1.3	The UAM vehicle's load factor shall not exceed -0.2 g at any given time during landing [6].	✓	Section 8.3
9-MIS-27-SYS-TEC-2.3.1	The propulsion unit shall have a specific energy consumption of 100,000 J/kg.	✓ 83,700 J/kg	Section 8.2
Navigation			
2-MIS-2-SYS-TEC-3.1.1	The UAM vehicle shall be able to determine its location within the accuracy of 0.1 m [56].	*	

Continued on next page

Table 22.1: *Compliance matrix of the mission, system, and subsystem requirements (Continued)*

1-MIS-1-SYS-TEC-3.2.1	The UAM vehicle shall use real-time weather data to optimize route planning to avoid adverse weather conditions.	✓	Chapter 13
1-MIS-1-SYS-TEC-3.1.2	The UAM vehicle shall be compatible with existing aviation navigation standards and protocols.	✓	Chapter 13
1-MIS-37-SYS-TEC-3.1.3	The UAM vehicle shall have sensors to measure airspeed, altitude and attitude.	✓	Chapter 13
Energy and Power			
18-MIS-26-SYS-TEC-4.1.1	The UAM vehicle and infrastructure system shall use no more than 100 MJ of energy for take-off.	✓ 19.3 MJ	Chapter 5 Chapter 6
18-MIS-26-SYS-TEC-4.1.2	The UAM vehicle shall use no more than 100,000 J of energy for cruise.	✓*	Chapter 5 Chapter 6
18-MIS-26-SYS-TEC-4.1.3	The UAM vehicle and infrastructure system shall use no more than 100 MJ of energy for landing.	✓	Chapter 5 Chapter 6
18-MIS-26-SYS-TEC-4.2.1	The UAM vehicle and infrastructure system shall use no more than 1000 kW of power for take-off.	✓ 941 kW	Chapter 6
18-MIS-26-SYS-TEC-4.2.2	The UAM vehicle shall use no more than 1000 kW of power for cruise.	✓*	Chapter 5 Chapter 6
18-MIS-26-SYS-TEC-4.2.3	The UAM vehicle and infrastructure system shall use no more than 1000 kW of power for landing.	✓ 770 kW	Chapter 6
18-MIS-26-SYS-TEC-4.2.7	The UAM vehicle shall use no more than 1000 kW of power for climb.	✓	Chapter 5
18-MIS-26-SYS-TEC-4.2.5	The UAM vehicle shall use no more than 1000 kW of power for descent.	✓	Chapter 5
18-MIS-26-SYS-TEC-4.2.6	The UAM vehicle shall use no more than 1000 kW of power for loiter.	✓	Chapter 5 Chapter 6
18-MIS-26-SYS-TEC-4.2.4	The UAM vehicle shall use no more than 1000 kW of power for reserves.	✓	Chapter 5 Chapter 6
18-MIS-26-SYS-TEC-4.3.1	Each UAM vehicle shall be able to transport 250 kg of mass for energy storage.	✓	Section 5.2.5 Section 6.2.4
18-MIS-26-SYS-TEC-4.3.3	The total installed power of the motors of the UAM vehicle shall be lower than 1000 kW [51].	✓	Chapter 5 Chapter 6
Stability and Control			
11-MIS-36-SYS-TEC-5.2.1	The UAM vehicle shall have stable phugoid.	*	
11-MIS-36-SYS-TEC-5.2.2	The UAM vehicle shall have stable aperiodic roll.	*	
11-MIS-36-SYS-TEC-5.2.3	The UAM vehicle shall have stable Dutch roll.	*	
11-MIS-36-SYS-TEC-5.2.4	The UAM vehicle shall have stable short period.	*	
2-MIS-2-SYS-TEC-5.4.1	The UAM vehicle shall be able to avoid obstacles at a vertical distance of at least TBD m.	✓*	Chapter 11
2-MIS-2-SYS-TEC-5.4.2	The UAM vehicle shall be able to avoid obstacles at a horizontal distance of at least TBD m.	✓*	Chapter 11
11-MIS-36-SYS-TEC-5.2.5	The UAM vehicle shall be statically stable for any distribution of the payload in the cabin.	✓	Chapter 11
11-MIS-36-SYS-TEC-5.2.6	The UAM vehicle shall be able to redistribute power to maintain stability in case of an engine failure	✓	Chapter 11
11-MIS-36-SYS-TEC-5.3	The UAM vehicle shall be able to roll 60 degrees in 1.3 seconds [42].	✓	Chapter 9
Aerodynamics			
2-MIS-2-SYS-TEC-6.1.1	The downwash caused by the UAM vehicle shall not impact the flying capability of another vehicle 152 m behind.	*	
1-MIS-1-SYS-TEC-6.2.1	The UAM vehicle shall have a stall speed lower than 25 m/s at landing configuration.	×25.4m/s*	Chapter 9
Support Infrastructure			
16-MIS-22-SYS-TEC-7.1.1	The take-off and landing area shall include at least one charging/refueling facility.	*	
16-MIS-22-SYS-TEC-7.1.2	Power of charging facility shall be at least TBD W.	*	
7-MIS-10-SYS-TEC-7.2.1	The take-off and landing area shall accommodate vertical take-off and landing.	✓	Chapter 15

Continued on next page

Table 22.1: *Compliance matrix of the mission, system, and subsystem requirements (Continued)*

16-MIS-23-SYS-TEC-7.1.3	At least one spare battery shall be present at each vertiport.	✓	Chapter 15
Structures			
7-MIS-10-SYS-TEC-8.4.1	The operative empty weight of the UAM vehicle shall not exceed 2300 kg.	✓ 1686 kg	Section 5.3 Section 6.3
7-MIS-10-SYS-TEC-8.4.2	The maximum take-off weight of the UAM vehicle shall not exceed 3175 kg [51].	✓ 2572 kg	Section 5.3 Section 6.3
7-MIS-10-SYS-TEC-8.3.1	G-forces during the takeoff and landing procedure shall not exceed TBD g.	✓*	Section 8.3
6-MIS-9-SYS-TEC-8.2.1	The UAM vehicle and infrastructure system shall resist all propulsive loads experienced throughout its flight regime.	✓	Chapter 10
6-MIS-9-SYS-TEC-8.1.1	The UAM vehicle shall resist all aerodynamic loads experienced throughout its flight regime.	*	
11-MIS-33-SYS-TEC-8	The UAM vehicle shall have fail-safe mechanisms in case of a structural failure.	× *	
11-MIS-38-SYS-TEC-8.5.1	The UAM vehicle shall be able to sustain a maximum load factor of 2.5 during all landing maneuvers	✓	Chapter 10
11-MIS-39-SYS-TEC-8.5.2	The UAM vehicle shall be able to withstand an ultimate load factor of 3.75 during landing	✓	Chapter 10
Subsystem Requirements			
Propulsion			
18-MIS-28-SYS-TEC-1.2.1-SUBSYS-PRP-1	The propulsion unit of the lifting vehicle shall provide at least 31 kN of thrust in fully vertical configuration at sea-level.	✓ 37847 N	Chapter 11
18-MIS-28-SYS-TEC-2.1.1-SUBSYS-PRP-3	The propulsion unit of the cruise vehicle shall provide at least 1000 N of thrust in fully horizontal configuration at sea-level.	✓	Chapter 11
Navigation			
2-MIS-2-SYS-TEC-3.1.1-SUBSYS-NAV-1	The UAM shall achieve a minimum update rate of GPS position data of TBD Hz.	*	
1-MIS-1-SYS-TEC-3.1.2-SUBSYS-NAV-2	The UAM vehicle shall maintain communication with ground-based air traffic control systems with a latency of less than TBD seconds.	*	
Energy and Power			
18-MIS-26-SYS-TEC-4.3.1-SUBSYS-ENP-1	The energy density of the energy storage system shall be at least 235 Wh/kg.	✓	Section 5.3

[1] https://www.airservicesaustralia.com/about-us/our-services/how-air-traffic-control-works/separation-standards/ [Accessed on 23 May 2024]

22.2.1. Additional Clarification

Below, the requirements that are met but call for more explanation are discussed. These requirements are indicated with ✓* in Table 22.1. Also, the requirements that could not have been fulfilled yet due to the early stage of the design process are discussed.

REQ-STK-1-MIS-1: Certification standards
The specifications of FAR Chapter 21.17 indicate that the vehicle(s) shall adhere to certain standards depending on the weight of the structure and the number of passengers. The lifting vehicle shall adhere to CS-27. The cruise vehicle shall adhere to CS-23. These regulations cover all aspects of design, construction, and operational safety to ensure the vehicles are airworthy and reliable. However, these regulations are extensive enough that at this stage of the design, it can not be established with certainty that both vehicles adhere to all regulations. However, the most important certifications such as the weight and the center of gravity determination, emergency procedures, climb performance, etc. are mentioned separately in the following (subsystem) requirements.

REQ-STK-5-MIS-6, -SYS-CON-1.1.1 until 1.1.4: Global warming potential
Multiple values for $CO_{2,eq}$ emissions for the production of lithium-ion batteries are reported. When an average value of 120 kg $CO_{2,eq}$/kWh is adopted, a pyrometallurgical recycling method with a 5.11 kg $CO_{2,eq}$/kWh emission is assumed, and CO_2 emission during use is neglected, together with the mass of the batteries and the specific energy density, the total CO_2 emission of the batteries during their lifetime can be estimated. When this is compared with the CO_2 emission of a diesel car, assuming its lifetime travel distance on average is 400000 km and its lifetime is about 15 years, the cruise and lifting vehicle produce over 20000 kg less CO_2 over a duration of 10 years. Furthermore, the CO_2 emissions for the production and recycling of the diesel car are not even taken into account.

Due to constraints in time and manpower, the specific amounts of NO_x and SO_2 emitted due to the production of the battery, charging of the batteries, and disposal of the batteries have not been analysed. However, it is assumed that during the operational phase, neither the lifting vehicle nor the cruise vehicle emits air pollutants.

REQ-STK-10-MIS-14-SYS-CON-1.2.2: Noise generation duration The amount of flights per day has not been determined at this stage of the design. Additionally, it depends on which distance the noise level is measured. At a distance of 100 meters, the experienced noise level is 77.6 dBA. This level is comparable to the sound of a dishwasher, and it can thus be assumed that this will not hinder the civilians.

REQ-STK-17-MIS-24 and 25: Wheelchair users
Wheelchair users will be able to use KoriAir to travel but under certain conditions. First, they must be able to remain in a seated position independently with the seating belts on. Additionally, a way of entering the cruise vehicle must be arranged by themselves if they are not able to do so on their own. Finally, the disabled person can take his or her wheelchair with him or her only when the wheelchair is foldable, and is folded less than 1.4 x 1.0 x 0.5 m^3, such that it fits in the additional storage space in the tailcone.

At this stage of the design, the vertiports or existing heliports that have been selected as locations for the take-off and landing pads are either helicopter landing parts of hospitals or ports that are on ground level. This means that they will be accessible for wheelchair users. Alternatively, vertiports may be placed atop buildings, where wheelchair accessibility will depend on the means of access to the building's top floor.

REQ-STK-5-MIS-7, -SYS-CON-1.3.1 and 1.3.2: Recyclability
Both the vehicles and the infrastructure have not been designed in such detail that it can be determined to what extent the individual components can be recycled. For sub-components that are made of metal alloys, such as the skid landing gear, the materials can be melted down and reused. These materials can then be repurposed for less demanding applications. This process is known as downcycling and is expected within the context of this project. This is because the aviation industry has high standards for materials, and it is difficult to meet these standards with recycled materials.

REQ-STK-5-MIS-8: Operational lifetime
The level of design detail for both vehicles and infrastructure does not allow for determining the precise lifetime of all components. This is influenced by the number of flights per year, the environmental conditions, the loading of the vehicles, the quality of several sub-components, and many more - interrelated - aspects. It can be estimated when more of these parameters are known in later stages of the design. However, the current design of the vehicles aims for an operational lifetime of 12 years.

REQ-STK-13-MIS-18: Operating costs
At this moment in the design phase, the cost of certain components such as the charging facilities, the rent or investment costs of the area of the vertiports, and insurance are not known. Additionally, it has not been determined how many flights will be flown with one combination of lifting and cruise vehicles per day. The cost per passenger per kilometre is also dependent on the price of electricity, which is subject to fluctuations over time. It can therefore not be determined at this point.

REQ-STK-16-MIS-22,23, -SYS-TEC-7.1.1 and 7.1.2: Charging and turnaround time
The charging and recharging infrastructure for the batteries has not been designed due to constraints in time and manpower. Consequently, necessary facilities for this purpose have not been developed and it is not possible to determine the exact time to fully charge both the lifting and the cruise vehicle.

REQ-STK-18-MIS-28 and 29: Block time
Due to time and manpower constraints, the intervals between the flights are not analysed in detail. It is therefore not yet possible to determine the block time of the vehicles. This also depends on the range of the missions, whether the cruise vehicle is required to fly at a higher altitude (as climbing takes more time than cruising flight), and if loitering is a common practice during flights.

REQ-STK-11-MIS-35 and -SYS-CON-3.5.1: Thermal management
Due to time constraints, it was not possible to analyse the amount of heat generated by the propulsion and power subsystem. This is a complex interaction between heat-generating components, the specific heat capacity of the materials near those components, and potential cooling due to airflow or other subsystems.

REQ-STK-5-SYS-CON-2.3.1: Bird strikes
This requirement has not been analysed in detail. The amount of birds potentially encountered is influenced by various factors, including the location of the flights, the time of flight, the season and weather, the altitude, and whether deterrents are used. It is estimated that a bird strike event occurs once every 2000 flights [30], but it is unsure if this includes both aircraft and helicopters and/or what types. Helicopters are generally more susceptible to bird strikes due to their lower cruise altitude. To get more specific numbers, bird strikes in helicopters should be investigated. Another source indicates that two light utility helicopters with a maximum speed of around 220 km/h were around 2-10 bird strikes per 10000 flight hours [10]. Given the average duration of a flight with KoriAir, it is assumed that this requirement can be met.

REQ-STK-2-MIS-2-SYS-CON-3.1.1: Municipality regulations
This depends on the region the flights are performed in. At this stage of the design, specific regulations of municipalities have not been checked. When the country and the specific location of the vertiports are determined, this can be researched. It has not been done for the municipalities of Amsterdam, Rotterdam, and The Hague due to time constraints.

REQ-STK-11-MIS-16-SYS-CON-3.3.2 and -4.1.1: Emergency evacuation procedures and loading of the payload
This requirement can be verified when a prototype has been built. This allows for real-life simulations of various situations and analyses if emergency evacuation protocols can be followed and performed in the required time frame.

REQ-STK-5-MIS-8-SYS-CON-3.2.2: Failure rate
At this stage of the design, not all systems and components of both vehicles are determined. Therefore, it is also not yet specified how certain elements interact with one another. It is thus not possible to estimate the failure rate of the system in its entirety. It must be mentioned, however, that estimating

the failure rate of a complex system such as those of multicopters and aircraft is challenging and it is often not feasible to expect a very accurate estimation of the failure rate of an entire system.

REQ-STK-4-MIS-4-SYS-CON-3.1.3 and 3.1.4: In-operation inspection and maintenance
At this stage of the design, maintenance is considered, albeit without delving deeply into specifics. Combined with what was mentioned earlier, that the specific flight hours have not been determined yet, it is not yet possible to satisfy these requirements. It is expected that these requirements will form part of the maintenance manual of both vehicles, and that the operating companies are required to strictly adhere to those.

REQ-STK-11-SYS-CON-3.4.1: Software
The software of both vehicles has not been a point of attention in this part of the design. Therefore, it is not possible to say that this requirement is met.

REQ-STK-9-SYS-CON-3.3.6: Faraday cage
Since the majority of the aircraft structure is made of metal, either aluminium or titanium, it is expected that this acts as a conductive outer shell, and safely conducts the charge. More detailed analysis is required when the design of both the lifting and the cruise vehicle advances.

REQ-STK-2-MIS-2-SYS-TEC-3.1.1 and -3.1.1-SUBSYS-NAV-1: Location determination
The specifics of the flight control system have not been yet considered, due to the limited amount of information about the data size. It is highly expected that this requirement will be met, due to the sensitivity of the coupling mechanism between the lifting and the cruise vehicle. The precision of the location determination has to be nearly perfect in order to allow for smooth and safe coupling. The accuracy of the location determination depends on the update rate of the GPS data. This requirement will be revisited when the flight control system is sized in even more detail.

REQ-STK-18-MIS-26-SYS-TEC-4.1.2 and 4.2.2: Energy and power use during cruise
When a conservative approach is adopted, and the energy consumption for a range of 50 km, at a cruise speed of 200 m/s for the entire distance is taken, the power used can be determined. This is approximated with $P = \frac{D}{V}$ where sea-level density is taken. This results in an energy consumption of less than 94 kJ.

REQ-STK-11-MIS-36-SYS-TEC-5.2.1 until 5.2.4: Stable eigenmotions
At the current stage of the design of both vehicles, the specific stability derivatives are not known, as they depend on intricate aerodynamic interactions and structural considerations. The detailed design phase and additional flight tests with a prototype or similar vehicle will play a critical role in determining these derivatives. Then, the response of the vehicles to various inputs and eigenmotions can be analyzed.

REQ-STK-2-MIS-2-SYS-TEC-5.4.1 and 5.4.2: Object avoidance
A specific avoidance system has not been designed in this stage of the design. However, it is implicitly assumed to be inherent in the flight control system. Additionally, given the required accuracy of the flight control of the two vehicles for the coupling procedure, and the high amount of sensors for that procedure, it can be safely assumed that either vehicle is able to detect and avoid obstacles, both horizontally and vertically.

REQ-STK-7-MIS-10-SYS-TEC-8.3.1: G-forces during take-off and landing
It has not been analyzed in detail at this stage of the design, but it is expected that with the maximum take-off and landing speed, the g-force felt by the passengers will be significantly below the value that is comfortable. This requirement is closely connected to REQ-STK-18-MIS-28-SYS-TEC-2.1.3.

REQ-STK-6-MIS-9-SYS-TEC-8.1.1: Aerodynamic loads
At this stage of the design, only the aerodynamic moment introduced in the fuselage structure due to the wing is considered. Additional loads due to gusts, torsional moments due to the vertical and horizontal tail, aerodynamic loads from control surface deflections, and the impact of asymmetric thrust have not been considered yet. It is however expected that no significant modifications are needed for the fuselage to withstand these loads, as the structure is able to withstand high load factors. However, these loads will be considered in the detailed design phase of the vehicles.

REQ-STK-2-MIS-2-SYS-TEC-6.1.1: Impact of downwash
The exact amount of downwash created by the cruise vehicle during horizontal flight has not been analyzed due to time and manpower constraints. It is expected that the minimal distance between either of the two vehicles and other (air)craft is enough to not have an adverse impact on the stability of those vehicles.

REQ-STK-1-MIS-1-SYS-TEC-3.1.2-SUBSYS-NAV-2: Latency of communication
This requirement is closely related to REQ-STK-2-MIS-2-SYS-TEC-3.1.1 as well as general requirements about the vehicles' object avoidance and general navigation. The amount of data that is required by the ground control systems to ensure safe, reliable and accurate flight has yet to be determined. Depending on the amount of data and the sensitivity of having the most up-to-date data, the latency of the data can be determined. At this stage of the design, this cannot be established.

22.2.2. Unfulfilled requirements

Below, the requirements that are not fulfilled at this stage of the design are discussed. This means that either the requirements need to be reconsidered, or the design needs additional alterations in order to meet those requirements. The details of this will be discussed per requirement in the following paragraphs.

REQ-STK-10-MIS-14-SYS-CON-1.2.1: Sound power level take-off and landing
For the current design, the sound power level - which is measured at 1 m distance from the rotors - is 128 dBA. It must be noted however, that no one outside the vehicle will be that close to the vehicles when they are taking off. For the passengers in the cabin of the cruise vehicle however, this might be a problem. Additional techniques might be needed to further reduce the noise level. This can include speakers which emit noise with frequencies that cancel out the sound waves. Also, a certain type of noise-cancelling foam can be used inside the cabin, and one can look into noise-cancelling headphones for the passengers. This will be part of the more detailed design of the vehicles, in a later stage of the project.

REQ-STK-15-MIS-21-SYS-CON-5.2.2: Payload volume
The volume available in the cabin for the luggage of the passengers is 0.176 m^3 in total, resulting from standard-sized carry-on baggage. However, since the design of the cruise vehicle has a relatively large tail cone, and the batteries occupy minimal space, it is expected that the remaining 0.454 m^3 - might the passengers need that space - can be placed in the tail cone.

REQ-STK-1-MIS-1-SYS-TEC-6.2.1: Stall speed
With the current wing, the maximum lift coefficient, wing surface area, maximum take-off weight, and using the air density at sea-level for the calculation, the cruise vehicle has a stall speed of 25.4 m/s. However, the additional lift created by the fuselage and the horizontal tail have not been taken into account. It is quite possible if that is included in the calculations, the cruise vehicle will meet the requirement. If this is not the case, the wing shall be redesigned; an airfoil with a larger camber, or resizing of the high-lift devices will make sure that the stall speed of the aircraft will be below the specified value.

REQ-STK-11-MIS-33-SYS-TEC-8: Fail-safe mechanism
As of now, the structure of the vehicles is designed such that it withstands the loads on the structure, including safety factors and load factors up to 3.75. However, no fail-safe mechanisms have been considered. This will be done in a later, more detailed design phase of the sub-components of the vehicles. It is expected that these mechanisms will add weight to the structure and thus should be carefully considered and designed.

23

Project Development

To ensure the design of KoriAir can be systematically continued after the preliminary design, it is important to set up the subsequent phases of the project. This chapter begins with a description of the project design and development in Section 23.1. It covers the steps that are taken after the preliminary design of the system to prepare the vehicle and infrastructure for production. The tasks involved are further detailed in a project Gantt chart in Section 23.2.

23.1. Design and Development Logic

This section describes the steps that need to be taken beyond the preliminary design of the vehicle. This 'Project Design and Development Logic' is shown in this section in the form of a diagram in Figure 23.1 and its associated activity descriptions.

The diagram lays out the action items in chronological order. The project design and development logic is split into four main parts: detailed design, a post-design stage, a post-authorization stage, and an end-of-life (EOL) stage. Although the project will include extensive design for the final product, only the steps up until the preliminary design are completed at this point. Therefore, the Design and Development Logic after the end of the current project begins with detailed design.

The Detailed Design phase is the last step of the design phase, in which the dimensions of the product will be finalized. Reference data, analysis tools, and expertise are utilized to build engineering models. Typical design tools include higher-order simulation, design for manufacturing and assembly, failure mode analysis, and more. With the use of these tools, the design can be finalized and the project can move to the next phase, which is manufacturing and testing.

After completion of the design phases, further actions must be taken. These activities can be grouped as the Post Design Processes. This process starts with planning for assembly, basic qualification then the Critical Design Review (CDR). The CDR is a crucial step of this design phase. The CDR ensures that the design presented is mature and appropriate to proceed to the full scale of design[1]. Once ensured that the full scaling is possible through CDR, the building process may begin. A manufacturing readiness review is conducted to ensure that the manufacturing process can be completed as planned. This process takes into consideration the availability of staff, availability of manufacturing equipment and facilities, skills of the manufacturing staff, and other elements of the manufacturing process. The building of hardware and therefore the vehicles/systems can now commence. The building process not only consists of manufacturing the product itself, but also the representative infrastructure in order to complete testing. Using representative infrastructures would be beneficial as it will reduce the risk of possible damage that could take place in case of using real-world infrastructure. After building elements that are required for testing, qualification testing and verification are conducted in order to ensure that the product operates as required. Lastly, the operational readiness must be reviewed to ensure that the product is ready to operate in different scenarios. After this phase, necessary certifications for vehicle and infrastructure are sought. The degree to which requirements are met is reviewed with acceptance testing, after which the vehicle and/or systems will be ready for mass production.

Once the aircraft is ready for production, it must be marketed towards potential customers and launched globally so it can begin being sold. Its infrastructure can be built (vertiports) or if there are

[1]https://nodis3.gsfc.nasa.gov/main_lib.cfm [Accessed on 21 May 2024]

existing landing pads they can be retrofitted with the necessary equipment to operate the aircraft. Then the vehicle will go into operation, where maintenance and revisions will be necessary occasionally to see if the aircraft is still airworthy. If after evaluation, the aircraft is not airworthy and cannot be repaired, the aircraft enter into their end of life (EOL) stage.

The EOL phase begins with determining the quality of the aircraft parts before disassembly begins. These parts are then re-used, if possible, or recycled. If they cannot be recycled, they will have to be correctly disposed of. In the case of the lithium-ion batteries, these are difficult to recycle and will be disposed of.

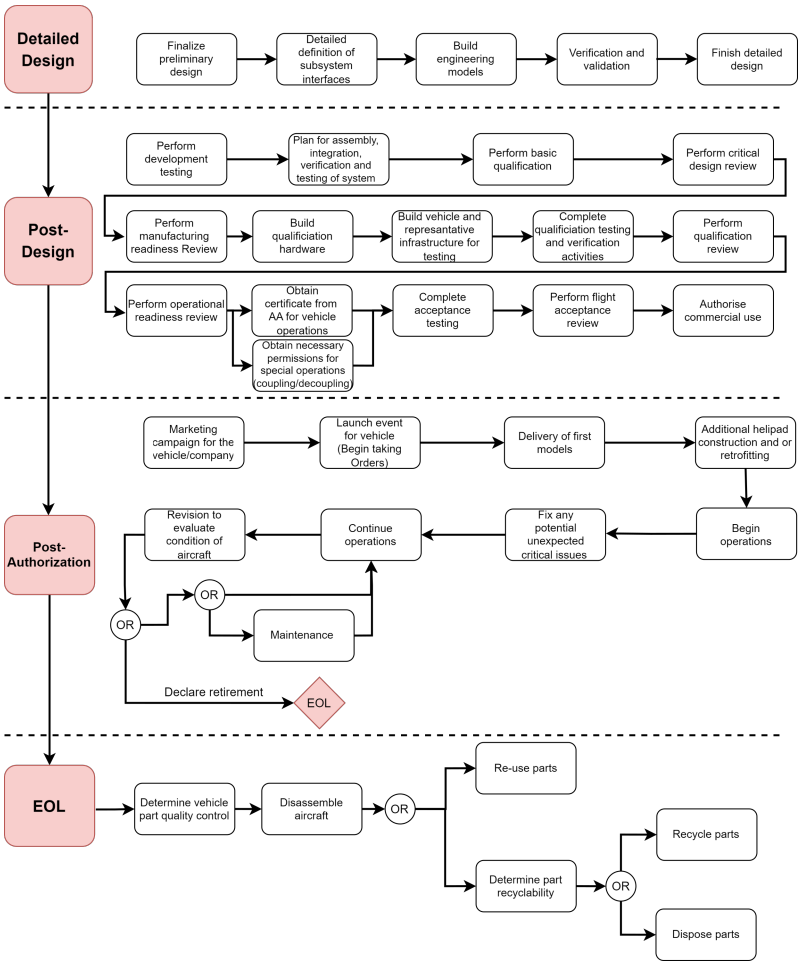

Figure 23.1: *Project design and development logic*

23.2. Project Gantt Chart

In this section, the development of a project plan by use of a Gantt chart will be done. The post preliminary design route is planned until full production. It starts from the preliminary design final phase and reached the full release of the vehicle into the market and the operations and end of life actions. The time intervals assigned to the tasks contain a 20 % contingency to take into account possible delays due to, among other things, supply of parts, tool damage and contract issues. It is complicated to predict the expected launch date of a vehicle in such an early design phase so it is expected this task distribution will be modified. It should be noted, that within the manufacturing tasks in the Gantt chart, there are also testing and quality assurance tasks carried out, as detailed in Figure 23.2.

ID	Name	2019	2024	2029	2034	2039
1	Preliminary Design Phase					
35	DSE presentation					
2	Post DSE meeting					
3	Implement DSE Feedback					
4	Feasability Study					
5	In-Depth Market Analysis					
6	Aerodynamic Analysis					
7	Structural Analysis					
8	Propulsion Analysis					
9	Coupling Analysis					
10	Performance Analysis					
11	Certification Analysis					
12	Avionics Design					
13	Safety Analysis					
14	Prototype Phase					
36	Prototype Manufacturing					
15	Component Testing					
16	Subsystem testing					
17	Subsystem Updates					
18	Prototypes Testing					
20	Wind-Tunnel Testing LiftingVehicle					
22	Performance Testing Lifting Vehicle					
19	Wind-Tunnel Testing Cruise Vehicle					
21	Performance Testing Cruise Vehicle					
23	Certification and Final Design Phase					
37	Logistics Certification					
24	Design Iterations					
25	Revision Testing					
26	Final Design Review					
27	Flight Manual					
28	Certification Testing					
29	Production Phase					
38	Manufacturing Logistics					
30	Manufacturing Vehicles					
32	Marketing of Vehicle					
33	Launch Event					
34	Begin Taking/Delivering Orders					
31	Quality Assurance					
39	Operations Phase					
41	Delivery of first Production Models					
42	Additional helipad construction and or retrofit…					
43	Begin operations					
44	Maintence					
45	Revision to evaluate condition of aircraft					
40	EOL Phase					
47	Disassemble aircraft					
46	Determine vehicle part quality control					
49	Determine part recyclability					
48	Re-use parts					
50	Recycle parts					
51	Dispose parts					

Figure 23.1: *Post preliminary design project GANTT chart*

24

Conclusion and Recommendations

The market of Urban Air Mobility (UAM) is a growing market with many opportunities. Various concepts with differing configurations are already on the market. However, a main problem within the field of UAM is its environmental impact, as it is flying through crowded urban areas. Additionally, noise is an important factor. Finally, vertical take-off and landing come with specific challenges and requirements. In this project, a UAM vehicle that performs a more efficient and quiet flight than current air taxi vehicles is designed.

In detail, the project provided the preliminary design of a system containing the cruise aircraft which is lifted up vertically by a multicopter and then takes off above building level. Together with the design of the vehicles, the coupling mechanism between the two vehicles and required infrastructure is also investigated. The design analysis proves this coupling along with the control system required is feasible. The coupling system is not limited to this project, but it also creates new possibilities in the aviation industry. The outcome of the project shows there is a UAM design which allows for an optimization of the cruise efficiency without the need to compromise it with the vertical flight capabilities. It follows, KoriAir can be a more energy efficient alternative to the conventional taxis and current UAM vehicles.

The design is also driven by the desire to reduce noise, as KoriAir aims to be implemented in cities. The implementation of small ducted rotors allows for a lower noise levels and thus smooth integration within the urban environment. Additionally, introducing active noise control in the cabin makes the operation of the vehicles quieter for the passengers. This lead to an observer noise level of 63.5 overall sound pressure level versus a conventional helicopter with levels up to 100. Along with the vehicles' design, the integration of the required infrastructure in urban areas was analyzed. It shows that even without large changes in the layout of the cities, KoriAir can be a significant improvement of travel time and availability for the agglomeration transport.

The current stage of the preliminary design is only a starting point for further development of the project. Like in every aircraft development program, all the subsystems can be developed in detail. However, there are two main subsystems which should be explored in the further stages of the project. First, further development and design of the coupling mechanism should be performed and second, a deeper exploration of the operation applications of the system should be analyzed.

The project concludes that it is possible to vertically take-off and land using a lifting vehicle coupled with a vehicle that does not have VTOL capabilities. As this is a novel idea, the assumptions made during the preliminary should be heavily researched as the design continues. Specifically, the aerodynamic interaction between two vehicles should be studied since this is currently the largest limiting unknown. Modelling this phenomenon can also lead to the better prediction of the motion of both vehicles. Then, it can be used to create a more advanced control system especially for the coupling phase. Additionally, recent developments in autonomous systems, communication methods, and precise position determination may aid in the coupling process.

Coupling also requires further development from the structural point of view. Currently, only static loading was analyzed, however to design the structure in detail it is necessary to consider also dynamic loading. For instance, the vibrations induced during coupling might create the additional constraints to the design of the attachments, and soft guiding. Moreover, further modelling of the transition process from soft guiding to full attachment must be done. The design developed in the preliminary

design phase shows the layout of the coupling mechanism, however, the exact design of the coupling components, locking parts, and soft coupling must be studied further.

Due to the lack of existence of the coupling concept in the market, the extensive testing must be performed. Mainly wind tunnel testing should be performed to obtain the detailed aerodynamic characteristics of the system. Since coupling and decoupling will be performed thousands of times during the lifetime of the vehicle, the additional fatigue testing of the most critical structures, such as soft guiding and couplers, must be performed. These tests would greatly improve the level of the detail that can be reached, and the results of these experiments can be used in the detailed design of the vehicles as well as in further studies about coupling and synchronization of aircraft.

Another important concept requiring further studies is the operation of the system. The current design proposes the lifting vehicle with the cruise vehicle capable of flying 50 km range and transporting 4 passengers. However, these two do not have to depend on each other. It is advised to perform further market analysis, as well as feasibility studies for different ranges, and payload configurations. Various cruise vehicles should be considered for different missions. It might be possible to travel for short distances without the necessity to decouple from the lifting vehicle. Similarly, the longer range vehicles should be also considered in the further studies, so that the idea of equipping non-VTOL vehicles with VTOL capabilities can be generalized and optimized.

From the operations point of view it is also crucial to develop a more detailed take-off and landing procedures. This must be done in cooperation with municipalities, airworthiness organizations, and passengers. These procedures will assure that the potential of the system will be used in a safe and non-disturbing manner. Also, by cooperating with airworthiness agencies, the certification standards for coupling mechanisms and operation of the lifting vehicles can be issued. Importantly, the areas for the take-off and landing should be created such that the system can be utilized safely. This should preceded by the release of the certification standards for UAM vehicles.

The aforementioned recommendations form guidelines for the further development of the project. Detailed design of both of the vehicles, and further studies on coupling and operation will make the design closer to entering service. Further development of this project has the potential to change the future of not only Urban Air Mobility but also the entire aviation industry.

Bibliography

[1] *AE1222-II: Aerospace Design & Systems Engineering Elements I*. Delft, 2021.

[2] Samuel Afari et al. "Review of Control Technologies for Quiet Operations of Advanced Air-Mobility". In: *Applied Sciences (Switzerland)* 13.4 (Feb. 2023).

[3] R K Amiet. *Noise Due to Turbulent Flow Past a Trailing Edge*. Tech. rep. 3. 1976, pp. 387–393.

[4] Faiza Arshad et al. *Life Cycle Assessment of Lithium-ion Batteries: A Critical Review*. May 2022.

[5] Alessandro Bacchini and Enrico Cestino. "Electric VTOL configurations comparison". In: *Aerospace* 6.3 (Mar. 2019).

[6] Mrunali Botre et al. "Validation of helicopter noise prediction system with flight data". In: *The Vertical Flight Society - Forum 75: The Future of Vertical Flight - Proceedings of the 75th Annual Forum and Technology Display*. Vertical Flight Society, 2019.

[7] J H Breeman. *Method for determining the time delay of the pitot-static tubing system of aircraft*. Tech. rep. National Aerospace Laboratory NLR, 1985.

[8] Arthur Brown and Wesley L. Harris. "Vehicle design and optimization model for urban air mobility". In: *Journal of Aircraft* 57.6 (2020), pp. 1003–1013.

[9] Steven R Bussolari. "Mode S data-line applications for general aviation Author". In: *Mode S data-line applications for general aviation 1994pp 313–328* 7.2 (1994), pp. 313–328.

[10] L.S. Buurma and A. Dekker. *Bird Strike in Aviation: Statistics, Analysis and Management*. Jerusalem: North Atlantic Treaty Organisation, 1992, p. 6377.

[11] Anjan Chakrabarty, Vaishali Hosagrahara, and Andrew Lei. *Design of UAM Network and Ecosystem Integration*. Tech. rep.

[12] E Coşkun and M H Doğru. "Investigation of the hub diameter effect on propeller thrust". In: *The International Journal of Materials and Engineering Technology (TIJMET)* 2022.1 (), pp. 43–47.

[13] Eugenio Denti, Roberto Galatolo, and Franscesco Schettini. "An AHRS Based on a Kalman Filter for the Intergation of Inertial, Magnetometric and GPS Data". In: *27th International Congress of the Aeronautical Sciences*. Nice, France, 210.

[14] By R Donald Riley. *Wind-tunnel Investigation and Analysis of the Effects of End Plates on the Aerodynamic Characteristics of an Unswept Wing*. Tech. rep. 1951.

[15] EADS Eurocopter. *Single Engine Twin Engine Ecureuil (Civil Version) Fennec (Military Version) Ecureuil EC130 B4*. Tech. rep. 2008.

[16] Easa. *Certification Specifications, Acceptable Means of Compliance and Guidance Material for Small Rotorcraft (CS-27)*. Tech. rep. 2023.

[17] Easa. *Easy Access Rules for Normal, Utility, Aerobatic and Commuter Category Aeroplanes (CS-23) (Initial issue)*. Tech. rep.

[18] Felicien F Fullmer. *Two-Dimensional Wind-Tunnel Investigation of Six Airfoil Sections for the Wing of the Vega XP2V-1 Airplane*. Tech. rep. 1945.

[19] Edoardo Grande et al. "Laminar Separation Bubble Noise on a Propeller Operating at Low Reynolds Numbers". In: *AIAA Journal* 60.9 (Sept. 2022), pp. 5324–5335.

[20] Author FP Grooteman. *Executive summary Transmission Loss analyses on fuselage panels Approach, numerical results and validation*. Tech. rep.

[21] Lisa Guerra. "Margins and Contingency Module - Space Systems Engineering". In: *NASA Exploration Systems Mission Directorate* (2008).

[22] Hanson Donald B. *Theory for Noise of Propellers in Angular Inflow With Parametric Studies and Experimental Verification*. Tech. rep. 1993.

[23] S J Hardy and M K Pipelzadeh. “Stress concentration factors for axial and shear loading applied to short flat bars with projections”. In: *The Journal of Strain Analysis for Engineering Design* 29.2 (Apr. 1994), pp. 93–100.

[24] Sighard F. Hoerner. *Fluid Dynamic Drag : Practical Information on Aerodynamic Drag and Hydrodynamic Resistance*. 2nd ed. 1965.

[25] Harvey H Hubbard. *National Advisory Committee For Aeronautics Technical Note 2024 Sound Measurements for Five Shrouded Propellers at Static Conditions*. Tech. rep.

[26] ICAO. “ICAO-Heliport-Design-04-30-2024”. In: 2.14 (2024).

[27] Robert T Jones. *The spanwise distribution of lift for minimum induced drag of wings having a given lift and a given bending moment*. Tech. rep. 1950.

[28] Ashraf M Kamal and Alex Ramirez-Serrano. “Design methodology for hybrid (VTOL + Fixed Wing) unmanned aerial vehicles”. In: *Aeronautics and Aerospace Open Access Journal* 2.3 (2018), pp. 165–176.

[29] Gabe Karpati et al. *Resource Management and Contingencies in Aerospace Concurrent Engineering*. Tech. rep.

[30] Arafat I. Khan, Rakesh K. Kapania, and Eric R. Johnson. “A review of soft body impact on composite structure”. In: *Collection of Technical Papers - Structures, Structural Dynamics and Materials Conference*. 2010.

[31] Oh Sang Kwon, Bong Ki Kim, and Jeong Guon Ih. “On the positioning of control sources in active noise control of three-dimensional interior space”. In: *KSME Journal* 8.3 (Sept. 1994), pp. 283–292.

[32] Xin Lai et al. *Critical review of life cycle assessment of lithium-ion batteries for electric vehicles: A lifespan perspective*. May 2022.

[33] Seongkyu Lee et al. *Turbulent boundary layer trailing-edge noise: Theory, computation, experiment, and application*. Oct. 2021.

[34] Liberty Aerospace. *Wiring Diagrams Chapter 91*. Tech. rep. 2009.

[35] Wanbo Liu and Willem A.J. Anemaat. “A refined method for wing weight estimation and a new method for wing center of gravity estimation”. In: *2013 Aviation Technology, Integration, and Operations Conference*. American Institute of Aeronautics and Astronautics Inc., 2013.

[36] Teppo Luukkonen. *Modelling and control of quadcopter*. Tech. rep. Espoo: Aalto University School of Science, Aug. 2011.

[37] Jack E Made and Donald W Kurtz. *N A Review of Aerodynamic Noise From Propellers, Rofors, and Liff Fans*. Tech. rep. 1970.

[38] Rodrigo Martinez-Val, Emilio Perez, and Jose Palacin. “Historical Perspective of Air Transport Productivity and Efficiency”. In: *43rd Aerospace Sciences Meeting and Exhibit*. Reston, Virigina: American Institute of Aeronautics and Astronautics, Jan. 2005.

[39] B. V. Mathiesen et al. *Smart Energy Systems for coherent 100% renewable energy and transport solutions*. May 2015.

[40] T.H.G. Megson. *Aircraft Structures for Engineering Students*. 16th ed. Oxford: Butterworth-Heinemann, 2016.

[41] MIL-F-8785C. “Military Specification: Flying Qualities of Piloted Airplanes”. In: ().

[42] Jessie Naor. *Opinion: Will eVTOLs Disrupt Traditional Aircraft Values?* Feb. 2024.

[43] *New Car and Van CO2 Guidance 2022*. Tech. rep. Vehicle Certification Agency, 2022.

[44] New Hampshire Department of Environmental Sciences. “All About Batteries”. In: *Environmental Fact Sheet* (2020).

[45] Nita M. and Scholz D. *Estimating the Oswald Factor from Basic Aircraft Geometrical Parameters*. Tech. rep. 2012.

[46] F. Oliviero. *Requirement Analysis and Design Principles for A/C Stabilty and Control (Part II)*. Delft, 2024.

[47] Ilona Paozalyte, Raimondas Grubliauskas, and Petras Vaitiekunas. "Research of railway noise pollution at the living area of railway station in Klaipėda city and designing of noise barrier". In: *ENVIRONMENTAL ENGINEERING*. 2011.

[48] Sylvain Pasquet. *RAMS Analysis for Aeronautics*. Tech. rep. ENAC, 2024.

[49] Jason L Pereira. *Hover and Wind-tunnel Testing of Shrouded Rotors for Improved Micro Air Vehicle Design*. Tech. rep.

[50] Lourenco Tercio Lima Pereira. "Project_Guide_2024_Spring_Group07". In: *TU Delft DSE* (2024).

[51] W. R. Pierson et al. "Sulfate Emissions from Vehicles on the Road". In: *Journal of the Air Pollution Control Association* 28.2 (1978), pp. 123–132.

[52] Walter D. Pilkey and Deborah F. Pilkey. *Peterson's Stress Concentration Factors*. Wiley, Nov. 2020.

[53] Daniel P. Raymer. *Aircraft Design: A Conceptual Approach*. Ed. by Joseph A Schetz. 6th ed. Blacksburg, Virginia: American Institute of Aeronautics and Astronautics, 2018.

[54] J. Roskam. *Part III: Layout Design of Cockpit, Fuselage, Wing and Empennage: Cutaways and Inboard Profiles*. 3rd ed. Lawrence, Kansas: Design, Analysis and Research Corportation (DARcorporation), 2002.

[55] Jhuma Sadhukhan and Mark Christensen. "An in-depth life cycle assessment (Lca) of lithium-ion battery for climate impact mitigation strategies". In: *Energies* 14.17 (Sept. 2021).

[56] Sigler Dean. *Flying the Atlantic Electrically – The Freedom Flight Prize*. Nov. 2020.

[57] Vinay Kumar Singh and Hridaya Nand Sah. "Applications of Transponders in Satellite Communication System". In: *Journal of Emerging Technologies and Innovative Research* 4.7 (2017), pp. 205–211.

[58] Frederick O. Smetana, Delbert C. Summey, and Donald W. Johnson. *RIDING AND HANDLING QUALITIES OF LIGHT AIRCRAFT - A REVIEW AND ANALYSIS*. Tech. rep. NORTH CAROLINA STATE UNIVERSITY, Mar. 1972.

[59] Egbert Torenbeek. *Synthesis of Subsonic Airplane Design*. 1st ed. Dordrecht: Delft University Press, 1982.

[60] G.W.H. Van Es. "Pitching-Moment Change Caused by High-Lift Devices on Wing-Body Configurations". In: *Journal of Aircraft* 40.2 (2003).

[61] Richard T Whitcomb. *A Design Approach and Selected Wind-tunnel Results at High Subsonic Speeds for Wing-tip Mounted Winglets*. Tech. rep. 1976.

[62] Yannian Yang et al. "Sizing of Multicopter Air Taxis—Weight, Endurance, and Range". In: *Aerospace* 11.3 (Mar. 2024).

[63] Xu Zhiyuan. *Interview with Zhiyuan Xu*. Delft, June 2024.